



HAL
open science

Elaboration and assessment of a new $\text{Ag}^\circ/\text{TIO}_2$ heterostructure intended to the label-free SERS detection of DNA

Lijie He

► **To cite this version:**

Lijie He. Elaboration and assessment of a new $\text{Ag}^\circ/\text{TIO}_2$ heterostructure intended to the label-free SERS detection of DNA. Materials. Université Grenoble Alpes, 2015. English. NNT : 2015GREAI004 . tel-01170993

HAL Id: tel-01170993

<https://theses.hal.science/tel-01170993>

Submitted on 2 Jul 2015

HAL is a multi-disciplinary open access archive for the deposit and dissemination of scientific research documents, whether they are published or not. The documents may come from teaching and research institutions in France or abroad, or from public or private research centers.

L'archive ouverte pluridisciplinaire **HAL**, est destinée au dépôt et à la diffusion de documents scientifiques de niveau recherche, publiés ou non, émanant des établissements d'enseignement et de recherche français ou étrangers, des laboratoires publics ou privés.

THÈSE

Pour obtenir le grade de

DOCTEUR DE L'UNIVERSITÉ DE GRENOBLE

Spécialité : **Matériaux, Mécanique, Génie Civil, Electrochimie**

Arrêté ministériel : 7 août 2006

Présentée par

Lijie HE

Thèse dirigée par **Valérie STAMBOULI**
et codirigée par **Michel LANGLET**

préparée au sein du **Laboratoire des Matériaux et du Génie Physique**
dans l'**École Doctorale I-MEP² : Ingénierie, Matériaux, Mécanique, Environnement, Energétique, Procédés, Production**

Élaboration et évaluation d'une nouvelle hétérostructure $\text{Ag}^{\circ}/\text{TiO}_2$ destinée à la détection par effet SERS sans marquage d'ADN

Thèse soutenue publiquement le **02 février 2015**,
devant le jury composé de :

M. Franz BRUCKERT

Professeur, Grenoble INP, Grenoble

Président

M. Marc LAMY DE LA CHAPELLE

Professeur, Université Paris 13, Paris

Rapporteur

Mme. Sophie LECOMTE

Directrice de Recherche, CNRS, Bordeaux

Rapporteur

M. Nicolas CLEMENT

Directeur de Recherche, CNRS, Lille

Examineur

Mme. Valérie STAMBOULI

Chargée de recherche, CNRS, Grenoble

Directrice de thèse

M. Michel LANGLET

Directeur de Recherche, CNRS, Grenoble

Codirecteur de thèse



Acknowledgement

I would never have been able to finish my dissertation without the guidance of my advisors, help from friends, and support from my family.

I would like to thank my thesis exam committee members: Prof. Franz Bruckert, Prof. Marc Lamy de la Chapelle, Dr. Sophie Lecomte, and Dr. Nicolas Clement for their time, interest, insightful questions, and helpful comments.

Foremost, I would like to express my deepest gratitude to my advisors, Dr. Michel Langlet and Dr. Valérie Stambouli, “mes chefs”, as I called them, for their excellent guidance, caring, patience, and providing me with an excellent atmosphere for doing research. Above all and the most needed, Michel, you provided me unflinching encouragement and support in various ways. I remember when I was struggling with this project and you told me to trust you, it was going to work out. I did and I could not be happier. Your truly scientist intuition exceptionally inspire and enrich my growth as a student, a researcher and a scientist want to be. I am indebted to you more than you know. Valérie, the joy and enthusiasm she has for your research was contagious and motivational for me, even during tough times in the Ph.D. pursuit. I am very thankful for your unreserved help and guidance and led me to finish my thesis step by step. Your crucial contributions made you the backbone of this research and so to this thesis, I am grateful in every possible ways.

I would like to give special thanks to Dr. Pierre Bouvier and Dr. Odette Chaix, whom I have worked with on Raman spectroscopy. Each of you have given of your time, energy, and expertise and I am richer for it. Pierre, thanks for the innumerable discussions, your help and suggestions have made a difference.

I am most grateful to the collaborators for lending me their expertise and intuition to my scientific and technical problems: Patrick Chaudouet, Béatrice Doisneau, Laëtitia Rapenne from LMGP, Clair-Marie Pradier and Christophe Calers from UPMC.

The administrative staffs in the LMGP are memorable not only for their prompt support but also for kind care: Colette (my lifesaver for several times), Josiane, Michèle, Virginie and others. I have especially benefited from the truly professional support from the technical staffs: Carman, Arnaud, Matthieu, Hervé, and Serge.

There is no way to express how much it meant to me to have been a member of the team CLEFS. These brilliant friends and colleagues inspired me over the last few years: David, Céline, Clairette, Mouna, Valentin, Thomas. Two persons at this team deserve a very special word of gratitude: one is Mouna, who has given me unreserved help in the beginning of this project; the other is David, who always had the right word for the occasion, who helped me handling different situations.

I would like to thank all the fun, nice, friendly colleagues and friends in LMGP: Mélanie, Shanting, Hironori, Yun Ji, Kanaparin, Marie, Claire M, Fab, Joseph, Flora, Ralph, Marlène, Dan, Simon, Pauline, Sophia, Karim, Quentin, Laurent, Sophie, Louis, and all the others, with whom I shared moments of anxiety but also excitement. Their presence was very important in a process that is often felt as tremendously solitaire. A warm word for Anne and Mamie Laure, who always managed to make me feel special.

To the amazing friends who have spent this period of my life with me: Xiqui, the voice of reason when it was needed, thank you for listening, offering me advice, and supporting me through this entire process. Freddy, the sweetest person I've ever met. Hong, for heart-warming kindness. Stacy, the dinners (mostly in Indian restaurants), traveling, erudite conversations, and even Candy Crush game were greatly appreciated. Lisi, for indulging my huge appetite for independent films. Liang and Géral, I'll never forget the many wonderful dinners and fun activities we've done together. To my friends scattered around the world: Manue, Lydia, Nina, Fathia, Stephane, Tamzin, Vincent, Esther, Chun... thank you for your thoughts, well-wishes, phone calls, e-mails, texts, visits, advice, and being there whenever I needed a friend.

I am especially grateful to my parents, who watched me from a distance while I worked towards my degree. The completion of this thesis will mean a lot to them. So I dedicate this thesis to my loving parents, without whose love, affection and encouragement this work would not have been possible.

Introduction	9
Chapter 1. SERS detection of DNA: state of the art	13
1. Introduction	13
2. Label-free biomolecular sensing context	13
3. A brief introduction to DNA molecule and its detection	14
4. Raman spectroscopy.....	16
4.1 Raman scattering phenomenon	16
4.2 Raman spectroscopy instrumentation	18
5. Overview of surface-enhanced Raman spectroscopy (SERS)	19
5.1 Discovery of SERS.....	19
5.2 Surface enhancement mechanisms.....	19
5.2.1 Electromagnetic enhancement	19
5.2.2 Chemical enhancement.....	21
5.2.3 SERS probes	22
5.3 Hot spots.....	22
6. Solid SERS substrates.....	23
6.1 General considerations.....	23
6.2 Structured surfaces.....	25
6.2.1 Island films.....	25
6.2.2 Electron-beam lithography substrates.....	25
6.2.3 Nanosphere lithography substrates.....	26
6.3 Nanoparticle-defined surfaces.....	27
6.3.1 Nanoparticles immobilized on solid substrates	27
6.3.2 Chemically and photochemically grown Ag ⁰ NPs on solid supports	30
7. Application of solid SERS biosensors for oligonucleotides detection	31
7.1 SERS biosensor for labeled- DNA detection	32
7.2 Label-free detection of DNA	34
7.2.1 Single-nucleobase detection	34
7.2.2 Single strand and double strands oligonucleotides detection	35
8. Conclusion.....	38
Chapter 2. Titanium dioxide and sol-gel processing: extrapolation to a new kind of SERS substrate	53
1. Introduction	53
2. Overview of titanium dioxide	53
2.1 Crystalline structure.....	53
2.2 Photo-induced properties.....	54
2.3 Photocatalytic activity	56
2.4 TiO ₂ -based photocatalytic reduction of metal cations	58
3. The sol-gel process	60
3.1 General principles.....	60
3.2 Adaptation to TiO ₂ sols	63
3.3 Film deposition by spin-coating.....	64
4. Extrapolation to an Ag⁰/TiO₂ SERS substrate: previous results.....	66

5. Conclusion.....	70
Chapter 3. Tailored silver nanoparticles for surface enhanced Raman spectroscopy substrates	75
1. Introduction	75
2. Characterizations.....	76
3. One-step photocatalytic reduction.....	76
3.1 Non-assisted photocatalytic reduction.....	76
3.2 Trisodium citrate (TSC)-assisted photocatalytic reduction.....	80
3.2.1 Influence of R_c for fixed UV duration.....	80
3.2.2 Effect of UV duration and $AgNO_3$ concentration.....	82
4. Seeded growth assisted photocatalytic reduction	84
4.1 Seeded growth principle and seed deposition	84
4.1.1 Morphological and structural characterizations	86
4.1.2 Self-limited growth/aggregation process: discussion	93
5. Conclusion.....	95
Chapter 4. First assessments of the Ag°/TiO_2 SERS substrate performances ..	99
1. Introduction	99
2. Spectroscopic characterizations	99
3. Preliminary spectroscopic studies	100
4. SERS spectra	103
5. SERS performance assessments	106
6. SERS performances of the Ag°/TiO_2 heterostructure: discussion.....	110
7. Conclusion.....	111
Chapter 5. SERS detection of homo-oligonucleotide single strands on Ag°/TiO_2 heterostructure: binding, orientation and ordering on Ag° NPs surface.....	115
1. Introduction	115
2. DNA material and immobilization process.....	116
2.1 DNA material: polybases- NH_2 and polybases	116
2.2 DNA immobilization process.....	117
3. Results	119
3.1 DNA concentrations effects.....	119
3.1.1 Surface chemical analyse by XPS.....	119
3.1.2 SERS analyses.....	122
3.2 Analyses at fixed concentration.....	125
3.2.1 Spectrum indexation of each polybase	125
3.3 DNA concentration-dependent reproducibility of SERS spectra	131
3.3.1 Range of lowest and highest DNA concentrations.....	131
3.3.2 Range of optimal DNA concentration	132
4. Discussion	135

4.1 Binding features and general molecular orientation.....	135
4.2 Concentration effects on the molecular orientation.....	137
4.3 Reproducibility of spectra at optimum concentration: role of the external NH ₂ linker.....	141
5. Conclusion.....	142
Chapter 6. SERS detection of complementary polybase pairs: mixture versus hybridization effects.....	147
1. Introduction	147
2. DNA materials and immobilization process	148
2.1 <i>In situ</i> hybridization	148
2.2 Single strand polybase mixture immobilization	150
2.3 General experimental features.....	150
3. Results	150
3.1 Equi-molar polyA-NH ₂ +polyT mixture vs. hybridized polyA-NH ₂ • polyT.....	150
3.1.1 Indexation of SERS spectra at fixed concentration	151
3.1.2 Influence of the concentration.....	153
3.1.3 Discussion.....	155
3.1.4 Summary.....	163
3.2 Equi-molar polyG-NH ₂ +polyC mixture vs. hybridized polyG-NH ₂ • polyC	164
3.2.1 Indexation of SERS spectra at fixed concentration	164
3.2.2 Influence of concentration	166
3.2.3 Discussion	168
3.2.4 Summary.....	171
4. Conclusion.....	171
Conclusion.....	175
List of publications	179

Introduction

The rapid and reliable detection of biomolecules, such as proteins, metabolites, peptides, or DNA sequences is of crucial importance to the progression of the medical diagnostic field. Research is continually progressing to develop more effective and sensitive approaches. Laser spectroscopic methods play a central role in this field, as they are capable to identify and structurally characterize the molecule of interest, for instance by providing its fingerprint and monitoring its structural changes. Therefore, vibration spectroscopic techniques such as *Raman spectroscopy* have drawn increasing attention due to their high structural information content. More recently, nanotechnology has opened a new horizon for biomolecular sensing. Accordingly, *Surface-Enhanced Raman Spectroscopy (SERS)* technique takes advantage of optical properties of metallic nanostructures, resulting in a strongly enhanced Raman signal that overcomes the traditional low sensitivity problem in Raman spectroscopy and provides a remarkably powerful tool for biomolecular sensing. In this context, the *label-free* strategies to detect biomolecules, and notably DNA molecules, are under intense development. Among all the label-free strategies, SERS technique provides a powerful, rapid, and sensitive method to analyze the structural fingerprint of molecules through the specific detection of Raman bands.

Many recent studies report on the label-free SERS detection of DNA strands before and/or after hybridization. However, the comparison of the resulting spectra remains very challenging. Indeed, from one paper to another one, fluctuations in both band position and peak intensity are found, leading to difficulties in extracting sustainable data. Moreover, the important aspect related to data reproducibility and repeatability on sample surface is not often addressed. If the SERS technique is a powerful and ultrasensitive tool to detect an analyte, many experimental parameters may compromise the data reliability, for example, the Raman cross section of molecules to be detected, the molecule orientation relatively to both the laser beam polarization and the exalting surface, the geometry of so-called “hot spots”, etc. In the specific case of DNA detection, two main parameters should be stressed. First, the characteristics of the DNA molecule itself involve various levels of compositional, structural, and conformational organizations depending on environmental and experimental conditions. Second, as for any other analyte, the characteristics of the SERS active substrate are crucial. The efficiency of such substrate relies in particular on the controlled creation of a large number of stable hot spots on a solid substrate. This can be achieved through either the homogeneous dispersion of well-designed metal nanoparticles (NPs) aggregates at the substrate surface or through the suitable structuration of a metallic substrate. Currently, available methods for the fabrication of such SERS solid substrates are generally either expensive and/or involve complex procedures for practical application. Thus, the easy and cheap

fabrication of SERS solid substrates in large areas, while maintaining a high enhancement factor (EF) and good reproducibility, still remains a challenge. The purpose of the thesis is to address this issue following a step by step experimental approach i/ by investigating a new bottom up experimental procedure, aiming at improving the uniformity of a $\text{Ag}^\circ/\text{TiO}_2$ heterostructure formed by photocatalytic reduction in order to optimize the derived SERS substrate performances, and ii/ by extrapolating such new type of substrate for the label-free SERS detection of DNA molecules before and after hybridization.

The content of this thesis covers 6 chapters.

In **chapter 1**, we introduce the reader to SERS technique, emphasizing principles and applications which we judge important as a background to SERS. In a first part, we start with the general principles of Raman spectroscopy and then describe in detail the mechanisms responsible for SERS. In a second part, we provide a review of common solid SERS substrates currently used and their applications in DNA molecule sensing.

In **chapter 2**, we present the methods and procedures that have been employed for the elaboration of a new type of SERS substrate. In a first part, we start with a brief overview of titanium dioxide and then describe the sol-gel protocol used to produce photocatalytic TiO_2 thin films. In a second part, we present an overview of the results previously obtained at LMGP, which showed the feasibility of an $\text{Ag}^\circ/\text{TiO}_2$ heterostructure elaborated through a photocatalytic reduction procedure and its potential as SERS substrate in view of the label-free DNA detection.

Chapter 3 is devoted to the optimization of the $\text{Ag}^\circ/\text{TiO}_2$ heterostructure elaboration conditions. We describe thorough investigations on the mechanisms leading to the controlled growth of Ag° NPs through a photocatalytic reduction process and show how a chemically assisted photocatalytic procedure enables to optimize the morphologic properties of Ag° NPs grown on the TiO_2 surface. In this chapter, we only focus on the morphology of Ag° NPs, while the SERS performances of derived $\text{Ag}^\circ/\text{TiO}_2$ heterostructure will be investigated in **chapter 4**. In the latter, we first study the pure Raman spectrum (without any SERS enhancement) of Rhodamine 6G (R6G) molecules on a bare silicon substrate (in the absence of Ag° NPs), followed by a detailed indexation of all the characteristic bands. Then we investigate the SERS performances of $\text{Ag}^\circ/\text{TiO}_2$ heterostructure elaborated in selected model conditions. These performances are in particular studied through the assessments of the detection limit, SERS enhancement factor, and SERS spectrum reproducibility of so-obtained substrates.

In **chapter 5**, we report for the first time a thorough study on the SERS spectra obtained in the case of the four homo-oligonucleotides, polyA, polyC, polyT, and polyG, functionalized or not by an external functional amino NH_2 linker, and immobilized on our solid $\text{Ag}^\circ/\text{TiO}_2$ SERS substrate. This enables us to study the influence of this NH_2 group on the respective SERS spectra and to draw conclusions on how DNA is immobilized on the platform. Furthermore, in addition to XPS analyses, we pay special attention to how the homo-oligonucleotide concentration influences the packing surface density of homo-oligonucleotides and their orientation with respect to the platform surface.

Based on our previous results, in **chapter 6**, we investigate the specific SERS features of complementary polybase pairs obtained after *in situ* hybridization directly performed on single strand polybases covered Ag° NPs surfaces. The polybase pairs are typically: polyA- NH_2 with polyT, and polyG- NH_2 with polyC. To support the results, the obtained SERS spectra are systematically compared with those obtained after the direct immobilization of mixtures containing the same complementary polybases. Since the polybases are not hybridized in these mixtures, derived SERS spectra serve as negative control, which enables us to investigate unambiguously the signature of hybridized polybases in SERS spectra by comparing the spectroscopic features of mixed and hybridized pairs. Then, we draw conclusions on how the DNA double strands are immobilized on the platform and we pay special attention to how their concentration influences their surface coverage density and their orientation with respect to the platform surface.

Finally, a conclusion closes this thesis with a summary of the main results and a presentation of future directions.

Chapter 1. SERS detection of DNA: state of the art

1. Introduction

The purpose of this chapter is to introduce the reader to *Surface-Enhanced Raman Spectroscopy*, which is one of the major techniques used for the *label-free* detection of bio-molecules. The general principles of Raman spectroscopy as well as the mechanisms responsible for SERS are described in detail. Then the chapter presents a review of common solid SERS substrates currently used and their applications in DNA molecule sensing.

2. Label-free biomolecular sensing context

Rapid and reliable detection of biomolecules, such as proteins, metabolites, peptides or DNA sequences is of vital importance to the progression of the medical diagnostic field. Research is continually progressing to develop more effective and sensitive approaches. Laser spectroscopic methods play a central role in this field, as they are capable to identify and structurally characterize the molecule of interest, for instance by providing its fingerprint and monitoring its structural changes. Therefore, vibration spectroscopic techniques such as *Raman spectroscopy* have drawn increasing attention due to their high structural information content. Elsewhere, nanotechnology has recently opened a new horizon for biomolecular sensing. Accordingly, *Surface-Enhanced Raman Spectroscopy (SERS)* technique takes advantage of optical properties of metallic nanostructures, resulting in a strongly enhanced Raman signal that overcomes the traditional low sensitivity problem in Raman spectroscopy and provides a remarkably powerful tool for biomolecular sensing. Specific examples of molecules detected by SERS include not only DNA [1-23], but also proteins [24-28], bacteria [29-31], and whole cells [32-34].

In this context and as will be detailed in next section, the *label-free* strategies to detect biomolecules, and notably DNA molecules, are under intense development. Such label-free strategies generally rely on the modification of a physical parameter of the transducer in response to the biological event, namely changes in the refractive index in the case of Surface Plasmon Resonance (SPR) [35-37], the conductivity in the case of electrical or electrochemical detection [38-40], the resonance frequency in the case of bio-MEMS (Micro Electro Mechanical Systems) [41, 42]. In these techniques, the detected signal is not necessarily specific of the molecule to be analyzed. In contrast, and among other advantages, SERS technique provides a powerful, rapid, and sensitive label-free method to analyze the structural fingerprint of molecules through the specific detection of Raman peaks [43]. In this chapter, we will focus on the SERS detection of DNA molecules.

3. A brief introduction to DNA molecule and its detection

It is well known that DNA (also called deoxyribonucleic acid) is the molecule which carries genetic codes. The sensitive and selective detection of DNA sequences is central in the modern bio-analysis. Generally speaking, the fundamental DNA structure can be simply perceived as a double helical structure: two DNA strands twisted around each other in the form of a double helix (Figure 1-1). Single DNA strands consist of a long chain of repeating subunits, which are called *nucleotides*. Each nucleotide is composed of three parts: a five-carbon cycle sugar, named as ribose, a phosphate group, and a nucleobase (Figure 1-2).

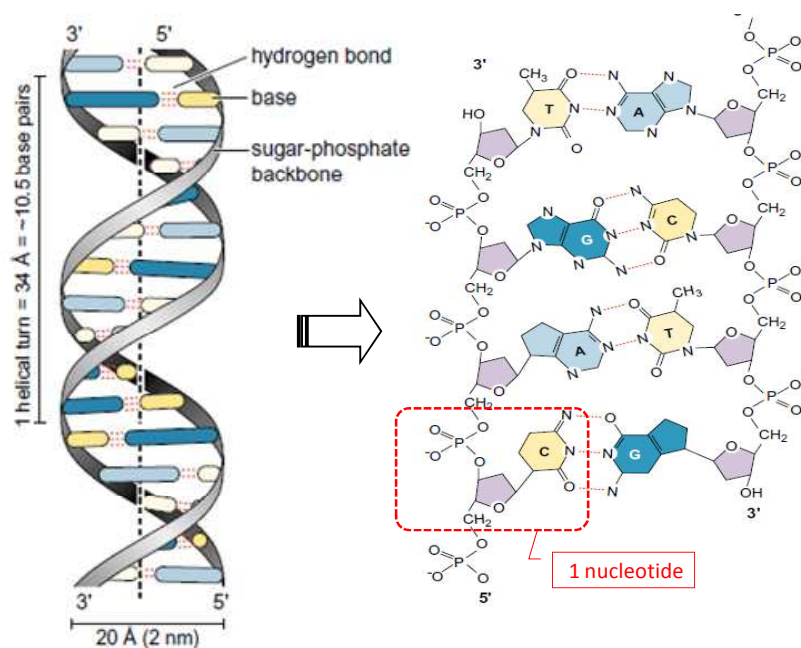


Figure 1-1: Schematic model of the DNA double helix showing the composition of the nucleotide subunit.

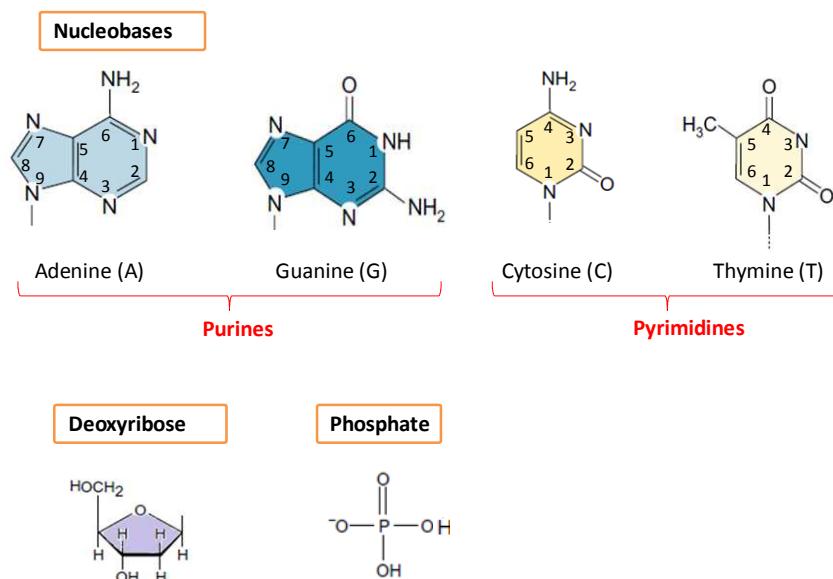


Figure 1-2: Components of DNA: bases, sugar, and phosphate.

The four nucleobases are nitrogen containing molecules which are divided into two classes, purines and pyrimidines [44]. The purines are *adenine* and *guanine*, which have the similar double carbon-nitrogen ring structure but with different attached groups (Figure 1-2), while *cytosine* and *thymine*, which have one single ring structure, are called pyrimidines. The hydrogen bonds between bases, which are referred to as “Watson-Crick” or “complementary” base pairing, provide a force holding the double helix together. This hydrogen bonding occurs in such a way that adenine is always paired with thymine, while guanine is always paired with cytosine, as illustrated in Figure 1-1.

As mentioned before, nucleotides are considered as the basic building blocks of DNA. They contain a phosphate joined to a sugar moieties, known as 2'-deoxyribose, to which the nucleobase is attached. Nucleotides are joined (polymerized) by a condensation reaction to form a DNA single strand chain [45]. If there is a small number of nucleotides (up to 30), this short strand is called oligonucleotide.

Generally speaking, there are two categories of techniques in the field of optical detection of DNA sequences: label-based detection and label-free detection. In the label-based detection, the target DNA sequences are labeled with fluorescent dyes and detected either by the fluorescence emission [46] or by SERS. The latter part will be detailed in section 7.1. Fluorescence-based detection is the most used and a well-established detection method. However it suffers from complex and expensive labeling processes and is also very susceptible to photo-bleaching under excitation conditions, which affects the detection limits. In contrast, in label-free detection, the target DNA sequences are not labeled and are detected

through their direct fingerprint. This approach potentially offers an easier and cheaper detection way. As will be detailed in following sections, the SERS technique can address DNA label-free detection needs. Before detailing the SERS phenomenon, it is firstly necessary to give a brief introduction to *Raman spectroscopy*.

4. Raman spectroscopy

4.1 Raman scattering phenomenon

The Raman scattering is an inelastic scattering effect discovered by C.V. Raman in 1921 in India. Raman himself observed a “modified” light scattering with altered wavelength and called the effect ‘a new type of secondary radiation’ in his original paper [47]. Since then, this type of scattering has been referred to as *Raman scattering or Raman effect*. This discovery awarded him a Nobel Prize in physics in 1930.

When light interacts with matter, the light (photons) may be absorbed or scattered. When dealing with molecules, the interaction with light is primarily determined by the energy levels of the degrees of freedom of the molecules. The scattering process can be classified into two groups:

Elastic scattering, also referred to as *Rayleigh scattering*, where the scattered photons have the same energy (E_S) as incident photons (E_L), i.e. $E_S = E_L$.

Inelastic scattering, where the scattered photons have different energy from that of incident photons, i.e. $E_S \neq E_L$.

Figure 1-3 presents the energy level diagram for Raman scattering process and Rayleigh scattering. The Rayleigh scattering process does not involve any energy change and the photons return to the same energy state (vibrational state). The Raman scattering process involves absorption of energy and the molecular energy lies between a ground vibrational state ($v = 0$) and a higher energy excited state ($v = 1$). This is referred to as *Stokes scattering*, i.e. $E_S < E_L$. Besides, molecules already in a vibrationally excited state ($v = 1$) can also scatter and return to the ground state ($v = 0$), transferring excess of energy to scattered photons. This is referred to as *anti-Stokes scattering*, i.e. $E_S > E_L$. Compared to Stokes scattering, anti-Stokes scattering is normally very weak.

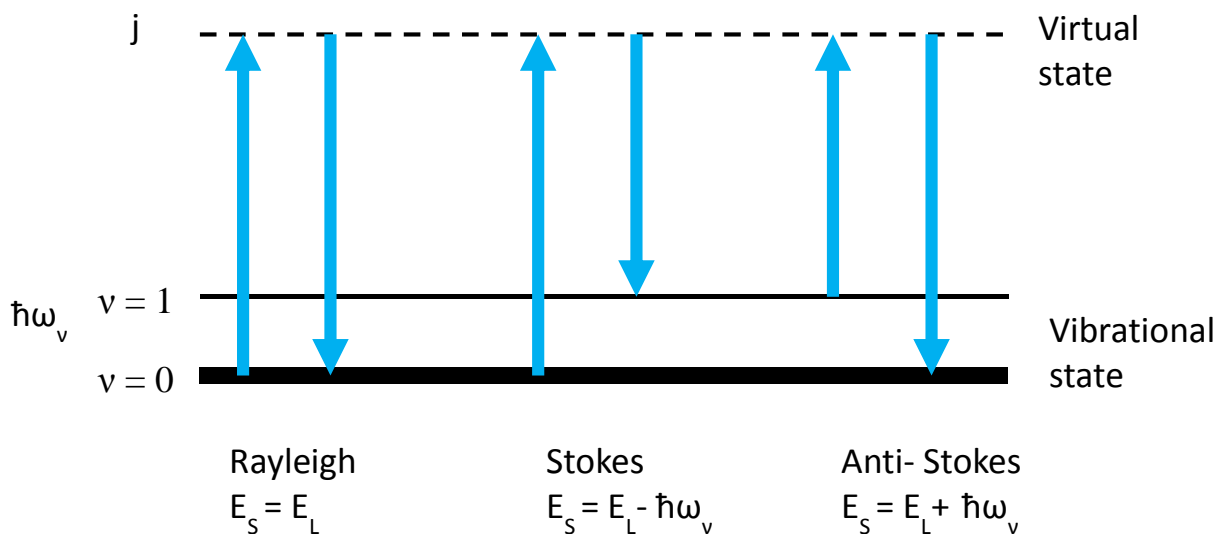


Figure 1-3: Diagram of Rayleigh and Raman scattering (from Smith 2005[48]). The lowest vibrational state $v = 0$ is shown at the foot with higher energy states above it.

The energy lost by the photons in the scattering event is called the *Raman shift* and is defined in energy as $E_R = E_L - E_S$. Raman shifts are commonly expressed in wavenumbers and will then be noted $\Delta\bar{\nu}_R$ (cm^{-1}). The modulus of the Raman shift corresponds to the wavenumber of the vibrational mode ($\bar{\nu}_v = \hbar\omega_v/hc$) involved in the scattering event, i.e. $\bar{\nu}_v = |\Delta\bar{\nu}_R|$. A typical *Raman spectrum* commonly depicts the Raman intensity variations as a function of the Raman shift (rather than wavelength). Peaks in the Raman spectrum correspond to specific vibrational modes of the molecule and the Raman shift, i.e. the peak position in wavenumber, depicts the vibrational energy of the corresponding mode [49]. The measurement and the analysis of signals arising from the Raman scattering are called *Raman spectroscopy*. In addition to IR spectroscopy, Raman spectroscopy is the main technique used for molecule identification. A Raman spectroscopy apparatus is constituted of several key components described hereafter and illustrated in Figure 1-4.

4.2 Raman spectroscopy instrumentation

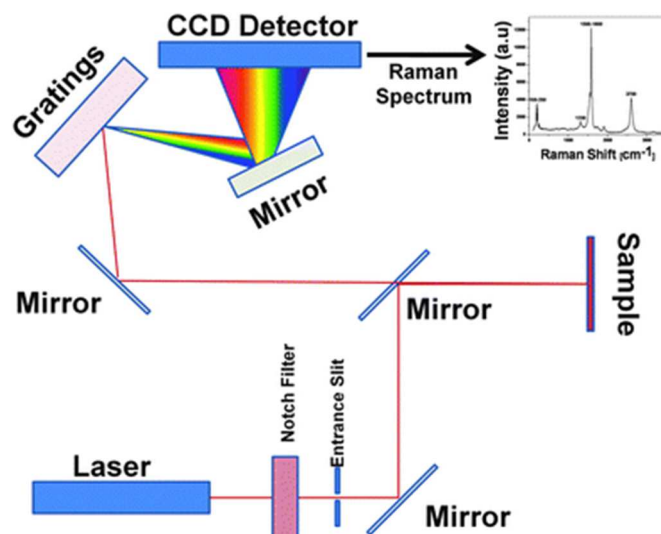


Figure 1-4: Schematic illustration of a Raman system [50].

Laser source

The laser source is generally He-Ne, Ar⁺, or Kr⁺ corresponding to different emission wavelengths in the visible range. He-Ne lasers emit a highly collimated beam of photons at a wavelength of 632.8 nm, Ar⁺ lasers emit at 488.0 and 514.5 nm, and Kr⁺ lasers emit at 530.9 and 647.1 nm [51]. A multitude of wavelengths is thus available today and the choice of laser wavelengths is dictated by the analyzed sample properties. The considerations for wavelength choice are: coupling of laser light to the system sensitivity, desired/undesired resonance phenomena, elimination of fluorescence emissions, avoiding photodecomposition of the sample under laser light, etc.

Sample cells

Raman spectra can be obtained in various media, i.e. solids, liquids or gases. For solid samples or molecular analytes adsorbed on a solid surface, minimum preparation is required. Using a Raman microscope, it is sufficient to focus on the sample visually. The focus of the laser onto the sample can be readily achieved as well as the analyses on small areas because of the small diameter of the laser beam (~1 μm) [52].

Wavelength selector

Wavelength selectors can be classified into several categories. The simplest device is an interference filter. Improved interference filters, made by a holographic process and referred to as notch filter, have recently been introduced [52]. The notch filter is designed to absorb all light frequencies of the incident laser beam. In common type of instruments, the scattered light is collected through the notch filter and

focused into several monochromators, which separate the different energies of the Raman scattering [49]. In addition, diffraction gratings are chosen in relation to the desired wavelength range and to improve the optical resolution of the spectrometer.

Transducer and Readout System

Historically, Raman spectrometers used photomultiplier tubes as detectors. However, this method is no longer used. Presently, most of Raman spectrometers are equipped with a two-dimensional multichannel charge-coupled device (CCD) detector. The multichannel detector provides a simultaneous detection of Raman signals in the entire frequency range in a reduced amount of time compared to a single-channel technique. The major advantage of multichannel CCD detector relatively to other multichannel detectors relies on a weaker readout noise [52, 53].

5. Overview of surface-enhanced Raman spectroscopy (SERS)

5.1 Discovery of SERS

The first paper reporting SERS phenomenon is attributed to Fleischmann in 1974, who described a strong enhancement of the Raman signal arising from pyridine adsorbed on a roughened silver electrode [54]. Shortly after, Jeanmaire and Van Duyne [55] and Albrecht and Creighton [56] demonstrated separately that the Raman signal enhancement factor (EF) of pyridine adsorbed on a roughened electrode system is 10^5 - 10^6 . Van Duyne, who named the phenomenon Surface-Enhanced Raman Spectroscopy [57] has claimed the discovery of SERS by his group in a recent publication [58]. They also have contributed to the knowledge in the enhancement mechanisms based on electromagnetic and chemical effects.

5.2 Surface enhancement mechanisms

The SERS enhancement phenomenon is not yet clearly understood, but two main concepts are still under discussion since the discovery of the SERS phenomenon, i.e. electromagnetic and chemical effects, which have dominated works in this field.

5.2.1 Electromagnetic enhancement

In SERS it is firstly well-admitted that the Raman signal of an adsorbed molecule is amplified through the specific and resonant excitation of localized surface plasmon resonances (LSPR) of the substrate [59], usually in the form of metal particles or roughened metal surfaces.

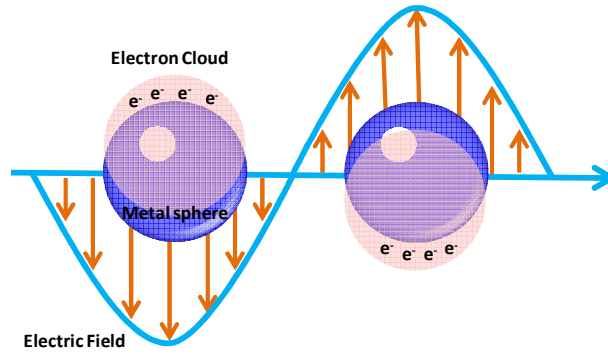


Figure 1-5: Illustration of the excitation of the LSPR of spherical nanoparticles by incident electromagnetic radiation [60].

LSPR is an optical phenomena generated by light when it interacts with conductive nanoparticles (NPs) whose size is smaller than the incident wavelength (Figure 1-5). Consequently, the magnitude of SERS enhancement is crucially dependent upon the SERS substrate. To understand the electromagnetic enhancement, one must consider the size, shape, and material (noble metal, i.e. Ag, Au, Pt) of nanoscale roughness [60]. Theoretical models have been proposed in the literature. The simplest description of electromagnetic enhancement is based on the model of isolated spheres (Figure 1-5) with a quasistatic description of the incident electromagnetic field. The field at the surface is described by [48]:

$$E_r = E_0 \cos \theta + g \left(\frac{a^3}{r^3} \right) E_0 \cos \theta \quad \text{Equation 1-1}$$

In which,

E_r and E_0 are the total electric field magnitude at a distance r from the sphere surface and at the sphere surface, respectively,

a is the radius of the sphere,

θ is the angle relative to the direction of the electric field,

g is a constant related to the dielectric constants such that,

$$g = \frac{\varepsilon_1(\nu_L) - \varepsilon_0}{\varepsilon_1(\nu_L) + 2\varepsilon_0} \quad \text{Equation 1-2}$$

Where, ε_0 and ε_1 are the dielectric constants of the medium surrounding the sphere and the metal sphere, respectively, and ν_L is the frequency of the incident radiation.

The diameter of the sphere is considered to be small compared to the wavelength of light. At some point, where the value of g reaches its maximum, the excitation of surface plasmon significantly increases the local field experienced by the molecule adsorbed on the surface [48]. The electromagnetic enhancement

mechanism brings typically a 3-4 orders of magnitude enhancement. Besides, electromagnetic enhancement does not demand direct contact between molecule and metal but it strongly decreases when increasing the distance between both, usually in a few nanometers [61]. However, LSPR is strongly dependant on the size and shape of metal NPs. Accordingly, the numerous papers devoted to the SERS effect report very different results concerning various aspects, i.e. different order of magnitude enhancement, different optimal shapes or sizes, different optimal detection wavelengths, depending on the studied analytes.

5.2.2 Chemical enhancement

Although the electromagnetic enhancement is considered to be the major contributor to the SERS effect, other mechanisms cannot be neglected. The chemical enhancement mechanism, which is less understood than electromagnetic enhancement, brings a 1-2 orders of magnitude enhancement to the Raman signal intensity. In the chemical mechanism, it is assumed that a specific interaction is created between the metal and the adsorbed molecule through the metal-adsorbate proximity [60-62]. An electronic coupling between molecule and metal, and the formation of an adsorbate-surface complex, results in an increased Raman cross section of the adsorbed molecule compared to the cross section of a 'free' molecule in a 'normal' Raman mode [61].

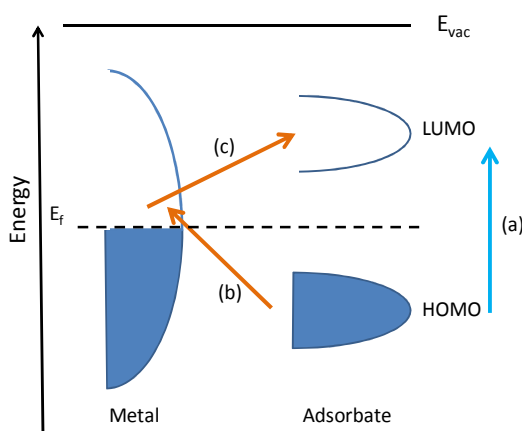


Figure 1-6: Energy level diagram for a 'molecule-metal system' showing possible resonant Raman processes involving only molecular states (path(a)) or both molecular and metallic states (paths (b) and (c)) [62].

This may be explained by the diagram illustrated in Figure 1-6: the highest occupied molecular orbital (HOMO) and the lowest unoccupied molecular orbital (LUMO) of the adsorbate are symmetrically placed in energy in relation to the Fermi level (E_f) of the metal. The possible resonant Raman process involves only molecular states (Figure 1-6: path (a)) or both molecular and metallic states (Figure 1-6: paths (b) and (c)) [61]. In this latter case, charge-transfer excitations (either from the metal to the

molecule or vice versa) can occur at about half the energy of the intrinsic intramolecular excitations of the adsorbate [62]. Unlike the electromagnetic enhancement mechanism, this mechanism requires direct contact between molecule and metal [63].

5.2.3 SERS probes

Dye molecules are often chosen as model analytes in fundamental studies or to develop SERS substrates because of their high intensity of Raman scattering, i.e. their high Raman cross-section. But for many applications (e.g. biomolecule sensing), we don't have the liberty to choose the probe and must adapt the probe with specifically optimized SERS substrates and spectrum acquisition conditions. Thus, two important questions arise:

- i/ can any molecule be attached to metallic substrate surface (usually silver or gold surface)? and
- ii/ will the resulting SERS signal be high enough for observation?

In principle, any molecule can be detected by SERS. But with weaker Raman scatterers, obtaining a detectable signal can be very challenging. As the electromagnetic enhancement drops dramatically when increasing the distance between the probe and the SERS substrate, the probe molecules must stay in close proximity to the SERS substrate, usually within a few nanometers, in order to ensure an intense SERS signals [64, 65]. Theoretical calculations have suggested that the field degradation length is about 2 nm [60, 66]. Thus, the ability to adsorb directly on the SERS substrate surface has become an important aspect for SERS probes. For this reason, many SERS studies have been performed on molecules with a terminal thiol (HS) or amine (NH₂) group allowing chemisorption to the substrate surface. Indeed these terminal groups, which are usually called functional groups, display strong chemical affinity for metal surfaces, typically gold or silver surfaces. This concept of probe/surface interaction has become an important part of SERS studies, i.e. studies dealing with a specific '*surface functionalization*'. In the context of biosensing, this often refers to as the modification of the SERS substrate surface for the selective attachment of specific biomolecule analytes.

5.3 Hot spots

While electromagnetic and chemical mechanisms have historically been considered as the main cause of SERS effect, more recent fundamental studies have demonstrated that the greatest Raman signal enhancement does not occur evenly around an isolated metal molecule, but is generally related to aggregates of metal NPs. It is attributed to "hot spots" located at the proper junction or gap between vicinal NPs (illustrated in Figure 1-7), where a dramatic enhancement of the EM field can occur. In the past few years, numerous publications pointed out the exciting fact that these hot spots provide giant enhancements in many cases [67-71]. For instance, several groups have demonstrated the possibility to achieve Rhodamine 6G single-molecule detection by Ag⁰-induced SERS, which corresponds to an enhancement factor (EF) of 10¹⁴ or more in the SERS spectra relative to normal Raman [38-40, 42]. The

precise reasons for this still remain the subject of intensive researches. However, it can be roughly explained using a simplified model of two vicinal metal spheres. As these latter approach each other, the electric fields produced by each individual particle start to interact, and this interaction strongly reinforces the electromagnetic field in certain regions of space. The resulting magnified electromagnetic field yields a huge enhancement of the Raman signal, which has ever been exploited for the SERS detection of many varieties of single molecules [67-74].

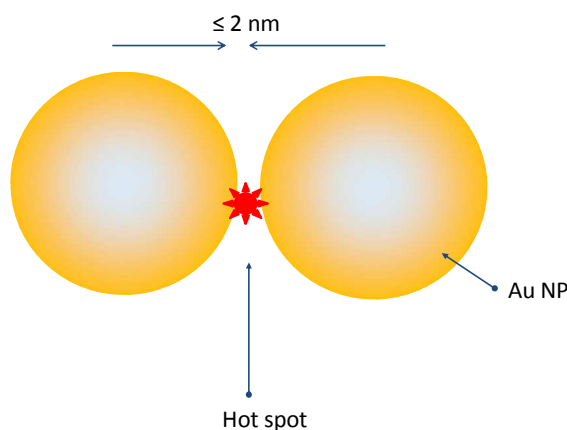


Figure 1-7: Idealized “hot spot” located at the proper junction or gap between vicinal NPs.

In these fundamental studies, hot spots were only observed on some isolated aggregates, but this finding has considerably reinforced the interest for SERS-based bio- and chemo-sensors, since the narrow and well-resolved Raman peaks directly provide a structural fingerprint of the analytes and allow a rapid and simultaneous detection of multiple analytes. In this applicative context, current challenges deal with the development of highly sensitive, tunable, robust, and reproducible SERS-active devices [75]. The high sensitivity of such devices relies in turn on the homogeneous creation of a large number of hot spots on a solid substrate, i.e. the homogeneous dispersion of well-designed metal NPs aggregates at the substrate surface or the suitable surface structuration of a metallic substrate.

6. Solid SERS substrates

6.1 General considerations

A SERS substrate is a general denomination for any plasmon-resonance supporting structure that can produce suitable Raman amplification [49]. Hereafter, we apply the classification proposed by Le Ru *et al.* in ref. [49], which divide SERS substrates into three categories:

- Metallic roughened electrodes.

- Metallic nanoparticles in solution, i.e. colloidal solutions.
- “Solid” substrates, i.e. nanoparticles dispersed onto solid surfaces or artificially structured surfaces.

Metallic roughened electrodes had great contributions to the initial development of SERS since its discovery, particularly with the studies of Otto *et al.*[12, 13]. Even though today their importance has decreased, electrodes still remain an important approach in SERS detection on solid substrates. We will not further discuss this category of solid SERS substrates, since the electrochemical mechanism on which they rely is very distant from the topic treated in this thesis.

Among the other two categories of SERS substrates, metal colloidal solutions play a very important role in SERS sensing. This second category addresses SERS experiments performed in liquid medium, which involve either Ag⁰ or Au⁰ nanoparticles in liquid suspensions [4, 76-80]. Great amounts of publications have proposed numerous methods to produce metallic nanoparticles in solution, including chemical and photo-chemical approaches. However, the main drawback of this approach is that the aggregation of nanoparticles in solution turns the reproducibility more challenging. Moreover, it is clear that this technique is not so simple to use in the case of portable biosensor.

In this chapter, we will thus focus on the third category of SERS substrates, new solid SERS substrate generation, which are in direct link with this thesis. Much effort has been devoted to improve the performances of such substrates. Because the SERS intensity depends on the excitation of the LSPR, it is important to control all the factors influencing the LSPR to maximize signal strength and ensure reproducibility [81]. Nanoscale roughness features such as the size, shape, and most important, interparticle spacing, are extremely useful properties to ensure that the incident laser light efficiently excites the LSPR [58]. Solid SERS substrates currently studied include nanoparticle-defined surfaces and rationally designed nanostructures, chosen because of their desired optical properties [11-13, 82, 83]. These substrates are discussed in detail in the following sections. It is worthwhile pointing out that i/ SERS detection on solid substrate can be performed either in liquid (or humid) conditions or in dry conditions; and ii/ SERS solid substrates are usually elaborated according to two main strategies depending on the choice of “top down” or “bottom up” technology. The top down strategy involves several routes of controlled etching of silver films. Historically, silver electrodes were electrochemically (top down) etched or roughened and SERS measurements were performed in liquid medium [12, 13, 15, 84]. The section 6.2 covers the SERS substrates obtained by directly fabricating nanostructures on a solid support. As previously mentioned, such approach is generally classified as ‘top down’, in contrast to the ‘bottom up’ methods covered in section 6.3.

6.2 Structured surfaces

6.2.1 Island films

Vapor-deposited island films were the most widely used substrates in the early stages of SERS studies [85-91]. Even if the vacuum-based system necessary for vapor deposition of metal film is relatively expensive and requires conscientious upkeep, the deposition procedure itself is straightforward and inexpensive [92]. So-deposited metal films are usually formed directly on substrates with controlled thicknesses and island morphologies by adjusting the deposition conditions [86, 90]. However, the enhancement factors achieved with these films (10^4 - 10^5) are well below those obtained with other SERS substrates (i.e. aggregated nanostructures) and the EF exhibits large fluctuations when measured in different places of a same substrate for pyridine molecules [88].

6.2.2 Electron-beam lithography substrates

One of the most obvious methods to produce regular structured surfaces is lithography, which can yield long-range ordered structures. However most lithographic techniques are not capable of producing features of size small enough to be truly SERS-active [75]. An exception to this trend relies on electron-beam lithography (EBL), which has been routinely used since the discovery of its feasibility to generate SERS-active structures (Figure 1-8 : (A), (B)) [93-102]. The most important advantage of the EBL approach is the possibility to control the metal nanoparticle size and shape and the interparticle distance with great accuracy [97, 103, 104]. Sepaniak *et al.* investigated the efficiency of EBL fabricated SERS substrates with different nanoscale features. Such efficiency was studied by measuring the SERS signal of Rhodamine 6G (R6G) adsorbed on a series of cubic, elliptical, and hexagonal nanopatterned pillars. Their results show that the size, geometry, and orientation of the particle primary axis relative to the excitation polarization vector, and particularly the density of nanoparticles, all have strong influence on the SERS substrate performances [103]. Gunnarsson *et al.* explored the influence of interparticle distance on the performances of circular and triangular silver nanoparticles substrates [105]. In a similar experiment, a metal nanoparticles array with an interparticle distance reduced to 1 nm resulted in extremely high SERS signals. Such metal nanoparticle arrays were fabricated by EBL combined with an angular evaporation technique [106]. The above examples show that EBL allows the optimization of periodic structures, shape, and spacing, potentially compatible with good SERS performances. However EBL is time-consuming, costly and not amenable to large-scale production.

In addition to EBL, new techniques such as nanoimprint lithography (NIL) have also been used as an effective tool for producing SERS-active structured substrates (Figure 1-8: (C), (D)). Several authors reported that this approach is able to fabricate reproducible and large-scale SERS-active substrates with

controlled topology, which allowed fundamental studies to be carried out on the enhancement factor (EF) dependence of the substrate optical properties [107-112].

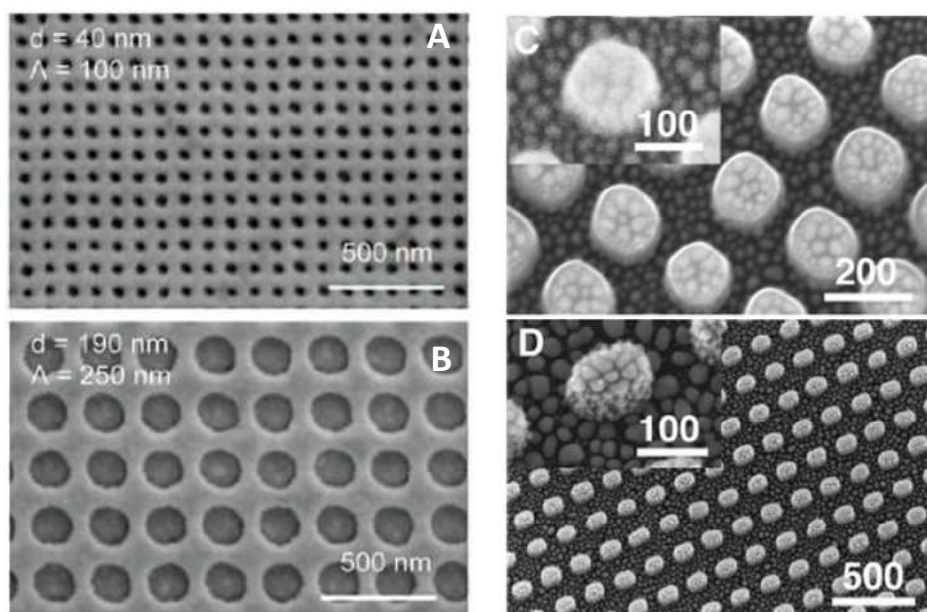


Figure 1-8: SERS substrates: (A-B) nanoholes array fabricated by EBL from ref.[93]; (C-D) pillared SERS-active substrates fabricated with a technique combining nanoimprint lithography with physical vapor deposition from ref.[107].

6.2.3 Nanosphere lithography substrates

In addition to the previous lithography approaches, the nanosphere lithography (NSL) has also been used historically for generating structured surface since it is a quite low cost method. In this method, micro- or nanospheres are used to template deposited metal film. This methodology improves the stability of the structure, which can be efficiently used in Raman investigations [113]. Derived “metal films over nanoparticles” (MFON) samples are often employed in fundamental SERS studies thanks to their well-characterized structures. For instance, Van Duyne and co-workers have performed a series of studies on NSL fabricated SERS substrates (Figure 1-9) [81, 114-118]. They have studied in detail wavelength-scanned surface enhanced Raman excitation spectroscopy, a technique where SERS enhancement is measured over a variety of laser excitation wavelengths. The SERS spectra of benzenethiol adsorbed on NSL-derived Ag° nanoparticle arrays were correlated with corresponding LSPR spectra of Ag° nanoparticle arrays [115]. The experiments demonstrated that the largest SERS enhancement occurs when the LSPR maximum is located between the excitation and the vibration wavelengths. The largest measured EF was $\sim 10^8$ for triangular nanoparticle arrays. By using a similar

NSL fabricated SERS substrate, which consisted of Ag° triangular nanopyramids, they have provided evidence of single molecule SERS detection of R6G for individual nanoparticles without nanogaps. The authors concluded that this NSL-derived nanopyramids are advantageous for SERS detection because their tunable LSPR makes them amenable for resonance Raman conditions of various analytes of interest, such as R6G-d₀ or R6G-d₄ [117]. However, NSL remains limited in terms of generated structures and topographies.

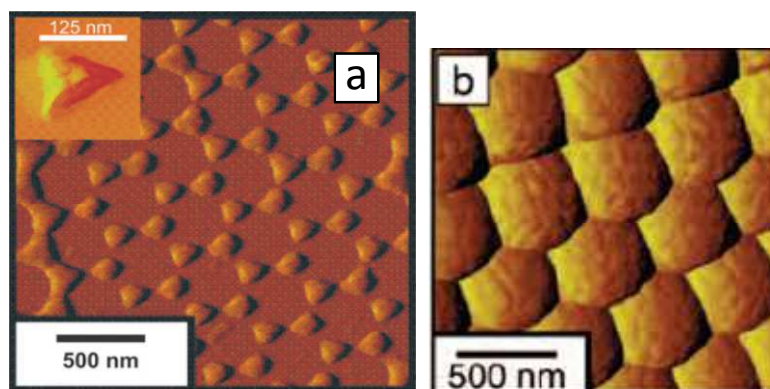


Figure 1-9: NSL generated structures from ref.[118].(a) Tapping-mode AFM image of the array;(b) Contact-mode AFM image of a silver film over nanosphere (Ag° FON) surface.

In all works described above, the engineered surface substrates allowed fundamental studies of the SERS phenomenon and yielded quite large and reproducible response. But such substrates involved costly and/or complex procedures, and were also quite limited in spacial resolution. Progresses in SERS have increasingly drawn attention of scientists from multiple disciplines. Numerous independent groups are now developing their own innovating substrates. Nanoparticle-defined surfaces are one of the important categories developed, among all the new SERS substrates, which are addressed in the following section.

6.3 Nanoparticle-defined surfaces

6.3.1 Nanoparticles immobilized on solid substrates

Nanoparticles which can be produced through wet chemistry methods have long been used in SERS experiments but generally in liquid suspensions. However, by immobilizing such NPs on a solid surface, the hot spots generated by interparticle junctions can be easily located and more readily controlled than if they are present in random colloidal aggregates [75]. One of the very first examples is reported by Natan and co-workers. They positioned both gold and silver nanoparticles monolayers onto a polymer-coated substrate yielding a highly active SERS surface. The procedure for nanoparticle immobilization

employed in their work is straightforward. The surface of glass substrates was firstly functionalized with functional groups through a surface polymerization. Then, metal NPs (Ag° , Au°) were linked to the substrate through multiple bonds between the colloidal metal and functional groups on the polymer, such as cyanide (CN), amine (NH_2), or thiol (SH) [119]. These Au° and Ag° nanoparticles-defined substrates present the ability to vary the particle size, shape, and interparticle spacing, which allowed the authors to improve the SERS response by optimizing these factors. This flexibility led to a large Raman enhancement as well as a better reproducibility than nanoparticles in suspension.

Since the immobilized colloids have proven to be useful for SERS detection, the concept behind this work has been expanded by many other authors [120-123]. Most of the works are based on a simple method involving the preparation of nanoparticles in liquid solution and their subsequent deposition onto a solid substrate, while more complex methods for synthesizing structured arrays of nanoparticles are also reported. These latter approaches involve assembling nanoparticles into structured porous films templated by colloidal crystals (CC) [124-130]. Such a convective assembly at high fractions was designed to generate large enhancement for SERS detection. Velev and co-workers have, for instance, demonstrated the feasibility of this approach and found that the highest Raman intensity is correlated to nanoporous substrates with three-dimensionally ordered micropores (Figure 1-10) [127, 128]. The authors assumed that derived fractal structures with high surface area and superior surface roughness provided additional increase of the Raman signal intensity obtained in the case of cyanide molecules [127]. The above-mentioned work demonstrates that the fractal structures are probably beneficial in the SERS enhancement. However, it is worthwhile pointing out that fractal structure is not a prerequisite, and extremely large enhancement can be generated without fractal structure if properly designed junctions (hot spots) are employed.

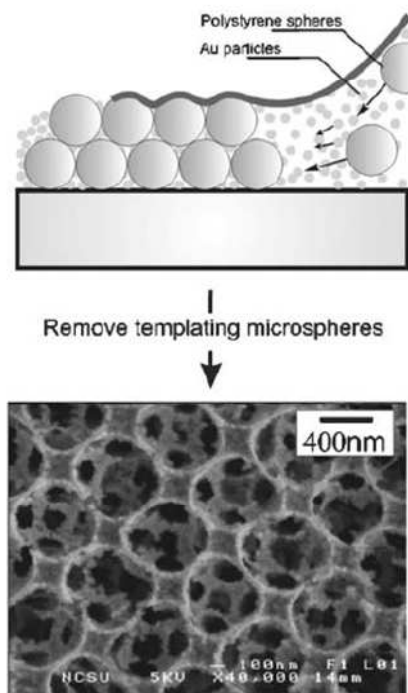


Figure 1-10: Schematic representation of the one-step template directed fabrication of structured porous SERS substrates, from ref. [127].

In addition, polymers [131-138] and biomolecules [75, 139-144] have been employed as binding agents for nanoparticles immobilization. For example, polyvinylpyrrolidone (PVP) was used to immobilize Ag° nanoparticles onto gold substrate for the detection of dipicolinic acid (DPA), a biomarker for bacterial spores. It was claimed that a strong SERS effect arises from such assemblies, which was supported by an enhancement factor of 10^6 [134]. While biomolecules, i.e. DNA molecules, were also widely used to attach nanoparticles, Mirkin and co-workers have demonstrated the feasibility of using Au° nanoparticles (NPs) - DNA conjugates as a functional SERS system to tailor the hot spots. They showed that Au° NPs functionalized with single-stranded DNA can be assembled into useful aggregates by using specific DNA interactions [139]. This method was then complemented by immobilizing this assemblies onto an underlying chip in a microarray format where the single-stranded DNA serves as binding agent [140]. An alternative approach was also reported by self-assembling probe-tethered metal nanoparticles to a “smooth” metal film using complementary target species. Figure 1-11 illustrates this structural arrangement. An Ag° particle is coupling with a planar silver surface via DNA hybridization. When the hybridization takes place, the close proximity between the particles and the metallic surface yields great EM enhancement, which leads to the formation of high intensity hot spots. The existence of such hot spots was confirmed by highly enhanced SERS signals of dye molecules adsorbed between particles and metallic surface [22]. Similar silver-plated DNA and gold nanoparticles assemblies were

reported by Moskovits and co-workers. They successfully detected by the SERS technique a protein (tagged by a SERS dye) bonded with DNA and also observed a large increase in the signal when decreasing the distance between analyte and metallic surface [144].

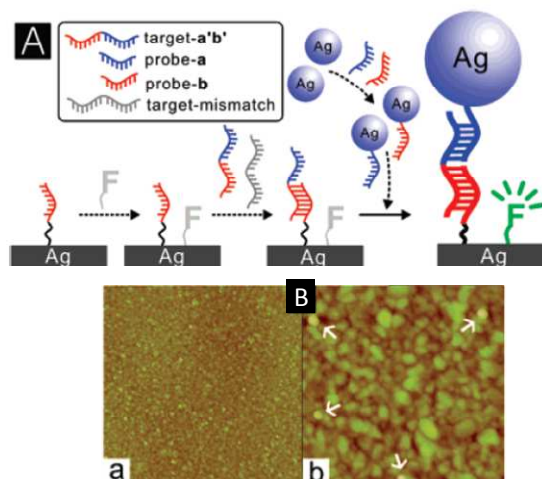


Figure 1-11: (A) Schematic illustration for the formation of SERS-active structure: a target strand ($a'b'$) is captured by probes on Ag° NPs and silver film, resulting in the creation of a SERS-active structure. Target DNA detection is confirmed by collecting the SERS signal of surface-bound Raman label, F . (B) AFM images of such SERS-active structure: (a) $5\ \mu\text{m} \times 5\ \mu\text{m}$ and (b) $1\ \mu\text{m} \times 1\ \mu\text{m}$. Arrows point to Ag° NPs on the surface [22].

Even though the above approaches yield large Raman enhancements, they still involve rather costly and complex procedures, which reduce their wide applications, and are size limited, which can be very restrictive when considering the detection of multiple analytes. Thus, there is still a real demand to develop new strategies for the easy and low cost fabrication of uniform and reproducible SERS-active substrates.

6.3.2 Chemically and photochemically grown Ag° NPs on solid supports

Ideally, SERS substrates should be cheap, robust, stable, active, reproducible, easily prepared and stored [92, 145]. They are also expected to have large-area uniformity. Metal NPs directly chemically or photochemically grown on solid supports are strong candidates for fulfilling the above requirements. These metal surfaces generally produced smaller enhancement factors, of approximately 10^4 - 10^5 , than previously described SERS structures. However, the important asset of these SERS substrates relies on the simplicity of their elaboration, which demands minimal background interferences. Besides, as they offer an optimum balance between reproducibility and Raman signal enhancement, these substrates appear promising for further chemical/biological sensing applications. However, compared to

previously described SERS substrates, such approach has been less investigated. Some studies provided procedures to chemically grow metal nanoparticles directly on solid supports [146-149]. For example, Au⁰ NPs and Ag⁰ NPs could be generated and embedded in a biopolymer (chitosan) through a simple wet chemical method. The resultant NPs-polymer film demonstrated control over the size and distribution of the produced nanoparticles, which appeared promising for several applications including the development of biosensors [146, 150].

The direct growth of Ag⁰ NPs by photocatalytic reduction on a TiO₂ support, leading to potentially SERS-active surfaces, has also been reported [92, 145, 151-153]. Unlike many other complex procedures, this simplified method does not require any template or binding agent. For instance, Mills *et al.* reported the photocatalytically assisted formation of so-called “fish scales” Ag⁰ coatings on TiO₂ surfaces. They studied the SERS activity of their samples but mentioned some irreproducibility of the Raman bands intensity of R6G molecules, which was attributed to the heterogeneous nature of the silver surface [151]. Besides, the Raman enhancement factor was not mentioned in this article. Other papers show the feasibility of this elaboration procedure but do not present any study on the mechanisms allowing a controlled growth of the Ag⁰ NPs, and SERS performances have not been investigated [154, 155]. Thus, there is a real need to perform thorough investigations on the mechanisms leading to the controlled growth of Ag⁰ NPs through a photocatalytic reduction process.

The chemical or photochemical procedure can also be used for the further growth/modification of metal nanoparticles previously deposited as “seeds” [156-158]. For example, Liz-Marzán and coworkers reported highly efficient and rather uniform Ag⁰ NPs arrays chemically grown from well-ordered and uniformly spaced Au⁰ seeds. However, an increase in concentration of “growth” solution resulted in the formation of large Ag⁰ NPs with variable shapes and sizes [156]. In another example, Au⁰ NPs labeled by Raman reporters (R6G) were assembled on glass and used as seeds to *in situ* grow silver-coated nanostructures. It was found that an optimized morphology yielded an important and reproducible SERS effect.

7. Application of solid SERS biosensors for oligonucleotides detection

In the field of biosensors, as previously explained, label-free strategies to detect biomolecules, notably DNA molecules, are under intense development. Theoretically, the SERS method provides a powerful, rapid and sensitive way to respond such a challenge, in particular on solid substrates. But surprisingly, most of the studies devoted to the DNA detection on a solid SERS substrate mention the use of a Raman active label linked to DNA because the signal is more easily detected than the weak Raman signal of a

label-free DNA molecule. In this context, the development of functional and simple SERS platforms for label-free DNA detection remains a challenge of prime interest. But, before to address this field, it is necessary to first consider the numerous studies devoted to the labeled-DNA SERS detection.

7.1 SERS biosensor for labeled- DNA detection

The Vo-Dinh's group is one of the pioneers in the development of the SERS detection for labeled-DNA molecules [34, 159-168]. In 1994, they reported for the first time a new type of DNA probe based on the SERS label detection. This method consisted of single strand DNA (probe), immobilized on a nitrocellulose filter, and then hybridized to its complementary DNA labeled with cresyl fast violet, a Raman-active dye. After hybridization, the double-stranded DNA was removed and transferred onto a SERS-active substrate for detection [165]. Using a similar concept, this group also demonstrated the feasibility of SERS detection of HIV gene [160] and cancer markers [159, 164, 169].

In 1996, Mirkin *et al.* [139] and Alivisatos *et al.* [170] demonstrated the feasibility of specific assemblies by attaching thiol modified single-stranded DNA sequences to single nanocrystals of Au⁰ NPs, forming thus an useful aggregation for DNA detection. Some years later, Cao *et al.* [140] achieved the multiplexed SERS detection of oligonucleotide targets by using gold nanoparticle probes labeled with oligonucleotides and a Raman-active dyes (i.e. Cy3). Six dissimilar DNA targets associated to six Raman-labeled nanoparticle probes were distinguished with a detection limit of 20 fM (Figure 1-12). Ever since, many studies have been performed with the similar DNA detection scheme [22, 143, 166, 171-174]. Thompson *et al.* reported the synthesis of oligonucleotide-silver nanoparticle conjugates and demonstrated their use in a sandwich assay format [175]. McKenzie *et al.* reported mixed metal nanoparticle assemblies taking advantage of the improved surface enhancement properties of Ag⁰ NPs and surface chemical modification benefits of Au⁰ NPs [176]. Graham and co-workers demonstrated the selective turning on of the SERS effect of DNA-functionalized Ag⁰ NPs through a target-dependent DNA hybridization assembly [177]. An alternative approach was also reported by Lim and coworkers who proposed the formation of DNA-modified Au⁰ NPs with a Raman-active dye (Bodipy Texas Red) positioned in the intern nanogap. The detection limit of this nanostructure was 10 fM [178].

A slightly different approach, based on a specific “sandwich type” of capture (probe) / target / reporter hybridization of DNA, has been widely used in other detection methods [179-181], including in labeled SERS detection [182-186].

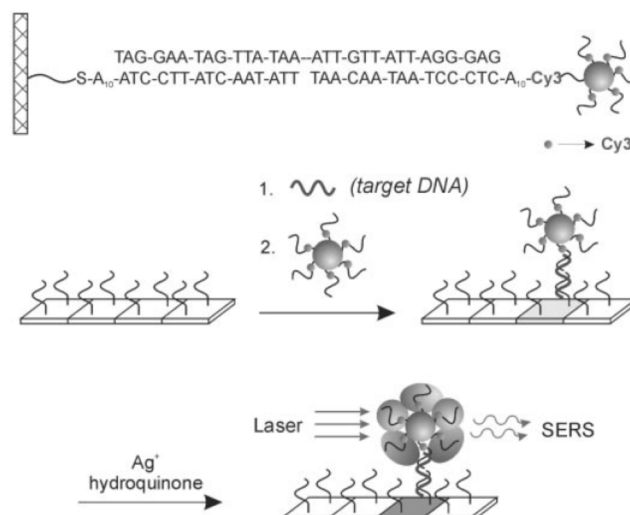


Figure 1-12: SERS probe consisting of a 13-nm-diameter Au° nanoparticle functionalized with oligonucleotide labelled with a Raman-active dye (Cy3) [140].

In this method, the capture DNA, hybridized to a target DNA, has a chain-end binding itself to the SERS-active substrate. Because the capture DNA length is shorter than the target DNA, after hybridization, there are still available base pairs left for hybridization with a dye-labeled reporter DNA. Employing this specific hybridization assay, Lee *et al.* reported a SERS-active substrate based on Ag° NPs grown on silicon nanowires and demonstrated the high sensitivity of this substrate by the detection of a dramatically low reporter DNA concentration of 1 fM [183]. Fan *et al.* also reported a very low detection limit of reporter DNA (10 pM) on Au° NPs-decorated graphene substrates grown by chemical vapor deposition. They also demonstrated the feasibility of detecting simultaneously two different DNA targets on the same substrate [182].

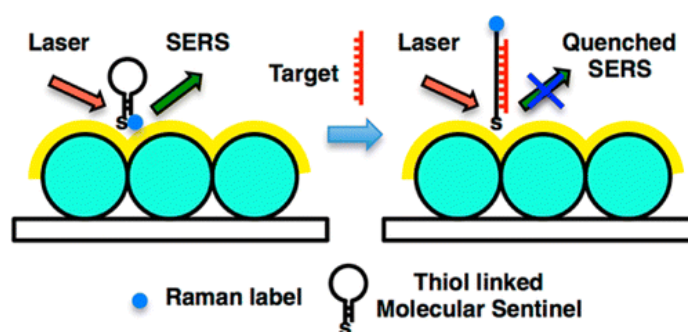


Figure 1-13: Label-free complementary target DNA detection scheme [163].

Recently, Vo-Dinh and coworkers developed a special SERS-based probe system for DNA detection, referred to as “molecular sentinel” (MS) [168]. The MS system, which is initially in solution, consists of a DNA hairpin probe sequence with one end tagged with a Raman-active dye (i.e. Cy3) and a nanoparticle attached at the other end. It is worth pointing out that this type of hairpin DNA sequence has been widely used in fluorescence-based “molecular beacon” system [187], which also plays an important role in the field of DNA detection [19, 20, 188]. However, the sensing principle of MS system is slightly different from that of molecular beacon. In the absence of target DNA, the probe DNA forms a hairpin loop, which maintains the Raman dye in a close proximity of the metal surface yielding intense SERS signals of the dye. Upon hybridization with target DNA, the dye is separated physically from the metal surface leading to decreased SERS signals [163], as illustrated in Figure 1-13. The usefulness and potential application of this MS system on a solid support is demonstrated by using a plasmonic ‘Nanowave’ chip. The authors have demonstrated that this chip is not limited to detect only one type of complementary target DNA [163] but also suitable for multiplex DNA detection [162].

7.2 Label-free detection of DNA

As explained before and in contrast with the large amount of SERS studies dealing with labeled-DNA detection, there are fairly few publications dealing with the SERS label-free detection of oligonucleotides, either in liquid colloidal suspensions or on a solid substrate.

7.2.1 Single-nucleobase detection

Some first studies focusing on DNA bases detection on a silver electrode were reported by Otto *et al.* in 1986 [12, 13]. In their work, spectra were acquired for the four single nucleobases using both normal Raman and SERS. The spectral band locations were compared. Comparisons between spectra revealed a significant shift in spectral lines between the normal Raman and SERS configurations [13]. Recently, direct spectroscopic detection of the four DNA nucleobases (adenine (A), guanine (G), cytosine (C) and thymine (T)) has been achieved on silver grass-like nanostructures [6]. The authors showed that the SERS signal intensities of the four bases increased in the order $T < C < A < G$. They concluded that the differences in SERS intensity are due to different adsorption strengths of the DNA bases. It is noticeable that the SERS literature on DNA is strongly dominated by the SERS detection of the adenine (A) nucleobase alone [9, 12, 13, 78, 189]. In addition to this well documented SERS detection of adenine, the detection of its derivatives such as adenosine [15, 190] and adenosine mono phosphate (AMP) [15, 189, 191, 192] is also reported because adenine and its products are important groups which strongly act in the metabolism in addition to the genome.

7.2.2 Single strand and double strands oligonucleotides detection

Homo-oligonucleotides single strands

Compared to adenine nucleobase, the SERS detection of other nucleobases (cytosine, guanine, or thymine) is rather few documented in the literature. This observation also prevails for homo-oligonucleotides (also called single base composition oligonucleotides in the literature). Mostly because of their flexible string aspect, and depending on the experimental conditions, various conformational changes can occur. This results in some orientation changes of each individual nucleobase to both the surface and laser beam polarization leading to some repercussions on the SERS spectra [193]. Compared to the simple nucleobase spectrum, an increase in the complexity of the resulting spectrum can be expected in term of reproducibility and variability of the band intensities. This is clearly illustrated by the investigations of E. Papadopoulou *et al.* who compared the spectra of both adenine, AMP and polyA on gold colloids (Figure 1-14) [194].

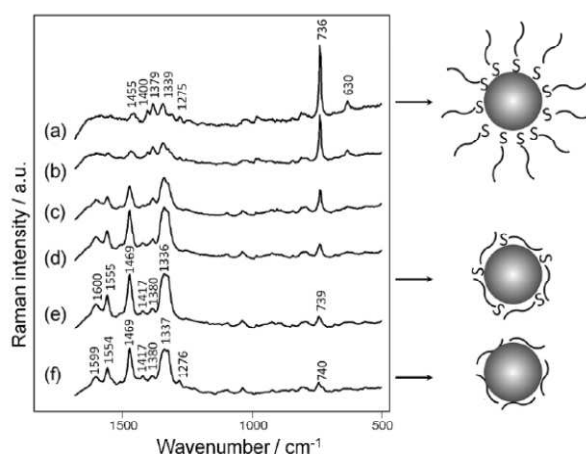


Figure 1-14: SERS spectra of 24-mer thiolated poly A at concentrations (a) - (e) 10^{-4} - 10^{-8} M and (f) 10^{-5} M unthiolated poly A on AuNP aggregated with $MgSO_4$ [194].

The authors conclude to some changes in the overall orientation leading to modifications in the SERS spectra. Elsewhere, Kundu *et al.* reported a solution pH dependence inducing conformational change of polyA adsorbed on silica core-gold nanoshell surfaces [191]. To the best of our knowledge, in addition to E. Papadoupoulou *et al.* [4] who studied the SERS spectra of the four homo-oligonucleotides, namely polyA, polyC, polyT, and polyG in colloid solutions, M. Green *et al.* were the rare authors to report on the SERS spectra of these homo-oligonucleotides, alone or in mixed solutions, immobilized on a solid substrate, i.e. a Si substrate supporting Ag° torus structures [43]. The measurements were performed in humid conditions. Generally speaking, the mentions about the reproducibility of the SERS spectra are rarely described. This reproducibility problematic is of concern in a recent paper, which reports on TERS (Tip Enhanced Raman Spectroscopy) experiments performed in dried conditions on polyA physisorbed

on mica [195]. Thus, in spite of the excellent resolution of TERS, it is clear that this technique is not so simple to use in the case of portable biosensor. That is why, before going further to the SERS detection of poly-oligonucleotides and DNA hybridization on solid SERS platform, it is very important to carefully study and index the SERS spectra of the four homo-oligonucleotides in very well-defined conditions.

Multibase oligonucleotides

The detection of multibase composition oligonucleotides (single strand) and their hybridization to complementary target DNA strand (double-strand) is another crucial area of biosensors applications. As previously mentioned, the spectra generated from multibase composition oligonucleotides chains rely greatly on their structures as well as on the experimental conditions. Thus, a comparison between published results shows clearly the complexity of the resulting spectra in term of reproducibility and variability of band intensities.

Some rare advances in achieving low limit of detection using complex three dimensions nanostructures have enabled the detection of unmodified single and/or double-stranded DNA (oligonucleotides). One example is reported by Lee *et al.* [196]. Using a substrate consisting of vertical silicon nanocone arrays coated with Ag^o NPs, the authors demonstrated the superior detection sensitivity for a reliable and label-free detection of DNA. However, the reproducibility of SERS spectra obtained in a relative small area (50 x 40 μm²) is not as successful as they claimed, when considering the need of rather large substrates for multibase detection. In another example, label-free detection of ssDNA probe before and after hybridization has been achieved on a very similar Ag^o NPs on silicon nanowires nanostructure [197]. Except for low concentrations, the Raman signal reproducibility is rather good, i.e. the variation of the Raman signal was less than 10% when the molecules amount spread on the substrate was more than 10⁻¹² mol. However, the probed substrate area was not mentioned in the paper. Another example of label-free DNA detection on an Ag^o toroid substrate was reported by Green and co-workers [43, 198, 199] (Figure 1-15). Spectra were obtained on probe oligonucleotides, as well as single-stranded probe DNA and double-stranded DNA molecules. The authors studied the influence of probe (ssDNA) concentration on the DNA hybridization in order to determine the optimal packing density of ssDNA for optimal hybridization [43]. However, the reproducibility of spectra was not specifically mentioned in the article.

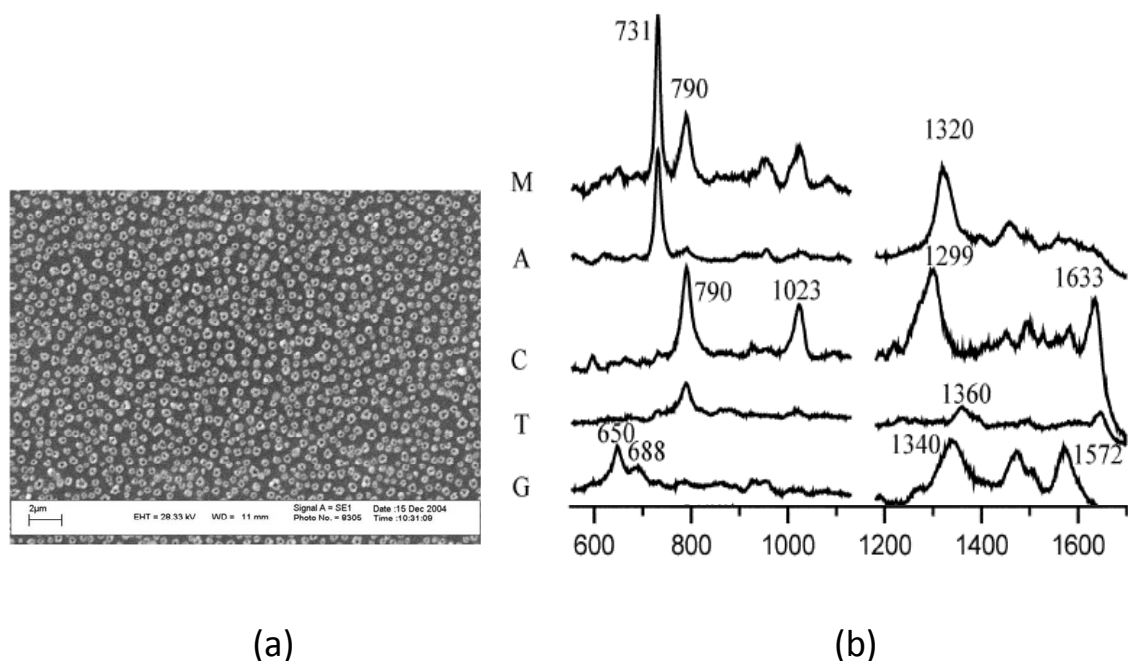


Figure 1-15: (a) SEM image of a silver torus structure on a SiO_2/Si substrate ; (b) SERS spectra of $4 \times 10^{-6} \text{ M}$ poly A (A), poly C (C), poly T(T), poly(G), and their equi-molar mixed solutions A + G+ T+ C (M), respectively, obtained from this SERS substrate [43].

Similarly, aligned Ag° nanorod arrays have been reported as a suitable substrate for label-free detection of ssRNA, dsRNA: DNA duplex [200], and micro-RNA hybridization [201]. In particular, a straightforward least-squares (LS) analysis combined with SERS technique has been employed to quantitatively determine the relative ratio of the four nucleotide components before and after hybridization for micro-RNA sequences [201]. This is the first demonstration of a combination of SERS and LS techniques used for capturing subtle changes in the spectra resulting from label-free hybridization. However, the accuracy of this approach needs to be further improved.

Halas and co-workers have performed numerous studies using nanoshell-based SERS substrates for the detection of single and double-stranded thiolated DNA oligomers. They observed that all the SERS spectra of DNA are dominated by a 736 cm^{-1} peak attributed to an adenine breathing mode, which makes it extremely difficult to distinguish the specific SERS signals of other bases [202]. To overcome this problem, they employed a specific adenine-free probe DNA sequence to enable the detection of target DNA upon its hybridization with 2-aminopurine-substituted probe DNA sequence [203]. Additionally,

the authors also investigated the orientation of dsDNA bond toward the Au^o nanoshell surface. This new study suggested that dsDNA adopted a tilted orientation at high packing densities, which was reduced for decreasing packing densities (Figure 1-16) [204]. However, the probed substrate area in these studies was quite small (i.e. about 3 μm x 30 μm).

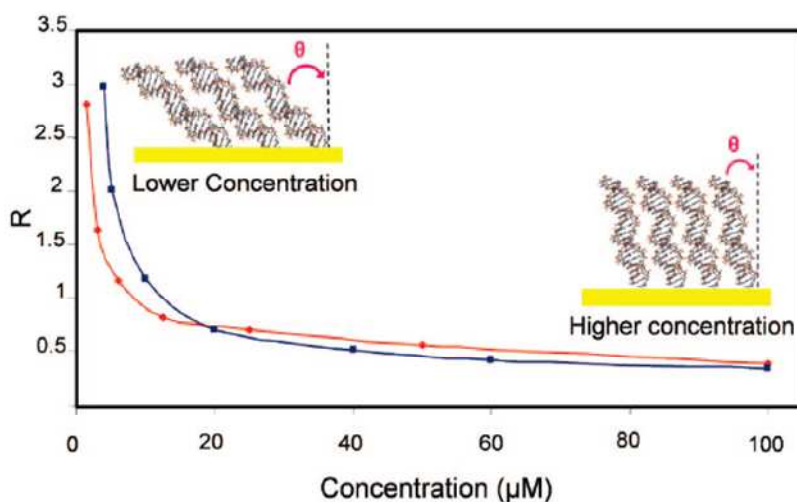


Figure 1-16: Guanine to adenine peak intensity ratio as a function of DNA concentration. Blue and red lines correspond to two different DNA molecules ($SA_{20}NI$ and $SA_{10}NI$ respectively, conjugated with their complementary sequence). Insets show schematics of variations of DNA orientation with packing density [204].

A last work of interest has to be cited. Qian *et al.*, have demonstrated a simple and label-free method to detect DNA based on a gold nanoplate films substrate. Various concentrations of this double-stranded DNA in solution ranging from 1.0×10^{-2} to 1.0×10^{-6} M were successfully detected [17]. Compared to methods previously presented, such method is simpler but exhibits rather smaller Raman enhancements and, one important feature, the sample size was not mentioned in the paper.

8. Conclusion

Since its discovery, SERS has been increasingly employed in the detection of biomolecules. In this latter context, label-free strategies to detect biomolecules notably DNA molecules are under intense development. SERS is a very powerful method to ensure label-free detection needs. Besides, SERS spectra of molecules adsorbed on a solid metallic nanostructure are much more stable and repeatable than those in metallic colloid suspension. In particular, fundamental studies have shown that dramatic enhancement of the EM field originates from hot spots located at the proper junction or gap between

vicinal metal NPs, leading to a strong intensity of SERS spectra. Thus the high sensitivity of SERS substrates relies on the homogeneous creation of a large number of hot spots on a solid substrate, i.e. the homogeneous dispersion of well-designed metal NPs aggregates at the substrate surface or the suitable structuration of a metallic substrate. Currently, available methods for the fabrication of such solid substrates include electron-beam lithography, nanosphere lithography or nanoparticles immobilized on solid substrates. These methods are generally either too expensive and/or involve too complex procedures for practical application. Thus, the easy and cheap fabrication of SERS solid substrates in large area, while maintaining high EF and good reproducibility, still remains a challenge.

Metal NPs chemically or photochemically grown on solid supports are strong candidates for fulfilling the above requirements of good SERS substrates. Some studies provided procedures to chemically or photochemically grow metal nanoparticles on solid supports, but they do not present enough data to envisage the controlled growth of the metal NPs compatible with good SERS substrate criteria. In particular, there is a real interest to perform thorough investigations on the mechanisms leading to the controlled growth of Ag° NPs through a photocatalytic reduction process. The purpose of the thesis is to address this issue, i/ by investigating a new bottom up approach, aiming at improving the uniformity of a $\text{Ag}^{\circ}/\text{TiO}_2$ heterostructure formed by photocatalytic reduction in order to optimize the derived SERS substrate performances; and ii/ by extrapolating such new type of substrate for the label-free SERS detection of DNA molecules before and after *in-situ* hybridization.

- [1] E. Papadopoulou and S. E. J. Bell, "Label-Free Detection of Nanomolar Unmodified Single- and Double-Stranded DNA by Using Surface-Enhanced Raman Spectroscopy on Ag and Au Colloids," *Chemistry – A European Journal*, vol. 18, pp. 5394-5400, 2012.
- [2] S. Basu, S. Jana, S. Pande, and T. Pal, "Interaction of DNA bases with silver nanoparticles: Assembly quantified through SPRS and SERS," *Journal of Colloid and Interface Science*, vol. 321, pp. 288-293, 2008.
- [3] P. Sandström, M. Boncheva, and B. Åkerman, "Nonspecific and Thiol-Specific Binding of DNA to Gold Nanoparticles," *Langmuir*, vol. 19, pp. 7537-7543, 2003.
- [4] E. Papadopoulou and S. E. J. Bell, "Label-Free Detection of Single-Base Mismatches in DNA by Surface-Enhanced Raman Spectroscopy," *Angewandte Chemie International Edition*, vol. 50, pp. 9058-9061, 2011.
- [5] A. Barhoumi and N. J. Halas, "Detecting Chemically Modified DNA Bases Using Surface-Enhanced Raman Spectroscopy," *The Journal of Physical Chemistry Letters*, vol. 2, pp. 3118-3123, 2011.
- [6] R. Liu, D. Zhang, C. Cai, Y. Xiong, S. Li, Y. Su, *et al.*, "NIR-SERS studies of DNA and DNA bases attached on polyvinyl alcohol (PVA) protected silver grass-like nanostructures," *Vibrational Spectroscopy*, vol. 67, pp. 71-79, 2013.
- [7] J. M. Benevides, S. A. Overman, and G. J. Thomas, "Raman, polarized Raman and ultraviolet resonance Raman spectroscopy of nucleic acids and their complexes," *Journal of Raman Spectroscopy*, vol. 36, pp. 279-299, 2005.
- [8] F. Feng, G. Zhi, H. S. Jia, L. Cheng, Y. T. Tian, and X. J. Li, "SERS detection of low-concentration adenine by a patterned silver structure immersion plated on a silicon nanoporous pillar array," *Nanotechnology*, vol. 20, p. 295501, 2009.
- [9] B. Giese and D. McNaughton, "Surface-Enhanced Raman Spectroscopic and Density Functional Theory Study of Adenine Adsorption to Silver Surfaces," *The Journal of Physical Chemistry B*, vol. 106, pp. 101-112, 2001.
- [10] E. Koglin, J. M. Séquaris, J. C. Fritz, and P. Valenta, "Surface enhanced raman scattering (SERS) of nucleic acid bases adsorbed on silver colloids," *Journal of Molecular Structure*, vol. 114, pp. 219-223, 1984.
- [11] J. Li and Y. Fang, "An investigation of the surface enhanced Raman scattering (SERS) from a new substrate of silver-modified silver electrode by magnetron sputtering," *Spectrochimica Acta Part A: Molecular and Biomolecular Spectroscopy*, vol. 66, pp. 994-1000, 2007.
- [12] C. Otto, F. F. M. De Mul, A. Huizinga, and J. Greve, "Surface enhanced Raman scattering of derivatives of adenine: the importance of the external amino group in adenine for surface binding," *The Journal of Physical Chemistry*, vol. 92, pp. 1239-1244, 1988.
- [13] C. Otto, T. J. J. van den Tweel, F. F. M. de Mul, and J. Greve, "Surface-enhanced Raman spectroscopy of DNA bases," *Journal of Raman Spectroscopy*, vol. 17, pp. 289-298, 1986.
- [14] J. S. Suh and M. Moskovits, "Surface-enhanced Raman spectroscopy of amino acids and nucleotide bases adsorbed on silver," *Journal of the American Chemical Society*, vol. 108, pp. 4711-4718, 1986.
- [15] T. Watanabe, O. Kawanami, H. Katoh, K. Honda, Y. Nishimura, and M. Tsuboi, "SERS study of molecular adsorption: Some nucleic acid bases on Ag electrodes," *Surface Science*, vol. 158, pp. 341-351, 1985.
- [16] N. E. Marotta, K. R. Beavers, and L. A. Bottomley, "Limitations of Surface Enhanced Raman Scattering in Sensing DNA Hybridization Demonstrated by Label-Free DNA Oligos as Molecular Rulers of Distance-Dependent Enhancement," *Analytical Chemistry*, vol. 85, pp. 1440-1446, 2012.
- [17] L. Bi, Y. Rao, Q. Tao, J. Dong, T. Su, F. Liu, *et al.*, "Fabrication of large-scale gold nanoplate films as highly active SERS substrates for label-free DNA detection," *Biosensors and Bioelectronics*, vol. 43, pp. 193-199, 2013.

- [18] R. P. Johnson, J. A. Richardson, T. Brown, and P. N. Bartlett, "A label-free, electrochemical SERS-based assay for detection of DNA hybridization and discrimination of mutations," *Journal of the American Chemical Society*, vol. 134, pp. 14099-14107, 2012.
- [19] S. Su, X. Wei, Y. Zhong, Y. Guo, Y. Su, Q. Huang, *et al.*, "Silicon Nanowire-Based Molecular Beacons for High-Sensitivity and Sequence-Specific DNA Multiplexed Analysis," *ACS Nano*, vol. 6, pp. 2582-2590, 2012.
- [20] X. Wei, S. Su, Y. Guo, X. Jiang, Y. Zhong, Y. Su, *et al.*, "A Molecular Beacon-Based Signal-Off Surface-Enhanced Raman Scattering Strategy for Highly Sensitive, Reproducible, and Multiplexed DNA Detection," *Small*, vol. 9, pp. 2493-2499, 2013.
- [21] A. K. Singh, S. A. Khan, Z. Fan, T. Demeritte, D. Senapati, R. Kanchanapally, *et al.*, "Development of a Long-Range Surface-Enhanced Raman Spectroscopy Ruler," *Journal of the American Chemical Society*, vol. 134, pp. 8662-8669, 2012.
- [22] G. Braun, S. J. Lee, M. Dante, T.-Q. Nguyen, M. Moskovits, and N. Reich, "Surface-Enhanced Raman Spectroscopy for DNA Detection by Nanoparticle Assembly onto Smooth Metal Films," *Journal of the American Chemical Society*, vol. 129, pp. 6378-6379, 2007.
- [23] H.-I. Peng, C. M. Strohsahl, K. E. Leach, T. D. Krauss, and B. L. Miller, "Label-Free DNA Detection on Nanostructured Ag Surfaces," *ACS Nano*, vol. 3, pp. 2265-2273, 2009.
- [24] D. A. Gish, F. Nsiah, M. T. McDermott, and M. J. Brett, "Localized surface plasmon resonance biosensor using silver nanostructures fabricated by glancing angle deposition," *Analytical chemistry*, vol. 79, pp. 4228-4232, 2007.
- [25] X. Qian, X. Zhou, and S. Nie, "Surface-enhanced Raman nanoparticle beacons based on bioconjugated gold nanocrystals and long range plasmonic coupling," *Journal of the American Chemical Society*, vol. 130, pp. 14934-14935, 2008.
- [26] N. T. K. Thanh and Z. Rosenzweig, "Development of an aggregation-based immunoassay for anti-protein A using gold nanoparticles," *Analytical chemistry*, vol. 74, pp. 1624-1628, 2002.
- [27] F. Wei, D. Zhang, N. J. Halas, and J. D. Hartgerink, "Aromatic amino acids providing characteristic motifs in the Raman and SERS spectroscopy of peptides," *The Journal of Physical Chemistry B*, vol. 112, pp. 9158-9164, 2008.
- [28] K. Nithipatikom, M. J. McCoy, S. R. Hawi, K. Nakamoto, F. Adar, and W. B. Campbell, "Characterization and application of Raman labels for confocal Raman microspectroscopic detection of cellular proteins in single cells," *Analytical biochemistry*, vol. 322, pp. 198-207, 2003.
- [29] T. A. Alexander, P. M. Pellegrino, and J. B. Gillespie, "Near-infrared surface-enhanced-Raman-scattering-mediated detection of single optically trapped bacterial spores," *Applied spectroscopy*, vol. 57, pp. 1340-1345, 2003.
- [30] N. E. Marotta and L. A. Bottomley, "Surface-enhanced Raman scattering of bacterial cell culture growth media," *Applied spectroscopy*, vol. 64, pp. 601-606, 2010.
- [31] M. Kahraman, M. M. Yazici, F. Sahin, and M. Çulha, "Convective assembly of bacteria for surface-enhanced Raman scattering," *Langmuir*, vol. 24, pp. 894-901, 2008.
- [32] D. Graham, K. Faulds, D. Thompson, F. McKenzie, R. Stokes, C. Dalton, *et al.*, "Functionalized nanoparticles for bioanalysis by SERRS," *Biochemical Society Transactions*, vol. 37, p. 697, 2009.
- [33] A. Sujith, T. Itoh, H. Abe, K.-i. Yoshida, M. S. Kiran, V. Biju, *et al.*, "Imaging the cell wall of living single yeast cells using surface-enhanced Raman spectroscopy," *Analytical and bioanalytical chemistry*, vol. 394, pp. 1803-1809, 2009.
- [34] J. P. Scaffidi, M. K. Gregas, V. Seewaldt, and T. Vo-Dinh, "SERS-based plasmonic nanobiosensing in single living cells," *Analytical and bioanalytical chemistry*, vol. 393, pp. 1135-1141, 2009.
- [35] S. Pan, J. Xu, Y. Shu, F. Wang, W. Xia, Q. Ding, *et al.*, "Double recognition of oligonucleotide and protein in the detection of DNA methylation with surface plasmon resonance biosensors," *Biosensors and Bioelectronics*, vol. 26, pp. 850-853, 2010.

- [36] H. Szmecinski, J. R. Lakowicz, J. M. Catchmark, K. Eid, J. P. Anderson, and L. Middendorf, "Correlation Between Scattering Properties of Silver Particle Arrays and Fluorescence Enhancement," *Applied Spectroscopy*, vol. 62, pp. 733-738, 2008.
- [37] M. Manesse, R. Sanjines, V. Stambouli, C. Jorel, B. Pelissier, M. Pisarek, *et al.*, "Preparation and Characterization of Silver Substrates Coated with Antimony-Doped SnO₂ Thin Films for Surface Plasmon Resonance Studies," *Langmuir*, vol. 25, pp. 8036-8041, 2009/07/21 2009.
- [38] F. Uslu, S. Ingebrandt, D. Mayer, S. Böcker-Meffert, M. Odenthal, and A. Offenhäuser, "Label-free fully electronic nucleic acid detection system based on a field-effect transistor device," *Biosensors and Bioelectronics*, vol. 19, pp. 1723-1731, 2004.
- [39] J. S. Daniels and N. Pourmand, "Label-Free Impedance Biosensors: Opportunities and Challenges," *Electroanalysis*, vol. 19, pp. 1239-1257, 2007.
- [40] M. Lee, K. Y. Baik, M. Noah, Y.-K. Kwon, J.-O. Lee, and S. Hong, "Nanowire and nanotube transistors for lab-on-a-chip applications," *Lab on a Chip*, vol. 9, pp. 2267-2280, 2009.
- [41] M. Alvarez and L. M. Lechuga, "Microcantilever-based platforms as biosensing tools," *Analyst*, vol. 135, pp. 827-836, 2010.
- [42] D. Ramos, J. Tamayo, J. Mertens, M. Calleja, L. G. Villanueva, and A. Zaballos, "Detection of bacteria based on the thermomechanical noise of a nanomechanical resonator: origin of the response and detection limits," *Nanotechnology*, vol. 19, p. 035503, 2008.
- [43] M. Green, F.-M. Liu, L. Cohen, P. Kollensperger, and T. Cass, "SERS platforms for high density DNA arrays," *Faraday Discussions*, vol. 132, pp. 269-280, 2006.
- [44] J. D. Watson, *Molecular biology of the gene*: Pearson Education India, 2004.
- [45] L. A. Allison, *Fundamental molecular biology*: John Wiley & Sons, 2009.
- [46] X. Fan, I. M. White, S. I. Shopova, H. Zhu, J. D. Suter, and Y. Sun, "Sensitive optical biosensors for unlabeled targets: A review," *Analytica Chimica Acta*, vol. 620, pp. 8-26, 2008.
- [47] C. V. Raman and K. S. Krishnan, "A new type of secondary radiation," *Nature*, vol. 121, pp. 501-502, 1928.
- [48] E. Smith and G. Dent, *Modern Raman spectroscopy: a practical approach*: John Wiley & Sons, 2005.
- [49] E. Le Ru and P. Etchegoin, *Principles of Surface-Enhanced Raman Spectroscopy: and related plasmonic effects*: Elsevier, 2008.
- [50] A. Biswas, T. Wang, and A. S. Biris, "Single metal nanoparticle spectroscopy: optical characterization of individual nanosystems for biomedical applications," *Nanoscale*, vol. 2, pp. 1560-1572, 2010.
- [51] S. R. Crouch and J. D. Ingle, *Spectrochemical analysis*: Prentice Hall, 1988.
- [52] J. R. Ferraro, *Introductory raman spectroscopy*: Academic press, 2003.
- [53] I. R. Lewis and H. Edwards, *Handbook of Raman spectroscopy: from the research laboratory to the process line*: CRC Press, 2001.
- [54] M. Fleischmann, P. J. Hendra, and A. J. McQuillan, "Raman spectra of pyridine adsorbed at a silver electrode," *Chemical Physics Letters*, vol. 26, pp. 163-166, 1974.
- [55] D. L. Jeanmaire and R. P. Van Duyne, "Surface Raman spectroelectrochemistry: Part I. Heterocyclic, aromatic, and aliphatic amines adsorbed on the anodized silver electrode," *Journal of Electroanalytical Chemistry and Interfacial Electrochemistry*, vol. 84, pp. 1-20, 1977.
- [56] M. G. Albrecht and J. A. Creighton, "Anomalously intense Raman spectra of pyridine at a silver electrode," *Journal of the American Chemical Society*, vol. 99, pp. 5215-5217, 1977.
- [57] R. P. Van Duyne, "Laser excitation of Raman scattering from adsorbed molecules on electrode surfaces," *Chemical and Biochemical Applications of Lasers*, vol. 4, p. 101, 1979.
- [58] C. L. Haynes, C. R. Yonzon, X. Zhang, and R. P. Van Duyne, "Surface - enhanced Raman sensors: early history and the development of sensors for quantitative biowarfare agent and glucose detection," *Journal of Raman Spectroscopy*, vol. 36, pp. 471-484, 2005.

- [59] B. Sharma, M. Fernanda Cardinal, S. L. Kleinman, N. G. Greeneltch, R. R. Frontiera, M. G. Blaber, *et al.*, "High-performance SERS substrates: Advances and challenges," *MRS bulletin*, vol. 38, pp. 615-624, 2013.
- [60] C. L. Haynes, A. D. McFarland, and R. P. V. Duyne, "Surface-Enhanced Raman Spectroscopy," *Analytical Chemistry*, vol. 77, pp. 338 A-346 A, 2005.
- [61] K. Kneipp, H. Kneipp, I. Itzkan, R. R. Dasari, and M. S. Feld, "Surface-enhanced Raman scattering and biophysics," *Journal of Physics: Condensed Matter*, vol. 14, p. R597, 2002.
- [62] A. Campion and P. Kambhampati, "Surface-enhanced Raman scattering," *Chem. Soc. Rev.*, vol. 27, pp. 241-250, 1998.
- [63] A. Otto, I. Mrozek, H. Grabhorn, and W. Akemann, "Surface-enhanced Raman scattering," *Journal of Physics: Condensed Matter*, vol. 4, p. 1143, 1992.
- [64] J. P. Camden, J. A. Dieringer, Y. Wang, D. J. Masiello, L. D. Marks, G. C. Schatz, *et al.*, "Probing the Structure of Single-Molecule Surface-Enhanced Raman Scattering Hot Spots," *Journal of the American Chemical Society*, vol. 130, pp. 12616-12617, 2008.
- [65] K. C. Bantz, A. F. Meyer, N. J. Wittenberg, H. Im, Ö. Kurtuluş, S. H. Lee, *et al.*, "Recent progress in SERS biosensing," *Physical Chemistry Chemical Physics*, vol. 13, pp. 11551-11567, 2011.
- [66] G. Schatz and R. Van Duyne, "In Handbook of Vibrational Spectroscopy; Chalmers, JM; Griffiths, PR, Eds," ed: Wiley: New York, 2002.
- [67] S. Nie and S. R. Emory, "Probing Single Molecules and Single Nanoparticles by Surface-Enhanced Raman Scattering," *Science*, vol. 275, pp. 1102-1106, February 21, 1997 1997.
- [68] Jiang, K. Bosnick, M. Maillard, and L. Brus, "Single Molecule Raman Spectroscopy at the Junctions of Large Ag Nanocrystals," *The Journal of Physical Chemistry B*, vol. 107, pp. 9964-9972, 2003.
- [69] A. M. Michaels, M. Nirmal, and L. E. Brus, "Surface Enhanced Raman Spectroscopy of Individual Rhodamine 6G Molecules on Large Ag Nanocrystals," *Journal of the American Chemical Society*, vol. 121, pp. 9932-9939, 1999.
- [70] A. M. Michaels, Jiang, and L. Brus, "Ag Nanocrystal Junctions as the Site for Surface-Enhanced Raman Scattering of Single Rhodamine 6G Molecules," *The Journal of Physical Chemistry B*, vol. 104, pp. 11965-11971, 2000.
- [71] K. Kneipp, H. Kneipp, V. B. Kartha, R. Manoharan, G. Deinum, I. Itzkan, *et al.*, "Detection and identification of a single DNA base molecule using surface-enhanced Raman scattering (SERS)," *Physical Review E*, vol. 57, pp. R6281-R6284, 1998.
- [72] K. Kneipp, Y. Wang, H. Kneipp, L. T. Perelman, I. Itzkan, R. R. Dasari, *et al.*, "Single molecule detection using surface-enhanced Raman scattering (SERS)," *Physical review letters*, vol. 78, p. 1667, 1997.
- [73] K. Kneipp, H. Kneipp, I. Itzkan, R. R. Dasari, and M. S. Feld, "Ultrasensitive chemical analysis by Raman spectroscopy," *Chemical reviews*, vol. 99, pp. 2957-2976, 1999.
- [74] K. Kneipp, Y. Wang, H. Kneipp, L. T. Perelman, I. Itzkan, R. R. Dasari, *et al.*, "Single Molecule Detection Using Surface-Enhanced Raman Scattering (SERS)," *Physical Review Letters*, vol. 78, pp. 1667-1670, 1997.
- [75] M. J. Banholzer, J. E. Millstone, L. Qin, and C. A. Mirkin, "Rationally designed nanostructures for surface-enhanced Raman spectroscopy," *Chemical Society Reviews*, vol. 37, pp. 885-897, 2008.
- [76] E. Papadopoulou and S. E. J. Bell, "Structure of Adenine on Metal Nanoparticles: pH Equilibria and Formation of Ag⁺ Complexes Detected by Surface-Enhanced Raman Spectroscopy," *The Journal of Physical Chemistry C*, vol. 114, pp. 22644-22651, 2010.
- [77] X. Gao, J. P. Davies, and M. J. Weaver, "Test of surface selection rules for surface-enhanced Raman scattering: the orientation of adsorbed benzene and monosubstituted benzenes on gold," *The Journal of Physical Chemistry*, vol. 94, pp. 6858-6864, 1990.

- [78] M. Pagliai, S. Caporali, M. Muniz-Miranda, G. Pratesi, and V. Schettino, "SERS, XPS, and DFT Study of Adenine Adsorption on Silver and Gold Surfaces," *The Journal of Physical Chemistry Letters*, vol. 3, pp. 242-245, 2012.
- [79] S. Lecomte and M. H. Baron, "Surface - enhanced raman spectroscopy investigation of fluoroquinolones - DNA - DNA gyrase - Mg²⁺ interactions. II. Interaction of pefloxacin with Mg²⁺ and DNA," *Biospectroscopy*, vol. 3, pp. 31-45, 1997.
- [80] J. Kneipp, H. Kneipp, and K. Kneipp, "SERS a single-molecule and nanoscale tool for bioanalytics," *Chemical Society Reviews*, vol. 37, pp. 1052-1060, 2008.
- [81] C. L. Haynes and R. P. Van Duyne, "Nanosphere lithography: a versatile nanofabrication tool for studies of size-dependent nanoparticle optics," *The Journal of Physical Chemistry B*, vol. 105, pp. 5599-5611, 2001.
- [82] R. Wen and Y. Fang, "An investigation of the surface-enhanced Raman scattering (SERS) effect from a new substrate of silver-modified silver electrode," *Journal of Colloid and Interface Science*, vol. 292, pp. 469-475, 2005.
- [83] J. Zhang, S. Song, L. Wang, D. Pan, and C. Fan, "A gold nanoparticle-based chronocoulometric DNA sensor for amplified detection of DNA," *Nat. Protocols*, vol. 2, pp. 2888-2895, 2007.
- [84] B. Giese and D. McNaughton, "Density functional theoretical (DFT) and surface-enhanced Raman spectroscopic study of guanine and its alkylated derivatives Part 2: Surface-enhanced Raman scattering on silver surfaces," *Physical Chemistry Chemical Physics*, vol. 4, pp. 5171-5182, 2002.
- [85] G. J. Kovacs, R. O. Loutfy, P. S. Vincett, C. Jennings, and R. Aroca, "Distance dependence of SERS enhancement factor from Langmuir-Blodgett monolayers on metal island films: evidence for the electromagnetic mechanism," *Langmuir*, vol. 2, pp. 689-694, 1986.
- [86] V. L. Schlegel and T. M. Cotton, "Silver-island films as substrates for enhanced Raman scattering: effect of deposition rate on intensity," *Analytical Chemistry*, vol. 63, pp. 241-247, 1991.
- [87] C. Jennings, R. Aroca, A. M. Hor, and R. O. Loutfy, "Surface-enhanced Raman scattering from copper and zinc phthalocyanine complexes by silver and indium island films," *Analytical Chemistry*, vol. 56, pp. 2033-2035, 1984.
- [88] H. Seki, "SERS of pyridine on Ag island films prepared on a sapphire substrate," *Journal of Vacuum Science and Technology*, vol. 18, pp. 633-637, 1981.
- [89] D. Weitz, S. Garoff, and T. Gramila, "Excitation spectra of surface-enhanced Raman scattering on silver-island films," *Optics letters*, vol. 7, pp. 168-170, 1982.
- [90] G. Kovacs, R. Loutfy, P. Vincett, C. Jennings, and R. Aroca, "Distance dependence of SERS enhancement factor from Langmuir-Blodgett monolayers on metal island films: evidence for the electromagnetic mechanism," *Langmuir*, vol. 2, pp. 689-694, 1986.
- [91] Y. Suzuki, M. Kobayashi, A. Hatta, and A. Otto, "Anomalous IR Absorption of the System Gold Island Film in Water or Methanol," *Japanese Journal of Applied Physics*, vol. 36, p. 4446, 1997.
- [92] K. L. Norrod, L. M. Sudnik, D. Rousell, and K. L. Rowlen, "Quantitative Comparison of Five SERS Substrates: Sensitivity and Limit of Detection," *Applied Spectroscopy*, vol. 51, pp. 994-1001, 1997.
- [93] N. Félidj, J. Aubard, G. Lévi, J. R. Krenn, A. Hohenau, G. Schider, *et al.*, "Optimized surface-enhanced Raman scattering on gold nanoparticle arrays," *Applied Physics Letters*, vol. 82, pp. 3095-3097, 2003.
- [94] D. P. Fromm, A. Sundaramurthy, A. Kinkhabwala, P. J. Schuck, G. S. Kino, and W. E. Moerner, "Exploring the chemical enhancement for surface-enhanced Raman scattering with Au bowtie nanoantennas," *The Journal of Chemical Physics*, vol. 124, pp. -, 2006.

- [95] N. Félidj, S. L. Truong, J. Aubard, G. Lévi, J. R. Krenn, A. Hohenau, *et al.*, "Gold particle interaction in regular arrays probed by surface enhanced Raman scattering," *The Journal of Chemical Physics*, vol. 120, pp. 7141-7146, 2004.
- [96] Q. Yu, P. Guan, D. Qin, G. Golden, and P. M. Wallace, "Inverted Size-Dependence of Surface-Enhanced Raman Scattering on Gold Nanohole and Nanodisk Arrays," *Nano Letters*, vol. 8, pp. 1923-1928, 2008.
- [97] N. A. Abu Hatab, J. M. Oran, and M. J. Sepaniak, "Surface-enhanced Raman spectroscopy substrates created via electron beam lithography and nanotransfer printing," *Acs Nano*, vol. 2, pp. 377-385, 2008.
- [98] L. Gunnarsson, E. Bjerneld, H. Xu, S. Petronis, B. Kasemo, and M. Käll, "Interparticle coupling effects in nanofabricated substrates for surface-enhanced Raman scattering," *Applied Physics Letters*, vol. 78, pp. 802-804, 2001.
- [99] M. Kahl, E. Voges, S. Kostrewa, C. Viets, and W. Hill, "Periodically structured metallic substrates for SERS," *Sensors and Actuators B: Chemical*, vol. 51, pp. 285-291, 1998.
- [100] S. W. Lee, Y.-B. Shin, K. S. Jeon, S. M. Jin, Y. D. Suh, S. Kim, *et al.*, "Electron beam lithography-assisted fabrication of Au nano-dot array as a substrate of a correlated AFM and confocal Raman spectroscopy," *Ultramicroscopy*, vol. 108, pp. 1302-1306, 2008.
- [101] J. Grand, S. Kostcheev, J.-L. Bijeon, M. L. De La Chapelle, P.-M. Adam, A. Rumyantseva, *et al.*, "Optimization of SERS-active substrates for near-field Raman spectroscopy," *Synthetic metals*, vol. 139, pp. 621-624, 2003.
- [102] J. C. Hulteen and R. P. Van Duyne, "Nanosphere lithography: a materials general fabrication process for periodic particle array surfaces," *Journal of Vacuum Science & Technology A*, vol. 13, pp. 1553-1558, 1995.
- [103] M. A. De Jesús, K. S. Giesfeldt, J. M. Oran, N. A. Abu-Hatab, N. V. Lavrik, and M. J. Sepaniak, "Nanofabrication of Densely Packed Metal–Polymer Arrays for Surface-Enhanced Raman Spectrometry," *Applied Spectroscopy*, vol. 59, pp. 1501-1508, 2005.
- [104] J. M. Oran, R. J. Hinde, N. Abu Hatab, S. T. Retterer, and M. J. Sepaniak, "Nanofabricated periodic arrays of silver elliptical discs as SERS substrates," *Journal of Raman Spectroscopy*, vol. 39, pp. 1811-1820, 2008.
- [105] L. Gunnarsson, E. J. Bjerneld, H. Xu, S. Petronis, B. Kasemo, and M. Käll, "Interparticle coupling effects in nanofabricated substrates for surface-enhanced Raman scattering," *Applied Physics Letters*, vol. 78, pp. 802-804, 2001.
- [106] J. Theiss, P. Pavaskar, P. M. Echternach, R. E. Muller, and S. B. Cronin, "Plasmonic Nanoparticle Arrays with Nanometer Separation for High-Performance SERS Substrates," *Nano Letters*, vol. 10, pp. 2749-2754, 2010.
- [107] R. Alvarez-Puebla, B. Cui, J.-P. Bravo-Vasquez, T. Veres, and H. Fenniri, "Nanoimprinted SERS-Active Substrates with Tunable Surface Plasmon Resonances," *The Journal of Physical Chemistry C*, vol. 111, pp. 6720-6723, 2007.
- [108] W. Wu, M. Hu, F. S. Ou, Z. Li, and R. S. Williams, "Cones fabricated by 3D nanoimprint lithography for highly sensitive surface enhanced Raman spectroscopy," *Nanotechnology*, vol. 21, p. 255502, 2010.
- [109] G. Kostovski, D. White, A. Mitchell, M. Austin, and P. Stoddart, "Nanoimprinted optical fibres: Biotemplated nanostructures for SERS sensing," *Biosensors and Bioelectronics*, vol. 24, pp. 1531-1535, 2009.
- [110] B. D. Lucas, J. S. Kim, C. Chin, and L. J. Guo, "Nanoimprint Lithography Based Approach for the Fabrication of Large - Area, Uniformly - Oriented Plasmonic Arrays," *Advanced Materials*, vol. 20, pp. 1129-1134, 2008.
- [111] B. Cui, Y. Cortot, and T. Veres, "Polyimide nanostructures fabricated by nanoimprint lithography and its applications," *Microelectronic engineering*, vol. 83, pp. 906-909, 2006.

- [112] B. Cui, L. Clime, K. Li, and T. Veres, "Fabrication of large area nanoprism arrays and their application for surface enhanced Raman spectroscopy," *Nanotechnology*, vol. 19, pp. 145302, 2008.
- [113] L. A. Dick, A. D. McFarland, C. L. Haynes, and R. P. Van Duyne, "Metal Film over Nanosphere (MFON) Electrodes for Surface-Enhanced Raman Spectroscopy (SERS): Improvements in Surface Nanostructure Stability and Suppression of Irreversible Loss," *The Journal of Physical Chemistry B*, vol. 106, pp. 853-860, 2001.
- [114] J. Zhao, A. Das, G. C. Schatz, S. G. Sligar, and R. P. Van Duyne, "Resonance Localized Surface Plasmon Spectroscopy: Sensing Substrate and Inhibitor Binding to Cytochrome P450," *The Journal of Physical Chemistry C*, vol. 112, pp. 13084-13088, 2008.
- [115] A. D. McFarland, M. A. Young, J. A. Dieringer, and R. P. Van Duyne, "Wavelength-Scanned Surface-Enhanced Raman Excitation Spectroscopy," *The Journal of Physical Chemistry B*, vol. 109, pp. 11279-11285, 2005.
- [116] X. Zhang, J. Zhao, A. V. Whitney, J. W. Elam, and R. P. Van Duyne, "Ultrastable Substrates for Surface-Enhanced Raman Spectroscopy: Al₂O₃ Overlayers Fabricated by Atomic Layer Deposition Yield Improved Anthrax Biomarker Detection," *Journal of the American Chemical Society*, vol. 128, pp. 10304-10309, 2006.
- [117] A. B. Zrimsek, A.-I. Henry, and R. P. Van Duyne, "Single Molecule Surface-Enhanced Raman Spectroscopy without Nanogaps," *The Journal of Physical Chemistry Letters*, vol. 4, pp. 3206-3210, 2013.
- [118] A. J. Haes, C. L. Haynes, A. D. McFarland, G. C. Schatz, R. P. Van Duyne, and S. Zou, "Plasmonic Materials for Surface-Enhanced Sensing and Spectroscopy," *MRS Bulletin*, vol. 30, pp. 368-375, 2005.
- [119] R. G. Freeman, K. C. Grabar, K. J. Allison, R. M. Bright, J. A. Davis, A. P. Guthrie, *et al.*, "Self-assembled metal colloid monolayers: an approach to SERS substrates," *Science*, vol. 267, pp. 1629-1632, 1995.
- [120] D. J. Maxwell, S. R. Emory, and S. Nie, "Nanostructured Thin-Film Materials with Surface-Enhanced Optical Properties," *Chemistry of Materials*, vol. 13, pp. 1082-1088, 2001.
- [121] H. Wang, C. S. Levin, and N. J. Halas, "Nanosphere Arrays with Controlled Sub-10-nm Gaps as Surface-Enhanced Raman Spectroscopy Substrates," *Journal of the American Chemical Society*, vol. 127, pp. 14992-14993, 2005.
- [122] K. W. Kho, Z. X. Shen, H. C. Zeng, K. C. Soo, and M. Olivo, "Deposition Method for Preparing SERS-Active Gold Nanoparticle Substrates," *Analytical Chemistry*, vol. 77, pp. 7462-7471, 2005.
- [123] K. L. Wustholz, A.-I. Henry, J. M. McMahon, R. G. Freeman, N. Valley, M. E. Piotti, *et al.*, "Structure-Activity Relationships in Gold Nanoparticle Dimers and Trimers for Surface-Enhanced Raman Spectroscopy," *Journal of the American Chemical Society*, vol. 132, pp. 10903-10910, 2010.
- [124] M. Baia, L. Baia, and S. Astilean, "Gold nanostructured films deposited on polystyrene colloidal crystal templates for surface-enhanced Raman spectroscopy," *Chemical Physics Letters*, vol. 404, pp. 3-8, 2005.
- [125] S. Kubo, Z.-Z. Gu, D. A. Tryk, Y. Ohko, O. Sato, and A. Fujishima, "Metal-Coated Colloidal Crystal Film as Surface-Enhanced Raman Scattering Substrate†," *Langmuir*, vol. 18, pp. 5043-5046, 2002.
- [126] P. M. Tessier, S. D. Christesen, K. K. Ong, E. M. Clemente, A. M. Lenhoff, E. W. Kaler, *et al.*, "On-Line Spectroscopic Characterization of Sodium Cyanide with Nanostructured Gold Surface-Enhanced Raman Spectroscopy Substrates," *Applied Spectroscopy*, vol. 56, pp. 1524-1530, 2002.
- [127] D. M. Kuncicky, S. D. Christesen, and O. D. Velev, "Role of the Micro- and Nanostructure in the Performance of Surface-Enhanced Raman Scattering Substrates Assembled from Gold Nanoparticles," *Applied Spectroscopy*, vol. 59, pp. 401-409, 2005.

- [128] D. M. Kuncicky, B. G. Prevo, and O. D. Velev, "Controlled assembly of SERS substrates templated by colloidal crystal films," *Journal of Materials Chemistry*, vol. 16, pp. 1207-1211, 2006.
- [129] L. Lu, I. Randjelovic, R. Capek, N. Gaponik, J. Yang, H. Zhang, *et al.*, "Controlled fabrication of gold-coated 3D ordered colloidal crystal films and their application in surface-enhanced Raman spectroscopy," *Chemistry of materials*, vol. 17, pp. 5731-5736, 2005.
- [130] S. Gaponenko, A. Gaiduk, O. Kulakovich, S. Maskevich, N. Strekal, O. Prokhorov, *et al.*, "Raman scattering enhancement using crystallographic surface of a colloidal crystal," *Journal of Experimental and Theoretical Physics Letters*, vol. 74, pp. 309-311, 2001.
- [131] W. Yuan and C. M. Li, "Direct Modulation of Localized Surface Plasmon Coupling of Au Nanoparticles on Solid Substrates via Weak Polyelectrolyte-Mediated Layer-by-Layer Self Assembly," *Langmuir*, vol. 25, pp. 7578-7585, 2009.
- [132] R. F. Aroca, P. J. G. Goulet, D. S. dos Santos, R. A. Alvarez-Puebla, and O. N. Oliveira, "Silver Nanowire Layer-by-Layer Films as Substrates for Surface-Enhanced Raman Scattering," *Analytical Chemistry*, vol. 77, pp. 378-382, 2004.
- [133] J. K. Daniels and G. Chumanov, "Nanoparticle-Mirror Sandwich Substrates for Surface-Enhanced Raman Scattering," *The Journal of Physical Chemistry B*, vol. 109, pp. 17936-17942, 2005.
- [134] H.-W. Cheng, S.-Y. Huan, H.-L. Wu, G.-L. Shen, and R.-Q. Yu, "Surface-Enhanced Raman Spectroscopic Detection of a Bacteria Biomarker Using Gold Nanoparticle Immobilized Substrates," *Analytical Chemistry*, vol. 81, pp. 9902-9912, 2009.
- [135] P. J. G. Goulet, D. S. dos Santos, R. A. Alvarez-Puebla, O. N. Oliveira, and R. F. Aroca, "Surface-Enhanced Raman Scattering on Dendrimer/Metallic Nanoparticle Layer-by-Layer Film Substrates," *Langmuir*, vol. 21, pp. 5576-5581, 2005.
- [136] R. Gunawidjaja, E. Kharlampieva, I. Choi, and V. V. Tsukruk, "Bimetallic Nanostructures as Active Raman Markers: Gold-Nanoparticle Assembly on 1D and 2D Silver Nanostructure Surfaces," *Small*, vol. 5, pp. 2460-2466, 2009.
- [137] Y. Han, S. Sukhishvili, H. Du, J. Cefaloni, and B. Smolinski, "Layer-by-Layer Self-Assembly of Oppositely Charged Ag Nanoparticles on Silica Microspheres for Trace Analysis of Aqueous Solutions Using Surface-Enhanced Raman Scattering," *Journal of Nanoscience and Nanotechnology*, vol. 8, pp. 5791-5800, 2008.
- [138] L. Yang, B. Yan, W. R. Premasiri, L. D. Ziegler, L. D. Negro, and B. M. Reinhard, "Engineering Nanoparticle Cluster Arrays for Bacterial Biosensing: The Role of the Building Block in Multiscale SERS Substrates," *Advanced Functional Materials*, vol. 20, pp. 2619-2628, 2010.
- [139] C. A. Mirkin, R. L. Letsinger, R. C. Mucic, and J. J. Storhoff, "A DNA-based method for rationally assembling nanoparticles into macroscopic materials," *Nature*, vol. 382, pp. 607-609, 1996.
- [140] Y. C. Cao, R. Jin, and C. A. Mirkin, "Nanoparticles with Raman Spectroscopic Fingerprints for DNA and RNA Detection," *Science*, vol. 297, pp. 1536-1540, 2002.
- [141] R. Jin, G. Wu, Z. Li, C. A. Mirkin, and G. C. Schatz, "What Controls the Melting Properties of DNA-Linked Gold Nanoparticle Assemblies?," *Journal of the American Chemical Society*, vol. 125, pp. 1643-1654, 2003.
- [142] E. Ringe, J. Zhang, M. R. Langille, C. A. Mirkin, L. D. Marks, and R. P. V. Duyne, "Correlating the structure and localized surface plasmon resonance of single silver right bipyramids," *Nanotechnology*, vol. 23, pp. 444005, 2012.
- [143] W. Yuan, H. P. Ho, R. Lee, and S. K. Kong, "Surface-enhanced Raman-scattering biosensor on nanoparticle island substrates for DNA detection," in *Optical Fiber Communication & Optoelectronic Exposition & Conference, 2008. AOE 2008. Asia*, pp. 1-1, 2008.
- [144] A. J. Bonham, G. Braun, I. Pavel, M. Moskovits, and N. O. Reich, "Detection of Sequence-Specific Protein-DNA Interactions via Surface Enhanced Resonance Raman Scattering," *Journal of the American Chemical Society*, vol. 129, pp. 14572-14573, 2007.

- [145] L. M. Sudnik, K. L. Norrod, and K. L. Rowlen, "SERS-Active Ag Films from Photoreduction of Ag⁺ on TiO₂," *Applied Spectroscopy*, vol. 50, pp. 422-424, 1996.
- [146] D. S. dos Santos, P. J. G. Goulet, N. P. W. Pieczonka, O. N. Oliveira, and R. F. Aroca, "Gold Nanoparticle Embedded, Self-Sustained Chitosan Films as Substrates for Surface-Enhanced Raman Scattering," *Langmuir*, vol. 20, pp. 10273-10277, 2004.
- [147] Y. Kitahama, T. Itoh, J.-i. Aoyama, K. Nishikata, and Y. Ozaki, "SERS fiber probe: fabrication of silver nanoparticles at the aperture of an optical fiber used for SNOM," *Chemical Communications*, pp. 6563-6565, 2009.
- [148] X. Li, W. Xu, J. Zhang, H. Jia, B. Yang, B. Zhao, *et al.*, "Self-Assembled Metal Colloid Films: Two Approaches for Preparing New SERS Active Substrates," *Langmuir*, vol. 20, pp. 1298-1304, 2004.
- [149] D. R. Whitcomb, B. J. Stwertka, S. Chen, and P. J. Cowdery-Corvan, "SERS characterization of metallic silver nanoparticle self-assembly within thin films," *Journal of Raman Spectroscopy*, vol. 39, pp. 421-426, 2008.
- [150] M. Potara, M. Baia, C. Farcau, and S. Astilean, "Chitosan-coated anisotropic silver nanoparticles as a SERS substrate for single-molecule detection," *Nanotechnology*, vol. 23, pp. 055501, 2012.
- [151] A. Mills, G. Hill, M. Stewart, D. Graham, W. E. Smith, S. Hodgen, *et al.*, "Characterization of Novel Ag on TiO₂ Films for Surface-Enhanced Raman Scattering," *Applied Spectroscopy*, vol. 58, pp. 922-928, 2004.
- [152] S. J. Henley and S. R. P. Silva, "Laser direct write of silver nanoparticles from solution onto glass substrates for surface-enhanced Raman spectroscopy," *Applied Physics Letters*, vol. 91, pp. -, 2007.
- [153] X. Zheng, D. Guo, Y. Shao, S. Jia, S. Xu, B. Zhao, *et al.*, "Photochemical Modification of an Optical Fiber Tip with a Silver Nanoparticle Film: A SERS Chemical Sensor," *Langmuir*, vol. 24, pp. 4394-4398, 2008.
- [154] E. Stathatos, P. Lianos, P. Falaras, and A. Siokou, "Photocatalytically Deposited Silver Nanoparticles on Mesoporous TiO₂ Films," *Langmuir*, vol. 16, pp. 2398-2400, 2000.
- [155] X. He, X. Zhao, and B. Liu, "Studies on a possible growth mechanism of silver nanoparticles loaded on TiO₂ thin films by photoinduced deposition method," *Journal of Non-Crystalline Solids*, vol. 354, pp. 1267-1271, 2008.
- [156] A. Sánchez-Iglesias, P. Aldeanueva-Potel, W. Ni, J. Pérez-Juste, I. Pastoriza-Santos, R. A. Alvarez-Puebla, *et al.*, "Chemical seeded growth of Ag nanoparticle arrays and their application as reproducible SERS substrates," *Nano Today*, vol. 5, pp. 21-27, 2010.
- [157] Y. Wang, W. Ren, S. Dong, and E. Wang, "Characterization and optimization of AuNPs labeled by Raman reporters on glass based on silver enhancement," *Journal of Raman Spectroscopy*, vol. 40, pp. 571-576, 2009.
- [158] Y.-L. JIN, W. QIN, Y. JIANG, M. WANG, J.-L. YAO, J. HUANG, *et al.*, "Surface Treatment and Surface Enhanced Raman Spectroscopic Studies on Au/Ag Alloy Nanoparticle Assembly," 2008.
- [159] M. Culha, D. Stokes, L. R. Allain, and T. Vo-Dinh, "Surface-Enhanced Raman Scattering Substrate Based on a Self-Assembled Monolayer for Use in Gene Diagnostics," *Analytical Chemistry*, vol. 75, pp. 6196-6201, 2003.
- [160] N. R. Isola, D. L. Stokes, and T. Vo-Dinh, "Surface-Enhanced Raman Gene Probe for HIV Detection," *Analytical Chemistry*, vol. 70, pp. 1352-1356, 1998.
- [161] C. G. Houry, S. J. Norton, and T. Vo-Dinh, "Investigating the plasmonics of a dipole-excited silver nanoshell: Mie theory versus finite element method," *Nanotechnology*, vol. 21, p. 315203, 2010.
- [162] H. Ngo, H.-N. Wang, T. Burke, G. Ginsburg, and T. Vo-Dinh, "Multiplex detection of disease biomarkers using SERS molecular sentinel-on-chip," *Analytical and Bioanalytical Chemistry*, pp. 1-10, 2014.

- [163] H. T. Ngo, H.-N. Wang, A. M. Fales, and T. Vo-Dinh, "Label-Free DNA Biosensor Based on SERS Molecular Sentinel on Nanowave Chip," *Analytical Chemistry*, vol. 85, pp. 6378-6383, 2013.
- [164] A. Pal, N. R. Isola, J. P. Alarie, D. L. Stokes, and T. Vo-Dinh, "Synthesis and characterization of SERS gene probe for BRCA-1 (breast cancer)," *Faraday Discussions*, vol. 132, pp. 293-301, 2006.
- [165] T. Vo-Dinh, K. Houck, and D. L. Stokes, "Surface-Enhanced Raman Gene Probes," *Analytical Chemistry*, vol. 66, pp. 3379-3383, 1994.
- [166] T. Vo-Dinh, D. L. Stokes, G. D. Griffin, M. Volkan, U. J. Kim, and M. I. Simon, "Surface-enhanced Raman Scattering (SERS) method and instrumentation for genomics and biomedical analysis," *Journal of Raman Spectroscopy*, vol. 30, pp. 785-793, 1999.
- [167] M. Wabuyele, F. Yan, and T. Vo-Dinh, "Plasmonics nanoprobe: detection of single-nucleotide polymorphisms in the breast cancer BRCA1 gene," *Analytical and Bioanalytical Chemistry*, vol. 398, pp. 729-736, 2010.
- [168] M. B. Wabuyele and T. Vo-Dinh, "Detection of Human Immunodeficiency Virus Type 1 DNA Sequence Using Plasmonics Nanoprobes," *Analytical Chemistry*, vol. 77, pp. 7810-7815, 2005.
- [169] T. Vo-Dinh, L. R. Allain, and D. L. Stokes, "Cancer gene detection using surface-enhanced Raman scattering (SERS)," *Journal of Raman Spectroscopy*, vol. 33, pp. 511-516, 2002.
- [170] A. P. Alivisatos, K. P. Johnsson, X. Peng, T. E. Wilson, C. J. Loweth, M. P. Bruchez, *et al.*, "Organization of 'nanocrystal molecules' using DNA," 1996.
- [171] N. H. Jang, "SERS Analysis of Self-Assembled Monolayers of DNA Strands on Gold Surfaces," *Notes*, vol. 31, pp. 213, 2010.
- [172] W. Xu, X. Xue, T. Li, H. Zeng, and X. Liu, "Ultrasensitive and selective colorimetric DNA detection by nicking endonuclease assisted nanoparticle amplification," *Angewandte Chemie International Edition*, vol. 48, pp. 6849-6852, 2009.
- [173] J. A. Dougan, C. Karlsson, W. E. Smith, and D. Graham, "Enhanced oligonucleotide-nanoparticle conjugate stability using thioctic acid modified oligonucleotides," *Nucleic acids research*, vol. 35, pp. 3668-3675, 2007.
- [174] L. Barrett, J. A. Dougan, K. Faulds, and D. Graham, "Stable dye-labelled oligonucleotide-nanoparticle conjugates for nucleic acid detection," *Nanoscale*, vol. 3, pp. 3221-3227, 2011.
- [175] D. G. Thompson, A. Enright, K. Faulds, W. E. Smith, and D. Graham, "Ultrasensitive DNA detection using oligonucleotide-silver nanoparticle conjugates," *Analytical chemistry*, vol. 80, pp. 2805-2810, 2008.
- [176] F. McKenzie, K. Faulds, and D. Graham, "Mixed metal nanoparticle assembly and the effect on surface-enhanced Raman scattering," *Nanoscale*, vol. 2, pp. 78-80, 2010.
- [177] D. Graham, D. G. Thompson, W. E. Smith, and K. Faulds, "Control of enhanced Raman scattering using a DNA-based assembly process of dye-coded nanoparticles," *Nature nanotechnology*, vol. 3, pp. 548-551, 2008.
- [178] D.-K. Lim, K.-S. Jeon, J.-H. Hwang, H. Kim, S. Kwon, Y. D. Suh, *et al.*, "Highly uniform and reproducible surface-enhanced Raman scattering from DNA-tailorable nanoparticles with 1-nm interior gap," *Nat Nano*, vol. 6, pp. 452-460, 2011.
- [179] R. Radtkey, L. Feng, M. Muralhidar, M. Duhon, D. Canter, D. DiPierro, *et al.*, "Rapid, high fidelity analysis of simple sequence repeats on an electronically active DNA microchip," *Nucleic Acids Research*, vol. 28, pp. e17-e17, 2000.
- [180] K. Wang, Z. Sun, M. Feng, A. Liu, S. Yang, Y. Chen, *et al.*, "Design of a sandwich-mode amperometric biosensor for detection of PML/RAR α fusion gene using locked nucleic acids on gold electrode," *Biosensors and Bioelectronics*, vol. 26, pp. 2870-2876, 2011.
- [181] K. Wang, J. Chen, J. Chen, A. Liu, G. Li, H. Luo, *et al.*, "A Sandwich-Type Electrochemical Biosensor for Detection of BCR/ABL Fusion Gene Using Locked Nucleic Acids on Gold Electrode," *Electroanalysis*, vol. 21, pp. 1159-1166, 2009.

- [182] S. He, K.-K. Liu, S. Su, J. Yan, X. Mao, D. Wang, *et al.*, "Graphene-Based High-Efficiency Surface-Enhanced Raman Scattering-Active Platform for Sensitive and Multiplex DNA Detection," *Analytical Chemistry*, vol. 84, pp. 4622-4627, 2012.
- [183] Y. He, S. Su, T. Xu, Y. Zhong, J. A. Zapien, J. Li, *et al.*, "Silicon nanowires-based highly-efficient SERS-active platform for ultrasensitive DNA detection," *Nano Today*, vol. 6, pp. 122-130, 2011.
- [184] M. Li, S. K. Cushing, H. Liang, S. Suri, D. Ma, and N. Wu, "Plasmonic Nanorice Antenna on Triangle Nanoarray for Surface-Enhanced Raman Scattering Detection of Hepatitis B Virus DNA," *Analytical Chemistry*, vol. 85, pp. 2072-2078, 2013.
- [185] T. Kang, S. M. Yoo, I. Yoon, S. Y. Lee, and B. Kim, "Patterned Multiplex Pathogen DNA Detection by Au Particle-on-Wire SERS Sensor," *Nano Letters*, vol. 10, pp. 1189-1193, 2010.
- [186] Z. Y. Jiang, X. X. Jiang, S. Su, X. P. Wei, S. T. Lee, and Y. He, "Silicon-based reproducible and active surface-enhanced Raman scattering substrates for sensitive, specific, and multiplex DNA detection," *Applied Physics Letters*, vol. 100, p. 203104, 2012.
- [187] A. Bonanni and M. Pumera, "Graphene Platform for Hairpin-DNA-Based Impedimetric Genosensing," *ACS Nano*, vol. 5, pp. 2356-2361, 2011.
- [188] J. E. N. Dolatabadi, O. Mashinchian, B. Ayoubi, A. A. Jamali, A. Mobed, D. Losic, *et al.*, "Optical and electrochemical DNA nanobiosensors," *TrAC Trends in Analytical Chemistry*, vol. 30, pp. 459-472, 3// 2011.
- [189] S. E. J. Bell and N. M. S. Sirimuthu, "Surface-Enhanced Raman Spectroscopy (SERS) for Sub-Micromolar Detection of DNA/RNA Mononucleotides," *Journal of the American Chemical Society*, vol. 128, pp. 15580-15581, 2006.
- [190] G. D. Chumanov and T. M. Cotton, "Surface-enhanced Raman scattering for discovering and scoring single-base differences in DNA," in *BIOS'99 International Biomedical Optics Symposium*, pp. 204-210, 1999.
- [191] J. Kundu, O. Neumann, B. G. Janesko, D. Zhang, S. Lal, A. Barhoumi, *et al.*, "Adenine- and Adenosine Monophosphate (AMP)-Gold Binding Interactions Studied by Surface-Enhanced Raman and Infrared Spectroscopies," *The Journal of Physical Chemistry C*, vol. 113, pp. 14390-14397, 2009.
- [192] E. Papadopoulou and S. E. J. Bell, "Surface-Enhanced Raman Evidence of Protonation, Reorientation, and Ag⁺ Complexation of Deoxyadenosine and Deoxyadenosine-5' - Monophosphate (dAMP) on Ag and Au Surfaces," *The Journal of Physical Chemistry C*, vol. 115, pp. 14228-14235, 2011.
- [193] G. J. Thomas Jr, J. M. Benevides, S. A. Overman, T. Ueda, K. Ushizawa, M. Saitoh, *et al.*, "Polarized Raman spectra of oriented fibers of A DNA and B DNA: anisotropic and isotropic local Raman tensors of base and backbone vibrations," *Biophysical Journal*, vol. 68, pp. 1073-1088, 1995.
- [194] E. Papadopoulou and S. E. J. Bell, "DNA reorientation on Au nanoparticles: label-free detection of hybridization by surface enhanced Raman spectroscopy," *Chemical Communications*, vol. 47, pp. 10966-10968, 2011.
- [195] R. Treffer, X. Lin, E. Bailo, T. Deckert-Gaudig, and V. Deckert, "Distinction of nucleobases—a tip-enhanced Raman approach," *Beilstein journal of nanotechnology*, vol. 2, pp. 628-637, 2011.
- [196] T.-T. Xu, J.-A. Huang, L.-F. He, Y. He, S. Su, and S.-T. Lee, "Ordered silicon nanocones arrays for label-free DNA quantitative analysis by surface-enhanced Raman spectroscopy," *Applied Physics Letters*, vol. 99, pp. 153116, 2011.
- [197] C. Yi, C.-W. Li, H. Fu, M. Zhang, S. Qi, N.-B. Wong, *et al.*, "Patterned growth of vertically aligned silicon nanowire arrays for label-free DNA detection using surface-enhanced Raman spectroscopy," *Analytical and Bioanalytical Chemistry*, vol. 397, pp. 3143-3150, 2010.
- [198] M. Green and F. M. Liu, "SERS substrates fabricated by island lithography: the silver/pyridine system," *The Journal of Physical Chemistry B*, vol. 107, pp. 13015-13021, 2003.

- [199] F. M. Liu, P. A. Köllensperger, M. Green, A. E. G. Cass, and L. F. Cohen, "A note on distance dependence in surface enhanced Raman spectroscopy," *Chemical Physics Letters*, vol. 430, pp. 173-176, 2006.
- [200] J. D. Driskell and R. A. Tripp, "Label-free SERS detection of microRNA based on affinity for an unmodified silver nanorod array substrate," *Chemical Communications*, vol. 46, pp. 3298-3300, 2010.
- [201] J. L. Abell, J. M. Garren, J. D. Driskell, R. A. Tripp, and Y. Zhao, "Label-Free Detection of Micro-RNA Hybridization Using Surface-Enhanced Raman Spectroscopy and Least-Squares Analysis," *Journal of the American Chemical Society*, vol. 134, pp. 12889-12892, 2012.
- [202] A. Barhoumi, D. Zhang, F. Tam, and N. J. Halas, "Surface-Enhanced Raman Spectroscopy of DNA," *Journal of the American Chemical Society*, vol. 130, pp. 5523-5529, 2008.
- [203] A. Barhoumi and N. J. Halas, "Label-Free Detection of DNA Hybridization Using Surface Enhanced Raman Spectroscopy," *Journal of the American Chemical Society*, vol. 132, pp. 12792-12793, 2010.
- [204] A. Barhoumi, D. Zhang, and N. J. Halas, "Correlation of Molecular Orientation and Packing Density in a dsDNA Self-Assembled Monolayer Observable with Surface-Enhanced Raman Spectroscopy," *Journal of the American Chemical Society*, vol. 130, pp. 14040-14041, 2008.

Chapter 2. Titanium dioxide and sol-gel processing: extrapolation to a new kind of SERS substrate

1. Introduction

In this chapter, we present the methods and procedures that have been employed for the bottom up elaboration of the SERS substrate. We start with a brief overview of titanium dioxide, with an introduction to its crystalline structure and photo-induced properties, and most particularly, its photocatalytic activity, which will be essential in this work. We then describe the sol-gel protocol used to produce TiO₂ thin films. We then present an overview of the results previously obtained at LMGP, which showed the possibility to form an Ag⁰/TiO₂ SERS substrate in view of label-free DNA detection through a photocatalytic reduction procedure. We finally conclude on the limitations of those results and the important necessity of further optimization studies.

2. Overview of titanium dioxide

Titanium dioxide (TiO₂) has been object of considerable attention for various applications due to its many attractive properties, including chemical and biological stability, non-toxicity, optical properties, and low cost [1]. For example, TiO₂ finds use in a wide range of important applications as anti-reflection coating in silicon solar cells and in many thin-film optical devices [2]. Titanium dioxide is also used for gas sensor applications due to the dependence of its electrical conductivity on the ambient gas composition [3]. It also plays a role as bone substitute and reinforcing mechanical support in the biocompatibility of bones implants [4]. Last but not least, titanium dioxide is well known for its excellent photocatalytic performances. Accordingly, a significant amount of applications based on its photo-induced properties has been reported over the last decades, which will be presented in detail in the following sections (see also a review in [5]).

2.1 Crystalline structure

Titanium dioxide has three different crystalline structure types - anatase, rutile and brookite - which can be discussed in terms of (TiO₆) octahedral units (Figure 2-1). Rutile has a tetragonal structure and the TiO₆ octahedron is slightly distorted [6]. Anatase also has a tetragonal structure and the TiO₆ octahedron is much more distorted [7]. Brookite belongs to the orthorhombic crystal system. Pure brookite without

rutile or anatase is rather difficult to prepare so that titanium dioxide is commercially available in two crystal structures: anatase and rutile. The difference in lattice structures of anatase and rutile determines different densities and electronic structures, leading to different band gaps (anatase: 3.20 eV; rutile: 3.02 eV). Anatase is the most photo-active polymorphic form of TiO_2 , probably due to a higher electron mobility, lower dielectric constant, and lower density. Rutile is the thermodynamically stable form of TiO_2 , and anatase is often readily transformed into rutile when heated at sufficient temperatures [1]. Kinetically, anatase is stable, i.e. its transformation into rutile at room temperature is so slow that it practically does not occur. Anatase can readily be synthesized through many sol-gel procedures. The sol-gel process will be presented in detail in section 3.

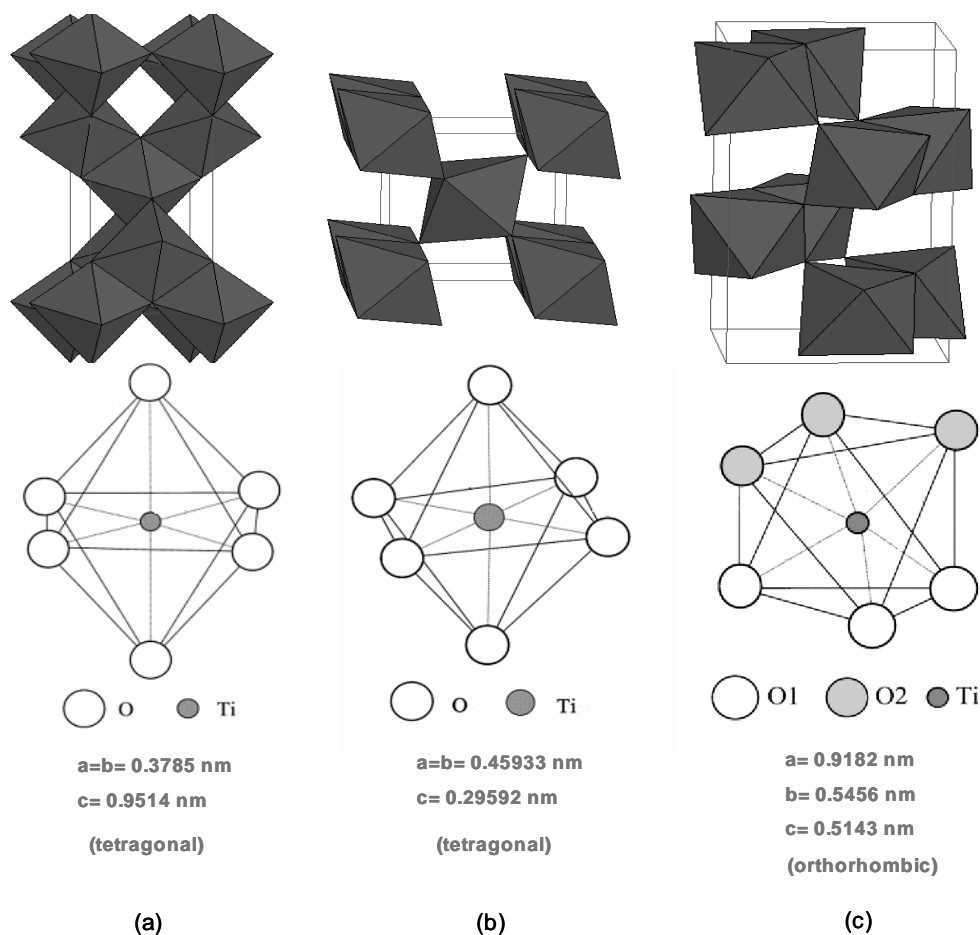


Figure 2-1: Crystal structures of anatase (a), rutile (b), and brookite (c).

2.2 Photo-induced properties

In 1972, Fujishima and Honda discovered that a TiO_2 electrode can decompose water to hydrogen and oxygen under UV exposition [8]. Since then, the photo-induced properties of TiO_2 , preferentially in its anatase form, have been the object of increasing interest for many kinds of applications. These properties originate from the semiconductor band gap. Photo-induced reactions proceed under UV-irradiation,

when photons have an energy equal to or greater than titania band gap energy (for anatase: $h\nu > 3.2$ eV, i.e. $\lambda < 380$ nm), which causes the promotion of an electron from the valence band to the conduction band. Consequently, the charge-carrier generation of photoelectrons (e^-) and holes (h^+) pairs is achieved according to the reaction Equation 2-1:



Such photogenerated electrons and holes have inspired many potential applications, as shown in Figure 2-2. For instance, the photogenerated electrons can be used to create electricity in photovoltaic solar cells. Both the electrons and holes can also participate to chemical reactions through multi-step redox mechanisms in photocatalysis. Various investigations have proved that TiO_2 is an excellent photocatalyst, which has been employed mostly in environmental and energy application, including photocatalytic treatment of wastewater, pesticide degradation, and water splitting to produce hydrogen [9]. The interest for TiO_2 has broadened again in 1997, when Wang et al. have found that titania surfaces exhibit a photo-induced superhydrophilicity, i.e. a water contact angle of zero degree under UV exposure [10]. This property has been largely studied, for instance for antifogging surface applications, since water cannot exist in the shape of drop but spreads flatly on the superhydrophilic surface. This property also ensues from holes photo-generated under UV irradiation. Photo-generated holes trapped by lattice oxygen of the TiO_2 network tend to weaken the bond between the titanium and oxygen atoms, which creates oxygen vacancies at the TiO_2 surface. Such oxygen vacancies can then be saturated by OH groups through a molecular or dissociative adsorption of atmospheric water, which yields a superhydrophilic surface characterized by a water contact angle of zero degree.

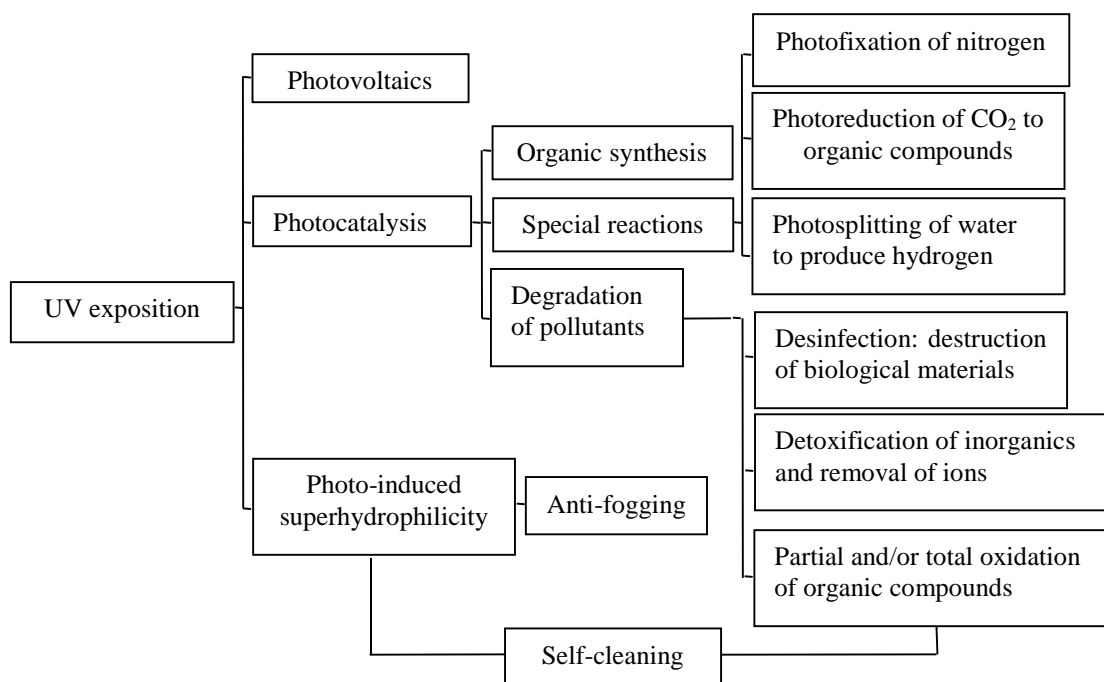


Figure 2-2: Applications of photo-active TiO_2 [5].

This photo-induced superhydrophilicity has been often associated to photocatalysis, since both phenomena have a common ground. Accordingly, the surface contamination can be photocatalytically decomposed and then washed away through a simple water rinsing operation without the need of detergent. These combined properties lead to “self-cleaning” surface applications, which are studied extensively by our group among many others. In this work, we principally took advantage of the photocatalytic activity of TiO_2 . This property is detailed in the next section.

2.3 Photocatalytic activity

The photocatalytic activity is a well-known process mostly employed to degrade or transform organic and inorganic compounds into less harmful substances. A heterogeneous photocatalytic system consists of semiconductor particles (photocatalysts), which are in close contact with a fluid phase (gas or liquid). When exposing the catalyst to light (radiation of sufficient energy), excited states are generated which enable subsequent processes like chemical reactions through redox mechanisms and molecular transformations. A simplified reaction scheme of the photocatalytic process in TiO_2 is illustrated in Figure 2-3. As previously mentioned, photocatalytic reactions induced by TiO_2 occur under UV-irradiation, when photons have energy equal or superior to the titania band gap energy. Excited electrons (e^-) in the valence band jump to the conduction band leaving behind holes (h^+).

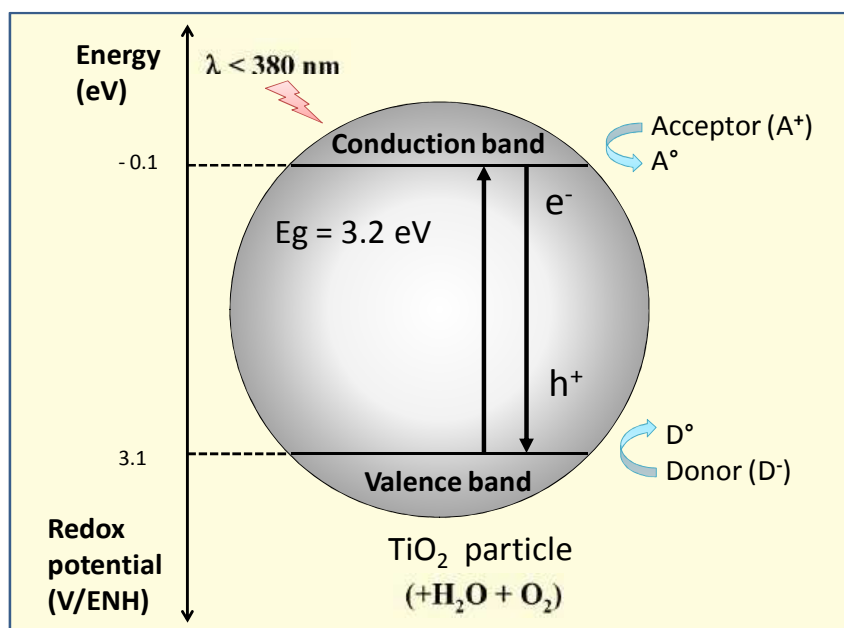
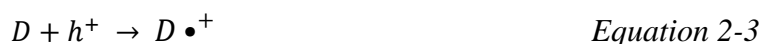


Figure 2-3: Schematic presentation of the photocatalytic process in a TiO_2 particle.

In electrically conducting material, i.e. metals, the electron-hole pairs are immediately recombined. In semi-conductors, a portion of these photoexcited electron-hole pairs diffuse to the catalyst surface and chemically react with an adsorbed donor (D) or acceptor (A) molecules. The photo-generated electron can reduce the acceptor molecule, while positive holes can oxidize donor molecules, as shown in the following equations:



A characteristic feature of anatase TiO_2 is the strong oxidation power of photo-generated holes (h^+). They can react in one-step oxidation reaction with water (Equation 2-4) or with surface hydroxyls to produce highly reactive hydroxyl radicals OH^\bullet (Equation 2-5).

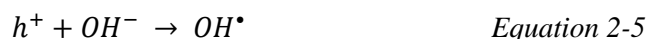


Photo-generated holes and OH^\bullet radicals, which are powerful oxidants, can be used to decompose adsorbed organic pollutants present at the TiO_2 surface. Besides, the photoelectrons are trapped by dissolved oxygen to form super-oxide ions ($\bullet \text{O}_2^-$):



These ions are also highly reactive radicals and are able to efficiently oxidize organic matter. However, the photocatalytic efficiency can be limited by electron-hole recombinations, which can occur either in the bulk (volume recombination) or at the surface (surface recombination), as shown in Figure 2-4.

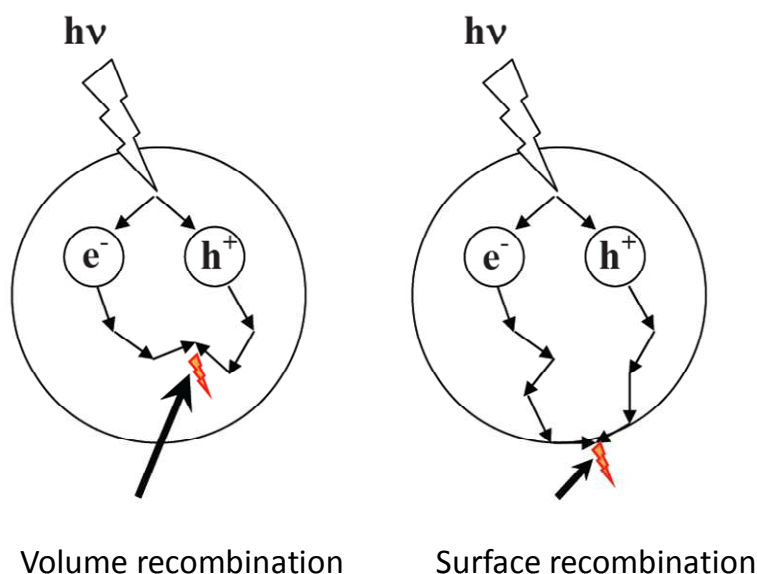
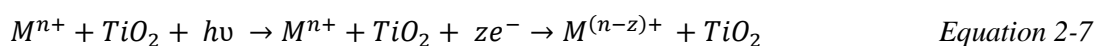


Figure 2-4: Electron-hole recombination pathways.

In recent years, the applications of TiO₂-based photocatalysts have been one of the most active areas in heterogeneous photocatalysis. The term photocatalysis usually describes the acceleration of the photoreaction rate induced by the catalyst. The photo-induced redox reactions of adsorbed substances have continuously grown in popularity, since they offer a low cost photochemical procedure for industrial applications. Let us note that previously described photocatalytic mechanisms are based on the oxidative power of photo-generated holes and derived radicals, which are mainly exploited for the oxidative decomposition of organic matter, for instance in self-cleaning surface applications. However, photo-generated electrons can also be exploited to induce reduction mechanisms. This approach, much less studied than the previous one, has been adapted by our group to grow noble metal nanoparticles (NPs) at the surface of TiO₂ films. It is presented in the next section.

2.4 TiO₂-based photocatalytic reduction of metal cations

In contrast to a great amount of publications reporting the oxidation reactions, much less studies report reduction reactions photo-induced by a TiO₂ photocatalyst, as illustrated in Equation 2-2 in the previous section. In this equation, the acceptor (*A*) can in particular be a metal cation (Mⁿ⁺) having a convenient redox potential to be transformed into a lower oxidation state (M^{(n-z)+}) [11]:



In proper conditions, this mechanism leads to the formation of metal particles (M°) at the TiO_2 surface. This photo-metallization process is often proposed for semiconductor photocatalyst modifications [12]. Photo-metallization involves the whole reduction of adsorbed metal cations by conduction band electrons, the anodic process being the oxidation of a liquid electrolyte, water or else, by valence band holes. According to Lin and Rajeshwar, two types of reduction mechanisms are possible for the photocatalytic removal of metal cations from the liquid solution: (i) direct reduction of the cations by the photogenerated electrons, and (ii) indirect reduction by intermediates generated by hole oxidation of added organics [13]. Certainly, the direct reduction pathway is the simplest one. For this direct reduction, the conduction band energy level must be more negative than the M^{n+}/M° redox potential, as shown in Figure 2-5 [11].

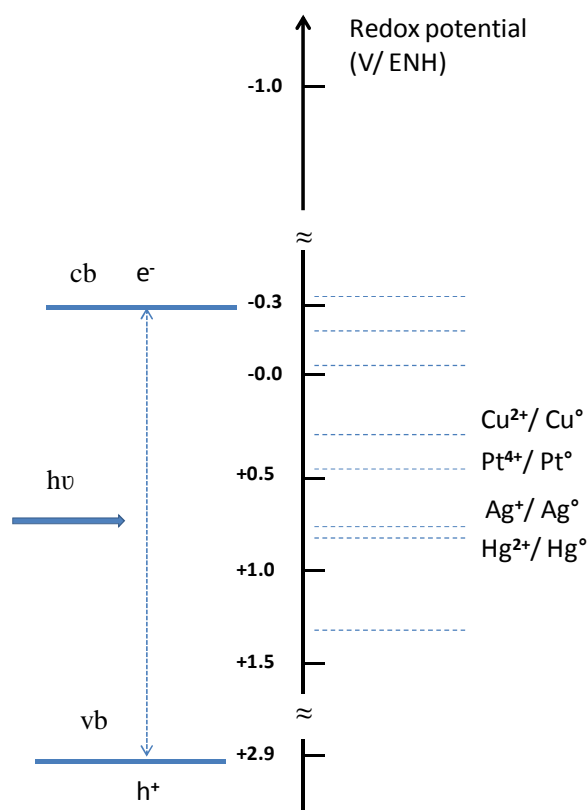


Figure 2-5: Positions of the redox potentials of various metallic M^{n+}/M° couples related to the energy level of the conduction (cb) and valence bands (vb) of TiO_2 [11].

For instance, conduction band electrons photo-generated by TiO_2 can reduce directly Ag^+ cations into Ag° . Accordingly, the photocatalytic deposition of metallic silver particles onto a TiO_2 surface has been well demonstrated for a long time in the literature. One of the very early studies was reported by Vondjidis *et al.* in the sixties [14]. They have studied the UV-induced darkening of a TiO_2 and silver nitrate mixture. More specifically, the first interpretations concerning the adsorption of Ag^+ cations on a TiO_2 surface and the conduction band electron transfer to Ag^+ cations were reported in the seventies

by Fleischauer and Shepherd [15]. In this study, silver particles were photocatalytically grown on a TiO₂ single crystal. In the eighties, Herrmann et al. confirmed this photocatalytic growth mechanism and concluded that the metal silver crystallites are formed from agglomeration of silver atoms individually reduced at the surface of powdered titania [16].

All these initial studies demonstrated the possibility to grow metal Ag⁰ particles on a TiO₂ surface through a photo-metallization process. However, most of the subsequent works were devoted to powdered or single crystals titania. In contrast, very few works addressed the photocatalytically assisted growth of Ag⁰ particles on TiO₂ thin films. Only some recent papers deal with this purpose. For instance, Mills et al have studied a photocatalytic reduction procedure to form so-called “fish scales” Ag⁰ coatings on TiO₂ surfaces for SERS applications [17]. Some other papers also show the feasibility of this elaboration procedure but do not present any study on the mechanisms allowing a controlled growth of the Ag⁰ NPs, and SERS performances have not been investigated [18, 19]. It is this approach, the controlled growth of Ag⁰ nanoparticles through a photocatalytic reduction mechanism, which will be studied in this thesis to propose a new Ag⁰ /TiO₂ SERS substrate.

3. The sol-gel process

3.1 General principles

TiO₂ thin films studied in this thesis have been deposited through a sol-gel route. In this section, we briefly summarize the important principles of the sol-gel process. Exhaustive details can be found in the “bible” of sol-gel by Brinker and Scherer in [20].

The sol-gel process is a wet chemistry method. Wet chemistry is a term which refers to a number of scientific techniques involving synthesis protocols of materials in liquid solution. It is widespread used today due to many attractive assets including low cost, easy control of stoichiometry, size and shape of particles formed in solution, synthesis of homogeneous materials, etc... Among many available wet chemistry methods, we will mention precipitation, solvothermal, combustion, electrochemical, or sol-gel methods. The sol-gel process can be used for preparing numerous inorganic or hybrid organic/inorganic compounds in a large variety of forms such as thin films, calibrated nanoparticles, monolithic glasses, or optical fibers, as shown in Figure 2-6. The assets of sol-gel are in particular intensively applied to thin films elaboration, providing for instance porous films with large specific surface areas or dense and mechanically resistant films, as well as allowing coverage of large and complex shape substrates.

The term ‘sol-gel’ refers to a process of transformation in which monomer or oligomer species dissolved in a liquid solution chemically react to form a so-called sol and subsequently aggregate to form a solid-like oxide network (gel). The ‘sol’ is typically a stable dispersion of colloidal particles, whose size range from $< 1\text{ nm}$ to $< 1\ \mu\text{m}$, arising from chemical precursors which can be classified into two different types depending on the involved ligands.

- Inorganic precursors: include inorganic salts such as nitrates, sulphates, chlorides, or acetates.
- Metal organic precursors: generally used as metal alkoxides ($\text{M}(\text{OR})_n$), which consist of an organic alcohol group (alkoxy, OR) attached to a metal (M) atom and react in a large variety of organic solvents. Metal alkoxides are the most widely used in sol-gel. In the next part of this section, we focus on such precursors.

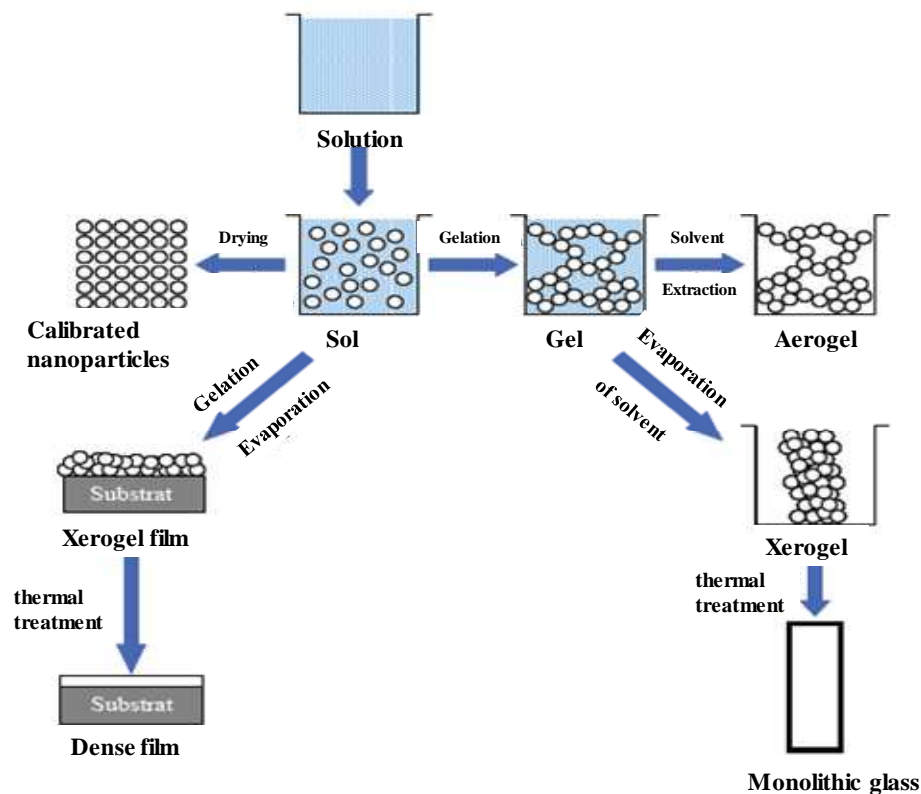


Figure 2-6: The potential of sol-gel process [20].

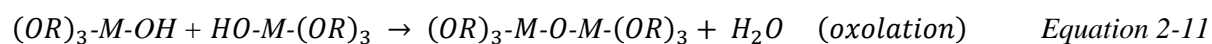
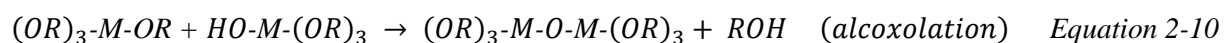
Metal alkoxides are firstly diluted in an organic solvent (generally alcohol). Their sol-gel transformation (liquid to solid transformation) occurs through an *inorganic* polymerization mechanism, which is based on two chemical reactions: hydrolysis and condensation. Metal alkoxides are generally strongly hydrolysable compounds when mixed with water. Thus, a hydroxyl group becomes attached to the metal atom through an OR-OH exchange:



In an extreme case, the alkoxy group may be completely hydrolyzed, i.e. all OR groups are replaced by OH ones:



However, hydrolysis generally stops before completion yielding $(HO)_n-M-(OR)_{4-n}$ species. The linkage of these partially hydrolyzed molecules can then occur through condensation reactions, leading to an oxide network gel. In the condensation reactions, protonated species are expelled either in the form of alcohol (alcoxolation) or water (oxolation):



The relative rates of hydrolysis and condensation determine the structure of the final gel. Accordingly, many studies have reported various methods to selectively control the rate of these reactions, i.e. acid or base catalysts are often used to enable a separation of the hydrolysis and condensation reactions [21]. Generally, acidic catalysts (e.g. HCl, HNO₃) increase hydrolysis rates, while basic catalysts (e.g. NaOH, NH₄OH) promote condensation.

Monomer or oligomer species grow in the liquid solution through multi-hydrolysis/condensation reactions (polycondensation), yielding increasingly larger inorganic polymeric clusters, and finally resulting in the formation of a wet gel. The gel formation can be accelerated by a concentration increase of reactive species induced by evaporation of the solvent, which rapidly occurs during thin film deposition procedures. Further solvent evaporation yields a wet to dry gel transformation. The dried gel is called xerogel and is often reduced in volume by a factor of 5 to 10 compared to the original wet gel. In the case of thin films, the sol→gel→xerogel transformation takes place within a few seconds. A sol-gel film can be prepared by common liquid phase deposition processes such as spin-coating (see section 3.3), as well as dip- or spray-coating.

The final xerogel consists of a porous and amorphous oxide network, which is constituted of M-O-M chains with hydrolyzed or not alkoxy groups at chain ends. In order to improve its characteristics, for instance its mechanical integrity, densification degree, or crystallization state, the xerogel is then thermally treated in air at more or less high temperature. Thermal treatment promotes the pyrolysis of remaining alkoxy and hydroxyl groups, yielding a pure oxide compound, and induces densification of the oxide network, which is for instance required for the formation of functional optical fibers, monolith

glasses, or thin films. Oxidation and densification particularly enhance the abrasion resistance of sol-gel derived thin films. Besides, the crystallization of thin films necessitates a complete pyrolysis of remaining alkoxy groups (or additional organic ligand). These species normally have good stability and act as structural impurities that inhibit crystallization at low temperature. Accordingly, crystalline anatase TiO₂ sol-gel films are usually processed at a relatively high temperature of 350°C or more [22-25].

3.2 Adaptation to TiO₂ sols

In contrast to certain alkoxides, such as Si ones, Ti alkoxides are extremely reactive to hydrolysis and polycondensation. It is a critical feature to be taken into account, because a too fast and uncontrolled reaction can rapidly promote the aggregation of large inorganic species, which can rapidly precipitate and settle in the solution. In that case, the sol is no longer adapted to the deposition of uniform films of optical quality. Two main routes can be implemented to overcome this problem and to finely control the reaction rates. The first one relies on a complexation of the alkoxide with a non-hydrolyzable chelating ligand, for instance acetic acid or acetylacetone. This ligand partially substitutes to the reactive alkoxy groups and reduces the overall reactivity in solution. This method has for instance been used in preliminary works performed at LMGP, which showed the feasibility of SERS detection on Ag⁰/TiO₂ heterostructure (see section 4) [26]. A second route to chemically stabilize the sol relies on a so-called peptization mechanism. This mechanism is based on electrostatic repulsions between reactive species positively (negatively) charged in sufficiently acidic (basic) conditions. These electrostatic repulsions reduce the contact between reactive species and therefore decrease the overall sol reactivity. It is this second route which has been used in this work to prepare a stable titanium oxide sol according to previous studies performed at LMGP [27].

This sol, which is hereafter called “mother solution” (MS), was obtained by mixing tetraisopropyl orthotitanate (TIPT, from Fluka) with deionized water, hydrochloric acid (HCl), and absolute ethanol as a solvent. The TIPT molar concentration in the solution was 0.4 M and the TIPT/H₂O/HCl molar composition was 1/0.82/0.13. The theoretical solution pH, calculated from the amount of HCl, is 1.27. It indicates a strongly acidic sol which can undergo a peptization process. Accordingly, the above MS preparation conditions give rise to a very stable sol, which indicates that no premature gelation or precipitation takes place in this solution. Consequently, such sol could be used for several weeks or months in reproducible film deposition conditions [27, 28]. In this protocol, the solution was aged at room temperature for 2 days prior to use for film deposition.

3.3 Film deposition by spin-coating

As previously mentioned, sol-gel films can be elaborated by several classical liquid phase deposition methods such as dip-, spray- or spin-coating. In the present study, we have used spin-coating for the deposition of TiO₂ thin films. Bornside *et al.* divided the spin-coating procedure into four stages, as shown in Figure 2-7 [29].

- In the first stage, an excess of liquid is delivered to the substrate at rest or spinning slowly (deposition).
- In the second stage, the liquid flows radially outward, driven by the centrifugal force created by the substrate rotated at high speed (spin-up).
- In the third stage, excess liquid now covering the substrate flows radially on the perimeter (spin-off).
- In the last stage, evaporation of solvent occurs, which promotes hydrolysis/condensation reactions leading to the formation of a dry gel (xerogel) film.

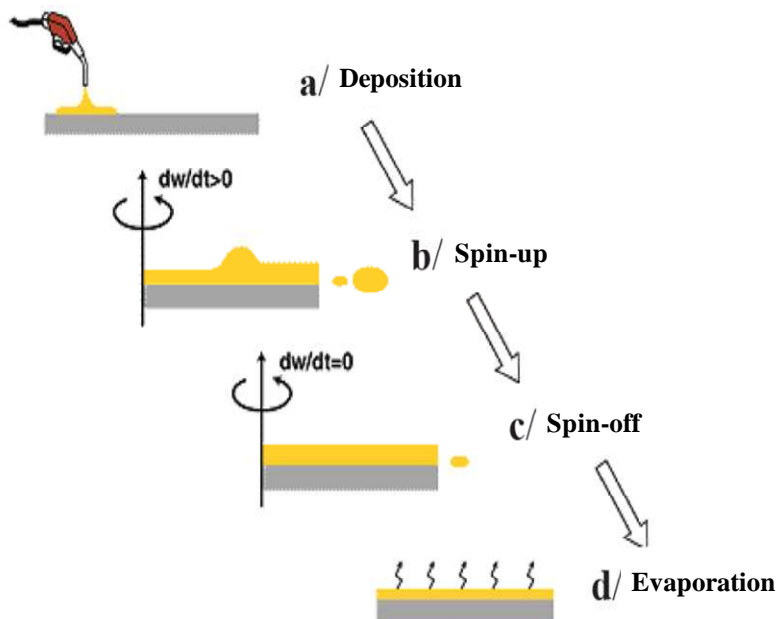


Figure 2-7: Stages of the spin-coating process [29].

According to these mechanisms, a uniformly thick liquid film tends to be formed during spin-off. Its thickness (h) is described by:

$$h(t) = \frac{h_0}{\left(1 + \frac{4\rho\omega^2 h_0^2 t}{3\eta}\right)^{\frac{1}{2}}} \quad \text{Equation 2-12}$$

After evaporation, the film becomes much thinner and the final xerogel film thickness is given by Equation 2-13:

$$h_{final} = \left(1 - \frac{\rho_{A'}}{\rho_A}\right) \left(\frac{3\eta e}{2\rho_{A'}\omega^2}\right)^{\frac{1}{3}} \quad \text{Equation 2-13}$$

In both equations, h_0 is the initial thickness, t is time, ω is the angular speed, ρ is the solution density, η is the solution viscosity, ρ_A is the mass of volatile solvent per unit volume, $\rho_{A'}$ is the initial value of this mass, and e is the evaporation rate that depends on the mass transfer coefficient.

MS derived TiO₂ films studied in the present work were deposited by using a SÜSS microtec CT 62 spin-coating instrument. The substrates were (100) silicon wafers of 3 x 3 cm² in size. Prior to be used, the silicon wafers were annealed at 500 °C for two hours and then stored in deionised water. Just before deposition, they were cleaned with ethanol and dried with air spray. Parameters that define the spinning process (i.e. spin-speed, acceleration, time, temperature) can result in important variations in the deposited film. It often requires to adapt a specific deposition procedure in relation to the sol characteristics, i.e. its dilution level, sol-gel reactivity, rheology, etc... In previous studies performed at LMGP, an optimized deposition procedure has been set up for the MS sol, which relies on an automatized program divided into three steps (Figure 2-8).

- In the first step, 300 µL of the sol (TIPT, HCl, absolute ethanol) are radially spread on a substrate at rest, and the substrate is then rotated at relatively high spin-speed of 3000 rpm for 1 second. This step serves to spread the sol over the substrate.
- Stabilized liquid films are then obtained by maintaining a 0 rpm spin-speed for 5 seconds.
- Evaporation of the solvent is finally controlled by centrifugal effect thanks to a low spin-speed of 100 rpm for 5 seconds.

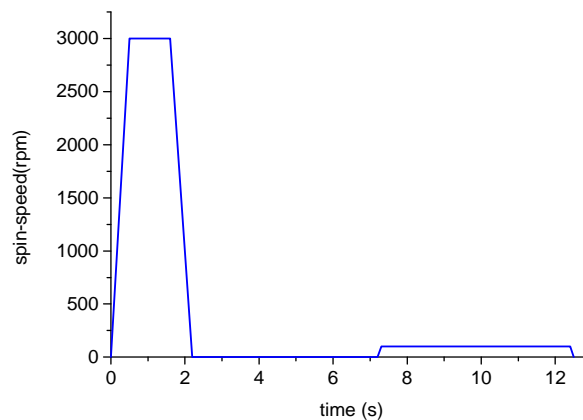


Figure 2-8: Spin-coating program for MS (mother solution) thin film deposition.

In such conditions, the so-obtained xerogel films exhibit uniform thickness and high optical quality, i.e. 90% of the substrate surface is coated with a thickness uniformity of about 1%, while the other 10% correspond to unavoidable edge and corner effects, where the thickness is greater than in the homogeneously coated area.

During the spin-coating procedure, MS films undergo a room temperature sol-gel transformation through hydrolysis/polycondensation reactions, which yields a solid amorphous xerogel film consisting of Ti-O-Ti chains with chain-end alkoxy and hydroxyl groups. This xerogel film is then annealed at 500°C and changes into a film crystallized in the anatase polymorphic form of TiO₂. This annealing temperature has been adopted according to previous studies showing that the best photocatalytic activity of TiO₂ MS films is obtained after a thermal treatment at 500 – 600°C [30, 31]. After thermal treatment, the films are cooled down to room temperature under ambient condition, stored in a plastic box, and kept in dark place opaque to UV radiation before use. The thickness of the film can be varied by using a multi-layer deposition procedure, i.e. through the repetition of deposition/thermal treatment cycles. According to previous studies, the film thickness plays an important role on the photocatalytic activity [30]. Contrary to our preliminary studies showing the feasibility of an Ag⁰/TiO₂ SERS substrate, where a seven-layers procedure was adopted, in this thesis a single-layer deposition procedure was preferred in order to reduce the time spent in the film elaboration. In these conditions, a 40 nm thickness was measured in the homogeneous area (90% of the substrate) after thermal treatment at 500 °C.

4. Extrapolation to an Ag⁰/TiO₂ SERS substrate: previous results

As mentioned before, this thesis relies on previous studies performed at LMGP, which showed the feasibility of a new Ag⁰/TiO₂ SERS substrate for the label-free detection of NH₂-terminated DNA molecules before and after their hybridization [26]. The substrate was elaborated through a photocatalytic reduction mechanism of silver nitrate (AgNO₃) adsorbed on a TiO₂ sol-gel film deposited in previously described conditions using a seven-layer deposition procedure. This bottom up approach led to Ag⁰/TiO₂ heterostructure constituted of metal Ag⁰ NPs dispersed at the surface of the TiO₂ film. As illustrated in Figure 2-9, these NPs exhibit isotropic shapes with a diameter ranging from few nanometers to several hundred of nanometers, i.e. a very broad size distribution, and appear heterogeneously dispersed on the TiO₂ surface. Despite such important drawbacks, these preliminary studies pointed out many potential assets of the proposed Ag⁰/TiO₂ SERS substrate [26].

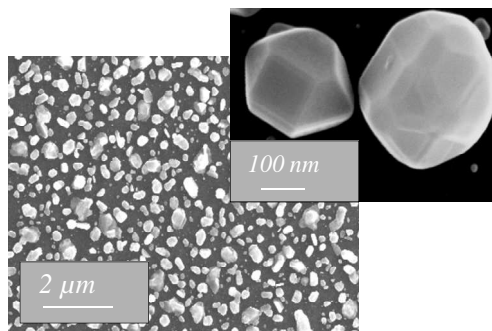


Figure 2-9: Low and high magnification FEG-SEM images of the TiO_2 film surface (dark area) after deposition of Ag° NPs (bright spots) [26].

First of all, this substrate takes advantage of its TiO_2 and Ag° components. Usually, a multistep and time consuming procedure is employed to graft DNA molecules on a traditional silicon substrate for further detection. This procedure particularly requires a silanization step, generally based on a preliminary surface functionalization using an amino-modified silicon alkoxide, followed by the use of a cross-linker molecule (glutaraldehyde) leading to a strong covalent bond between the amino groups of the functionalized substrate surface and amino groups constituting the NH_2 -terminated DNA molecules. In the previous studies, it was shown that the specificities of the proposed $\text{Ag}^\circ/\text{TiO}_2$ SERS substrate allowed a simplified one-step grafting procedure. It was assumed that this one-step procedure relied on the direct attachment of NH_2 -terminated DNA molecules on Ag° NPs, owing to the affinity of these latter toward amino groups, which led to the direct DNA grafting through the formation of Ag-N bonds. These results also pointed out the interest of a photo-hydrophilic TiO_2 surface. Since bare TiO_2 surface areas (uncoated with Ag° NPs) exhibited a superhydrophilic behavior after exposition to UV light during the photo-metallization step yielding Ag° NPs, it allowed an improved spreading of DNA-containing aqueous drops deposited on the substrate surface, which led to an enhancement in the uniform distribution of DNA molecules attached on the SERS substrate. This observation pointed out the interest to set up a photocatalytic reduction procedure leading to the alternation of Ag° -coated and TiO_2 bare areas, contrarily to the procedure proposed by others such as Mills *et al.*, which led to the photocatalytic deposition of an Ag° film totally covering the TiO_2 surface [17].

According to previously described features [26], it was possible to achieve the label-free SERS detection of DNA molecules grafted on the $\text{Ag}^\circ/\text{TiO}_2$ heterostructure (Figure 2-10 a), while pure Raman measurements (in the absence of Ag° NPs) did not allow such a detection (Figure 2-10 b), which pointed out the interest of a label-free SERS detection procedure. In particular, Raman bands of adenine and cytosine nucleobases constituting the DNA molecules were clearly identified through the SERS

detection. Previous results also allowed drawing conclusions on the spectral changes upon hybridization of the probe DNA molecules with complementary ones. In particular, these studies showed that hybridization causes a change in the relative intensity of the bands attributed to adenine and cytosine (Figure 2-10 c). It provided a direct way to differentiate single strand and double strand DNA obtained before and after hybridization, respectively, and attested that hybridization can be detected through DNA Raman spectra measured from the SERS platform.

However, the SERS spectra exhibited a weak signal/noise ratio as well as poor intensity reproducibility when measured in different areas of a same substrate, which restrained the reliability of conclusions drawn from these spectra and clearly demonstrated that the SERS substrate still required important optimization efforts.

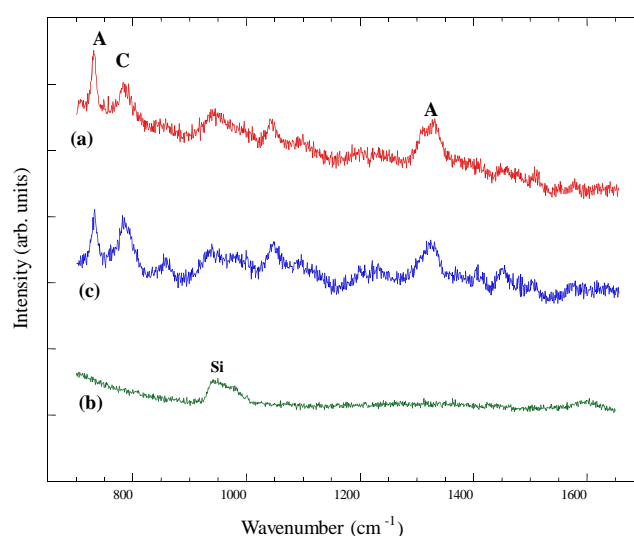


Figure 2-10: Raman spectra of single-stranded DNA grafted on an Ag[°]/TiO₂ heterostructure (a) and grafted on a bare (uncoated by Ag[°] NPS) TiO₂ film, where only the second order Si Raman line of the substrate is visible (b), and Raman spectrum of double-stranded DNA after hybridization on the Ag[°]/TiO₂ heterostructure (c). Main DNA lines are assigned to adenine (A) and cytosine (C) Raman modes.

These previous studies also showed that specificities arising from a sol-gel procedure responded to a very important challenge when considering DNA detection applications, i.e. the possibility to perform multiplexed analyses through a spatially addressed detection in order to rapidly and easily identify numerous biomolecules of different natures grafted on a single sample. The feasibility to answer such a challenge was demonstrated through the spatially addressed detection of a same DNA molecule grafted on a photo-patterned SERS substrate. For that purpose, a sol-gel procedure previously developed at LMGP was used [32]. Since, for time consuming reasons, this procedure could not be further exploited in the present thesis, it is only briefly summarized here. As explained before, a Ti-based sol can be chemically stabilized through the complexation of the titanium alkoxide with a chelating agent. In previous studies conducted at LMGP, it was shown that such a complexation can be performed using

Benzoyl-Acetone (BzAc) as a chelating agent, which yielded a Ti-BzAc alkoxo complex in solution. It was shown that, in proper conditions, derived TiO₂ xerogel films deposited at room temperature from this solution are chemically unstable and can easily be removed by washing in ethanol. Conversely, an exposure of these films to UVA light induces a photolytic decomposition of the Ti-BzAc complex, leading to an enhanced chemical stability of the xerogel film toward ethanol washing. A selective UVA exposition, through a mask or by laser exposition, associated to solubility contrasts between areas exposed or not to UVA light, finally enabled to implement a procedure leading to a fine photo-patterning of such sol-gel photoresists through a simplified one-step protocol. This simplified photo-patterning procedure is schematically represented in Figure 2-11. TiO₂ patterned films could in turn be crystallized in the anatase form through a thermal treatment at 500 °C yielding photocatalytic and photo-hydrophilic TiO₂ patterns [32].

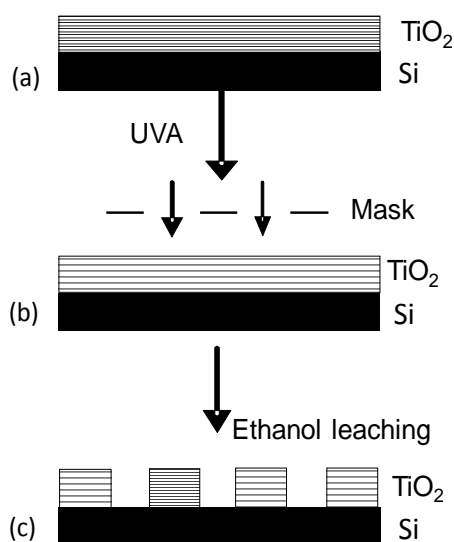


Figure 2-11: Photo-patterning of a sol-gel derived TiO₂ photoresist.

In further studies performed at LMGP to demonstrate the feasibility of an Ag⁰/TiO₂ SERS substrate, this protocol was used to pattern circular TiO₂ spots of 150 μm diameter (Figure 2-12 a) [26]. A subsequent photocatalytic reduction process yielded the selective growth of Ag⁰ NPs on the TiO₂ spots, while no Ag⁰ NPs could be grown on bare silicon substrate (uncoated by TiO₂ spots) areas. Finally, single strand DNA molecules were selectively immobilized on derived Ag⁰/TiO₂ spots using the previously described one-step grafting procedure, and their detection on different spots was achieved through SERS measurements. These measurements clearly indicated the presence of DNA on the spot surfaces, while no DNA could be detected on bare silicon regions. It is illustrated in Figure 2-12 b for the label-free detection of double strand (hybridized) DNA molecules. However, here again, the SERS

spectra suffered from a weak signal/noise ratio and poor intensity reproducibility when measured on different spots (spectra presented in Figure 2-12 b are a selection of best results).

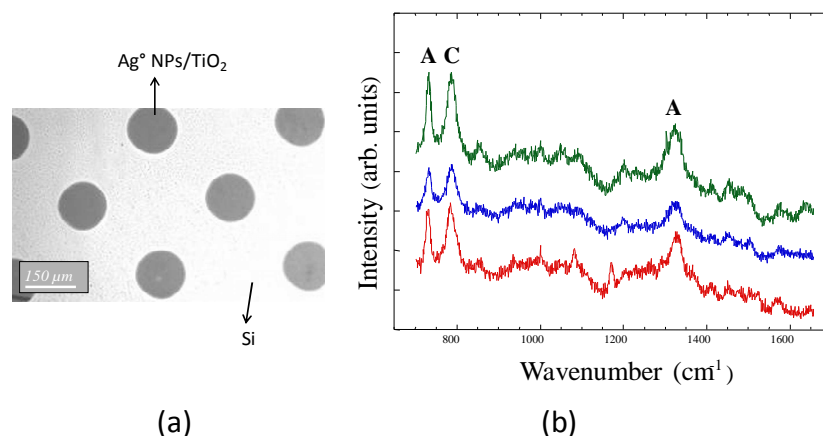


Figure 2-12: Optical image of photo-patterned $\text{Ag}^\circ/\text{TiO}_2$ spots (a), and Raman spectra of label-free double strand DNA immobilized on different photo-patterned $\text{Ag}^\circ/\text{TiO}_2$ spots. The main DNA lines are assigned to adenine (A) and cytosine (C) Raman modes.

According to these preliminary studies and despite some promising results, both the broad size dispersion and poor surface distribution of Ag° NPs grown on the TiO_2 film, as illustrated in Figure 2-9, appeared to be a strong drawback of this new SERS substrate, which affects the reproducibility, intensity, and reliability of DNA Raman spectra. On the one hand and based on the assumption that, in the case of the proposed one-step grafting procedure, DNA is mainly bonded to Ag° NPs (this particularly raises question about how to find additional experimental evidences of this grafting process), the size, amount, and surface distribution of Ag° NPs govern the amount of sites available for DNA grafting and hence the amount of DNA to be detected by Raman spectroscopy. On the other hand, as explained in chapter 1, their morphology, i.e. their size, shape, shape and size uniformity, aggregation state (hot spots), is also expected to intrinsically influence the Ag° NPs SERS activity. All these conclusions stress the importance to perform further studies in order to better control the morphology of Ag° NPs and their distribution on the SERS platform.

5. Conclusion

TiO_2 is a very versatile material owing to the multiplicity of its inherent properties. Its photo-induced properties (photocatalytic activity, photo-hydrophilicity), particularly when it is crystallized in its

anatase polymorphic form, largely contribute to the high interest devoted to TiO₂. In particular, this material can readily be deposited in the form of functional thin films through sol-gel routes. In recent studies performed at LMGP, the photo-induced properties of sol-gel derived TiO₂ thin films have been exploited to demonstrate the feasibility of a new Ag⁰/TiO₂ SERS substrate for label-free detection of DNA. In this bottom up approach, SERS active metal Ag⁰ NPs were grown on the TiO₂ film surface through a photocatalytic reduction procedure. Derived Ag⁰/TiO₂ heterostructure exhibited many assets, which were firstly assessed through the SERS detection of NH₂-terminated DNA molecules and their hybridization. According to specificities arising from the photo-induced properties of the TiO₂ film in association with a sol-gel procedure, such a SERS substrate also allowed the implementation of a simplified one-step grafting of DNA molecules and the possibility to perform a multiplexed spatially addressed detection of these molecules. However, these substrates still suffer from several drawbacks, which require further important optimizations. Among many other questions to address, it is crucial to perform further studies in order to better control the morphology of Ag⁰ NPs and their distribution on the SERS platform. The influence of these parameters on the SERS activity and the detection performances of the platform (reproducibility, durability, sensitivity, selectivity, reliability) constitutes the first main objective of this thesis. Besides, and as explained in chapter 1, before considering the SERS detection of complex multi-base DNA molecules, it is essential to improve the reliability of SERS detection on “simpler” single-base DNA molecules. This aspect constitutes the second main objective of this thesis.

- [1] A. Di Paola, M. Bellardita, and L. Palmisano, "Brookite, the least known TiO₂ photocatalyst," *Catalysts*, vol. 3, pp. 36-73, 2013.
- [2] H. A. Macleod, *Thin-film optical filters*: CRC Press, 2001.
- [3] N. Kumazawa, M. Rafiqul Islam, and M. Takeuchi, "Photoresponse of a titanium dioxide chemical sensor," *Journal of Electroanalytical Chemistry*, vol. 472, pp. 137-141, 1999.
- [4] Y. Leng, N. Huang, P. Yang, J. Chen, H. Sun, J. Wang, *et al.*, "Structure and properties of biomedical TiO₂ films synthesized by dual plasma deposition," *Surface and Coatings Technology*, vol. 156, pp. 295-300, 2002.
- [5] O. Carp, C. L. Huisman, and A. Reller, "Photoinduced reactivity of titanium dioxide," *Prog. Solid State Chem.*, vol. 32, p. 33, 2004.
- [6] X. Chen and S. S. Mao, "Titanium dioxide nanomaterials: synthesis, properties, modifications, and applications," *Chemical reviews*, vol. 107, pp. 2891-2959, 2007.
- [7] A. L. Linsebigler, G. Lu, and J. T. Yates Jr, "Photocatalysis on TiO₂ surfaces: principles, mechanisms, and selected results," *Chemical reviews*, vol. 95, pp. 735-758, 1995.
- [8] A. Fujishima and K. Honda, "Photolysis-decomposition of water at the surface of an irradiated semiconductor," *Nature*, vol. 238, pp. 37-38, 1972.
- [9] S. M. Gupta and M. Tripathi, "A review of TiO₂ nanoparticles," *Chinese Science Bulletin*, vol. 56, pp. 1639-1657, 2011.
- [10] R. Wang, K. Hashimoto, A. Fujishima, M. Chikuni, E. Kojima, A. Kitamura, *et al.*, "Light-induced amphiphilic surfaces," *Nature*, vol. 388, p. 431, 1997.
- [11] M. I. Litter, "Heterogeneous photocatalysis: transition metal ions in photocatalytic systems," *Applied Catalysis B: Environmental*, vol. 23, pp. 89-114, 1999.
- [12] Y. Nosaka, K. Norimatsu, and H. Miyama, "The function of metals in metal-compounded semiconductor photocatalysts," *Chemical physics letters*, vol. 106, pp. 128-131, 1984.
- [13] W. Y. Lin and K. Rajeshwar, "Photocatalytic Removal of Nickel from Aqueous Solutions Using Ultraviolet - Irradiated TiO₂," *Journal of the Electrochemical Society*, vol. 144, pp. 2751-2756, 1997.
- [14] W. Clark and A. Vondjidis, "An infrared study of the photocatalytic reaction between titanium dioxide and silver nitrate," *Journal of Catalysis*, vol. 4, pp. 691-696, 1965.
- [15] P. D. Fleischauer, H. K. A. Kan, and J. R. Shepard, "Quantum yields of silver ion reduction on titanium dioxide and zinc oxide single crystals," *Journal of the American Chemical Society*, vol. 94, pp. 283-285, 1972.
- [16] J.-M. Herrmann, J. Disdier, and P. Pichat, "Photocatalytic deposition of silver on powder titania: consequences for the recovery of silver," *Journal of Catalysis*, vol. 113, pp. 72-81, 1988.
- [17] A. Mills, G. Hill, M. Stewart, D. Graham, W. E. Smith, S. Hodgen, *et al.*, "Characterization of Novel Ag on TiO₂ Films for Surface-Enhanced Raman Scattering," *Applied Spectroscopy*, vol. 58, pp. 922-928, 2004.
- [18] E. Stathatos, P. Lianos, P. Falaras, and A. Siokou, "Photocatalytically Deposited Silver Nanoparticles on Mesoporous TiO₂ Films," *Langmuir*, vol. 16, pp. 2398-2400, 2000.
- [19] X. He, X. Zhao, and B. Liu, "Studies on a possible growth mechanism of silver nanoparticles loaded on TiO₂ thin films by photoinduced deposition method," *Journal of Non-Crystalline Solids*, vol. 354, pp. 1267-1271, 2008.
- [20] C. J. Brinker and G. W. Scherer, *Sol-gel science: the physics and chemistry of sol-gel processing*: Gulf Professional Publishing, 1990.
- [21] E. A. Barringer and H. K. Bowen, "High-purity, monodisperse TiO₂ powders by hydrolysis of titanium tetrathoxide. 2. Aqueous interfacial electrochemistry and dispersion stability," *Langmuir*, vol. 1, pp. 420-428, 1985.
- [22] J. Yu, X. Zhao, and Q. Zhao, "Photocatalytic activity of nanometer TiO₂ thin films prepared by the sol-gel method," *Materials Chemistry and Physics*, vol. 69, pp. 25-29, 2001.

- [23] T. Yoko, L. Hu, H. Kozuka, and S. Sakka, "Photoelectrochemical properties of TiO₂ coating films prepared using different solvents by the sol-gel method," *Thin Solid Films*, vol. 283, pp. 188-195, 1996.
- [24] J. Yu, X. Zhao, and Q. Zhao, "Effect of surface structure on photocatalytic activity of TiO₂ thin films prepared by sol-gel method," *Thin solid films*, vol. 379, pp. 7-14, 2000.
- [25] N. Negishi and K. Takeuchi, "Preparation of TiO₂ thin film photocatalysts by dip coating using a highly viscous solvent," *Journal of sol-gel science and technology*, vol. 22, pp. 23-31, 2001.
- [26] M. Langlet, I. Sow, S. Briche, M. Messaoud, O. Chaix-Pluchery, F. Dherbey-Roussel, *et al.*, "Elaboration of an Ag⁰/TiO₂ platform for DNA detection by surface enhanced Raman spectroscopy," *Surface Science*, vol. 605, pp. 2067-2072, 2011.
- [27] M. Langlet, M. Burgos, C. Coutier, C. Jimenez, C. Morant, and M. Manso, "Low temperature preparation of high refractive index and mechanically resistant sol-gel TiO₂ films for multilayer antireflective coating applications," *Journal of sol-gel science and technology*, vol. 22, pp. 139-150, 2001.
- [28] M. Langlet, A. Kim, M. Audier, C. Guillard, and J. M. Herrmann, "Liquid phase processing and thin film deposition of titania nanocrytallites for photocatalytic applications on thermally sensitive substrates," *Journal of Materials Science*, vol. 38, pp. 3945-3953, 2003.
- [29] D. E. Bornside, C. W. Macoscko, and L. E. Scriven, "On the modeling of spin coating," *J.Imaging.Tech*, vol. 13, pp. 122-130, 1987.
- [30] M. Langlet, S. Permpoon, D. Riassetto, G. Berthomé, E. Pernot, and J. C. Joud, "Photocatalytic activity and photo-induced superhydrophilicity of sol-gel derived TiO₂ films," *Journal of Photochemistry and Photobiology A: Chemistry*, vol. 181, pp. 203-214, 2006.
- [31] M. Fallet, S. Permpoon, J. L. Deschanvres, and M. Langlet, "Influence of physico-structural properties on the photocatalytic activity of sol-gel derived TiO₂ thin films," *Journal of Materials Science*, vol. 41, pp. 2915-2927, 2006.
- [32] S. Briche, Z. Tebby, D. Riassetto, M. Messaoud, E. Gamet, E. Pernot, *et al.*, "New insights in photo-patterned sol-gel-derived TiO₂ films," *Journal of Materials Science*, vol. 46, pp. 1474-1486, 2011.

Chapter 3. Tailored silver nanoparticles for surface enhanced Raman spectroscopy substrates

1. Introduction

In the previous chapter, we described a new bottom up approach based on a photocatalytic reduction mechanism at the surface of sol-gel deposited TiO_2 thin films. We showed that this low cost wet chemistry procedure yields $\text{Ag}^\circ/\text{TiO}_2$ heterostructure with a promising potential as new SERS substrates. However, the photocatalytic reduction mechanism led to a large dispersion in the size of SERS-active Ag° NPs and to a poorly homogeneous distribution of these NPs at the TiO_2 surface, which required further important optimization to improve the reproducibility of the Raman bands intensity. As mentioned in section 5 of chapter 1, very few works have been devoted to the photocatalytically assisted growth of Ag° NPs on TiO_2 substrates for SERS. Thus, there is a real need to perform thorough investigations on the mechanisms leading to the controlled growth of Ag° NPs through a photocatalytic reduction process. It is the aim of this chapter, where we only focus on the morphology of Ag° NPs, while the SERS performances of derived Ag/TiO_2 heterostructure will be investigated in the next chapter.

Numerous chemical or photo-chemical methods have been proposed in the literature to grow Ag° NPs in liquid solution. These methods are based on the use of specific chemical reagents and yield liquid suspensions of size and shape controlled Ag° NPs. For instance, the weak reducing activity of ascorbic acid (AA) [1-3] and the stabilizing effect of tri-sodium citrate (TSC) [4-7] have often been used, in combination or not, to tailor the size and shape of metal NPs through a single growth or a two-step seeded growth procedure in liquid solution. While such approaches have shown a huge potential to form metal NPs in liquid suspension, their extrapolation to the controlled immobilization of Ag° NPs on a solid substrate has rarely been investigated. Actually, only some rare reports mention the use of AA and/or TSC to grow Ag° NPS on solid substrates through chemical approaches [8, 9], and we could not find any report describing the use of such chemical reagents to assist the photocatalytically induced growth of Ag° NPs on a substrate. In this chapter, we present new studies on a chemically assisted seeded growth procedure aiming at improving the uniformity of $\text{Ag}^\circ/\text{TiO}_2$ heterostructure formed by photocatalytic reduction. We mainly study how this procedure enables a controlled growth of Ag° NPs in various amounts leading to the homogeneous dispersion or aggregation of these NPs at the surface of TiO_2 films. First, we present a one step photocatalytic reduction procedure employing TSC as stabilizing agent. Then, we apply a two-step TSC-assisted seeded growth procedure aiming at improving the

uniformity of derived Ag⁰ /TiO₂ heterostructure. We finally conclude by discussing a possible self-limited growth/aggregation process of Ag⁰ NPs.

2. Characterizations

The morphology (size, distribution, aggregation level) of Ag⁰ NPS was investigated by Field Emission Gun - Scanning Electron Microscopy (FEG-SEM) imaging using a FEI Quanta FEG 250 apparatus operated at 20 kV in secondary electron mode. NPs counting was realized from FEG-SEM images on several 1.5 x 1.5 μm² areas using the *Image-Pro Plus V4* software. The surface coverage rate (SCR) of Ag⁰ NPs was estimated on several 3 x 3 μm² areas using the *Image J* software. A Philips XL 30 SEM operated at 10 kV was employed for energy dispersive X-ray (EDX) analyses. The Ag (Lα) / Ti (Kα) peak intensity ratio deduced from EDX measurements was used to study the amount of deposited silver on several 360 x 480 μm² areas. Since the Ti peak intensity only accounts for the TiO₂ film, whose thickness is fixed at 40 nm, the Ag / Ti EDX ratio (in at%) is directly related to the silver amount and allows reliable comparisons between different elaboration conditions. In order to support the above analysis, we also performed X-ray photoelectron spectroscopy (XPS) characterizations. XPS spectra were acquired at Laboratoire de Réactivité des Surfaces (LRS-UPMC) using a SPECS (Phoibos 100-5 MCD) X-ray photoelectron spectrometer equipped with a monochromatised aluminum (Al Kα) X-ray source (hν = 1486.6 eV) powered at 10 mA and 15 kV and a Phoibos 100 hemispherical energy analyzer at a constant take-off angle of 90°. The spectra were calibrated with respect to the C1s peak at 284.8 eV. Structural studies were performed through cross-section Transmission Electron Microscopy (TEM) observations using a JEOL-2010 LaB6 instrument operated at 200 keV. Selected Area Electron Diffraction (SAED) patterns associated to TEM images and Fast Fourier transform (FFT) performed on high resolution TEM (HRTEM) images were employed to get insights in the crystallographic state of Ag⁰ NPs.

3. One-step photocatalytic reduction

3.1 Non-assisted photocatalytic reduction

As mentioned in chapter 2, when a TiO₂ thin film is exposed to UVA light (λ < 380 nm), it promotes the formation of electrons (e⁻) and holes (h⁺) pairs, which induce redox mechanisms at the film surface. The photo-induced electrons can for instance promote the reduction of Ag⁺ cations adsorbed at the film surface, which leads to the formation of metal Ag⁰ NPs. However, as mentioned in different papers, this photo-reduction mechanism can rapidly lead to the uncontrolled growth of NPs with a large size

distribution [10, 11]. In Figure 3-1, we schematically propose a model to illustrate this feature. Over the first stages of the photocatalytic reduction, Ag^+ cations adsorbed at the film surface form metal nuclei induced by the reduction ability of photo-electrons and, once these nuclei exceed a threshold critical size, Ag° NPs start growing. Over the subsequent stages of the photocatalytic reduction, new Ag^+ cations adsorb and new Ag° NPs start growing, while previously formed Ag° NPs undergo further growth. It rapidly yields some size heterogeneity of the NPs (Figure 3-1a).

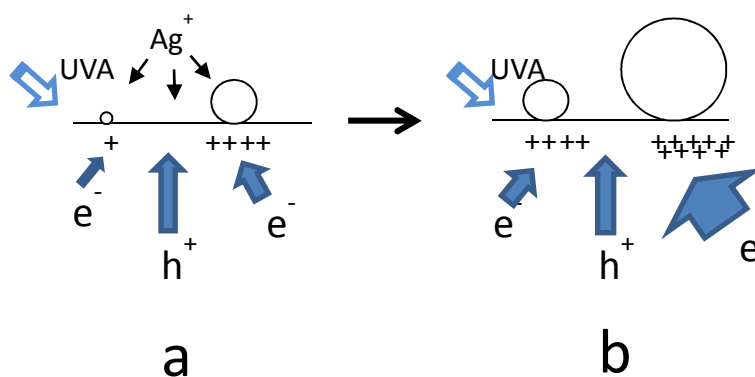


Figure 3-1: Proposed schematic representation of the mechanisms leading to Ag° NPs at the surface of a TiO_2 film over a single-step photocatalytic process: (a) and (b) depict phenomenological evolutions over UVA exposure.

This heterogeneity can in turn be strongly amplified by Schottky barrier effects at the metal-semiconductor interfaces. These effects have been previously studied in the team by D.Riassetto during his thesis at LMGP in the case of platinum NPs dispersed on the surface of TiO_2 thin films [12]. It is inferred that the mechanisms can be extrapolated to Ag° NPs. Schottky barriers promote an electron depletion in the surface regions of the semiconductor film in contact with metal NPs. Over UVA exposure, photo-induced electrons are thus preferentially directed toward the surface regions where metal NPs have initially been grown (Figure 3-1a) and subsequently transferred to these NPs where they contribute to further particle growth through the reduction of newly adsorbed Ag^+ cations (cathodic process, Figure 3-1b). Photo-induced holes are concomitantly directed toward the bare TiO_2 surface areas where they are harvested by the liquid electrolyte (anodic process). This spatial separation reduces the recombination probability of holes and electrons. It favors a greater flux of photo-electron reaching the surface and thus an enhanced photocatalytic reduction rate. Besides, since the electron depletion is all the more pronounced as metal NPs exhibit a larger size, photo-induced electrons are preferentially directed toward largest NPs, which promotes the preferential growth of these NPs to the detriment of the smallest ones and dramatically accelerates a heterogeneous growth of the NPs (Figure 3-1b).

This description can probably explain previous results obtained in the team by I.Sow at LMGP [10]. As illustrated in FEG-SEM images of Figure 2-9 in chapter 2, these previously studied growth conditions

led to nearly spherical Ag° NPs heterogeneously distributed at the substrate surface. The NPs diameter ranged from a few nanometers (which probably traduces NPs formed in the ultimate stages of the photocatalytic process) to several hundred of nanometers (NPs grown since the early stages of the photocatalytic process). Well faceted NPs illustrated in the high magnification FEG-SEM image of Figure 2-9 in chapter 2 also indicate that even largest NPs consisted of single-crystal (non-aggregated) particles.

In this thesis, several approaches have been investigated to improve the size uniformity of photocatalytically grown Ag° NPs. We firstly inferred that a slower growth would be more easily controlled and would favor the formation of more uniform NPs. Thus, compared to previous works, several adjustments have been performed to reduce the photocatalytic growth kinetic. Compared to the previous one (100 mM), the AgNO_3 concentration in liquid solution has been considerably decreased (0.2 or 2 mM) to reduce the probability of Ag^+ cation adsorption and the subsequent NPs growth kinetic. Since the photocatalytic rate increases with the thickness of our TiO_2 films [13], we also reduced the film thickness by using a single-layer deposition procedure yielding a 40 nm thickness instead of the ~250 nm thickness previously achieved from a 7-layers deposition procedure. This choice also allowed to considerably reduce the duration of the elaboration procedure. The nature of the AgNO_3 dilution medium has also a strong impact, since its capacity to harvest photo-induced holes at the film surface decreases the hole-electron recombination probability and increases the flux of photo-induced electrons reaching the film surface to promote the Ag^+ reduction. Contrary to previous works, where a water-ethanol liquid medium was used to take advantage of the strong hole-harvesting activity of ethanol, a pure water medium of weaker hole-harvesting power has been used in the present work. The FEG-SEM image of Figure 3-2a typically illustrates the morphology of Ag° NPs obtained in these new conditions. Compared to previous works, the effects of a reduced photocatalytic activity are clearly evidenced by a much smaller mean size of Ag° NPs uniformly dispersed at the film surface. However, this image also shows that the Ag° SCR (Surface Coverage Rate) is quite weak and FEG-SEM image analyses illustrated in the inset indicate that the NPs still exhibit some important size heterogeneity.

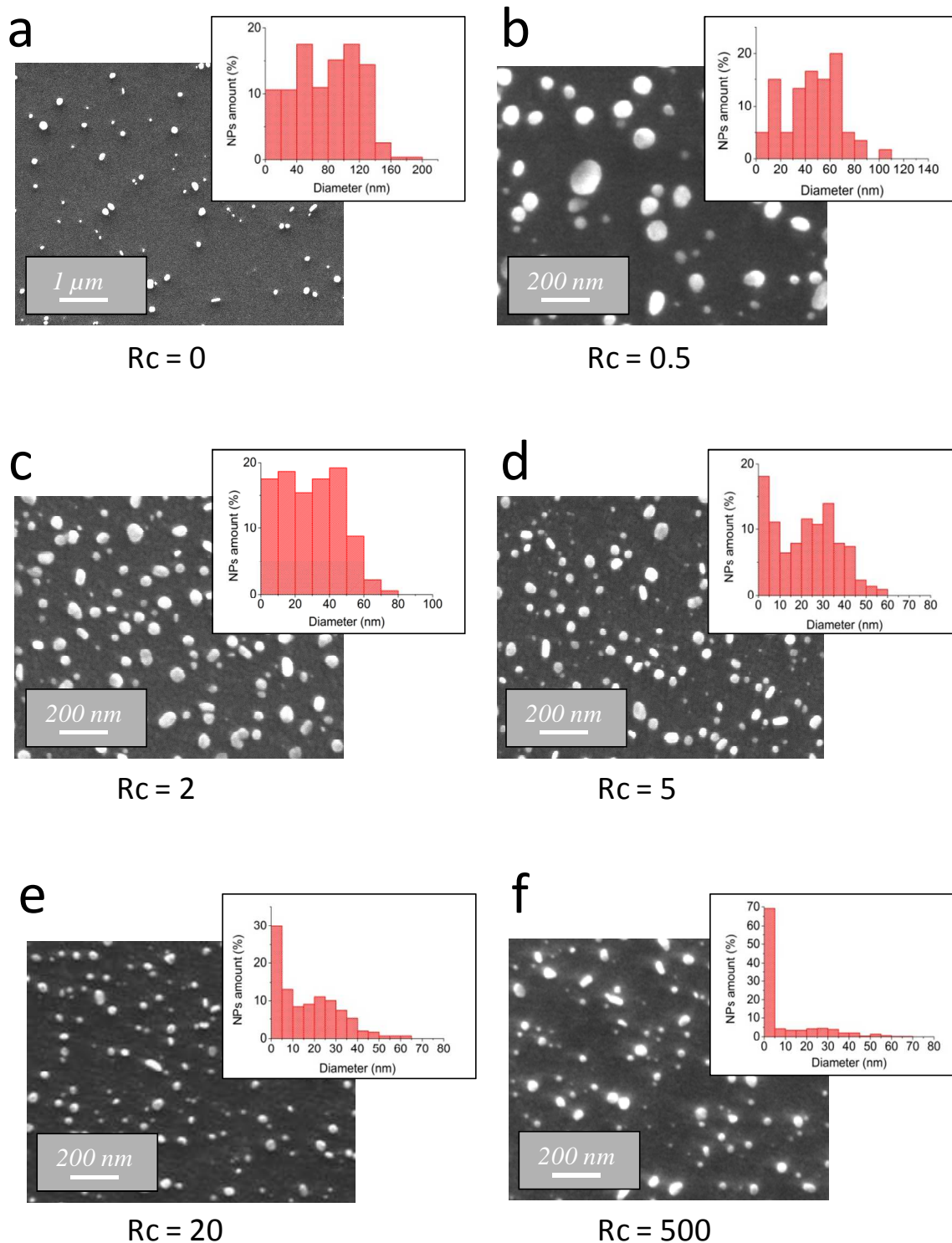


Figure 3-2: FEG-SEM images of Ag° NPs formed through a photocatalytic process as studied in the present work for an AgNO₃ concentration of 0.2 mM, an UVA exposure duration of 5 min, and with different TSC/AgNO₃ molar ratio (Rc) ranging from 0 to 500. The insets illustrate the Ag° NPs diameter distribution deduced from the analysis of different FEG-SEM images.

3.2 Trisodium citrate (TSC)-assisted photocatalytic reduction

3.2.1 Influence of Rc for fixed UV duration

New approaches have thus been studied to favor a large amount of Ag⁰ NPs with improved size uniformity. The photocatalytic reduction of AgNO₃ has firstly been chemically assisted by TSC. In first experiments, the AgNO₃ concentration and UVA exposition duration were fixed at 0.2 mM and 5 min, respectively, and the TSC / AgNO₃ molar ratio, so-called Rc ratio, was varied from 0 to 500. The effects of TSC on the NPs growth can be summarized by a bi-regime mechanism, which has firstly been evidenced by EDX measurements (Figure 3-3).

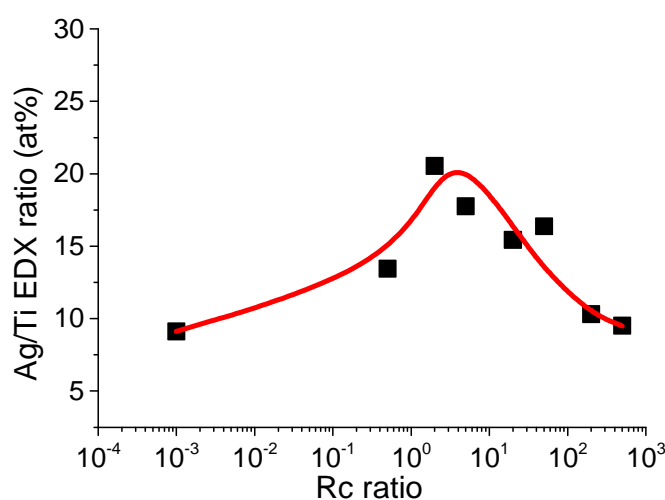


Figure 3-3: Influence of the Rc ratio on the Ag/Ti EDX ratio for an UVA exposure duration and AgNO₃ concentration fixed at 5 min and 0.2 M, respectively.

The Ag / Ti EDX ratio sharply increased when increasing the Rc ratio from 0 to around 5, and then underwent a continuous decrease when increasing again the Rc ratio up to 500. These trends are supported by FEG-SEM images of Figures 3-2a to f and their inset. Compared to a photocatalytic growth without TSC (Figure 3-2a), these images show that increasing the Rc ratio up to 5 (Figures 3-2b to d) continuously reduces the NPs size and concomitantly increases the number and size homogeneity of NPs dispersed at the TiO₂ surface (insets of Figures 3-2b to d). Image analyses showed that the mean diameter of NPs formed from a Rc ratio of 5 was about 30 nm even if some larger particles with a diameter ranging up to 60 nm could still locally be observed (inset of Figure 3-2d). As illustrated in Figures 3-2 e and f, further size reduction and homogeneity improvements remained very minor when increasing the Rc ratio above 5. Besides, a second family of smaller particles with a diameter of 5-10 nm started appearing for a Rc ratio of 5 (inset of Figure 3-2d). The inset of Figure 3-2e shows that the

relative amount of these new particles sharply increased when increasing the Rc ratio up to 20 and these small particles became all the more predominant as the Rc ratio increased up to 500 (inset of Figure 3-2f), i.e. the relative amount of 30 nm diameter NPs continuously decreased.

It is well known that TSC stabilizes or slows down the chemically assisted growth of Ag° NPs because citrate anions efficiently cap crystallographic planes of growing NPs [4-7, 9]. This effect has for instance been used, in association with other chemicals, to promote the preferential growth of shape-tailored Ag° NPs (cubic, triangular plates, or else) in liquid suspension. In the present study, since no other chemical was used, the FEG-SEM images of Figures 3-2b to f show that TSC essentially promoted an isotropic growth of NPs, similarly to what occurs in the absence of this chemical (Figure 3-2a), and it also strongly reduced the size and increased the uniformity and number of the Ag° NPs. In studies devoted to the photochemical (non photocatalytic) growth of Ag° NPs in liquid suspension, it has been reported that TSC can also act as a photo-reducer [14]. In our conditions, as illustrated in Figures 3-2a to d, it is possible that, when increasing the Rc ratio up to a threshold value around 5, this photo-reducing effect contributes to an increasing number of Ag° NPs. On the one hand, the photo-reducing activity of TSC may act in synergy with the photocatalytic mechanism to reduce adsorbed Ag^+ cations at the film surface. On the other hand, by preventing the hole-electron recombination through the efficient harvesting of photo-induced holes at the film surface, the TSC photo-reducer may induce a greater amount of photo-induced electrons prone to react through a photocatalytic surface mechanism. However, our results show that the photo-chemical activity of TSC does not alter the uniformity neither contribute to an accelerated growth of large NPs, which means that TSC-induced capping effects predominate in the growth mechanism. Besides, the photo-reducing activity of TSC can also promote the formation of small Ag° NPs in the liquid solution, which can in turn adsorb on the substrate. This assumption may explain the formation of two families of NPs above a Rc value of 5, i.e. 5-10 nm NPs formed in solution and subsequently adsorbed, which coexist with 30 nm NPs photocatalytically grown at the substrate surface. As the Rc ratio increases above 5, the TSC-induced photo-reduction may prematurely consume Ag^+ cations in solution, thus decreasing the amount of adsorbed cations available for a photocatalytic reduction at the film surface, which would explain why 30 nm NPs are progressively replaced by 5-10 nm ones. This feature may in turn explain EDX data when increasing the Rc ratio above 5. Indeed, the Ag / Ti EDX ratio accounts for the amount of deposited silver atoms. It means that this ratio is not only influenced by the number of deposited NPs but also by their volume. Considering that, compared to NPs of around 30 nm diameter, the volume of NPs with a 5-10 nm diameter is reduced by one or two orders of magnitude, it is obvious that these latter small particles insignificantly contribute to the EDX ratio. It may explain why the Ag / Ti ratio continuously decreases when these small NPs progressively replace larger ones for Rc values increasing above 5 (Figure 3-3).

3.2.2 Effect of UV duration and AgNO₃ concentration

In the following and according to previous features, the Rc ratio has been fixed at 5 in order to reduce both the mean size of photocatalytically grown NPs and the amount of the second family of smaller NPs. However, even for this Rc value, the FEG-SEM image of Figure 3-2d shows that the SCR of Ag⁰ NPs was still rather weak. Accordingly, no significant SERS enhancement could be observed on such Ag⁰/TiO₂ heterostructure. The weak SCR probably traduces that, in these new studies, we adopted conditions governed by a too weak photocatalytic activity and/or UVA exposure duration. Accordingly, keeping a Rc ratio of 5 and an UVA exposure duration of 5 min, we could significantly improve the SCR by increasing the AgNO₃ concentration from 0.2 to 2 mM, and the corresponding Ag / Ti EDX ratio was concomitantly amplified by a factor 3 (Figure 3-4). Keeping a same Rc ratio of 5 and an AgNO₃ concentration of 2 mM, we could again increase the SCR by prolonging the UVA exposure from 5 to 60 min. The corresponding Ag / Ti EDX ratio was again amplified by a factor 3 (Figure 3-5), i.e. by about one order of magnitude compared to the conditions illustrated in Figure 3-2d for a same Rc ratio.

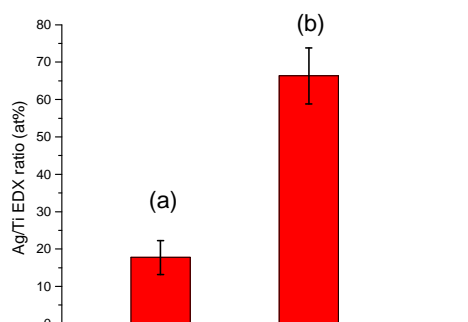


Figure 3-4: Ag/Ti EDX ratio for an UVA exposure duration fixed at 5 min and an AgNO₃ concentration fixed at 0.2 mM (a) and 2 mM (b).

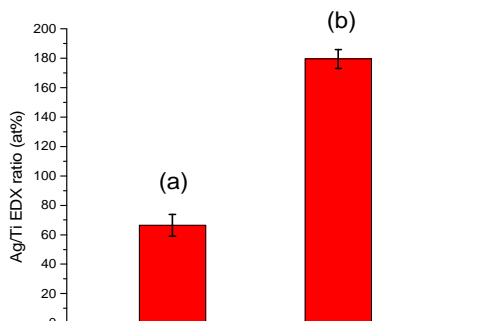


Figure 3-5: Ag/Ti EDX ratio for an AgNO₃ concentration fixed at 2 mM and an UVA exposure duration fixed at 5 min (a) and 60 min (b).

These new conditions are illustrated by the FEG-SEM images of Figure 3-6. The low magnification image of this figure depicts the alternation of regions of weak and strong SCR. On the one hand, the high magnification FEG-SEM image of this figure reveals that regions of weak coverage consist of individually dispersed small NPs (30 nm or less in diameter), which arise from previously discussed TSC-assisted growth mechanisms. On the other hand, this high magnification image reveals that regions with a high SCR correspond to aggregates of NPs. In that case, aggregation features did not allow a precise quantification of the NPs size through the analysis of FEG-SEM images, but grain boundaries observed in the high magnification image on Figure 3-6 indicate that the diameter of NPs constituting these aggregates lies within the 50-100 nm range. However, the low magnification image of this figure also shows that these aggregates exhibit a rather heterogeneous size and distribution at the substrate surface.

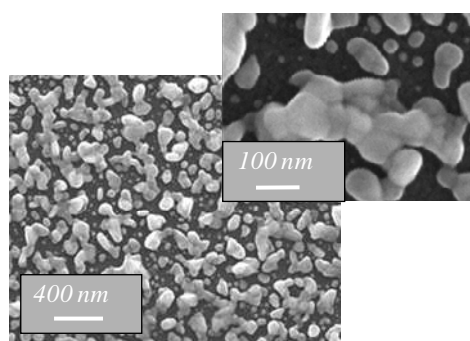


Figure 3-6: FEG-SEM images of Ag⁰ NPs formed through a photocatalytic process, as studied in the present work for an AgNO₃ concentration of 2 mM, an UVA exposure of 60 min, and a Rc ratio of 5.

These features yield two kinds of conclusions concerning the TSC effects. On the one hand, they show that previously detailed capping effects of TSC do not sufficiently prevent a heterogeneous growth and surface distribution of NPs when increasing the photocatalytic activity and/or UVA exposure duration. On the other hand, TSC strongly influences the photocatalytic growth of these NPs. Indeed, in contrast to Ag⁰ heterostructure studied in previous works, which constituted of heterogeneous single-crystal NPs the size of which ranged up to several hundred of nanometers (Figure 2-9 in chapter 2), data illustrated in Figure 3-6 show that TSC favors the growth of much smaller NPs of 100 nm or less in diameter. As will be discussed in next sections, this small size is in turn governed by aggregation features induced by TSC. According to these studies, in the following, the AgNO₃ concentration and Rc ratio have definitely been fixed at 2 mM and 5, respectively, and we have developed a new procedure involving a two-step seeded growth process to further improve the uniform growth and aggregation of Ag⁰ NPs.

4. Seeded growth assisted photocatalytic reduction

4.1 Seeded growth principle and seed deposition

The expected effects of a two-step seeded growth assisted photocatalytic reduction are illustrated in Figure 3-7. This procedure firstly relies on the preliminary dispersion of small and homogeneous Ag° NPs at the TiO_2 film surface (seed step). Then, when subsequently exposed to UVA light in the presence of an AgNO_3 liquid solution, so-obtained $\text{Ag}^\circ/\text{TiO}_2$ heterostructure will undergo previously described photocatalytic growth mechanisms governed by Schottky barrier effects (growth step). However, contrary to the mechanisms illustrated in Figure 3-1, and according to their homogeneous size and uniform dispersion at the film surface, it is expected that each metallic seed will attract a comparable amount of photo-electrons, which should induce further growth of uniform metal NPs through the photo-reduction of newly adsorbed Ag^+ cations (Figure 3-7a). Over subsequent UVA exposure stages, so-grown NPs will create an enhanced electron depletion at the metal-semiconductor interface, which should attract an increased amount of photo-electrons and accelerate the NPs growth rate. However, since so-grown NPs exhibit a similar size, Schottky barrier effects are still expected to induce a comparable attraction of photo-electron toward each NPs, which should preserve the NPs size uniformity over subsequent photo-induced growing steps (Figure 3-7b). As will be discussed in sections 4.1.2, this growth process is expected to finally stop owing to aggregation features.

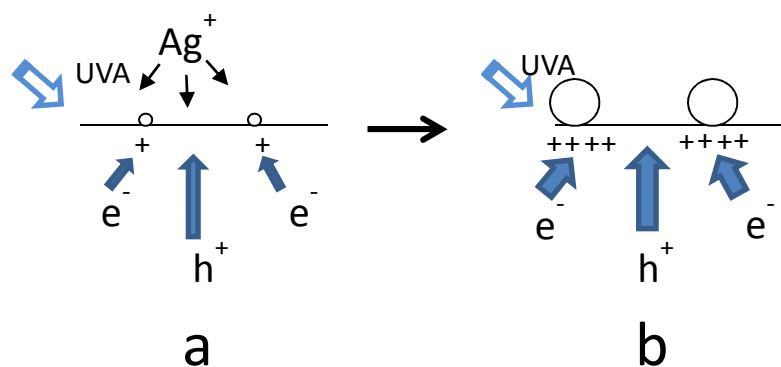


Figure 3-7: Proposed schematic representation of the mechanisms leading to Ag° NPs at the surface of a TiO_2 film over a seeded growth photocatalytic process in the early stages of the growth/aggregation process: (a) and (b) depict phenomenological evolutions over UVA exposure.

Various seeded growth routes have been proposed in the literature to synthesize size- and/or shape-controlled Ag° NPs in liquid suspension through chemical or photochemical mechanisms. Ascorbic acid (AA) is often used as a chemical agent during the growth step. Its weak reducing activity allows a slow and well-controlled growth at the surface of seeds preliminary formed in liquid solution [3, 5-7]. Some

authors have also extrapolated the mechanisms to chemically assist a seeded growth of Ag° NPs at the surface of solid substrates [8, 9]. Though more rarely reported in the literature, the weak reducing activity of AA has also been used to directly grow (one-step growth) small Ag° NPs in liquid solution in the presence of specific co-reagents [1, 2]. In the present work, we have adapted such an AA assisted growth (one-step) to preliminarily deposit seeds at the surface of our substrates in order to promote a subsequent seeded growth assisted photocatalytic reduction. To the best of our knowledge, such a procedure has never been reported in the literature.

The seed deposition has been implemented using a dual AgNO_3 and AA spin-coating deposition (Figure 3-8). The spin-coating procedure was adopted to uniformly disperse AgNO_3 and AA species on $3 \times 3 \text{ cm}^2$ substrates. Usually, AgNO_3 and AA are easily diluted in water. In this work, these species were diluted in absolute ethanol instead of water for two reasons. On the one hand, owing to its low surface tension compared to water, ethanol is more prone to uniformly spread diluted species during the liquid phase spin-coating procedure and subsequent solvent evaporation step. On the other hand, since AA should promote a cathodic reduction mechanism, the higher oxidative power of ethanol is expected to play a synergetic role in the balancing anodic mechanism. However, the amount of deposited AgNO_3 and AA species was limited by the reduced dilution ability of ethanol, i.e. the concentration of AgNO_3 and AA was fixed at 0.02 and 0.05M, respectively. For this reason, we employed a multilayer deposition procedure to increase the amount of deposited seeds.

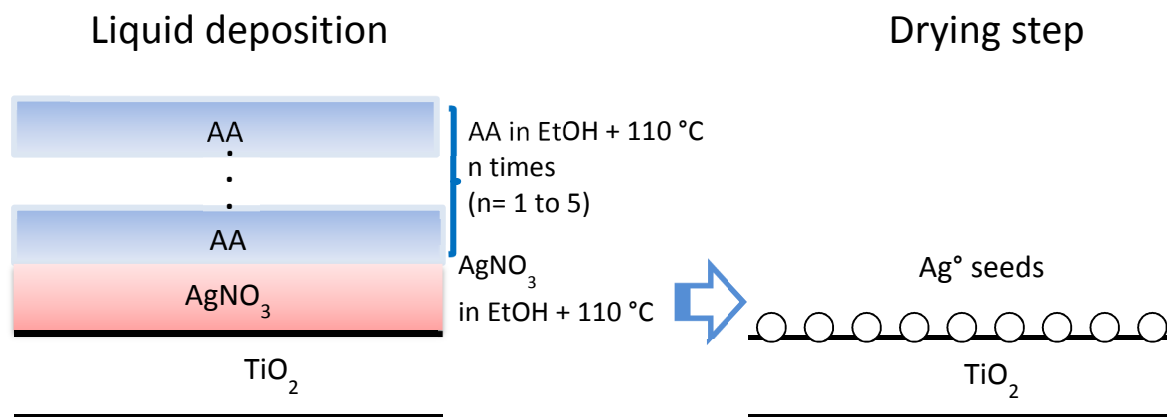


Figure 3-8: Schematic presentation of n -seed layer deposition ($n=1$ to 5).

Figures 3-9a and b show the FEG-SEM images and size histograms of so-deposited Ag° seeds after a 1-seed layer ($\text{AgNO}_3 + \text{AA}$) deposition and a 5-seed layer deposition, respectively. From the Figure 3-9a, it is clear that a rather small amount of seeds are dispersed at the substrate surface. They exhibit a narrow size distribution with an average diameter around 15-20 nm. Increasing the number of deposition

operations of AA significantly enhances the amount of deposited seeds and only promotes a minor increase of their size, since the average seed diameter ranges between 20 and 25 nm (Figure 3-9b). In any cases, this AA-assisted chemical approach yielded NPs much smaller than those obtained in our best TSC-assisted photocatalytic conditions (Figure 3-2d), since NPs of diameter above 35 nm were never observed.

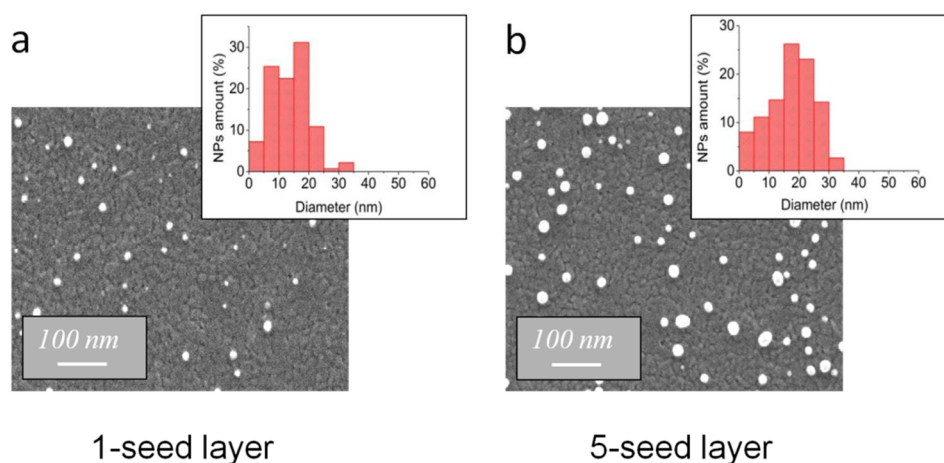


Figure 3-9: FEG-SEM images of Ag° seeds formed through an AA-assisted spin-coating deposition using a 1-seed layer (a) and a 5-seed layer procedure (b). The insets illustrate the Ag° seeds diameter distribution deduced from the analysis of different FEG-SEM images.

4.1.1 Morphological and structural characterizations

SEM characterizations

The TSC-assisted photocatalytic reduction process was then employed to grow Ag° NPs on AA-deposited seeds. Figure 3-10 depicts how, for a fixed seed layers number of 3 (a fixed UVA exposure duration of 60 min), a variation of the UVA exposure duration (of the seed layers number) influences the Ag/Ti EDX ratio and the Ag° SCR. This figure shows that the EDX ratio and SCR are primarily controlled by the UVA exposure duration. The SCR rapidly increases over the first ten minutes of UVA exposure and then undergoes a much slower increase (Figure 3-10a). In contrast, the EDX ratio follows a more gradual increase over a 60 min UVA exposure (Figure 3-10b). This influence of the UVA exposure duration is illustrated by the FEG-SEM images of Figures 3-10b to d for a 3-seed layer. After 10 min of UVA exposure, some aggregates of Ag° NPs start appearing and coexist with some dispersed small NPs (Figure 3-11b).

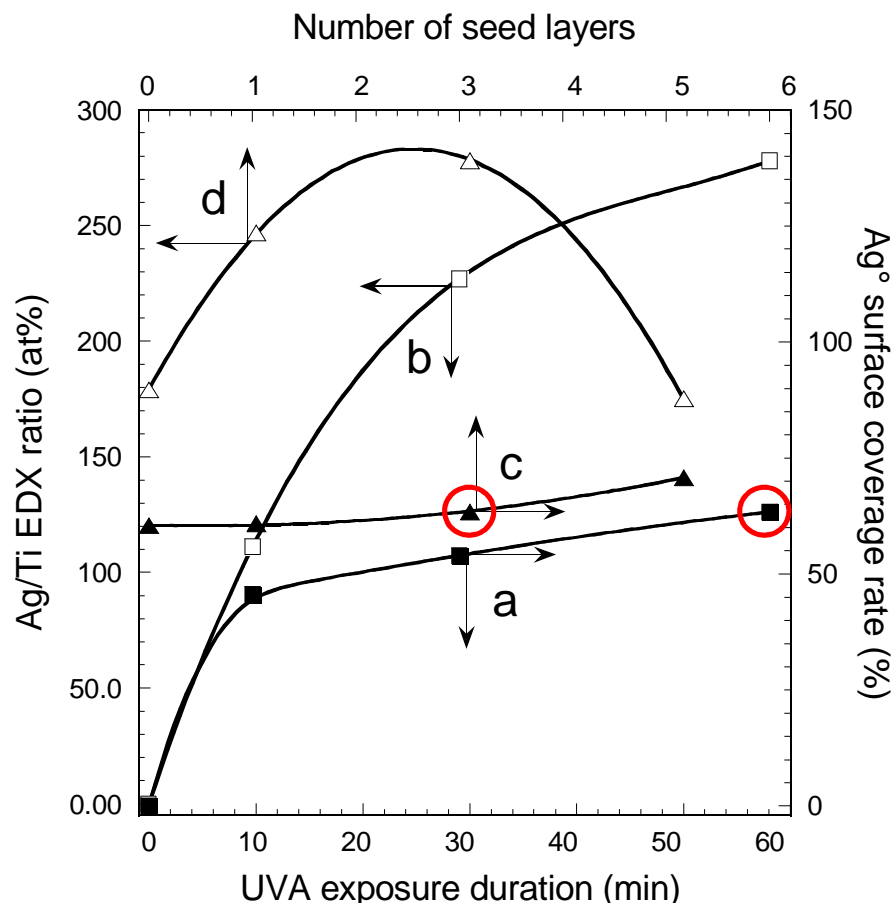


Figure 3-10: Influence of the UVA exposure duration on the Ag° SCR (a) and the Ag/Ti EDX ratio (b) for a number of seed layers fixed at 3, and influence of the seed layer number on the Ag° SCR (c) and the Ag/Ti EDX ratio (d) for an UVA exposure duration fixed at 60 min. The seeded growth TSC-assisted photocatalytic process was performed using a Rc ratio of 5 and an AgNO₃ concentration of 2 mM. The circles indicate conditions that have subsequently been tested by XPS.

Compared to the FEG-SEM image of Figure 3-6 in the absence of seeds, aggregates formed on a 3-seed layer exhibit a more uniform size and surface distribution. After 30 min of UVA exposure, some aggregates are observed to grow through a percolation phenomenon, keeping a fairly uniform size and surface distribution, and the number of individually dispersed NPs concomitantly decreases (Figure 3-11c). This trend is again enhanced after 60 min of UVA exposure, which leads to the total and uniform percolation of previously formed aggregates (Figure 3-11d). The high magnification FEG-SEM images illustrated in the insets of Figures 3-11b to d also indicate that these trends are accompanied by a growth of the NPs constituting the aggregates. While initially aggregated particles exhibit a rather spherical shape with a diameter of about 50 nm (inset of Figure 3-11b), further UVA exposure leads to more oblong particles whose smaller dimension is still close to 50 nm while the greater dimension reaches about 100 nm after a 60 min exposure (inset of Figure 3-11d).

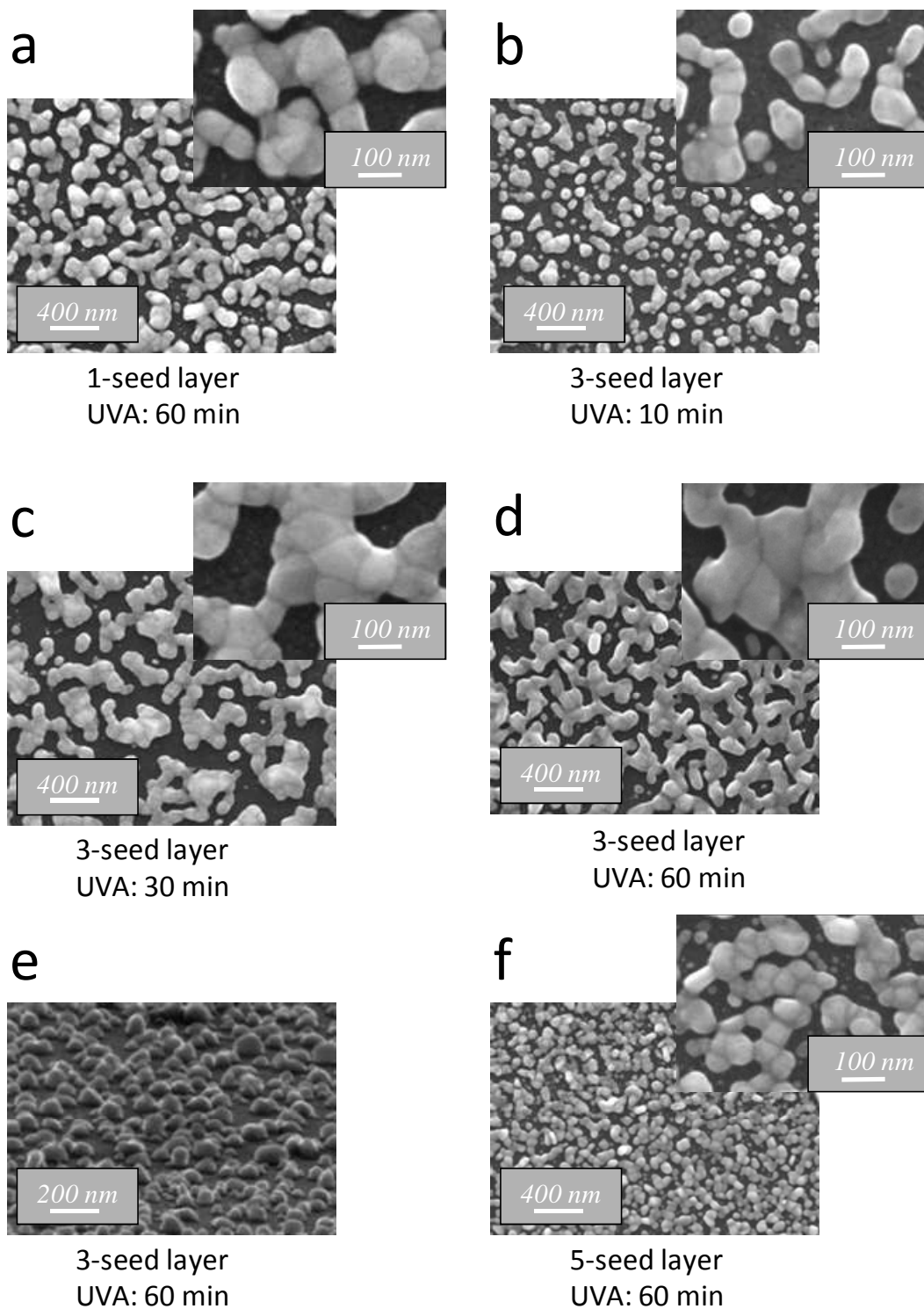


Figure 3-11: FEG-SEM images of Ag° NPs formed through a seeded growth TSC-assisted photocatalytic process for different UVA exposure duration and different seed layers. The Rc ratio is equal to 5, and AgNO_3 concentration is equal to 2 mM.

The corresponding perspective FEG-SEM image (Figure 3-11e) shows that the profile of Ag⁰ NPs is quite isotropic, which indicates that the NPs also undergo a growth along the direction perpendicular to the substrate surface, i.e. a volume increase, and this image confirms a typical NPs size ranging between 50 and 100 nm. Volume increase trends illustrated in Figures 3-11b to e can in turn explain data depicted in Figures 3-10a and b. Indeed, the Ag/Ti EDX ratio accounts for the total amount of deposited silver atoms. It means that, for a given number of deposited NPs, this ratio is influenced by volume effects, while SCR accounts for surface effects, which can in turn explain why the EDX ratio (Figure 3-10b) increases more markedly than the SCR (Figure 3-10a) when the NPs size increases over a prolonged UVA exposure.

As illustrated in Figure 3-10c for a fixed UVA exposure duration of 60 min, the number of seed layers induces more complex variations of the Ag⁰ SCR and Ag/Ti EDX ratio. The former undergoes a rather weak increase as the number of seed layers increases from 0 to 3 (Figure 3-10c), while the latter significantly increases (Figure 3-10d). The FEG-SEM images of Figure 3-6, Figure 3-11a, and Figure 3-11d support these trends. They show that, while the surface coverage of Ag⁰ NPs undergoes only minor variation, the size (volume) of the NPs significantly increases. When further increasing the number of seed layers from 3 to 5, the SCR continues to weakly increase (Figure 3-10c) but the EDX ratio undergoes a significant jump (Figure 3-10d). These trends are illustrated by the FEG-SEM images of Figures 3-11d and f, showing that the slight surface coverage increase, associated to an increase of the seed layers number from 3 to 5, is accompanied by a strong decrease of the NPs size (volume), which supports a jump of the EDX ratio. Interestingly and in contrast to aggregated particles formed from a 3-seed layer, even after a 60 min UVA exposure aggregated NPs formed from a 5-seed layer still exhibit a rather spherical shape with a diameter of about 50 nm (Figure 3-11f). A similar influence of the number of seed layers was also observed for shorter UVA exposure durations (not illustrated here).

XPS characterizations

XPS measurements were performed on a bare TiO₂ and a TSC-based Ag⁰/TiO₂ heterostructure surface, respectively. This Ag⁰/TiO₂ heterostructure was formed on a 3-seed layer after a 60 min UVA exposure, as illustrated in FEG - SEM images of Figures 3-10d and e. The survey spectrum of our substrate surface is presented in Figure 3-12. This survey analysis was carried out in a common binding energy range of 0-1100 eV in order to identify all the elements present on the surface. The XPS spectrum reveals the presence of all the elements listed in Figure 3-12. A main peak of Ag, as well as other less intense peaks of O, Ti, N, and C are identified. The important information derived from this spectrum are the binding energies of the lines (to identify the different elements) and the peak areas (to quantify the amount of each element).

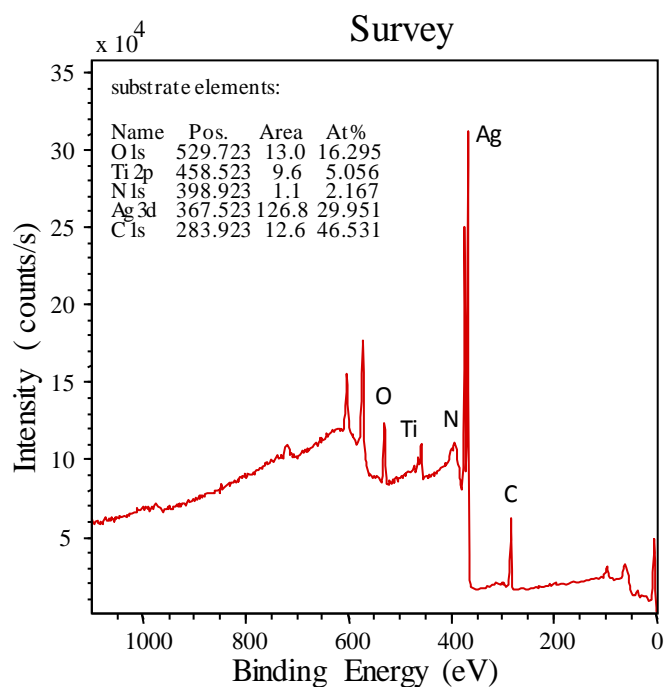


Figure 3-12: XPS survey spectra of an $\text{Ag}^\circ/\text{TiO}_2$ SERS substrate surface.

To get a more precise set of data on the given survey spectrum and provide better quantification and chemical bonding information, the detailed high resolution spectra of some selected peaks (i.e. Ti, Ag) are presented in Figure 3-13. Notably, the Ti 2p peaks are presented in Figure 3-13a and b for the bare TiO_2 substrate and for the $\text{Ag}^\circ/\text{TiO}_2$ substrate, respectively. The Ag peaks are presented in Figure 3-13c. Two series of peaks appear at 458.9/464.6 eV and 368.2/374.0 eV. Those values correspond to the doublets Ti 2p_{3/2/1/2} (Figures 3-13 a and b) and Ag 3d_{5/2/3/2} (Figure 3-13c), respectively, with binding energies and energy separations (Δ) characteristic of metallic silver (Ag°) and oxidized titanium (TiO_2). It appears that, in the presence of Ag° NPs, the intensity of the Ti 2p peaks is about one order of magnitude weaker (Figure 3-13b) than that of the Ag 3d peaks (Figure 3-13c). It is firstly due to the weaker photo-ionization cross section of titanium compared to silver. It also depicts that the XPS TiO_2 film signal is partially screened by Ag° NPs deposited on the film surface. Accordingly, compared to a bare TiO_2 film (Figure 3-13a), the intensity of Ti peaks is attenuated by a factor 3 after deposition of the Ag° nanoparticles (Figure 3-13b). It indicates that about two third of the TiO_2 surface is covered with Ag° nanoparticles, since we assume that the titanium peak is fully screened when covered by Ag° particles of 50-100 nm diameter. These findings are in very good accordance with the data depicted in Figures 3-10 a and c (see circles), which show that for the same substrate formed on a 3-seed layer after a 60 min UVA exposure, the SCR of Ag° NPs is about 65%.

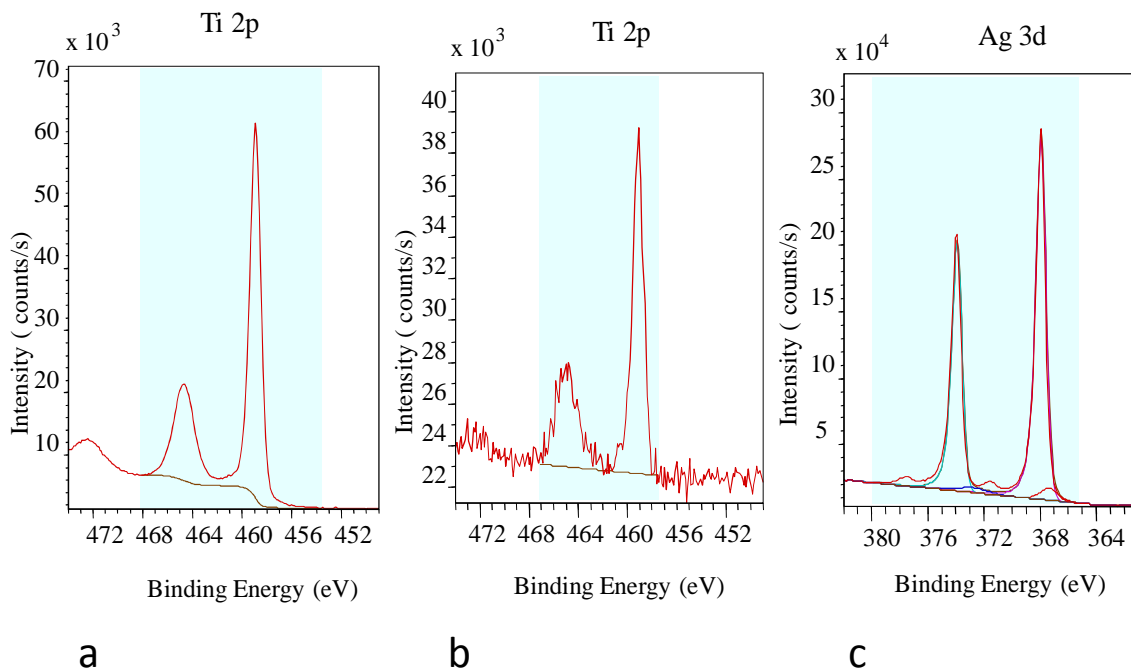


Figure 3-13: High resolution spectra of Ti 2p in the case of a bare TiO₂ substrate (a) and in the case of Ag⁰/TiO₂ SERS substrate (b), and high resolution spectrum of Ag 3d in the case of the same SERS substrate surface (c).

TEM characterizations

Figure 3-14 depicts cross section TEM images of a TSC-based Ag⁰/TiO₂ heterostructure formed on a 3-seed layer after a 60 min UVA exposure, as previously illustrated in FEG-SEM images of Figures 3-10d and e. Owing to weight contrast effects, silver particles are expected to produce darker features than TiO₂ ones, and this darkening effect is all the more pronounced as Ag⁰ NPs are larger owing to an attenuated transmission of the electron beam. Accordingly, TEM images of Figures 3-12a and b unambiguously depict the presence of Ag⁰ NPs at the surface of a TiO₂ film. They confirm the uniform 40 nm thickness of the TiO₂ film and the presence of several aggregated particles at the TiO₂ surface, the size of which ranges between 50 and 100 nm. The high magnification TEM image of Figure 3-14b particularly illustrates two types of clean interfaces. The first one is located between the Ag⁰ NPs and the TiO₂ surface. This clean interface typically arises from a photocatalytic growth mechanism at the TiO₂ surface. The second one is located between vicinal aggregated Ag⁰ NPs. This clean interface suggests that the photocatalytic growth proceeds until Ag⁰ NPs closely contact each others, after what the growth is blocked at the grain boundaries.

The inset of Figure 3-14a also illustrates the SAED pattern of a single Ag⁰ NPs constituting an aggregate. An indexation of this pattern depicts a particle orientated along the [110] zone axis of the centred face cubic (CFC) structure of metallic silver, and dark spots observed in the pattern are assigned to reticular plane families of this structure, i.e. (-11-1), (1-1-1), (00-2), and (-220) planes. The analysis of various patterns allowed a systematic assignment of reticular planes to the CFC structure of metallic silver. This assignment confirms the metallic state of photocatalytically grown Ag⁰ NPs. Besides, well resolved spots observed in the SAED patterns indicate that each aggregated NPs consists of a single-crystal particle. Figure 3-14c shows the HRTEM image of an interfacial area between two aggregated NPs. Lines observed in this image correspond to reticular planes assigned to the CFC structure of metallic silver. On the one hand, the diffraction pattern derived from a FFT of this HRTEM image (not shown here) depicts a particle (darker one) orientated along the [110] zone axis of the centred CFC structure of metallic silver and allows identifying the orientation of different reticular planes, for instance (111) ones as illustrated in this figure. On the other hand, a FFT of the vicinal particle (brighter one) HRTEM image depicts the same kinds of reticular planes, but with a marked disorientation compared to the previous particle. This disorientation firstly indicates that, while Ag⁰ NPs grown and aggregated at the surface of the TiO₂ film consist of single crystal particles, the photocatalytic growth does not involves any epitaxial mechanism at the TiO₂ surface. Besides, for both observed Ag⁰ NPs, Figure 3-14 indicates the absence of any crystallographic defect, e.g. disorientation of the reticular planes, even at the grain boundary. It suggests that Ag⁰ NPs aggregated at the TiO₂ surface does not undergo any interfacial atomic diffusion, which would lead to an eventual coalescence mechanism, and confirms that the NPs growth is stopped at the grain boundaries.

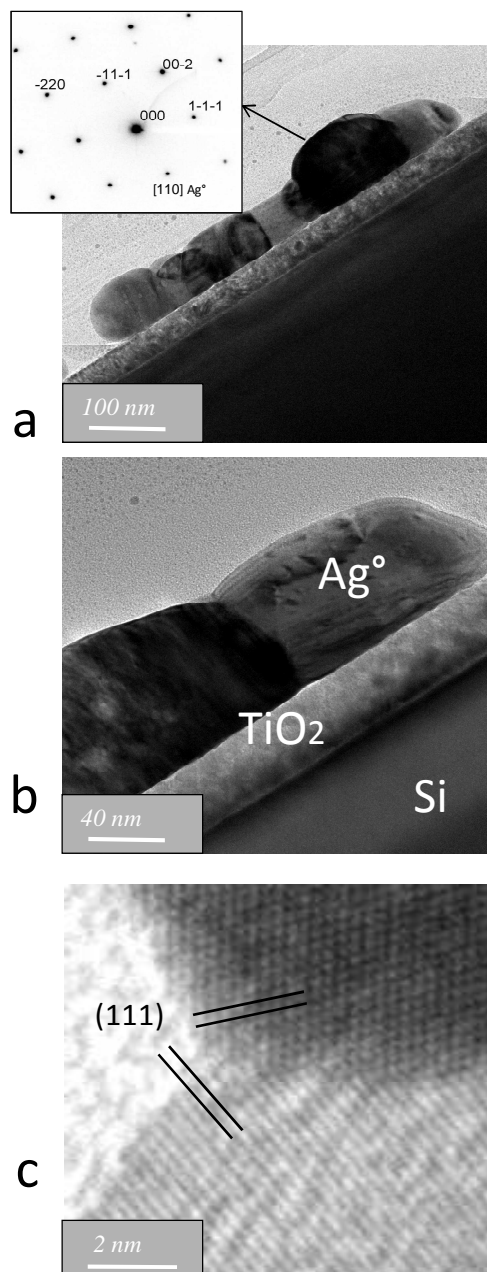


Figure 3-14. Cross section TEM images of a TSC-based $\text{Ag}^\circ/\text{TiO}_2$ heterostructure formed on a 3-seed layer after a 60 min UVA exposure: low magnification TEM image showing several aggregated Ag° NPs and the SAED pattern associated to one of these NPs orientated along the $[1\ 1\ 0]$ zone axis, with its assignment to different reticular plane families of the CFC structure of metallic silver (a), high magnification TEM image of aggregated Ag° NPs (b), and HRTEM image showing the orientation of $(1\ 1\ 1)$ reticular planes in two vicinal Ag° NPs (c).

4.1.2 Self-limited growth/aggregation process: discussion

SEM and TEM data of Figure 3-11 and Figure 3-14 indicate that the previously described seeded growth assisted photocatalytic process allows increasing the amount of deposited Ag° NPs while preserving a fairly good size uniformity and surface distribution of the NPs. These features are in turn associated

with the development of NPs aggregates uniformly distributed at the substrate surface. As illustrated by the FEG-SEM image of Figure 3-6, aggregation features specifically arise from a TSC-assisted photocatalytic reduction mechanism. However, this mechanism alone is not sufficient to prevent a heterogeneous growth and surface distribution of Ag° NPs. In contrast, data of Figure 3-11 show that the TSC photocatalytic process assisted by a seeded growth mechanism greatly improves the uniformity in size and surface distribution of such NPs and derived aggregates. This result firstly relies on previously presented seeded growth mechanisms illustrated in Figure 3-7, which explain how uniform NPs of rather spherical shape can be obtained in the initial growth stages. In the following, we discuss a model that illustrates the subsequent seeded growth stages leading to the formation of tailored aggregates of NPs. Over the photocatalytic process, some growing particles start to contact each other as illustrated in Figure 3-11b. The contact probability certainly relies on the surface distribution of initially deposited seeds, i.e. the NPs contact is all the more fast in regions that initially exhibit a greater surface density of seeds. Once the NPs contact is established, FEG-SEM and TEM images suggest that the growth process is stopped at the grain boundaries. In contrast, these NPs can still undergo an additional growth in directions where no granular contact has been established (or eventually in the direction perpendicular to the substrate surface) through a reaction with newly adsorbed Ag^+ cations, which would explain that, in certain conditions, oblong aggregated particles are obtained over a prolonged UVA exposure (Figure 3-11d). However, our results show that this additional growth process takes place in a limited extent and, for a fixed seed-layer number and UVA exposure duration, aggregated NPs exhibit a fairly uniform and small size. It suggests that the NPs growth is governed by a self-limited process induced by aggregation mechanisms. A proposed self-limited growth process is schematically illustrated in Figure 3-15.

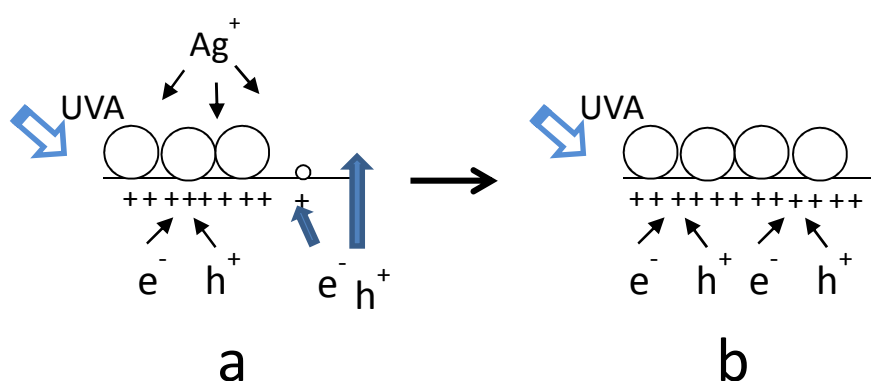


Figure 3-15: Proposed schematic representation of the mechanisms leading to Ag° NPs at the surface of a TiO_2 film over ultimate stages of the growth/aggregation process: (a) and (b) depict phenomenological evolutions over UVA exposure.

As explained before and illustrated in Figure 3-1 and Figure 3-7, the photocatalytic reduction mechanism relies on a reaction of photo-electrons with Ag^+ cations adsorbed at the TiO_2 film surface. This photo-reduction mechanism is all the more efficient as the recombination of photo-electrons and photo-holes is prevented by an enhanced photo-hole harvesting in Ag° -free areas of the TiO_2 film surface. When the aggregation of Ag° NPs starts, the aggregates block any pathway allowing the photo-holes to reach bare TiO_2 film surface. This feature promotes a total electron-hole recombination beneath the aggregates and stops the growth of aggregated NPs (Figure 3-15a). Accordingly, previous works performed in the team showed that a suitable distribution of platinum NPs at the surface of TiO_2 films strongly increased the photocatalytic activity of these films owing to an efficient electron-hole separation induced by Schottky barrier effects, while the photocatalytic activity was totally cancelled above a platinum NPs SCR threshold owing to electron-hole recombination [12]. However, while the growth of aggregated Ag° NPs is stopped, vicinal isolated seeds or NPs can still undergo further growth (Figure 3-15a). The growth of these new NPs will stop once they contact initially developed aggregates owing to previously described grain boundary and electron-hole recombination features (Figure 3-15b). It yields some kind of self-limited growth mechanism governed by aggregation features. Besides, and as explained before, the initial aggregation of growing NPs is all the more prone to occur as the surface density of dispersed seeds is greater. As illustrated in Figures 3-9a and b, increasing the number of seed layers significantly increases the surface density of dispersed seeds. It may in turn explain why the development of NPs aggregates and the associated blockage of the aggregated NPs growth are faster when the photo-reduction process is performed on a 5-seed layer compared to a 3-seed one, and thus, why much smaller and isotropic aggregated NPs are produced in the former case (Figure 3-11f).

5. Conclusion

The deposition of Ag° NPs has been studied through a chemically assisted photocatalytic reduction process on the surface of sol-gel deposited TiO_2 thin films exposed to UVA light in order to propose a low cost liquid solution elaboration procedure of SERS substrates. Field Emission Gun-Scanning Electron Microscopy, Transmission Electron Microscopy, and Energy Dispersive X-ray characterizations have been used to assess how the chemical assistance of the photocatalytic reduction process enables an enhanced uniformity of the Ag° NPs deposition. TSC firstly enables a considerable reduction in the NPs growth kinetic and favors the dispersion of rather small and uniform NPs, but when these NPs are deposited in great amount, they tend to heterogeneously aggregate at the substrate surface. Secondly, an AA-assisted seeded growth procedure, by allowing a self-controlled growth-aggregation process relying on Schottky barrier effects, enables the formation of a great amount of NPs uniformly aggregated. Moreover, various combinations of the seed amount and UVA exposure duration enable to

selectively control the amount, aggregation state, and size of deposited NPs. According to SERS literature, the high sensitivity of a SERS substrate relies on the homogeneous creation of a large number of hot spots on a solid substrate, i.e. the homogeneous dispersion of well-designed metal NPs aggregates at the substrate surface. Therefore, uniform aggregates obtained in this work are highly susceptible to induce hot spots, thus providing strong local electromagnetic fields, and resulting in a large enhancement of Raman signals of the adsorbed molecules. This feature will be addressed in the following chapter, where the SERS detection performances of an Ag^o/TiO₂ heterostructure will be investigated using Rhodamine 6G chosen as a model analyte.

- [1] I. Sondi and B. Salopek-Sondi, "Silver nanoparticles as antimicrobial agent: a case study on *E. coli* as a model for Gram-negative bacteria," *Journal of Colloid and Interface Science*, vol. 275, pp. 177-182, 2004.
- [2] Y. Qin, X. Ji, J. Jing, H. Liu, H. Wu, and W. Yang, "Size control over spherical silver nanoparticles by ascorbic acid reduction," *Colloids and Surfaces A: Physicochemical and Engineering Aspects*, vol. 372, pp. 172-176, 2010.
- [3] K. G. Stamplecoskie, J. C. Scaiano, V. S. Tiwari, and H. Anis, "Optimal Size of Silver Nanoparticles for Surface-Enhanced Raman Spectroscopy," *The Journal of Physical Chemistry C*, vol. 115, pp. 1403-1409, 2011.
- [4] B. Wiley, Y. Sun, B. Mayers, and Y. Xia, "Shape-Controlled Synthesis of Metal Nanostructures: The Case of Silver," *Chemistry – A European Journal*, vol. 11, pp. 454-463, 2005.
- [5] J. Zeng, Y. Zheng, M. Rycenga, J. Tao, Z.-Y. Li, Q. Zhang, *et al.*, "Controlling the Shapes of Silver Nanocrystals with Different Capping Agents," *Journal of the American Chemical Society*, vol. 132, pp. 8552-8553, 2010.
- [6] Q. Zhang, Y. Hu, S. Guo, J. Goebel, and Y. Yin, "Seeded Growth of Uniform Ag Nanoplates with High Aspect Ratio and Widely Tunable Surface Plasmon Bands," *Nano Letters*, vol. 10, pp. 5037-5042, 2010.
- [7] J. Zeng, X. Xia, M. Rycenga, P. Henneghan, Q. Li, and Y. Xia, "Successive Deposition of Silver on Silver Nanoplates: Lateral versus Vertical Growth," *Angewandte Chemie International Edition*, vol. 50, pp. 244-249, 2011.
- [8] L. He, J. Huang, T. Xu, L. Chen, K. Zhang, S. Han, *et al.*, "Silver nanosheet-coated inverse opal film as a highly active and uniform SERS substrate," *Journal of Materials Chemistry*, vol. 22, pp. 1370-1374, 2012.
- [9] S. Chang, Z. A. Combs, M. K. Gupta, R. Davis, and V. V. Tsukruk, "In situ Growth of Silver Nanoparticles in Porous Membranes for Surface-Enhanced Raman Scattering," *ACS Applied Materials & Interfaces*, vol. 2, pp. 3333-3339, 2010.
- [10] M. Langlet, I. Sow, S. Briche, M. Messaoud, O. Chaix-Pluchery, F. Dherbey-Roussel, *et al.*, "Elaboration of an Ag⁰/TiO₂ platform for DNA detection by surface enhanced Raman spectroscopy," *Surface Science*, vol. 605, pp. 2067-2072, 2011.
- [11] A. Mills, G. Hill, M. Stewart, D. Graham, W. E. Smith, S. Hodgen, *et al.*, "Characterization of Novel Ag on TiO₂ Films for Surface-Enhanced Raman Scattering," *Applied Spectroscopy*, vol. 58, pp. 922-928, 2004.
- [12] D. Riassetto, F. Roussel, L. Rapenne, H. Roussel, S. Coindeau, O. Chaix, *et al.*, "Synthesis and functionalities of noble metal nanoparticles formed through simple all-inorganic photochemical procedures," *Journal of Experimental Nanoscience*, vol. 5, pp. 221-243, 2010.
- [13] M. Langlet, S. Permpoon, D. Riassetto, G. Berthomé, E. Pernot, and J. C. Joud, "Photocatalytic activity and photo-induced superhydrophilicity of sol-gel derived TiO₂ films," *Journal of Photochemistry and Photobiology A: Chemistry*, vol. 181, pp. 203-214, 2006.
- [14] M. Maillard, P. Huang, and L. Brus, "Silver Nanodisk Growth by Surface Plasmon Enhanced Photoreduction of Adsorbed [Ag⁺]," *Nano Letters*, vol. 3, pp. 1611-1615, 2003.

Chapter 4. First assessments of the $\text{Ag}^\circ/\text{TiO}_2$ SERS substrate performances

1. Introduction

The SERS effect arising from Ag° NPs has particularly been studied in the literature using Rhodamine 6G (R6G) as a model analyte to perform fundamental studies or to study SERS-based devices because of the strong Raman cross section of this molecule. In this chapter, R6G was also used to provide first insights in the SERS performances of $\text{Ag}^\circ/\text{TiO}_2$ heterostructure whose optimization has been described in chapter 3. Let us recall that such substrate exhibits a great amount of Ag° NPs aggregates, which are highly uniform in structure and are susceptible to contribute to a large SERS enhancement (hot spots). Here after, we question the potential sensitivity, stability, and reproducibility of our substrates and therefore intend to test their performances by measuring the SERS signal of R6G molecules adsorbed on the surface. The area-to-area and substrate-to-substrate variability in the SERS response is particularly examined. We will first study the pure Raman spectrum (without any SERS enhancement) of R6G on a bare silicon substrate (in the absence of Ag° NPs). Then we will investigate the SERS performances of $\text{Ag}^\circ/\text{TiO}_2$ heterostructure elaborated in selected model conditions. These performances are in particular studied through the assessments of the detection limit and SERS enhancement factor (EF) of so-obtained substrates.

2. Spectroscopic characterizations

Raman measurements were carried out using a Jobin-Yvon/Horiba LabRam spectrometer equipped with a liquid nitrogen CCD detector. The experiments were conducted in micro-Raman mode at room temperature on areas of around $100 \times 100 \mu\text{m}^2$. Spectra were collected in a backscattering geometry, using the 514 nm green line of an argon ion laser. The light was focused to a $1 \mu\text{m}^2$ spot using a 50x long working distance objective. An accumulation time of 10 s and a laser power of $78 \mu\text{W}$ at the sample surface were used to record spectra in the $270 - 1860 \text{ cm}^{-1}$ range. The spectrometer was calibrated using the Raman spectrum of the Si substrate. R6G (the formula of which is present in Figure 4-1) was used as standard probe molecule to investigate the SERS enhancement of our samples. Small pieces of $3 \times 3 \text{ mm}^2$ were cut from the $3 \times 3 \text{ cm}^2$ substrate. Then, $10 \mu\text{L}$ aliquots of R6G liquid solutions of different concentrations were spread on these substrate pieces and dried in oven at 60°C for 10 min. For reference pure Raman spectra, drops of R6G diluted in absolute ethanol with a concentration of 10^{-3} M were deposited on bare silicon substrates. For SERS spectra, drops of R6G diluted in deionized water with

concentrations ranging from 10^{-4} to 10^{-10} M were deposited on silicon substrates coated with $\text{Ag}^\circ / \text{TiO}_2$ heterostructure. The same equipment was also used to collect the fluorescence spectrum of R6G in the 520 - 670 nm range. For that purpose, R6G was diluted in deionized water with a concentration of 10^{-3} M and the spectra were acquired in liquid solution with an accumulation time of 10 s and a laser power of $1 \mu\text{W}$.

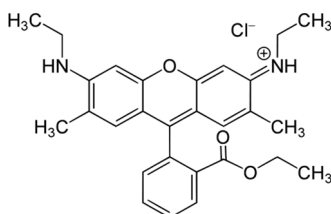


Figure 4-1: Formula of R6G.

3. Preliminary spectroscopic studies

As detailed in the previous chapter, numerous morphologies of Ag° NPs deposited at the surface of TiO_2 films can be expected through a variation of the seed layer number and UVA exposure duration combinations, which may in turn specifically influence the SERS effect arising from derived $\text{Ag}^\circ/\text{TiO}_2$ heterostructure. Such studies obviously go beyond the topics of the present thesis. Hereafter, we focus on Raman studies performed to assess the assets of our seeded growth procedure in terms of intensity and reproducibility of the SERS signal. The pure Raman (non-SERS) spectrum of R6G deposited on bare silicon substrates was firstly studied. In preliminary essays, we observed that successive R6G spectrum acquisitions, performed in a same place of the solid substrate, led to a continuous decrease in the Raman bands intensity, and this feature occurred both for pure Raman and SERS spectra. On the one hand, it is known that, even at low laser power, electron transfers at the surface of Ag° NPs can cause the photo-reduction of various kinds of adsorbed analyte molecules, which can complicate their SERS detection [1]. On the other hand, fundamental studies performed on the SERS detection of the single-molecule showed that R6G intrinsically exhibits instability caused by photo-induced mechanisms, leading to Raman signal blinking or progressive decrease in the signal intensity [2-5].

In our case, the signal intensity decrease was also observed when R6G Raman spectra were acquired on a bare silicon wafer, which shows that this decrease is not due to any Ag° -induced photo-reduction mechanism or any eventual TiO_2 -induced photocatalytic decomposition, but intrinsically arises from the photo-instability of R6G. According to this instability, we adopted a rather short accumulation time (10 s) and low laser power ($78 \mu\text{W}$) for the acquisition of pure Raman and SERS spectra. In these conditions, it appeared that the pure Raman detection required a strong amount of deposited R6G, i.e. a

strong concentration of R6G in liquid medium. Accordingly, no R6G detection could be performed for a concentration lower than 10⁻³ M. Water is classically employed as a dilution medium of R6G molecules. However, when deposited from a strongly concentrated water solution, we observed that R6G tended to pack in localized regions heterogeneously distributed on the substrate surface. It probably depicts aggregation features related to the high surface tension of water. Accordingly, the R6G heterogeneous distribution led to very irreproducible Raman spectra. In contrast, the low surface tension of ethanol yielded a fairly uniform dispersion of R6G molecules at the substrate surface leading to quite reproducible Raman spectra. Thus, contrary to SERS studies performed from R6G diluted in weak concentration in water, pure Raman studies were performed from a 10⁻³ M ethanolic solution of R6G.

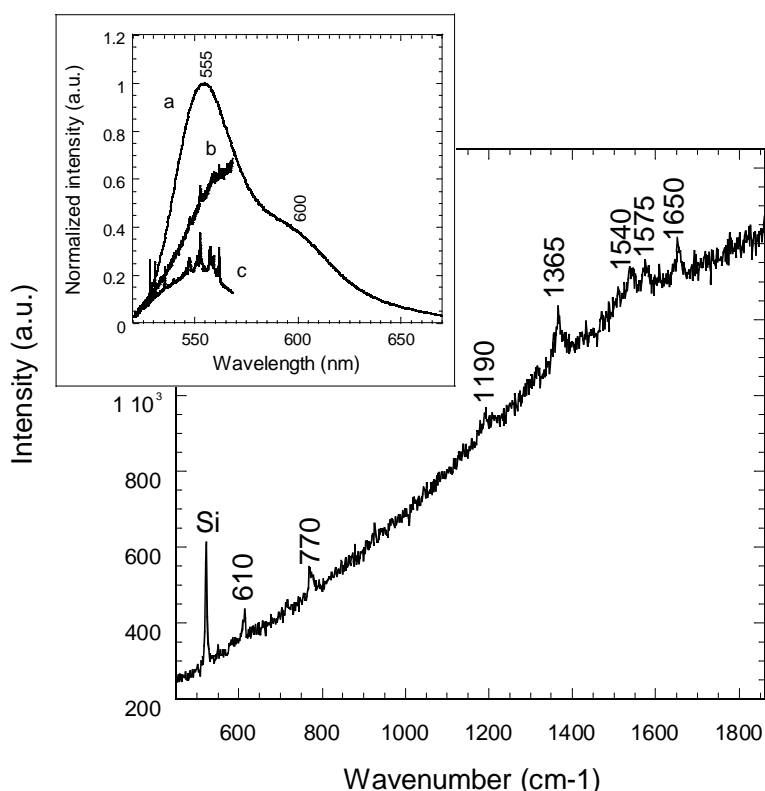


Figure 4-2: Raman spectrum of R6G deposited on a bare silicon substrate from a 10⁻³ M ethanolic solution. The inset compares the fluorescence spectrum of R6G diluted in water (10⁻³ M) (a), the Raman spectrum measured on a bare silicon substrate (b), and the SERS spectrum measured on a Ag^o/TiO₂ heterostructure coated with a 10⁻⁶ M R6G aqueous solution (c). In the inset, the intensities of the fluorescence and Raman spectra have been arbitrarily normalized to permit a clear comparison.

The pure Raman spectrum of R6G dispersed on silicon is illustrated in Figure 4-2. Except a band at 520 cm⁻¹, which corresponds to the silicon substrate, all other bands were observed in the 600 - 1700 cm⁻¹ spectral range and unambiguously attributed to R6G (Table 4-1), including bands at around 610 cm⁻¹ (C-C in-plane bending), 770 cm⁻¹ (C-H out-of-plane bending), 1190 cm⁻¹ (C-H in-plane bending), and a set of bands at 1365, 1540, 1575, and 1650 cm⁻¹ (aromatic C-C stretching) [6]. The spectra exhibit a

poor signal/noise ratio and all the bands are weakly intense, which depicts the limitations of a pure Raman detection. These bands are also observed to grow on a strongly sloped baseline, which is attributed to the fluorescence of R6G when exposed to a green laser source.

Band position (cm ⁻¹)	Assignments
610	C-C in-plane bending
635*	C-C in-plane bending
660*	C-C in-plane bending
770	C-H out-of-plane bending
925*	C-H out-of-plane bending
1085*	C-H out-of-plane bending
1125*	C-H in-plane
1180-1190	C-H in-plane bending
1310*	C-O-C stretching
1365	aromatic C-C stretching
1420*	aromatic C-C stretching
1510*	aromatic C-C stretching
1540	aromatic C-C stretching
1570-1575	aromatic C-C stretching
1600*	aromatic C-C stretching
1650	aromatic C-C stretching

*Table 4-1 : Vibrational assignments of main R6G Raman bands experimentally observed. The symbol * indicates bands not observed in pure Raman configuration but only by SERS [6].*

As illustrated in the inset of Figure 4-2, the fluorescence spectrum of R6G in water exhibits a marked intensity maximum centered at 555 nm with a shoulder around 600 nm. It is known that R6G in liquid solution undergoes molecular aggregation in the form of dimers or higher aggregates, and the fluorescence of R6G monomers occurs around 550 nm while dimerization or aggregation features lead to a fluorescence intensity maximum located at slightly higher wavelength [7, 8]. The R6G fluorescence

band is thus a convolution of both components and, as dimerization/aggregation becomes predominant, an increase in the relative intensity of the high wavelength component leads to a progressive red-shift of the overall fluorescence band. Accordingly, the fluorescence spectrum illustrated in the inset of Figure 4-2 is similar to that mentioned by other authors when R6G monomers are essentially present and coexist with a weak fraction of dimers or higher aggregates [8]. The inset of Figure 4-2 also suggests that the baseline of the Raman spectrum corresponds to the low wavelength edge of the R6G fluorescence spectrum. However, compared to this latter, the Raman spectrum traduces a red-shifted fluorescence. Actually, in the spectral range accessible in our acquisition conditions, the fluorescence intensity maximum is not observed in the Raman spectrum. It is likely that, even when diluted in ethanol, the deposition of R6G on a solid substrate leads to a certain degree of dimerization or aggregation, which would explain a red-shift of the fluorescence band.

4. SERS spectra

SERS spectra were acquired from R6G diluted in water in concentrations ranging from 10^{-4} to 10^{-10} M and subsequently deposited on Ag⁰/TiO₂ heterostructure. In this low concentration range, it was considered that R6G molecules diluted in water are not heterogeneously aggregated once deposited on the solid substrate, which will be verified in the following. A TSC-based Ag⁰/TiO₂ heterostructure formed on a 3-seed layer after a 60 min UVA exposure, whose morphology is illustrated in Figures 3-10d and e of the previous chapter and recalled in the right inset of Figure 4-3, has been chosen as a model SERS substrate to assess the assets of the seeded growth procedure. The SERS spectra of R6G diluted in water in various concentrations and deposited on such heterostructure are illustrated in Figure 4-3.

Spectra shown in this figure depict a bi-regime trend governed by a threshold R6G concentration of 10^{-5} M. The Raman bands intensity did not increase when increasing the R6G concentration above this threshold value (left inset of Figure 4-3), and even decreased when further increasing the R6G concentration (not illustrated here). These features suggest that, above a certain concentration, R6G molecules are deposited in the form of a multilayer instead of a monolayer. It means that R6G molecules deposited at the top surface of the multilayer do not contact Ag⁰ NPs and cannot undergo SERS detection, but only a pure Raman detection. Since this latter is expected to induce a negligible signal compared to a SERS one, it would explain that a R6G concentration increase above 10^{-5} M does not yield an enhanced Raman signal. Optical absorption features can also explain that a strong excess of deposited R6G reduces the flux of green light reaching the R6G/Ag⁰ interfaces, which would in turn reduce the SERS detection when the R6G concentration excessively increases.

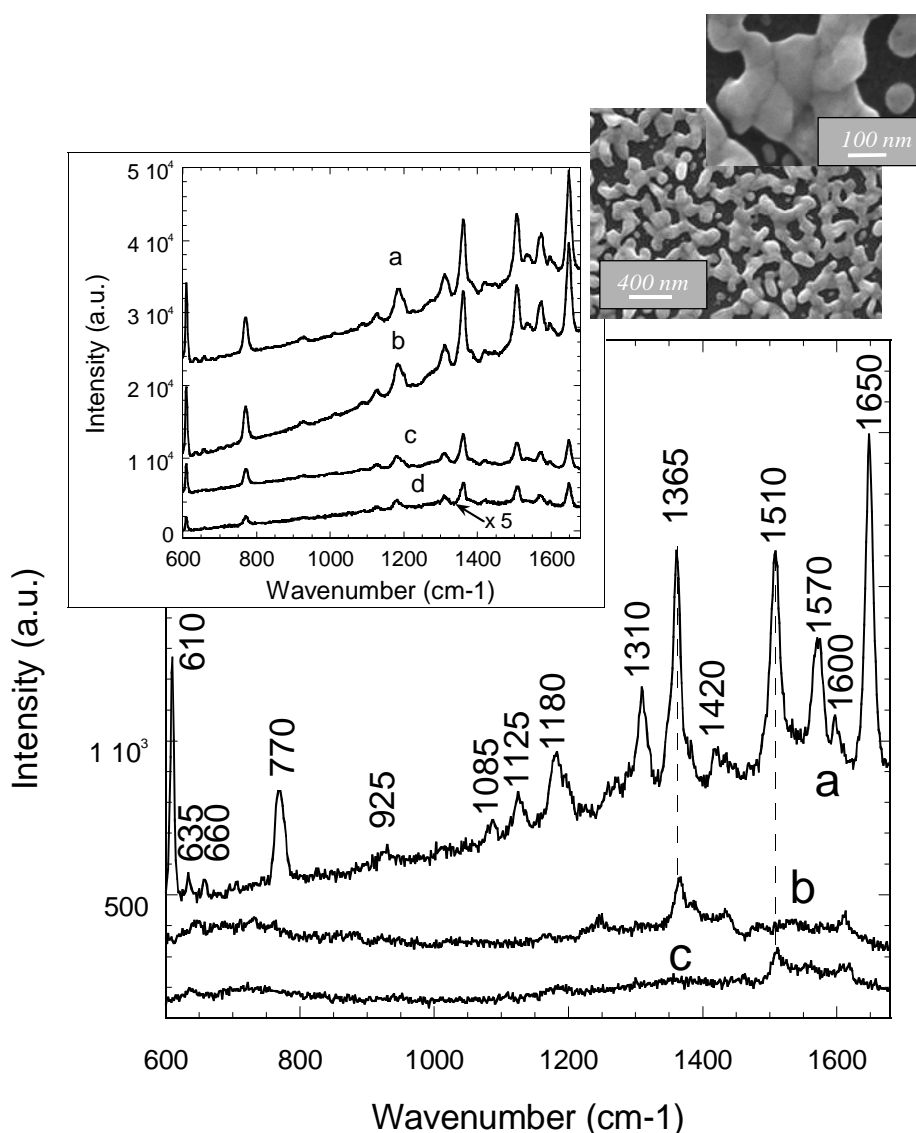


Figure 4-3: SERS spectra collected on an $\text{Ag}^\circ/\text{TiO}_2$ heterostructure formed on a 3-seed layer after 60 min of UVA exposure (inset on the right). Measurements were performed for a R6G concentration in water of 10^{-8} M (a), 10^{-9} M (b), and 10^{-10} M (c). The inset on the left shows the SERS spectra for a R6G concentration of 10^{-4} M (a), 10^{-5} M (b), 10^{-6} M (c), and 10^{-7} M (d). In the inset (d), the band intensity has been multiplied by a factor 5.

A decrease of the R6G concentration below the threshold value of 10^{-5} M leads to several observations. First of all, the previously mentioned sloped baseline, attributed to the R6G fluorescence, is still depicted in the SERS spectra. It should be mentioned that this baseline lies in a spectral range where the plasmon resonance of Ag° NPs can also influence the Raman spectrum baseline [2-5]. However, spectra illustrated in the left inset of Figure 4-3 clearly show that the slope of this baseline continuously decreases when decreasing the R6G concentration below 10^{-5} M. This trend contradicts the assumption of a plasmon resonance contribution, since for similarly synthesized SERS substrates the plasmon

resonance should not vary, but it fully supports a decreasing fluorescence intensity when the amount of deposited R6G diminishes. Interestingly, while the fluorescence intensity maximum could not be observed when R6G was deposited from concentrated solutions, owing to the previously mentioned red-shifting caused by dimerization or aggregation features, this maximum was clearly observed in the 1400-1500 cm⁻¹ range of the SERS spectra when R6G was deposited from concentrations of 10⁻⁶ M or less. As illustrated in the inset of Figure 4-2, for such weak concentrations, the wavelength position of this maximum closely agrees with that of the fluorescence maximum. These observations suggest that, when R6G is deposited from a sufficiently diluted solution, dimerization or aggregation features occurring at the substrate surface and inducing a red-shifted fluorescence are strongly reduced.

Figure 4-3 and its left inset also show that, while the Raman bands intensity gradually decreases when decreasing the R6G concentration below 10⁻⁵ M, well defined R6G bands with a very good signal/noise ratio are still observed even for a 10⁻⁸ M concentration (Figure 4-3a), which depicts the strong Raman signal amplification induced by the SERS effect. The SERS amplification also enables the detection of new R6G bands (Table 4-1), which did not appear in the pure Raman spectra, including bands at 635 and 660 cm⁻¹ (C-C in-plane bending), 925 and 1085 cm⁻¹ (C-H out-of-plane bending), 1125 cm⁻¹ (C-H in-plane bending), 1310 cm⁻¹ (C-O-C stretching), 1420, 1510, and 1600 cm⁻¹ (aromatic C-C stretching) [30]. Furthermore, Figure 4-3 and its inset show that, while the SERS detection does not significantly modify the position of R6G bands compared to the pure Raman spectrum of Figure 4-2, it yields a selective amplification of the Raman bands. This feature is particularly appreciable for the 1310 and 1510 cm⁻¹ bands, which were not detected in the pure Raman spectrum and exhibit strong intensities in the SERS spectra. This observation has not been elucidated yet and will require further investigations. Figure 4-3 finally indicates that the R6G detection is not limited to a 10⁻⁸ M concentration since, even after deposition from a 10⁻⁹ (Figure 4-3b) or a 10⁻¹⁰ M concentration (Figure 4-3c), R6G bands were still observed. However, for such weak concentrations, only some R6G bands could selectively be detected, and their intensity and wavenumber position randomly varied when spectrum acquisitions were performed in different places of a 100 x 100 μm² area. Actually, this selective detection can also be observed in SERS spectra presented by others when R6G was deposited from much diluted solutions, but the authors did not mention and discuss it [9, 10]. It has been reported that the Raman bands of the R6G single molecule undergo “blinking” on the second time-scale when exposed to laser excitation, which is characterized both by on/off behavior and intensity fluctuations, and is attributed to thermal or laser driven alternative desorption and re-adsorption of R6G molecules [3-5]. In our experimental conditions, when R6G is deposited from strongly diluted solutions, it is inferred that only a small number of R6G molecules are illuminated by the laser beam. Owing to the short acquisition time (10 s), it is therefore likely that the Raman spectrum punctually illustrates a transitory state of this desorption/adsorption process. The spectral position and intensity of detected Raman bands can in turn

depict the punctual orientation of the adsorbed R6G molecules in this transitory state, i.e. the nature of chemical bonds in contact with Ag⁰ NPs that can be detected by SERS. In contrast, when a large amount of R6G molecules are deposited, i.e. for a concentration of 10⁻⁸ M or more in our conditions, the Raman spectrum statistically averages all possible desorption/adsorption states and exhibits the whole set of R6G Raman bands with reproducible relative intensities.

5. SERS performance assessments

According to previous data, it can be considered that the detection limit of our Ag⁰/TiO₂ heterostructure ranges between 10⁻⁸ and 10⁻¹⁰ M. Another way to assess the SERS performances of this heterostructure relies on the determination of the EF using the standard equation,

$$EF = (I_{SERS}/I_{RAMAN}) \times (N_{RAMAN}/N_{SERS}) \quad [1]$$

where I_{SERS} (I_{RAMAN}) and N_{SERS} (N_{RAMAN}) account for the intensity of a given R6G band and the number of molecules illuminated by the laser beam in SERS (pure Raman) conditions, respectively [1, 9-11]. Since SERS and pure Raman measurements were performed in identical acquisition conditions, and a same volume of R6G solution was deposited on substrates of identical dimensions (3x4 mm²) in both cases, we considered that the N_{RAMAN}/N_{SERS} ratio could be estimated from the ratio of R6G concentrations in solution. This estimation, which has already been proposed by other authors [11], provides a fairly reliable assessment of the EF order of magnitude, and a more precise assessment would be illusory owing to the uncertainty on the I_{RAMAN} value measured from the poorly defined reference Raman bands illustrated in Figure 4-2. Using the SERS spectra derived from the deposition of a 10⁻⁸ M R6G solution (Figure 4-3a), an EF value of 10⁶ has been deduced from the intensity of the 610 and 1365 cm⁻¹ bands. We should mention that it is quite difficult to rigorously compare the EF of our heterostructure with data published by others because the authors often adopt very different adaptations of the equation [1], which leads to rather ambiguous comparisons [12]. Accordingly, while some authors mentioned a similar EF of the R6G detection on their Ag⁰-based SERS substrates, they reported on very different detection limits ranging between 10⁻⁸ and 10⁻¹⁴ M [1, 9, 10]. However, according to the EF and detection limit of our Ag⁰/TiO₂ heterostructure, we can globally draw following conclusions. On the one hand, the detection sensitivity presented in this paper is clearly inferior to that recently mentioned by some authors, who reported on EF values and detection limits of R6G in the 10⁸-10¹⁴ and 10⁻¹⁴-10⁻¹⁸ M ranges, respectively, but these authors proposed costly and complex procedures, as presented in chapter 1 [8-10]. On the other hand, the performances of our SERS substrate elaborated through a low cost liquid solution approach are fairly comparable to those recently obtained by others when using

alternative liquid solution procedures, which led to an EF value around 10^7 and a detection limit of R6G ranging between 10^{-8} and 10^{-12} [1, 10].

The assets of our heterostructure also rely on a very good reproducibility of the SERS spectra, which in turn arises from the implementation of a seeded growth procedure. It should be mentioned that, when several authors report on the good sensitivity of their SERS substrates, they rarely mention the reproducibility of spectra acquired on different areas of their substrates [9, 11, 13] and, when such criteria are considered, they are investigated on very small areas of $100 \times 100 \mu\text{m}^2$ or less [1, 10]. In the following, we discuss the spectrum reproducibility assessed on our heterostructure for a 10^{-6} M R6G aqueous solution. In order to study how the seeded growth procedure influences the SERS spectra reproducibility, we preliminarily studied a TSC-based Ag⁰/TiO₂ heterostructure formed in the absence of seed, whose morphology is illustrated in Figure 3-6 of the previous chapter and recalled in the inset of Figure 4-4. Several spectra randomly acquired in various places of a same $100 \times 100 \mu\text{m}^2$ area showed that the R6G bands intensity fluctuated over one order of magnitude (Figure 4-4), which demonstrated the strong irreproducibility of the SERS detection. As discussed below, this irreproducibility depicts the heterogeneous distribution of Ag⁰ NPs and/or aggregates of NPs in so-formed heterostructure.

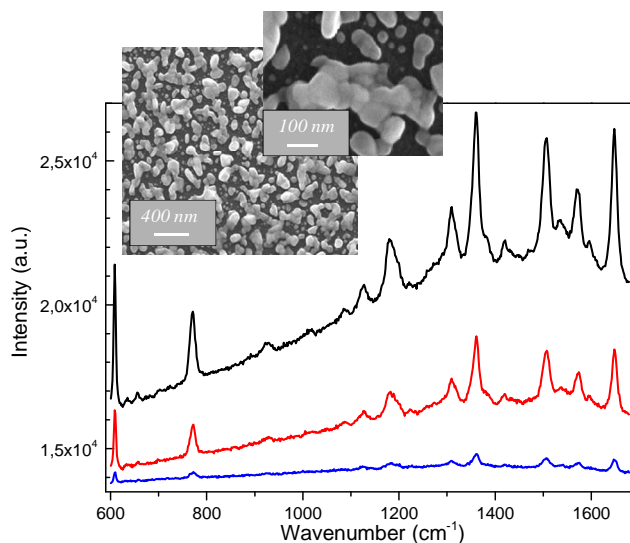


Figure 4-4: Raman spectra randomly measured in different areas of a $100 \times 100 \mu\text{m}^2$ SERS substrate, elaborated in the absence of seed after 60 min of UVA exposure (SEM images in inset), and coated with a 10^{-6} M R6G aqueous solution.

Same studies were then performed on our model Ag⁰/TiO₂ heterostructure formed on a 3-seed layer after 60 min of UVA exposure. A relative standard deviation (RSD) of around 10% in the intensity of the 610 and 1365 cm^{-1} R6G bands was deduced from investigations performed on different $100 \times 100 \mu\text{m}^2$ areas (Figure 4-5 and its inset).

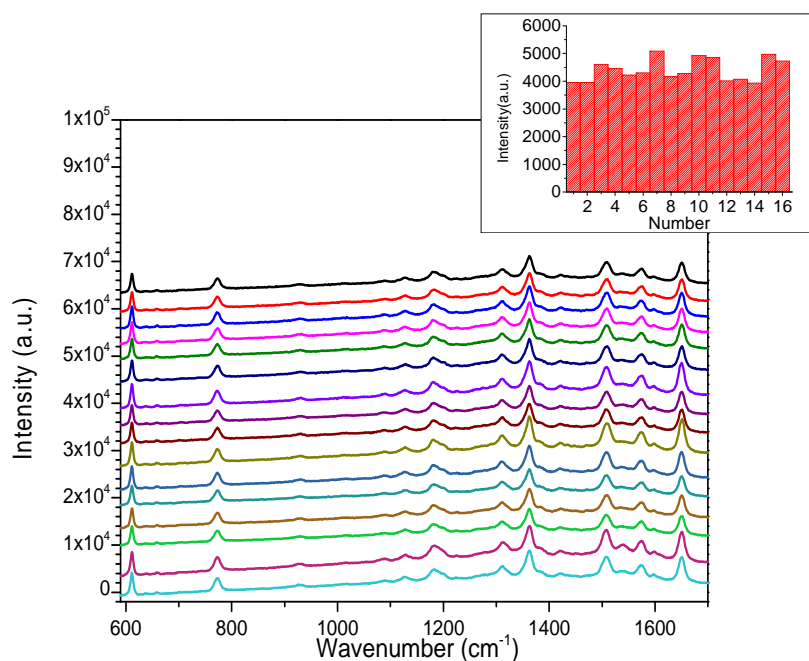


Figure 4-5: Raman spectra randomly measured in different areas of a $100 \times 100 \mu\text{m}^2$ SERS substrate, formed on a 3-seed layer after 60 min of UVA exposure, and coated with a 10^{-6} M R6G aqueous solution. The inset illustrates the intensity of the 610 cm^{-1} band measured in the different areas.

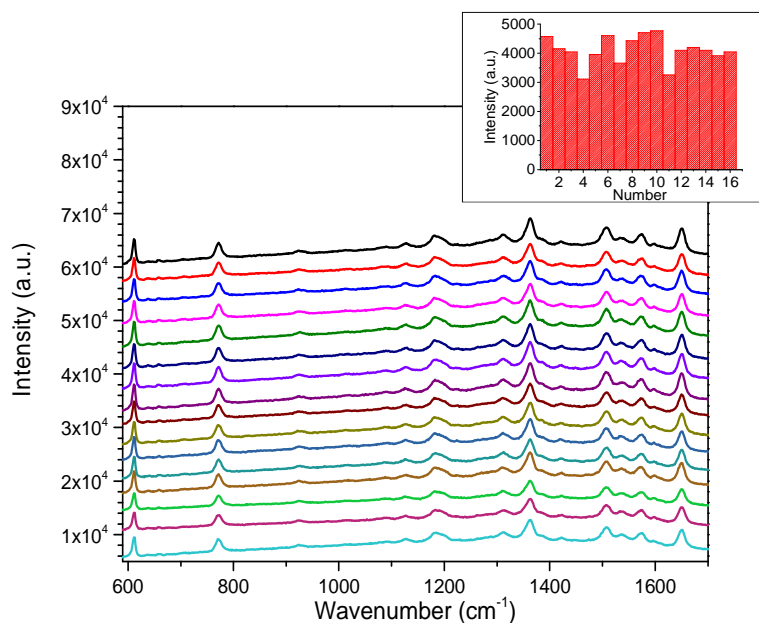


Figure 4-6: Raman spectra randomly measured in different areas of a $3 \times 4 \text{ mm}^2$ SERS substrate, formed on a 3-seed layer after 60 min of UVA exposure, and coated with a 10^{-6} M R6G aqueous solution. The inset illustrates the intensity of the 610 cm^{-1} band measured in the different areas.

This very good reproducibility is closely comparable to data reported by other authors in investigations performed on similarly small areas [1, 10]. Then, we also performed statistical studies on the whole surface of R6G-coated 3x4 mm² substrates. As illustrated in Figure 4-6 and its inset, a similarly good reproducibility of the SERS spectra, i.e. an intensity RSD of around 12%, was also evidenced on the whole surface of such substrates. As far as we know, such reproducibility on so large substrates has never been reported before for the detection of R6G on Ag^o-derived SERS substrates. As explained in introduction, a large size SERS substrate is an important criterion to consider for potential applications to the detection of multiple analytes. We also studied the spectra reproducibility in different 3x4 mm² areas of several samples elaborated in successive photocatalytic synthesis runs (Figure 4-7). This investigation showed that 80% of the spectra exhibited an intensity RSD of about 20% (see ellipsis in Figure 4-7), while the 20% remaining spectra diverged from this trend but systematically exhibited a Raman intensity amplified by a factor around 2 compared to the previous spectra. These data obviously depict a greater dispersion of the Raman intensities compared to those measured on individual 3 x 4 mm² substrates. However, it is worthwhile mentioning that, in this case, the experimental dispersion accounts both for the sample-to-sample SERS reproducibility and the SERS reproducibility over the whole surface (3 x 3 cm²) of each substrate, which actually depicts a rather good robustness of our elaboration procedure. Several measurements performed on different samples aged in the dark over a one-month period finally showed that the Raman intensity fluctuated within the previously defined sample-to-sample dispersion, which also indicates a good stability of our SERS substrates sensitivity over aging.

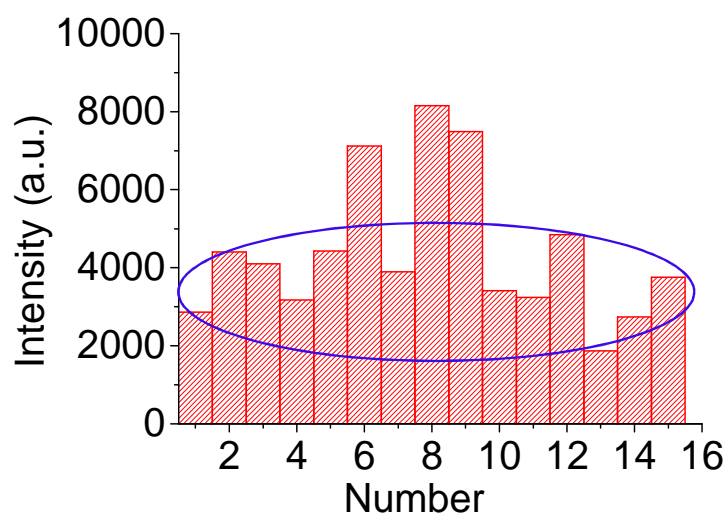


Figure 4-7: Mean intensity of the 610 cm⁻¹ band averaged from several measurements on 100 × 100 μm² areas arising from different 3 × 4 mm² pieces of different 3 × 3 cm² samples, formed on a 3-seed layer after 60 min of UVA exposure, and coated with a 10⁻⁶ M R6G aqueous solution. The ellipsis illustrated the 80% of the measured bands that exhibit an intensity RSD of about 20%.

6. SERS performances of the Ag⁰/TiO₂ heterostructure: discussion

The reproducibility of SERS spectra collected on our model Ag⁰/TiO₂ heterostructure derived from a seeded growth procedure can be discussed as follows. It firstly proves that, when diluted in water in sufficiently weak concentration, R6G does not undergo heterogeneous aggregation once deposited on the solid substrate. Besides, the spectrum reproducibility is a direct consequence of the uniform distribution of Ag⁰ NPs and/or aggregates of Ag⁰ NPs at the substrate surface. It is generally considered that the Ag⁰-based SERS effect firstly relies on the size and shape of metal NPs, which in turn govern chemical and electromagnetic mechanisms leading to a Raman signal enhancement [12, 14-17]. As illustrated in Figures 3-10d and e of chapter 3, NPs constituting our model Ag⁰/TiO₂ heterostructure exhibit a shape varying from spherical to oblong and a typical dimension ranging between 50 and 100 nm. These shape and size variations might eventually modify the Raman bands intensity in SERS spectra, which is denied by the reproducibility of spectra collected on this model heterostructure. It probably means that the SERS effect in our samples is not intrinsically governed by the shape and size of individual NPs. FEG-SEM images illustrated in Figure 3-10 of chapter 3 show that the morphologies of different heterostructure studied in this work are governed by the aggregation of Ag⁰ NPs. As mentioned in introduction, hot spots derived from aggregation features can in turn strongly amplify the Raman bands intensity. However, it has been reported that all kinds of Ag⁰ NPs aggregates do not necessarily induce hot spots, which means that, depending on their morphology (short on long linear aggregates, linear or 2D aggregates...), various kinds of aggregates can differently influence the SERS amplification arising from hot spots [2, 4]. These considerations can in turn explain important differences in the bands intensity reproducibility evidenced on heterostructure grown in the absence or the presence of seeds. Indeed, in the former case Figure 4-4 inset illustrates strongly heterogeneous aggregation features, while in the latter case, a rather uniform aggregation takes place leading to percolating aggregates (Figure 4-3 inset on the right). It does not mean that the aggregates morphology illustrated in this latter case provides the best situation for an optimized SERS amplification, but at least that the uniform aggregation at the laser beam scale (1 μm diameter) governs the reproducibility of the SERS spectra. As mentioned before, the influence of the aggregates morphology derived from different seeded growth procedures on the SERS intensity should be the object of further studies, which go beyond the topic of this thesis. Besides, the Raman bands intensity not only depends on the SERS effect, but also on the ability of SERS substrates to efficiently fix the analyte molecules, i.e. the experimental procedure used to adsorb the analyte on the solid substrate. Let us note that this feature may partially explain some ambiguities between the EF and detection limit values mentioned by different authors. In our case, two R6G adsorption mechanisms can be envisaged. On the one hand, owing to their affinity for Ag⁰ NPs, N-H bonds of the R6G molecule can induce the fixation of R6G through Ag-N binding [6, 14]. This situation is adapted to an efficient SERS detection through short-range interactions between

the R6G molecules and Ag⁰ NPs or aggregates of NPs. On the other hand, it has been reported that the alkoxy group of the R6G molecule has a particular chemical affinity for a TiO₂ surface [8]. In our case, the fixation of R6G on inter-aggregates bare TiO₂ areas would reduce the SERS detection owing to long-range interactions between the R6G molecules and Ag⁰ NPs. It means that a greater coverage rate of Ag⁰ NPs or aggregates of NPs should favor an improved R6G detection. This feature should also be the object of further investigations. In this thesis and owing to their robustness, we were encouraged to study our SERS substrates for the detection of bio-molecules of applicative interest, i.e. DNA molecules. It is the second main objective of the thesis, on which we focus in the next chapters.

7. Conclusion

Raman studies, performed on Ag⁰/TiO₂ heterostructure derived from a chemically assisted photocatalytic reduction procedure, show that the SERS amplification does not seem to intrinsically rely on the shape and size of individual NPs, but is more probably governed by hot spots induced by aggregation features. Accordingly, the homogeneous aggregation of NPs induced by a TSC-based photocatalytic reduction associated to an AA-based seeded growth leads to good SERS performances, a 10⁶ EF and a detection limit of R6G ranging between 10⁻⁸ and 10⁻¹⁰ M, as well as a good reproducibility of the R6G SERS spectra on rather large substrates. As illustrated in the previous chapter, various combinations of the seed amount and UVA exposure duration allow to selectively control the amount, aggregation state, and size of deposited NPs. It will be of particular interest to study in the future the respective influence of these parameters on the analyte adsorption and SERS performances. In the present state, it is considered that our SERS substrates has been proven to be sufficiently robust and reproducible to be extended to the detection of bio-molecules of applicative interest, such as DNA molecules whose Raman detection is by far less easy than that of R6G molecule studied in the present chapter. These features will be addressed in the next chapters.

- [1] Z. Y. Jiang, X. X. Jiang, S. Su, X. P. Wei, S. T. Lee, and Y. He, "Silicon-based reproducible and active surface-enhanced Raman scattering substrates for sensitive, specific, and multiplex DNA detection," *Applied Physics Letters*, vol. 100, pp. 203104, 2012.
- [2] S. Nie and S. R. Emory, "Probing Single Molecules and Single Nanoparticles by Surface-Enhanced Raman Scattering," *Science*, vol. 275, pp. 1102-1106, February 21, 1997.
- [3] A. M. Michaels, M. Nirmal, and L. E. Brus, "Surface Enhanced Raman Spectroscopy of Individual Rhodamine 6G Molecules on Large Ag Nanocrystals," *Journal of the American Chemical Society*, vol. 121, pp. 9932-9939, 1999.
- [4] A. M. Michaels, Jiang, and L. Brus, "Ag Nanocrystal Junctions as the Site for Surface-Enhanced Raman Scattering of Single Rhodamine 6G Molecules," *The Journal of Physical Chemistry B*, vol. 104, pp. 11965-11971, 2000.
- [5] J. A. Dieringer, R. B. Lettan, K. A. Scheidt, and R. P. Van Duyne, "A Frequency Domain Existence Proof of Single-Molecule Surface-Enhanced Raman Spectroscopy," *Journal of the American Chemical Society*, vol. 129, pp. 16249-16256, 2007.
- [6] P. Hildebrandt and M. Stockburger, "Surface-enhanced resonance Raman spectroscopy of Rhodamine 6G adsorbed on colloidal silver," *The Journal of Physical Chemistry*, vol. 88, pp. 5935-5944, 1984.
- [7] R. Vogel, M. Harvey, G. Edwards, P. Meredith, N. Heckenberg, M. Trau, *et al.*, "Dimer-to-Monomer Transformation of Rhodamine 6G in Aqueous PEO-PPO-PEO Block Copolymer Solutions," *Macromolecules*, vol. 35, pp. 2063-2070, 2002.
- [8] R. Vogel, P. Meredith, M. D. Harvey, and H. Rubinsztein-Dunlop, "Absorption and fluorescence spectroscopy of rhodamine 6G in titanium dioxide nanocomposites," *Spectrochimica Acta Part A: Molecular and Biomolecular Spectroscopy*, vol. 60, pp. 245-249, 2004.
- [9] E. Galopin, J. Barbillat, Y. Coffinier, S. Szunerits, G. Patriarche, and R. Boukherroub, "Silicon Nanowires Coated with Silver Nanostructures as Ultrasensitive Interfaces for Surface-Enhanced Raman Spectroscopy," *ACS Applied Materials & Interfaces*, vol. 1, pp. 1396-1403, 2009.
- [10] L. He, J. Huang, T. Xu, L. Chen, K. Zhang, S. Han, *et al.*, "Silver nanosheet-coated inverse opal film as a highly active and uniform SERS substrate," *Journal of Materials Chemistry*, vol. 22, pp. 1370-1374, 2012.
- [11] X. T. Wang, W. S. Shi, G. W. She, L. X. Mu, and S. T. Lee, "High-performance surface-enhanced Raman scattering sensors based on Ag nanoparticles-coated Si nanowire arrays for quantitative detection of pesticides," *Applied Physics Letters*, vol. 96, pp. 053104, 2010.
- [12] M. J. Banholzer, J. E. Millstone, L. Qin, and C. A. Mirkin, "Rationally designed nanostructures for surface-enhanced Raman spectroscopy," *Chemical Society Reviews*, vol. 37, pp. 885-897, 2008.
- [13] Y.-C. Liu, C.-C. Yu, and S.-F. Sheu, "Low concentration rhodamine 6G observed by surface-enhanced Raman scattering on optimally electrochemically roughened silver substrates," *Journal of Materials Chemistry*, vol. 16, pp. 3546-3551, 2006.
- [14] Jiang, K. Bosnick, M. Maillard, and L. Brus, "Single Molecule Raman Spectroscopy at the Junctions of Large Ag Nanocrystals," *The Journal of Physical Chemistry B*, vol. 107, pp. 9964-9972, 2003.
- [15] C. L. Haynes, C. R. Yonzon, X. Zhang, and R. P. Van Duyne, "Surface - enhanced Raman sensors: early history and the development of sensors for quantitative biowarfare agent and glucose detection," *Journal of Raman Spectroscopy*, vol. 36, pp. 471-484, 2005.
- [16] K. G. Stamplecoskie, J. C. Scaiano, V. S. Tiwari, and H. Anis, "Optimal Size of Silver Nanoparticles for Surface-Enhanced Raman Spectroscopy," *The Journal of Physical Chemistry C*, vol. 115, pp. 1403-1409, 2011.

- [17] J. Zeng, X. Xia, M. Rycenga, P. Henneghan, Q. Li, and Y. Xia, "Successive Deposition of Silver on Silver Nanoplates: Lateral versus Vertical Growth," *Angewandte Chemie International Edition*, vol. 50, pp. 244-249, 2011.

Chapter 5. SERS detection of homo-oligonucleotide single strands on $\text{Ag}^\circ/\text{TiO}_2$ heterostructure: binding, orientation and ordering on Ag° NPs surface

1. Introduction

According to the reliability of our optimized SERS platform (as illustrated in detail in the previous chapter with highly reproducible R6G SERS spectra), we were encouraged to perform extensive studies on the detection of homo-oligonucleotide single strands (also referred to as polybases, to simplify). Homo-oligonucleotides are obtained after polymerization of identical nucleotides, derived from adenine (A), cytosine (C), guanine (G), or thymine (T) nucleobases, leading to polyA, polyC, polyG, or polyT molecules (Figure 5-1).

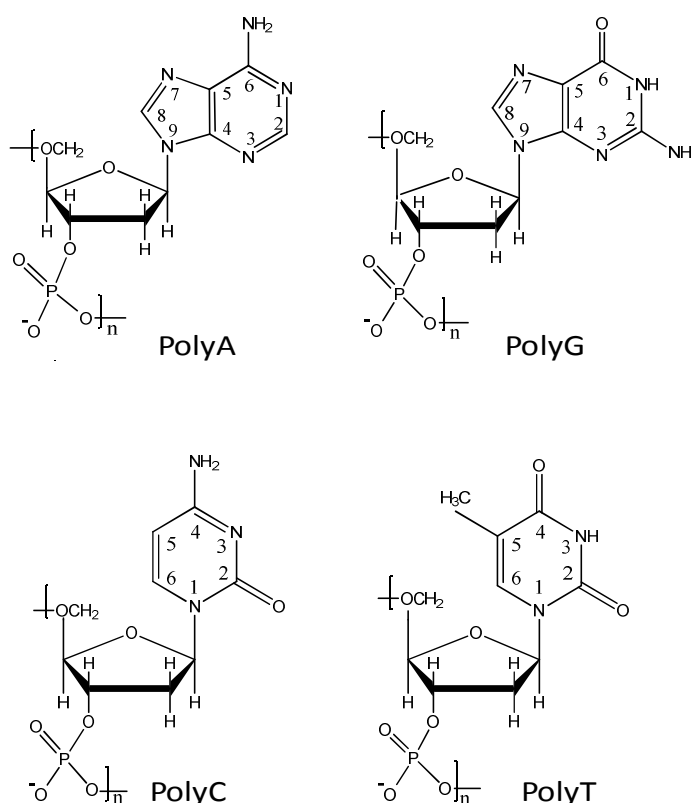


Figure 5-1: Molecular structure and N atom labeling of polyA, polyC, polyG, and polyT.

In this chapter, we report for the first time a fundamental and thorough study of the SERS spectra obtained in the case of the four homo-oligonucleotides, polyA, polyC, polyG, and polyT, immobilized on our solid Ag^o/TiO₂ SERS platform. These homo-oligonucleotides are functionalized or not by an external functional amino NH₂ linker. This enables us to study the influence of this NH₂ group on the respective SERS spectra and to draw conclusions on how DNA is immobilized on the platform. Furthermore, on the basis of XPS analyses, we pay special attention to how the homo-oligonucleotide concentration in solution influences the SERS behavior and reproducibility. It enables us to discuss how their concentration influences the packing surface density of homo-oligonucleotides and their orientation with respect to the platform surface.

2. DNA material and immobilization process

2.1 DNA material: polybases-NH₂ and polybases

The DNA molecules studied here are homo-oligonucleotide single-strands, purchased from Biomers (Germany). Their sequence is detailed in Table 5-1. There are two groups of polybases, depending on the presence or the absence of an external functional NH₂ group at the 5' extremity of the strand, as schematized in Figure 5-2. The polybases will be labeled polybases-NH₂ or polybases, respectively, in which the bases corresponds to A, C, G, or T (as seen in Figure 5-2).

Polybase		Sequence
External group NH ₂ functionalized polybase	PolyA-NH ₂	5' NH ₂ T5-A15 3'
	PolyC-NH ₂	5' NH ₂ T5-C15 3'
	PolyT-NH ₂	5' NH ₂ T20 3'
	PolyG-NH ₂	5' NH ₂ T5-G15 3'
NH ₂ free polybase	PolyA	5' T5-A15 3'
	PolyC	5' T5-C15 3'
	polyT	5' T20 3'
	polyG	5' T5- G15 3'

Table 5-1 : Polybase sequence details: polyA, polyC, polyT, and polyG in the presence or not of an external functional NH₂ group. Note: T₅ is a spacer commonly used for DNA hybridization on biosensor surfaces.

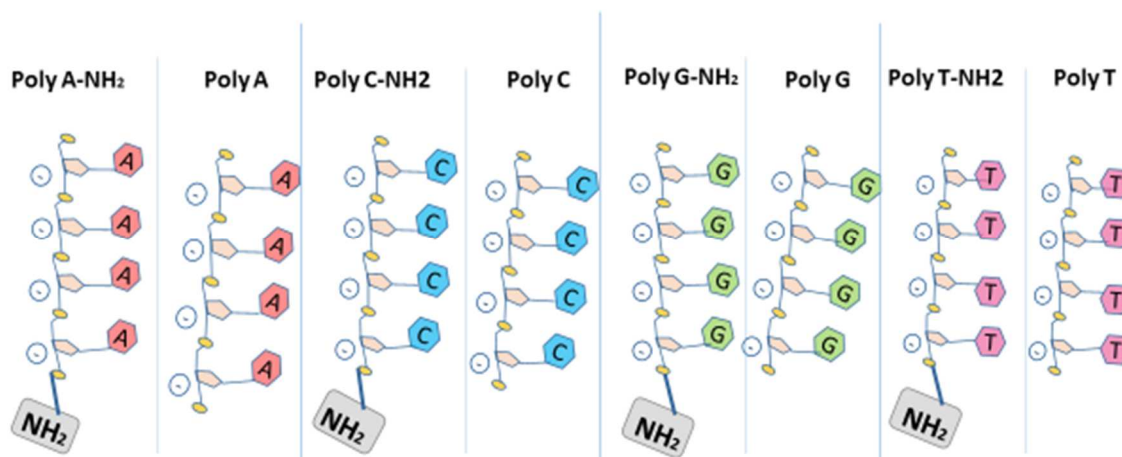


Figure 5-2: Schematic representation of the two kinds of polybases following the presence or the absence of the external NH_2 linker: polybases- NH_2 and polybases.

As mentioned in chapter 2 (section 4), our SERS platform benefits from important assets in respect to the DNA immobilization. On the one hand, NH_2 -modified DNA molecules can be directly immobilized on the platform through a simplified protocol that does not involve a traditional multi-step and time consuming silanization process [1]. It is assumed that this direct immobilization arises from the affinity of Ag° metal surface to N atoms of NH_2 amino groups, which favours the DNA grafting through the formation of Ag-N bonds. On the other hand, the DNA immobilization benefits from the photohydrophilicity of a TiO_2 surface, i.e. such a surface exposed to UVA light exhibits a superhydrophilic behaviour. Thus, after the photocatalytic reduction step leading to Ag° NPs, the photo-induced superhydrophilicity of bare TiO_2 areas (not coated by Ag° NPs) enables a good spreading of the DNA aqueous solution, leading to a rather uniform immobilization of DNA on the SERS platform. Accordingly, both features allow a simplified immobilization protocol.

2.2 DNA immobilization process

We have performed extensive studies to optimize the direct grafting of polybases on the SERS substrates while attempting to maintain the integrity and adhesion of Ag° NPs on the TiO_2 surface. In this aim, different grafting solutions have been preliminary tested, as illustrated in the Table 5-2. According to these studies, we have successfully established an optimized standard procedure, which has definitively been employed in all experiments. The polybases were diluted in an aqueous solution of monobasic sodium phosphate NaH_2PO_4 ($C = 0.3\text{M}$). This moderately acidic solution ($\text{pH} = 4.5$) preserves the

integrity of Ag⁰ NPs, avoiding both their peel off from the TiO₂ surface and any corroding reaction. For each studied polybase, with or without NH₂ external group, the concentration of DNA solution has been varied from 1 to 100 μM.

Tested grafting solution	Pure deionized water	Monobasic sodium phosphate: H ₂ PO ₄ ⁻ , Na ⁺ in pure deionized water C=0.3 M, pH=4.5	Dibasic sodium phosphate: HPO ₄ ²⁻ , 2Na ⁺ in pure deionized water C=0.3 M, pH= 9
Acquisition of SERS spectra	Random	Yes	No

Table 5-2: Tested solutions for the grafting of ssDNA and corresponding results in term of SERS spectrum acquisition.

The Ag⁰/TiO₂ substrates were cut in 7x7 mm² square pieces immediately after photo-reduction under UVA light for 60 min. Then, a 10 μL volume droplet of the polybase-containing aqueous solution was deposited on the substrate surface (Figure 5-3). In these conditions and due to the high hydrophilicity of the substrate, the drop naturally spreads over the surface with a contact angle value measured to be around 10°. After one night incubation at room temperature under ~ 35% relative humidity, the droplet was rinsed with deionized water and then dried for one hour at room temperature, ready for SERS experiments.

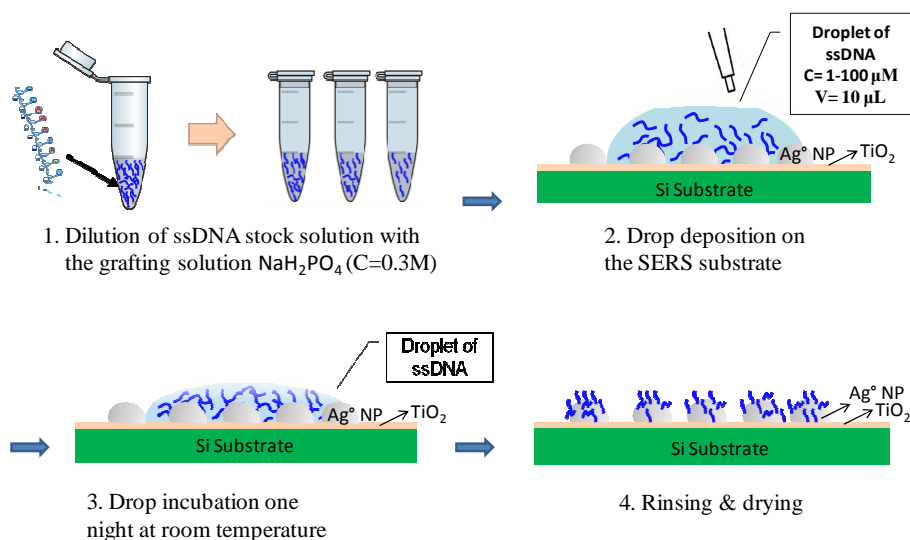


Figure 5-3: Schematic representation of the optimized ssDNA grafting procedure on the 7×7mm² Ag⁰/TiO₂ SERS substrate immediately after UVA exposure.

The chemical properties of the extreme surface of the Ag^o/TiO₂ SERS platforms after polybases deposition were characterized by XPS, using the procedure described in chapter 3 (section 4.1.1).

The same Raman equipment, as previously described in chapter 4 (section 2), was used to collect the SERS spectra of all polybases, except that in this case we used the $\lambda=632.8$ nm red line of a He-Ne laser. An accumulation time of 20 seconds and a laser power of *ca.* 1 mW at the sample surface were used to record spectra in the 600-1600 cm⁻¹ range. For each experiment, as for R6G Raman characterization, we systematically investigated two different 100 x 100 μm^2 areas of a same 7x7 mm² substrate and six spectra were collected in different places of each probed areas.

3. Results

3.1 DNA concentrations effects

3.1.1 Surface chemical analyse by XPS

To prove that DNA molecules are effectively present and correctly grafted on our SERS substrates, we performed XPS analyses. The measurements were performed on SERS substrates coated with polyA-NH₂ strands, chosen as model DNA molecules. The solutions concentrations were fixed at 0, 1, 5, 10, and 50 μM .

In a first step, let us observe the results obtained for a concentration of 10 μM . Similarly to the survey of the bare substrate (Figure 3-12, chapter 3), the new survey (not shown here) still exhibits the presence of Ag 3d and Ti 2p peaks. Their high resolution spectra are reported in Figures 5-4 a and b, respectively. The new information is brought by the presence of N 1s and P 2p peaks, whose high resolution spectra are reported in Figures 5-4 c and d, respectively. The P 2p peak, located at a binding energy of 132.9 eV, is highly characteristic of the phosphate groups of DNA backbone, while the N 1s peak is characteristic of the N containing nucleobases. The N1s peak fit can be reasonably described by using two components with binding energy separation of $\Delta E=1.5$ eV (Figure 5-4c). One component is located at 400.5 eV and the other one at 399.0 eV. Both of them feature the several chemical environments of the N atom within the adenine nucleobase (-NH₂, -NH-, and =N-). According to the XPS study achieved by Opdahl et al. on polyA adsorbed on Au surface, the lowest energy component features the strong chemisorption interaction between the N elements of the adenine nucleobase and the metal surface [2]. It would confirm that, in our case, the polyA-NH₂ is strongly bond to the Ag^o surface. However, we cannot exclude that some DNA molecules are also bound on bare TiO₂ areas of the SERS substrate. It is for instance known that phosphate groups have a particular affinity for metal oxide surfaces. This feature has particularly been used to attach phosphopeptides on titanium dioxide surfaces [3]. The

mechanism involves a bidentate binding mode in which two oxygen atoms are involved to link titanium and phosphorus atoms. This process is all the more efficient as the fixation procedure is performed in acidic conditions owing to an enhanced affinity of negatively charged phosphate groups to the positively charged TiO_2 surface [4]. Let us recall that our DNA immobilization procedure was performed in (moderately) acidic conditions ($\text{pH} = 4.5$).

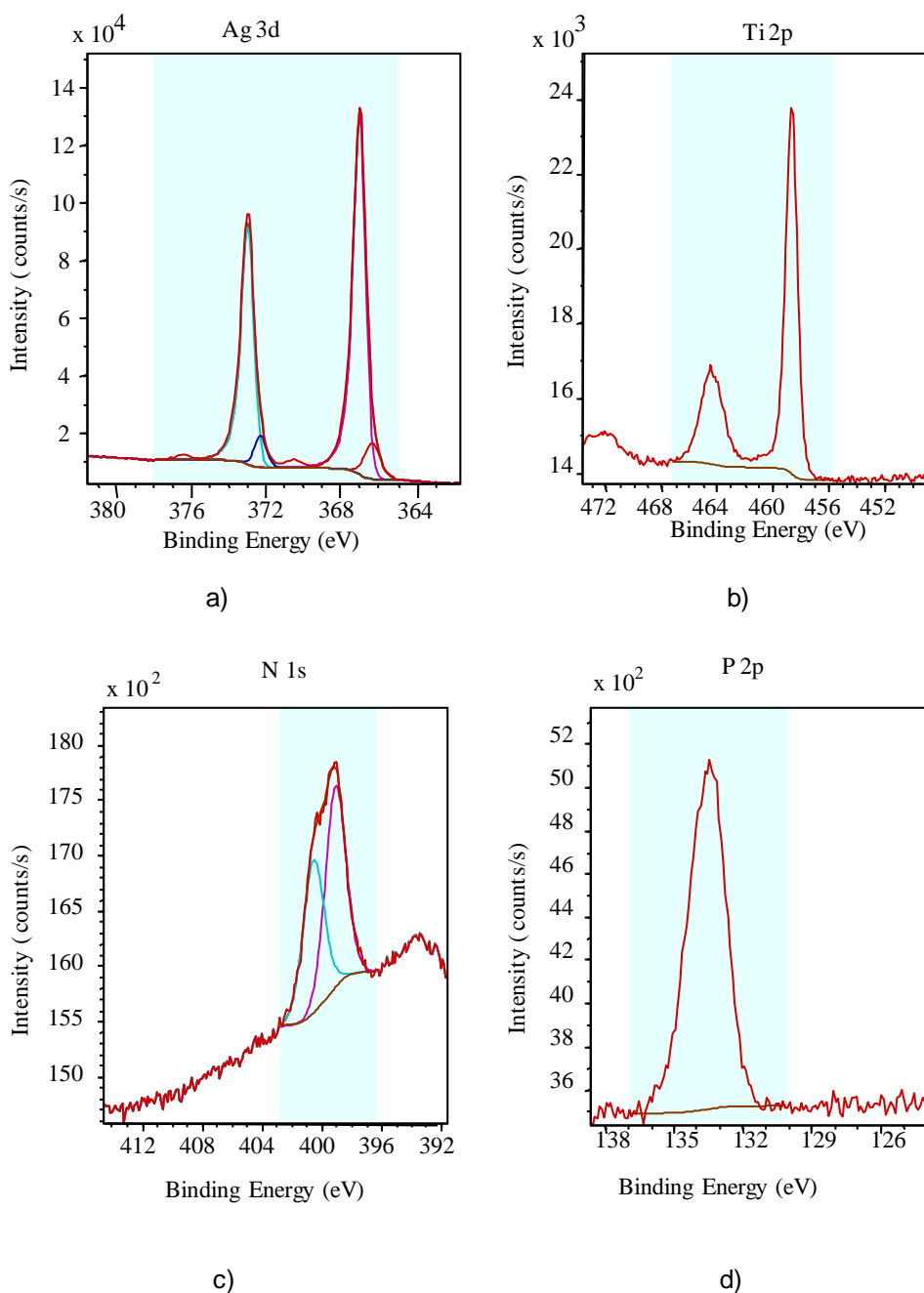


Figure 5-4: High resolution XPS spectra of four principal elements of the polyA-NH₂ (10 μM) covered Ag^o/TiO₂/Si substrate: (a) Ag 3d; (b) Ti 2p; (c) N 1s; and (d) P 2p.

Whether polyA molecules are fixed on Ag⁰ NPs or on bare TiO₂ areas is an important issue because, in the former case (Ag-N bonds), polyA is directly in contact with SERS active NPs, a favorable configuration for SERS, whereas in the latter case (grafting on Ag⁰ free TiO₂ areas), the DNA molecules may be located far from the active NPs, and thus may not be detected by SERS. The response to this uncertainty is brought from the observation of the respective evolutions of the Ag and Ti doublets intensity as a function of polyA-NH₂ concentration. Figure 5-5 first shows that, in the whole range of tested concentrations (0-50 μM), the grafting of polyA-NH₂ induced no variation in the titanium signal intensity. In contrast, the silver signal jumps down when the polyA-NH₂ concentration increases to 5-10 μM.

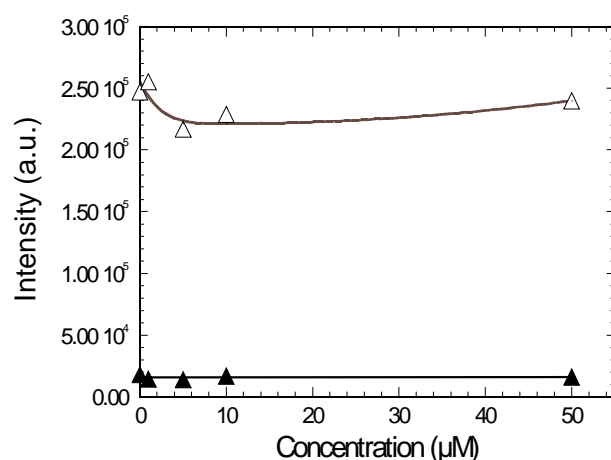


Figure 5-5: Intensity of the Ti 2p (▲) and Ag 3d (Δ) XPS doublets as a function of the polyA-NH₂ concentration in solution.

In other words, adsorbed polybase molecules partially screen the Ag⁰ signal but not the TiO₂ one, which clearly indicates that polyA-NH₂ molecules are preferentially grafted on Ag⁰ NPs. As previously mentioned, such a preferential adsorption on Ag⁰ NPs may be explained by the greater affinity of N atoms to Ag⁰ NPs, compared to that of P atoms to the TiO₂ surface. This feature is linked to the fact that, under our moderately acidic immobilization conditions, the TiO₂ film surface is only slightly positively charged (the isoelectric point of TiO₂ ranges between pH values of 5 and 6) and cannot strongly bind negatively charged phosphate groups. However, further increase in the polyA-NH₂ concentration above a 10 μM threshold value does not promote any further decrease of the Ag signal. It even seems that this signal slightly increases when the polyA-NH₂ concentration increases above 10 μM. As will be discussed later in the chapter, this behavior likely arises from the concentration dependence of the DNA molecules organization (distribution and orientation) at the SERS substrate surface.

To summarize, the XPS analyses evidenced the following results:

- The presence of DNA molecules is confirmed by the appearance of N 1s and P 2p XPS peaks around 400 and 133 eV, respectively.
- The DNA molecules are preferentially located on the Ag⁰ NPs and not on the TiO₂ surface, as deduced from the respective evolutions of the Ti 2p and Ag 3d signals following DNA concentration.
- The concentration dependence of the Ag 3d peak intensities evidences the existence of an optimum concentration ranging from 5 to 10 μM for DNA molecules on Ag⁰ NPs surface.

3.1.2 SERS analyses

3.1.2.1 Spectra of polyA-NH₂ and polyC-NH₂

The SERS spectra were acquired for DNA concentrations ranging from 1 to 100 μM for the four polybases-NH₂ and polybases. For all studied molecules, a similar trend was observed with respect to their concentration, regardless of the presence or absence of the external NH₂ linker. As an illustration, we present the typical spectra obtained in the case of polyA-NH₂ (Figure 5-6) and polyC-NH₂ (Figure 5-7) for concentration values of 1, 5, and 100 μM. At this step, we essentially focus on the general behavior of spectra and on the main characteristic bands of polyA-NH₂ and polyC-NH₂. The latter are the in-plane ring breathing modes (IPRBM) located at 735 cm⁻¹ and 792 cm⁻¹ for polyA-NH₂ and polyC-NH₂, respectively. A thorough study of all the other bands for all polybases will be described in section 3.2.1.

- At the lowest concentration (around C = 1 μM), as illustrated in Figures 5-6a and 5-7a, the intensities of the main DNA band lines of polyA and polyC are particularly weak, while bands of the substrate, the spectrum of which is presented in Figure 5-8, are clearly visible, in particular, bands at 640 cm⁻¹ and in the 940-1000 cm⁻¹ range which correspond to anatase TiO₂ film and Si second order, respectively.
- For intermediary concentrations (5 to 10 μM), illustrated in Figures 5-6b and 5-7b for a concentration of 5 μM, two observations can be made. On the one hand, in both cases spectra display a greater average intensity of the DNA bands, while the substrate bands are strongly attenuated. On the other hand, all spectra exhibit good reproducibility, both in their general behaviors and in their intensities. This important aspect will be more extensively studied in section 3.3.2.
- In contrast, for higher concentrations (around C = 100 μM), the spectral intensities exhibit non-reproducible features as illustrated in Figures 5-6c and 5-7c for polyA-NH₂ and polyC-NH₂, respectively. These particular features will be detailed in section 3.3.1.

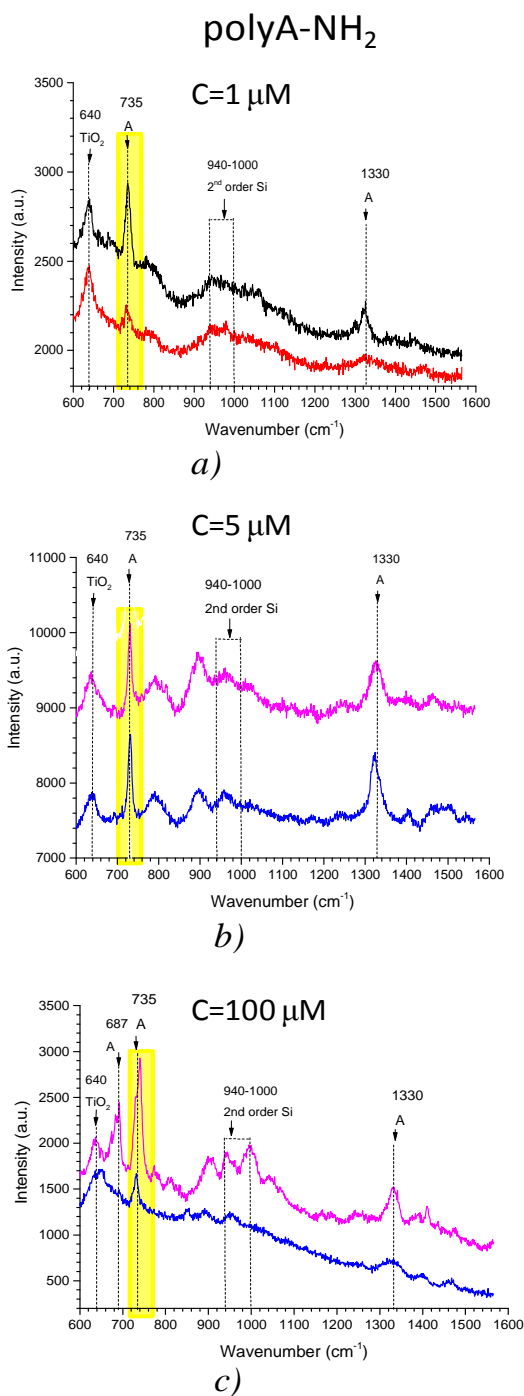


Figure 5-6: SERS spectra of polyA-NH₂ acquired for different concentrations ranging from 1 to 100 μM on two different areas of the Ag⁰/TiO₂ platform surface.

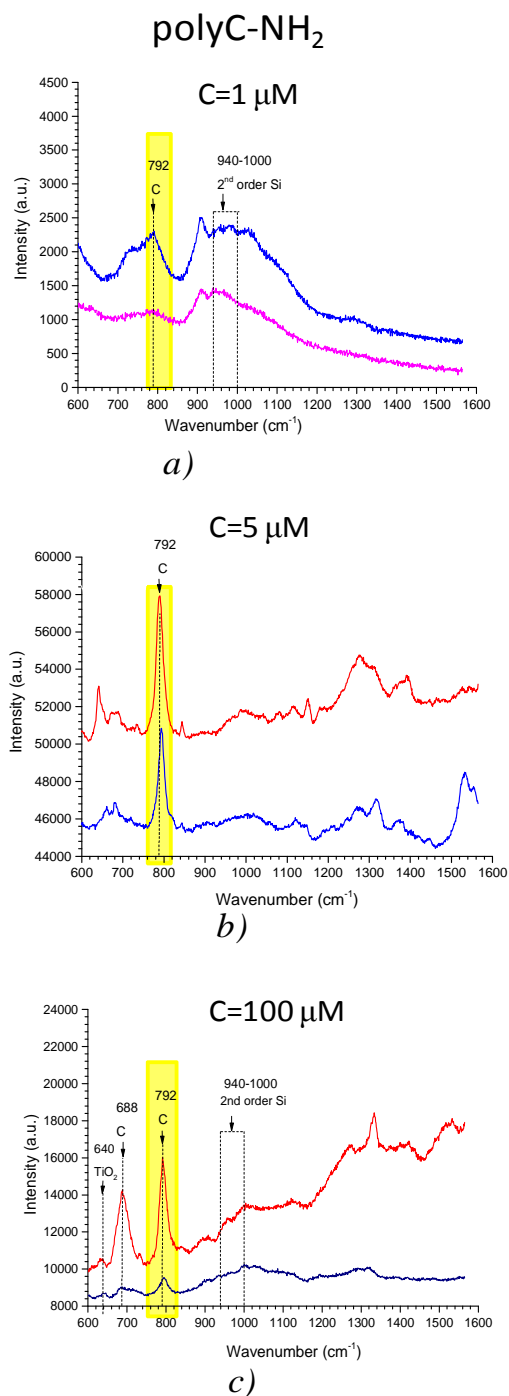


Figure 5-7: SERS spectra of polyC-NH₂ acquired for different concentrations ranging from 1 to 100 μM on two different areas of the Ag⁰/TiO₂ platform surface.

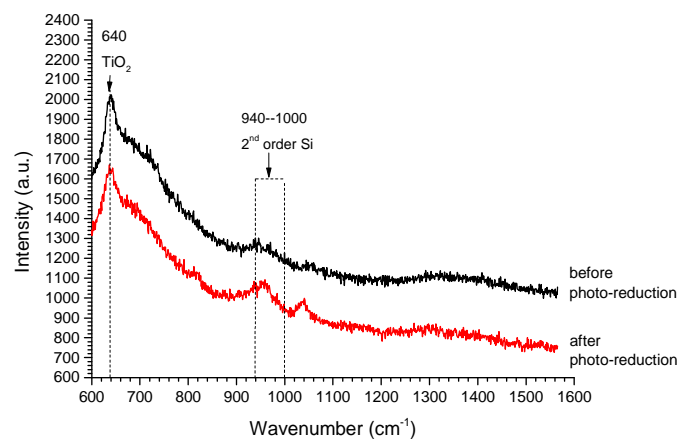


Figure 5-8: Raman spectra of a DNA free $\text{Ag}^\circ/\text{TiO}_2$ substrate before and after the process of UVA photoreduction.

To better emphasize the effect of the DNA concentration on SERS spectra, we chose to investigate the concentration dependence of the main DNA band intensities, i.e. IPRBM, for the different studied polybases. The results are presented in the following.

3.1.2.2 Evolution of the IPRBM following DNA concentration

The evolution of IPRBM are reported in Figure 5-9 in the case of the 735 cm^{-1} band for polyA-NH₂ and polyA, as well as in the case of the 792 cm^{-1} band for polyC-NH₂ and polyC. In the four cases, an optimal concentration yielding a maximal intensity is clearly observed between 5 and 10 μM . Owing to this maximum of intensities, SERS studies presented in the following sections have been performed at a fixed concentration of 5 or 10 μM . In particular, the thorough indexation of the four studied polybases-NH₂ and polybases is detailed in this section.

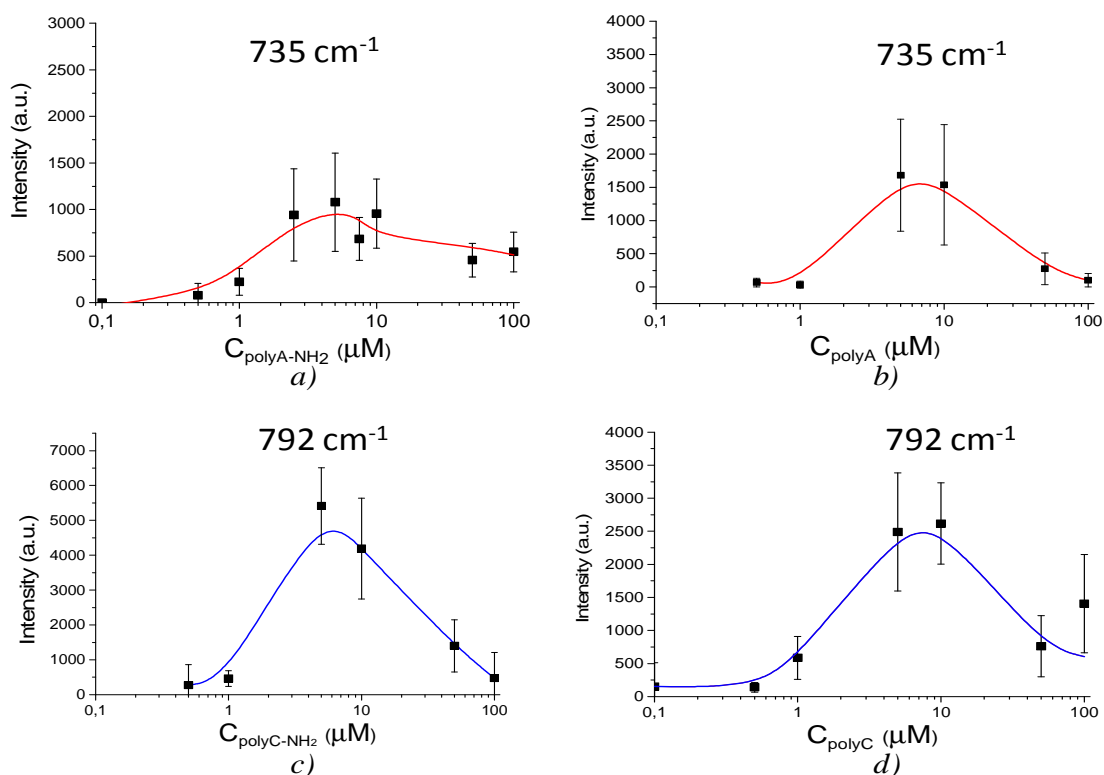


Figure 5-9 : Respective intensity evolutions of the 735 cm^{-1} and 792 cm^{-1} in-plane vibration band as a function of the concentration in solution of polybase for a) polyA-NH₂, b) polyA, c) polyC-NH₂, and d) polyC.

3.2 Analyses at fixed concentration

3.2.1 Spectrum indexation of each polybase

Typical spectra of the four studied NH₂-modified and NH₂-free polybases are reported in Figure 5-10 to Figure 5-13. Before going further in the investigation of each polybase spectrum, it is first necessary to point out some common bands which are systematically present in all spectra. These very weak bands, the intensity of which is more or less significant depending on the spectra, correspond to vibration modes arising either from the substrate material or from the DNA backbone bindings. As previously mentioned regarding the substrate material, a first band located at 640 cm^{-1} corresponds to the TiO₂ film, while a second one in the range $940\text{--}1000\text{ cm}^{-1}$ corresponds to the Si 2nd order (Figure 5-8). Regarding the DNA backbone, many small bands in the $800\text{--}1100\text{ cm}^{-1}$ spectral range depict C-O bonds of ribose and phosphate groups. It is known that such species present many Raman bands such as $842, 900, 960, 995, 1000,$ and 1010 cm^{-1} ones [5]. However, owing to their weak intensity, these bands can hardly be indexed in our spectra. All other bands are due to ring vibration modes of the four studied polybases, whose indexation is summarized in Table 5-3 according to various references cited in the literature. Hereafter, we firstly detail the main DNA bands in the case of NH₂-modified polybases, and then extend our observations to NH₂-free polybases.

Table 5-3: Vibrational assignments for each polybase

Band position (cm ⁻¹)	Tentative assignments				Ref.
	PolyA	PolyC	PolyG	PolyT	
656			In, breath R6		[6-8]
687	Out, def R5, R6 (tors C4-C5-C6, w N3-C4-N9)				[9-11]
688		Out, bend C5-C4, N3-C4			[6]
700			In, bend (ring)		[9, 12]
706				In, ring breath	[13]
730			Out, def R6 (w N1-C2-N3), tors NH ₂		[7]
735	In, ring breath				[9-11, 14]
786	Out, def R6 (w C4-C5-C6, w C8-H)				[9-11, 14]
792		In, ring breath			[6, 15-17]
798			Mentioned but not indexed in ref.		[6]
799				In, ring breath	[6, 13, 18]
850			In, def R6-R5		[8, 9, 12]
889			In, NH bend		[8]
957			In, def R5 (sqz N7-C8-N9)		[6, 7]
1138			In, bend C8-H, str C4-N9, rock NH ₂		
1212				In, str C5-C6, bend CH ₃ , str N3-C4, C6-N1	[7, 13, 18]
1235			In, pyrimidic character		[8, 9, 12]
1260		In, str C4-N3			[17]
1280		In, str C2-N3			[16, 17]
1295			In, str N7-C8, C2-N3, bend N1-H		[7]
1312				In, bend N3-H, C6-H	[7, 13]
1315		In, str N1-C6+ C5-C6			[6, 15]
1328			In, bend C8-H, str C5-N7-C8		[6]
1333	In, ring skeleton vibration: str C5-N7, N1-C2, bend C2-H, C8-H				[6, 9-11, 14]
1380		In, bend C=C-H			[6, 15, 17]
1380				In, bend C5-Me	[6, 13, 18]
1385			In, str C2-N3, C6-N1, C5-C6, C4-N9, C5-N7		[6, 8]
1402	In, bend C2-H, str C8-N7, N1-C2				[9, 10]
1463	In, str C2-N3, N1-C6, bend C2-H, sciss NH ₂				[9-11]
1463				In, sciss CH ₃ , bend C6-H	[13, 18]
1468			In, str N7=C8 & C8-N9		[8, 9, 12]
1472		In, str C4-N3 + C2-N3			[15, 17]
1484		In, str N1-C6 + str N3-C4			[6]
1495				bend C6-H, N-H	[7, 13, 18]
1532			In, str C=C, str N3-C4		[8, 9]
1535	In, str N3-C4, N1-C6, C5-N7, N7-C8, sciss NH ₂				[9, 12]

Note : In, in-plane; out, out of plane; bend, bending; def, deformation; wag, wagging; R5, five-membered ring; R6, six-membered ring; tors, torsion; sciss, scissoring; ring breath, in-plane ring breathing mode; sqz, squeeze.

3.2.1.1 Case of polybases-NH₂

- **PolyA-NH₂** (Figure 5-10a): As commonly reported in the literature for polyA, as well for the adenine nucleobase, the spectrum is largely dominated by a sharp band at 735 cm⁻¹, which corresponds to in-plane ring breathing mode, and to a lesser extent by a multicomponent band centered around 1330 cm⁻¹. The latter is attributed to mix in-plane stretching motions of the six membered ring skeleton vibration modes [6, 9-11, 14]. The most intense component of this band, located at 1333 cm⁻¹, can be reasonably attributed to the N7-C5 stretching mode [6, 9-11, 14]. Some additional in-plane vibration modes can also be observed at 1402 cm⁻¹, 1463 cm⁻¹, and 1535 cm⁻¹. In addition, some weak bands corresponding to out of plane vibration modes can be distinguished at 687 cm⁻¹ [9-11] and at 786 cm⁻¹ [9-11, 14]. It is interesting to note that the relative intensity of aforementioned bands markedly differs from the ones reported by E. Papadopoulou *et al.* for polyA at a concentration of 10⁻⁶ M in various colloidal solutions [19]. In their case, the 735 cm⁻¹ band is the least intense whereas, depending on the used colloids, either the 1333 cm⁻¹ or the 1463 cm⁻¹ band is the most intense. These differences with our spectra should be attributed to various effects of the different polyA environment.

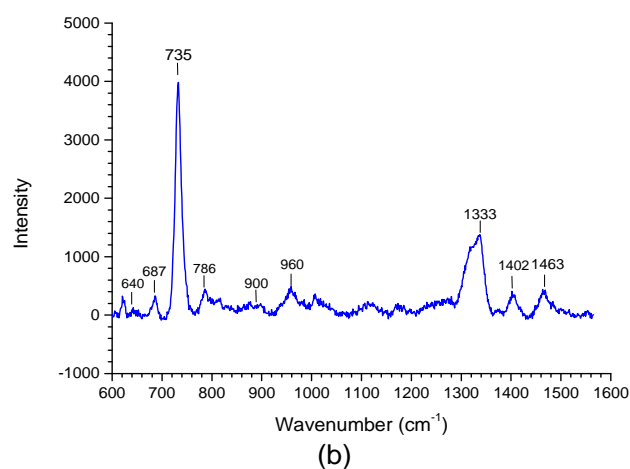
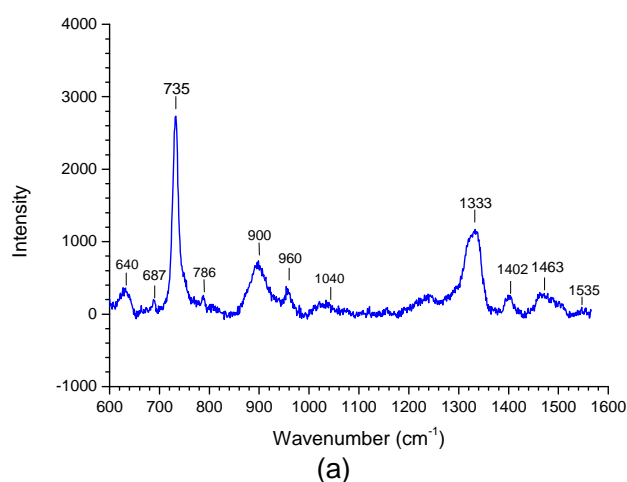


Figure 5-10: SERS spectra of polyA-NH₂ (a) and polyA (b) obtained for a concentration of 10. 10⁻⁶ M in solution.

- **PolyC-NH₂** (Figure 5-11a): The spectrum exhibits a dominant cytosine band at 792 cm⁻¹ corresponding to the in-plane ring breathing mode and, at higher frequencies (1250-1500 cm⁻¹), a group of less intense but still marked bands [6, 15-17]. In this latter spectral range, the dominant band located at 1315 cm⁻¹ is associated with the skeleton vibration [6, 15]. It is mainly surrounded by four bands corresponding to, on a one hand, C4-N3 stretching at 1260 cm⁻¹ and C2-N3 stretching at 1280 cm⁻¹ [16, 17], and on the other hand, two bands at 1380 cm⁻¹ corresponding to C=C-H bending and at 1484 cm⁻¹ corresponding to N1-C6 and N3-C4 stretching modes [6, 15, 17]. In addition to these in-plane vibrations, one can also clearly observe at 688 cm⁻¹ a small band corresponding to out of plane vibrations [6].

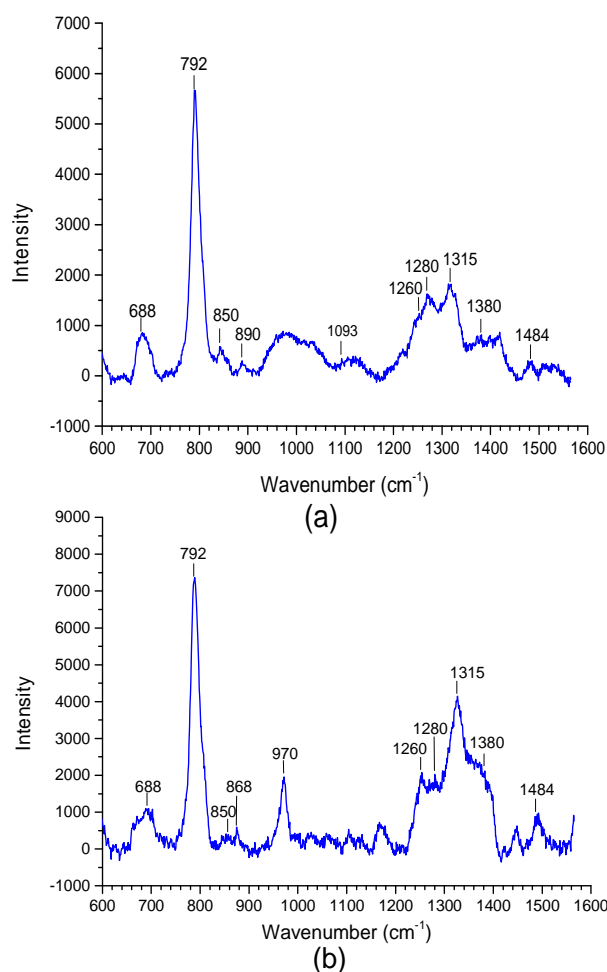


Figure 5-11: SERS spectra of (a) polyC-NH₂ and (b) polyC for a concentration of 10. 10⁻⁶ M in solution.

- **PolyG-NH₂** (Figure 5-12a): The most important band of guanine is easily seen at 656 cm⁻¹, which corresponds to in-plane ring stretching mode [6-8]. Remarkably, in addition to the 656 cm⁻¹ band, the spectrum is characterized by numerous well defined bands of medium intensity, the indexation of which is summarized in Table 5-3. They are mainly assigned to in-plane vibration modes (no reference has

been found to index the 798 cm^{-1} band, even if this band has already been observed by others [14]). Beside all these in-plane vibration features, a small band is clearly observed at 730 cm^{-1} , which corresponds to out of plane bending mode [7]. Previously, Green et al. discerned for the first time the presence of Raman bands around 688 cm^{-1} [14]. From these bands, they deduced that at least two kinds of polyG adsorption configurations occurred on the substrate.

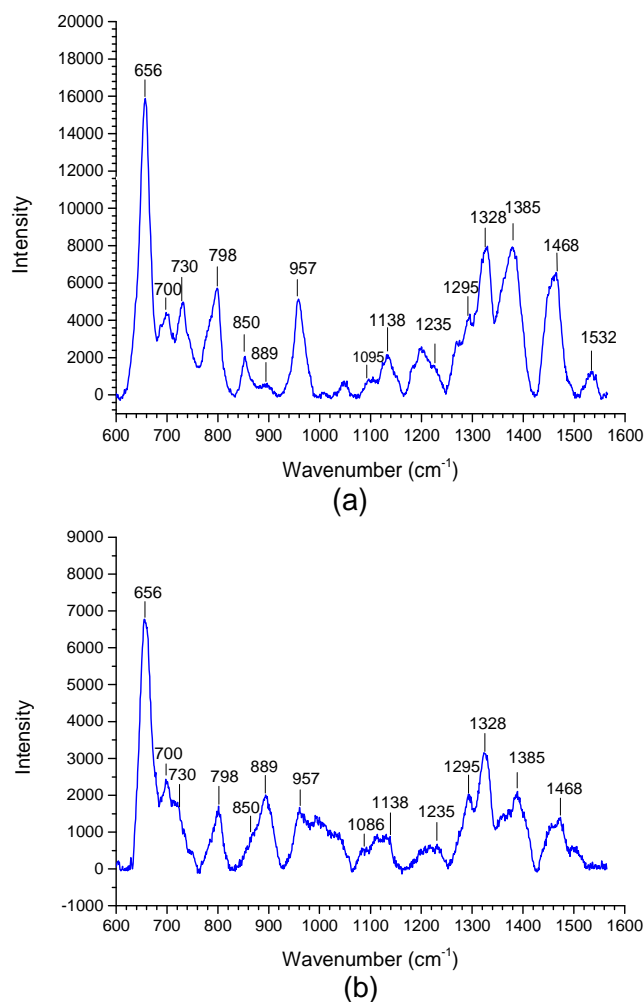


Figure 5-12: SERS spectra of (a) polyG-NH₂ and (b) polyG obtained for a concentration of $10 \cdot 10^{-6}\text{ M}$ in solution.

- **PolyT-NH₂** (Figure 5-13a): The spectrum displays a major band at 799 cm^{-1} corresponding to the in-plane ring breathing mode [6, 13, 18]. This location is clearly distinct from the similar vibration band of cytosine located at 792 cm^{-1} (Figure 5-11a), which is contrary to the results of Green et al. who reported a similar position for polyC and polyT [14]. At higher frequencies, a line located at 1212 cm^{-1} corresponds to different in-plane C-N stretching modes [7, 13, 18], while a line at 1312 cm^{-1} and another one at 1380 cm^{-1} are assigned to N3-H and C6-H in-plane bending modes and to C5-methyl, respectively

[19]. Interestingly, in the case of polyT-NH₂, we could not identify any band assigned to out of plane vibration modes.

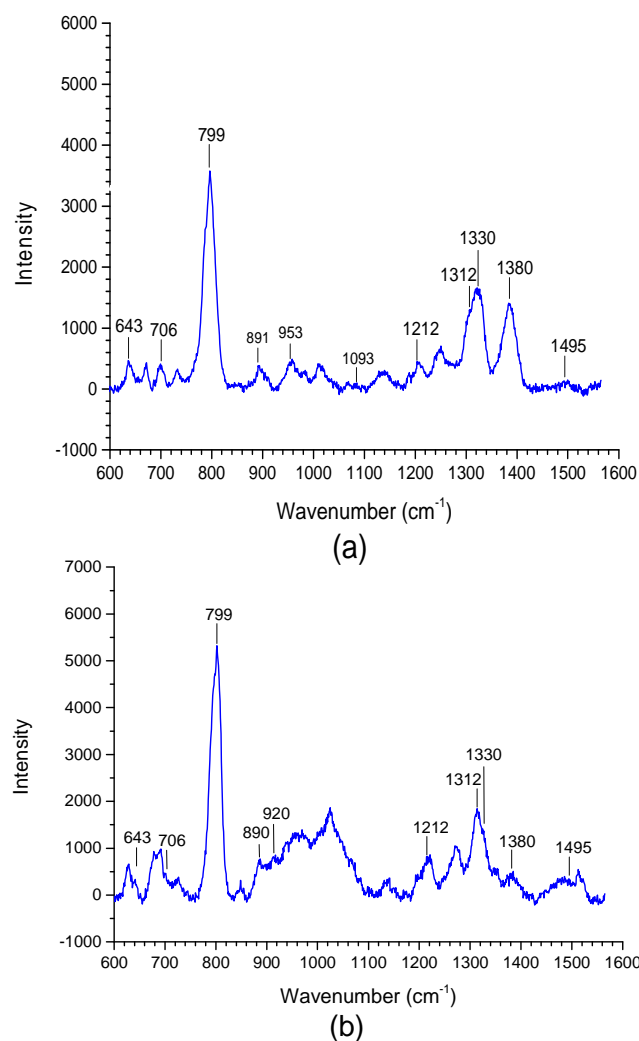


Figure 5-13: SERS spectra of (a) polyT-NH₂ and (b) polyT obtained for a concentration of 10. 10⁻⁶ M in solution.

3.2.1.2 Case of NH₂-free polybases

In comparison to NH₂-modified polybases (Figures 5-10a to 5-13a), two main analyses can be made in the case of NH₂-free polybases, whose spectra are illustrated in Figures 5-10b to 5-13b. On the one hand, previously described secondary bands are again detected but compared to that of NH₂-modified polybases, their relative intensities are somewhat modified. We also observed in some rare cases additional bands not observed in the case of NH₂-modified polybases, in particular a band located at 970 cm⁻¹ in the case of polyC, which could not be assigned. A discussion of these differences, which depict secondary spectral features, is beyond the scope of this thesis. On the other hand, similarly to NH₂-modified polybases, the spectra of NH₂-free polybases are strongly dominated by in-plane breathing

modes (at 656, 735, 792, and 799 cm^{-1} for the different NH_2 modified or not polybases). Besides, the intensity of such vibration modes exhibits similar orders of magnitude, regardless of the presence or absence of NH_2 external groups. In contrast, for the concentration illustrated here (10 μM), out of plane bands are extremely weak (polyA, polyC, polyG) or even absent (polyT). All these features will be discussed in the following.

To summarize, this description of the four polybases SERS spectra, obtained in the case of NH_2 modification or not, depicts the reliability and efficiency of our solid SERS substrate both in terms of sensitivity and resolution, which enabled us to clearly index the main and secondary lines. Even if our spectra are sometimes in contradiction with spectra mentioned by others, they could be interpreted unambiguously according to the overall literature. In addition, when they are compared to spectra found in the literature, if the polyA spectra are globally similar to the ones commonly reported, the spectra of the other polybases exhibit quite high resolution and signal/noise ratio. Actually, and to the best of our knowledge, it is the first time that spectra of all four polybases spectra have been the object of such a complete (even if non-exhaustive) indexation on a same solid SERS substrate. In addition, from the comparison between polybases- NH_2 and polybases spectra, we did not emphasize significant differences between the spectra obtained in both cases. As a consequence, the external NH_2 linker seems to be not essential for the molecules immobilization on the Ag^0 surface. Based on this thorough indexation of polybases- NH_2 and polybases spectra, we then focus on the problematic of spectrum reproducibility according to the DNA concentration.

3.3 DNA concentration-dependent reproducibility of SERS spectra

In this part, SERS spectra were acquired in a 600-950 cm^{-1} spectral range for concentrations ranging from 1 to 100 μM for the four studied polybases. As detailed in section 3.1.2 of this chapter, and already illustrated in the Figures 5-6, 5-7, and 5-9 for polyA- NH_2 and polyC- NH_2 , two main domains of concentrations can be distinguished. The first domain corresponds to the optimal range of concentration ($C = 5\text{-}10 \mu\text{M}$). The second one is located on each side of the previous domain, below and above the optimal concentration range. In this section, we focus on the reproducibility of SERS spectra in the two domains of concentration. We recall that, for each concentration, spectra are acquired in six different places of two areas of a same substrate.

3.3.1 Range of lowest and highest DNA concentrations

This range of concentration is not further illustrated by spectra in this section and, for illustrations, the reader should refer to examples depicted in Figures 5-6a and c and Figures 5-7a and c in the case of

polyA-NH₂ and polyC-NH₂, respectively. At lowest concentrations as well as highest ones, and for all studied polybases, the Raman peak intensities are particularly weak (Figure 5-9) and their reproducibility is very poor. Actually, the main IPRBM band of each polybase varies by one order of magnitude when measured in different places of a same substrate. In addition, we noticed important fluctuations in the relative intensity of the different Raman bands previously indexed for each base. Besides, a particular feature has to be mentioned in the case of highest concentrations. For each polybase, and as illustrated in Figures 5-6c (band at 687 cm⁻¹) and 5-7c (band at 688 cm⁻¹) in the case of polyA-NH₂ and polyC-NH₂, respectively, at highest concentrations, the out of plane vibration modes are particularly enhanced. In contrast, and as illustrated in Figures 5-10 to 5-13, at weaker concentrations these modes are weakly intense or even absent (polyT and polyT-NH₂). Such specific feature will be discussed in section 4.1.

3.3.2 Range of optimal DNA concentration

3.3.2.1 Case of polybases-NH₂

In contrast to the previous concentration range, for intermediary concentrations of 5 to 10 μM, (illustrated in Figures 5-14 a to d for a polybase-NH₂ concentration of 5 μM), a comparison of twelve spectra measured in different places of a same substrate depicts a rather good reproducibility in the Raman band intensities.

This reproducibility has been assessed through the calculation of the relative standard deviation (RSD) value of the IPRBM band intensity for each polybase. The corresponding values are reported in Figure 5-14. In the case of polyA-NH₂ (Figure 5-14a), only one spectrum diverges from this reproducibility trend and a calculation of the intensity RSD value, performed from the twelve spectra for the dominant IPRBM adenine band at 735 cm⁻¹, leads to a value of 39% (Figure 5-14a). A good spectrum reproducibility is also obtained in the case of polyC-NH₂ for a same concentration (Figure 5-14b). For this polybase, the intensity RSD measured on the dominant IPRBM band of cytosine at 792 cm⁻¹ is equal to 21%. Such rather weak RSD values were also obtained for the other two studied polybases in the same concentration range and in the presence of external NH₂ groups, i.e. 27% for polyG-NH₂ and 39% for polyT-NH₂ (Figures 5-14 c and d).

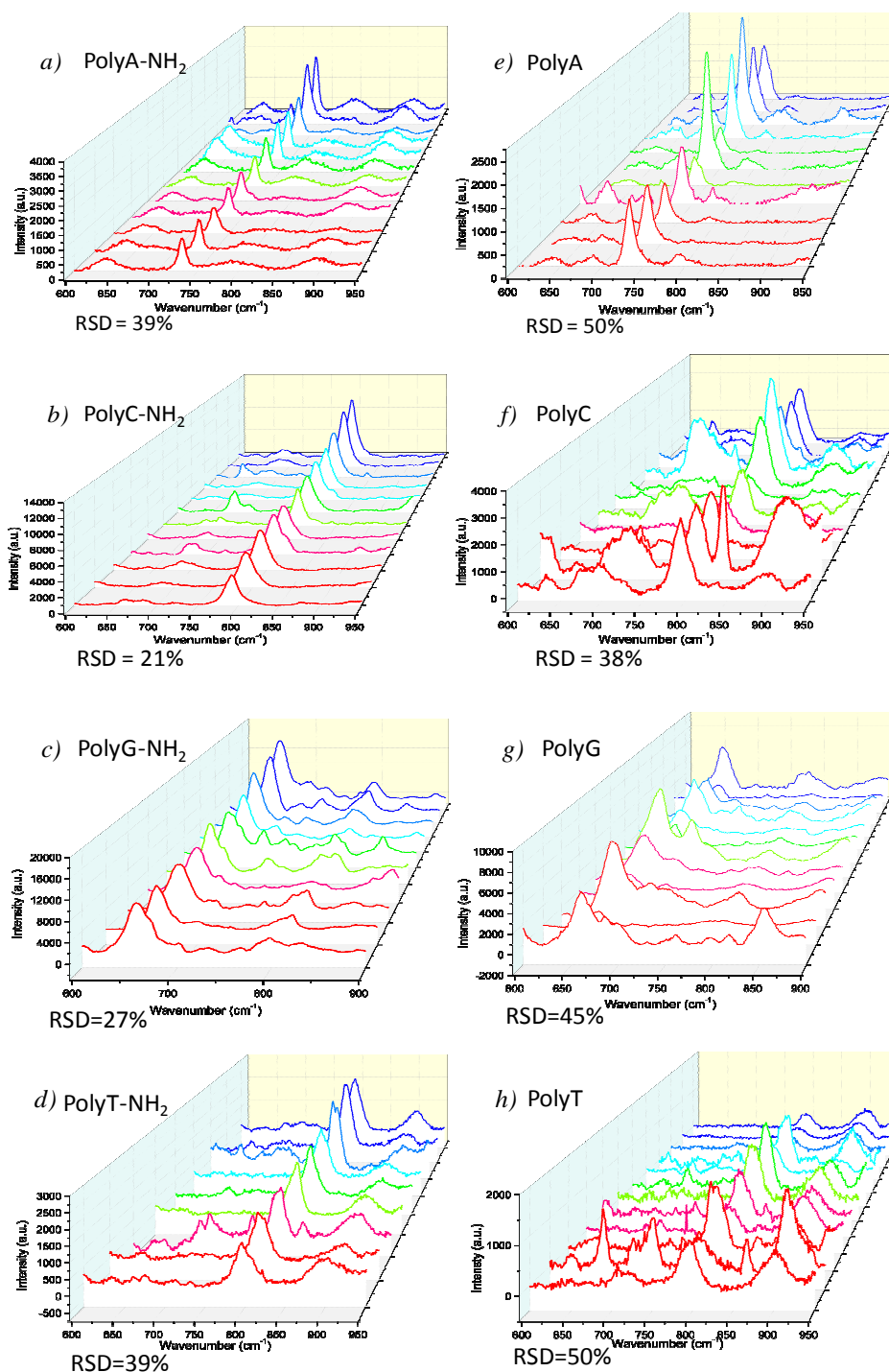


Figure 5-14: SERS spectra acquired in twelve different places for a concentration $C = 5 \mu\text{M}$ from two different $100 \times 100 \mu\text{m}^2$ areas of a same $7 \times 7 \text{mm}^2$ $\text{Ag}^\circ/\text{TiO}_2$ substrate for (a) polyA-NH₂, (b) polyC-NH₂, (c) polyG-NH₂, (d) polyT-NH₂, (e) polyA, (f) polyC, (g) polyG, and (h) polyT.

We note that these values are obviously larger than the RSD previously reported for R6G on the same kind of SERS substrate (10-12%) (chapter 4, section 5), but they still reveal a rather good reproducibility of the spectral intensities for all the studied polybases. This reproducibility i/ illustrates the detection performances of our SERS substrate, and ii/ confirms that, in this concentration range, our simplified immobilization procedure leads to a uniform grafting of DNA molecules on the substrate surface. To the best of our knowledge, such a reproducibility for all these polybases has never been reported before on a same solid SERS substrate.

3.3.2.2 Case of NH₂-free polybases

The behavior of twelve SERS spectra is reported in Figures 5-14 e to h for polyA, polyC, polyG, and polyT. When comparing the spectrum of each NH₂-modified polybase (Figures 5-14 a to d) with the spectrum of its NH₂-free counterpart (Figures 5-14 e to h), it firstly appears that the Raman band intensities are rather comparable. However, in the latter case, the spectra display a lower degree of reproducibility. The RSD values have been calculated from the IPRBM band for all the NH₂-free polybases and are reported in the Figures 5-14 e to h. These values are summarized in Figure 5-15 together with the values for polybases-NH₂ in view of comparison. The RSD values obtained for all NH₂-free polybases are systematically higher than those of polybases-NH₂. The fluctuation increase is more pronounced for polyC (about + 50 %) and it ranges around + 25 % for polyA and polyT. Compared to their NH₂-modified counterpart, this systematic and general trend suggests that, while it does not play an essential role in the polybases immobilization on Ag⁰ NPs, the NH₂ linker should play a role in the reduction of the SERS intensity fluctuations, which will be discussed in next section. Finally, Figure 5-15 also shows that the reproducibility (the RSD values) of NH₂-modified and NH₂-free polybases follows the same trend, i.e. the reproducibility varies in the order polyA (-NH₂) ~ polyT (-NH₂) < polyG (-NH₂) < polyC (-NH₂). It suggests therefore that, regardless the effect of NH₂-modification, the reproducibility is also intrinsically influenced by the polybase nature. Besides, whatever the NH₂ modification or not, it is worthwhile noticing the high intensity and reproducibility of polyC and polyT bases, despite their weak Raman cross section.

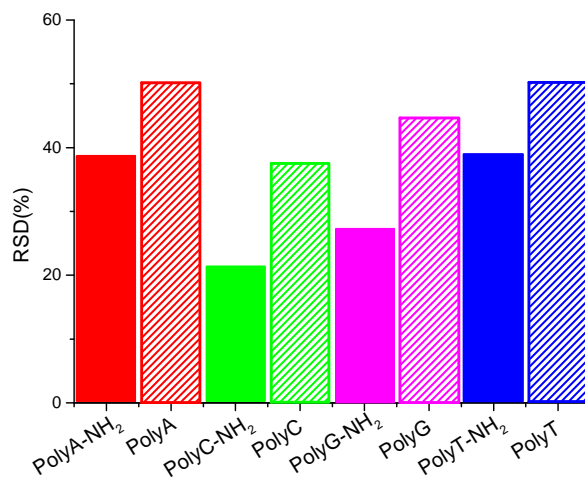


Figure 5-15: RSD calculated from the in-plane ring breathing vibrational mode intensities of all polybases ($C = 5 \mu\text{M}$), corresponding to twelve spectra obtained in two different $100 \times 100 \mu\text{m}^2$ areas of a same $\text{Ag}^\circ/\text{TiO}_2$ substrate.

4. Discussion

4.1 Binding features and general molecular orientation

Thanks to XPS measurements, it has been clearly proved that the DNA molecules are preferentially grafted on the Ag° NPs, presumably via N atoms. The reliability of the SERS spectra obtained on our $\text{Ag}^\circ/\text{TiO}_2$ platform for the four studied polybases enables us to propose further discussions on the DNA immobilization mechanisms. The first important point regards the comparison between the spectra obtained for NH_2 -functionalized polybases and the ones obtained for NH_2 -free polybases. Regardless of the polybase types, the SERS spectra exhibit rather comparable Raman band intensities in the presence or absence of external NH_2 linkers. This result shows that the immobilization of NH_2 -free polybases on the Ag° surface is as efficient as in the case of the NH_2 -terminated polybases, meaning that the external NH_2 linker is not essential for the immobilization of the polybases on the Ag° surface. Consequently, it is likely that the internal exocyclic NH_2 groups of nucleobases are involved in the grafting as well as the intern N atoms: NH or CN bonds (see Figure 5-1). This assumption is reinforced by the particular case of NH_2 -free polyT. This polybase does not possess any internal NH_2 group, but only one internal N3 atom (Figure 5-1), which is believed to be involved in the immobilization on Ag° NPs as it is depicted on Figure 5-16a.

It is supposed that the immobilization mechanism involving internal N atoms of polyT can also be at least partially extrapolated to the other NH_2 -modified or NH_2 -free polybases. This assumption is strengthened by the following observations. For all NH_2 -modified or NH_2 -free polybase concentrations, the spectra are dominated by IPRBM of each individual nucleobase (Figures 5-6 and 5-7). According to

the SERS selection rules of the electromagnetic field theory, the vibration modes involving large changes of the polarisability perpendicular to the platform surface are enhanced [9, 20]. Thus, the dominant IPRBM suggests that individual bases constitutive of the polybases are mainly oriented perpendicularly to the Ag° NPs surface [4, 21, 22]. Since the individual bases are also orientated perpendicularly to the polybase chains axis, it shows that the polybase chains are lying preferentially flat on the surface. In the case of both polyA and polyG, NH_2 , N1, N3, and N7 groups may be involved in this preferential orientation (Figures 5-16 b and c). In the case of polyC, NH_2 and N3 may be involved (Figure 5-16d), whereas only N3 would be involved in the case of polyT (Figure 5-16a).

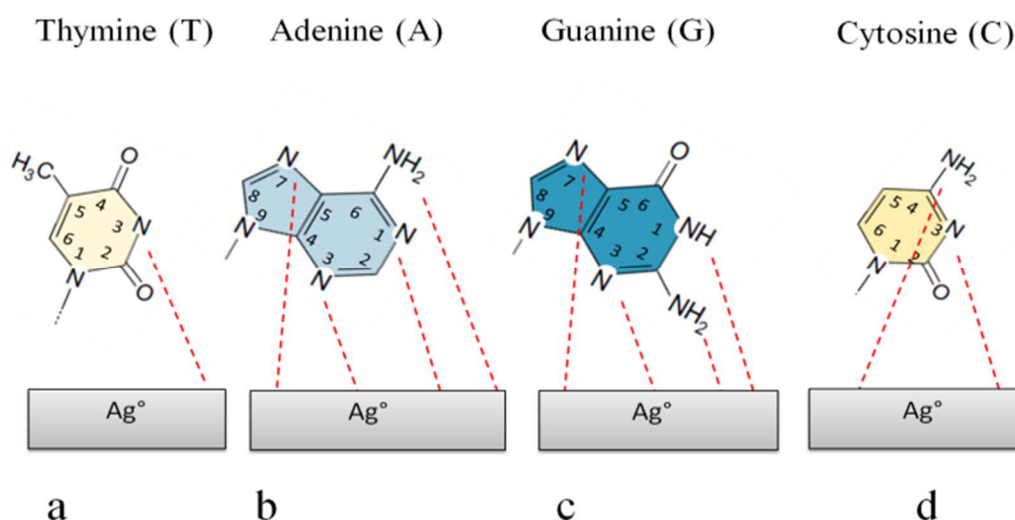


Figure 5-16: Schematic representation of the possible chemical binding between the internal and available N groups of polybases and the Ag° NPs surface in the case of polyT (a), polyA (b), polyG (c), and polyC (d).

The similar results obtained in the case of polybases functionalized or not with terminal NH_2 groups can be compared with the ones of Papadopoulou et al. who studied the adsorption of thiolated and unthiolated polyA on Au colloids, as illustrated in Figure 5-17 [23]. These authors also observed similarities between spectra obtained in the case of thiolated polyA at low concentration ($C=10^{-8}$ M) and SERS spectra obtained in the case of unthiolated polyA ($C=10^{-5}$ M). If the thiolated polyA may not only bind nonspecifically to the gold surface through its nucleobases but also via its external sulfur atoms (Figure 5-17a), the unthiolated polyA can only bind nonspecifically via the nucleobases (Figure 5-17b). Due to similarities between the spectra, the authors concluded that the overall polyA orientation is flat on the Au° colloidal surface.

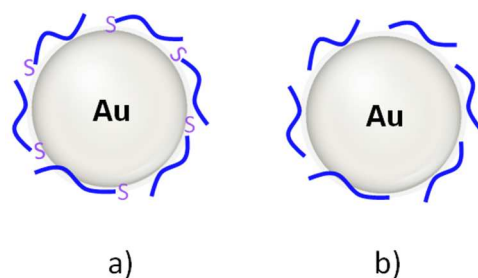


Figure 5-17: Schematic representation of the orientations of ssDNA with respect to the surface of Au colloid: a) case of thiolated polyA, b) case of unthiolated polyA (after ref. [23]).

This preferential orientation of DNA strands was also deduced by Herne *et al.* from ellipsometry measurements performed on HS-DNA chains on gold surface [24]. Indeed, the measured thickness of the HS-DNA coating was five times weaker than the theoretical value of the molecule length, meaning that the probed chains were not perpendicular to the gold surface but lied flat. However, contrarily to Papadopoulou *et al.* [23], the authors did not report on the DNA concentration in their experiments. These data would have been of interest since the amount of DNA immobilized on the surface is an important parameter which has a direct influence on the molecular orientation. This feature is addressed in the following part of the discussion. Concerning our SERS platform, it would be interesting in further experiments to precisely discriminate which of the N-containing groups are primarily involved in the immobilization of each polybase. If some studies have already been performed in this aim, only with adenine base and in the case of solid platforms in dried conditions [10, 11], to our knowledge, no or very few investigations are reported on polyA, polyC, polyG, and polyT.

In summary, our results provide compelling evidence that i/ the polybases are mainly lying preferentially flat on the Ag^o NPs surface independently of the presence of the external NH₂ linker, and ii/ the immobilization mechanism largely involves the internal N-containing groups of the nucleobases.

4.2 Concentration effects on the molecular orientation

As mentioned before (section 1 of this chapter), the amount of DNA immobilized on the surface, i.e. the concentration in solution, is an important parameter which has a direct influence on both the surface coverage and the molecular orientation. These features are deduced from XPS data of Figure 5-5 and from SERS data of Figures 5-6, 5-7 and 5-9. We propose different immobilization mechanisms following the different concentrations. They are discussed hereafter and are schematically illustrated in Figure 5-18.

On the one hand, we observed that the in-plane ring breathing band intensities increase when increasing the polybase concentration up to 5-10 μM (Figure 5-9). At this threshold concentration, they exhibit a

rather good reproducibility when probing in various areas of the substrate (Figures 5-14 and 5-15). At the same time, out of plane bands are almost not observed. These features indicate an important coverage rate of DNA molecules, which undergo a homogeneous 2D dispersion, i.e. a flat orientation of the molecules on the Ag⁰ NPs surface, as previously discussed and schematically illustrated in Figure 5-18a. It is supported by a decreasing XPS signal of Ag⁰ NPs up to this threshold concentration of 5-10 μM (Figure 5-5), showing the gradual screening of the Ag⁰ NPs signal by an enhanced amount of immobilized polybase molecules. On the other hand, very different trends are observed when increasing again the DNA concentration above 5-10 μM. First, the Ag⁰ NPs XPS signal slightly increases, which suggests a decreased coverage rate of Ag⁰ NPs by the polybase molecules, while the intensity of in-plane breathing Raman bands concomitantly decreases. At the same time, the in-plane bands exhibit a poor reproducibility when probed in different areas of the substrate (Figures 5-6c and 5-7c). In addition, the out of plane bands exhibit a significant enhancement. This latter trend has been observed in the SERS spectra of all studied NH₂-modified or NH₂-free polybases. It is illustrated in Figures 5-6c and 5-7c where we observe an enhancement of the out of plane band of adenine (687 cm⁻¹) and cytosine (688 cm⁻¹), respectively. The intensity increase of such out of plane bands may feature a change in the orientation of some nucleobases. Indeed, contrarily to previous trends observed at weaker concentrations, the enhancement of out of plane bands suggests that some individual nucleobases may be orientated parallel to the surface, which would indicate a more or less vertical orientation of corresponding polybase molecules, as depicted in Figure 5-18b. Such an orientation feature has already been reported by others in the case of polyG-quadruplex formation [22, 25].

This analysis leads us to propose a tentative description of the orientation and packing density of polybase molecules immobilized in the case of strong concentrations. For reasons that are not yet clear, we assume that, at strong concentrations, the molecules do not undergo a uniform 2D distribution, as postulated for weaker concentrations, but are locally packed in the form of 3D aggregates heterogeneously distributed on the SERS surface. Compared to weaker concentration trends, such aggregation is expected to leave numerous Ag⁰ areas uncoated by polybase molecules, and this trend should be amplified as the concentration increases. It is possible that this aggregation takes place during the post-incubation drying of the DNA-containing aqueous droplet in the case of strong polybase concentrations. This description is in agreement with all our experimental observations. First, the heterogeneous distribution of polybase molecules is supported by the non-reproducibility of SERS bands when probing on different areas of the substrate (Figures 5-6c and 5-7c). Second, XPS data traduce a balance between Ag⁰ areas coated or uncoated with polybase molecules. It would explain that, since the amount of uncoated Ag⁰ areas is expected to increase when increasing the polybase concentration above 10 μM, the silver XPS signal does not further decrease and even slightly increases when increasing the polybase concentration.

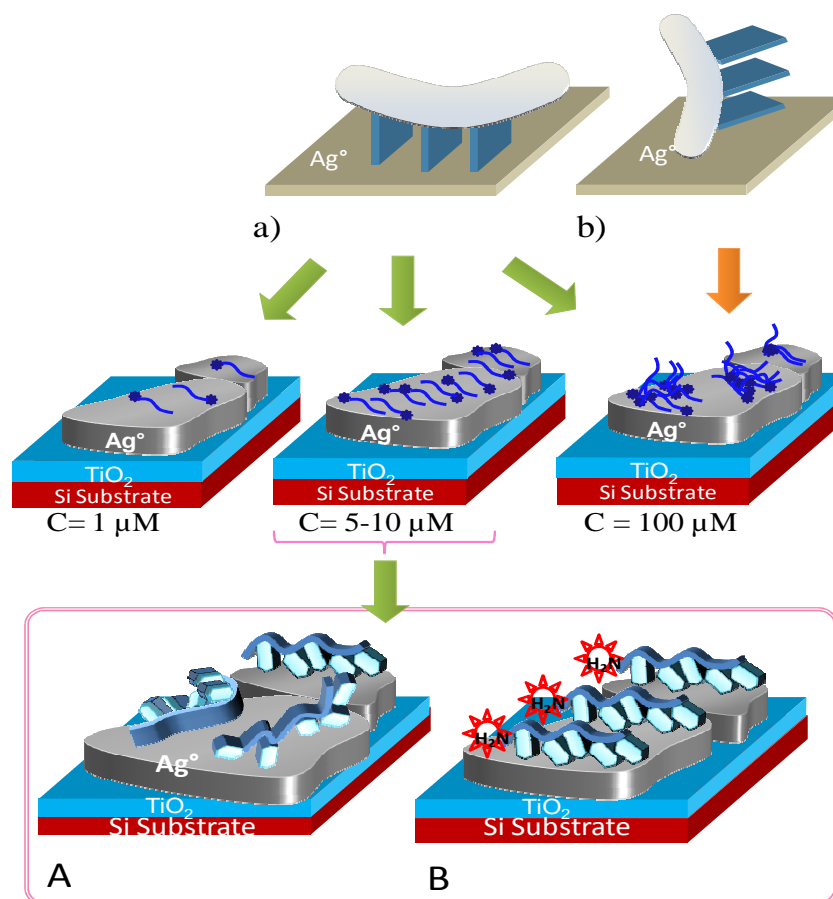


Figure 5-18: Schematic model presenting the polybase molecules on the Ag° NPs and showing the correlation between their orientation, distribution, and concentration in the case of both NH_2 -modified and NH_2 -free polybases, the so-called “probe grafting model”.

Upper: orientation of nucleobases (rectangles) with respect to Ag° surface a) the nucleobases are oriented perpendicularly to the surface so that the overall polybases lie flat on the surface, b) the nucleobases are oriented parallelly to the surface, more or less tilted, so that the overall polybases stand up on the surface.

Middle: evolution of the surface distribution of polybases as a function of polybase concentration in solution. For the lowest concentration ($C = 1 \mu\text{M}$), the Ag° surface coverage by polybases is weak while for the optimum of concentration ($5\text{-}10 \mu\text{M}$), the polybases are homogeneously distributed on the whole surface. In this concentration ranges, the polybases lie flat (a). For the strongest concentration, ($C = 100 \mu\text{M}$), due to some 3D aggregation, some polybases lie flat (a) while some others stand up (b).

Lower: for the optimum of concentration ($5\text{-}10 \mu\text{M}$), structural models of the two possible configurations for single strand polybases adsorbed on Ag° NPs surface. The nucleobases are represented by the rectangular-like shape; (A) case of NH_2 -free polybases: the strands are randomly oriented; (B) case of polybases with NH_2 external linker: the strands are extended and less randomly oriented than in case (A).

In addition, with the assumption of 3D aggregates, polybase molecules present at the surface of these aggregates are not in close contact with SERS active NPs and can no longer be detected by SERS. We can also imagine that, contrarily to polybase molecules in contact with Ag⁰ NPs, which are expected to be strongly linked on these NPs through Ag-N bonds, molecules constituting the aggregates are not so strongly fixed and may be washed away during the post-incubation rinsing step. In both cases, an increase in the 3D packing when increasing the polybase concentration can explain a decrease in the intensity of dominant (in-plane) bands of the SERS spectra. This decrease can finally be supported by a concomitant increase in the intensity of out of plane bands. Indeed, it is likely that in 3D aggregates, steric hindrance effects do not allow the polybase molecules to be uniformly orientated flat on the surface. More presumably, these aggregates are constituted of molecules showing heterogeneous orientations (Figures 5-18, C = 100 μM). Roughly speaking, flat and vertically orientated molecules are expected to constitute these aggregates and can explain the enhanced intensity of out of plane bands. Such supposed orientation changes induced by the concentration of the polybases can be compared with the deductions from Papadopoulou et al. in the case of thiolated polyA immobilized on colloid gold surfaces [23]. The authors correlated spectral modifications with the increase of the polyA concentration (from 10⁻⁸ to 10⁻⁴ M) to orientation changes. When increasing the concentration, the polyA molecules were assumed to change from a conformation where they bind nonspecifically to the surface through the nitrogen atoms of nucleobases, to another conformation where they bind only through the external thiol linker, leading to polyA molecules standing up vertically on the surface. In our case, we deduce that such a phenomenon occurs regardless the presence or not of the external NH₂ groups, which suggests that these latter are not necessary for the vertical orientation of the DNA molecules. Obviously, these descriptions rely on first interpretations and will require further analyses.

In summary, we can distinguish three different ranges of DNA concentrations, in which we can describe the organization of DNA molecules and their components on the Ag⁰ surface by starting from the smallest components, i.e. the nucleobases, up to the chain packing densities. These features are summarized in the Table 5-4.

	DNA concentration		
	Low (1 μM)	Optimum (5-10 μM)	High (100 μM)
Nucleobase orientation	Perpendicular	Perpendicular	Random
Chain conformation	Flat	Flat	Random
Surface coverage	Low	Homogeneous	Heterogeneously distributed
Packing density	Low	2D monolayer	3D aggregates

Table 5-4: Summary table of our results presenting the proposed organization of polybases relatively to the Ag° surface as a function of the DNA concentration in solution.

4.3 Reproducibility of spectra at optimum concentration: role of the external NH_2 linker

From the above discussion, it can be understood that the external NH_2 linker does not play a key role in the polybase immobilization on the Ag° surface. Indeed, the DNA molecules are mainly lying flat on the surface thanks to the nucleobase internal N atoms, independently of the presence of the external NH_2 linker. Therefore the question arises about the usefulness of the latter.

Let us examine more carefully the results obtained in the optimum concentration range (5-10 μM). At these concentrations, we assume that the polybase chains adopt a flat orientation on the Ag° NPs surface and their packing density is described by a homogeneous 2D monolayer (Figure 5-18, $C = 5\text{-}10 \mu\text{M}$). But within this monolayer, owing to the flexible string structure of the sugar-phosphate backbone [26], we can suppose that the individual and localized conformation of the polybase chains is random. It can vary depending on how the nucleobases are locally positioned relatively to the Ag° surface, while maintaining their ring axis perpendicular to the metal surface. Barhoumi et al. explained that single-strand DNA can adsorb on metal surfaces in randomly coiled conformations. These conformations can be modified towards a more relaxed, linear, and extended conformation thanks to a gentle thermal pretreatment [26]. Elsewhere, in the case of G-rich strands, formation of some secondary structures has been observed and may have also a certain effect on the polybase conformation [27]. Thus, we see that the adsorption of individual single strand polybases can result in various conformations/configurations on the metal surface. The consequence of this would be a severe limitation in the quality, reproducibility, and uniformity of SERS spectra. As explained previously, Barhoumi et al. succeeded to reduce these variations through a specific pretreatment, the effect of which allowed a more linear conformation of the chains [26]. As a consequence, the DNA chains were more ordered on the metal surface.

In our case, we have shown in section 4.3.2 that the fluctuations of SERS spectra are systematically reduced when the polybases chains are functionalized by the external NH_2 linker. Indeed, the RSD values of the IPRBM intensity are systematically weaker in the case of polybases- NH_2 compared to NH_2 -free polybases (Figure 5-15). This systematic trend indicates that the external NH_2 linker does play a role in the reduction of SERS spectrum fluctuations. By analogy to the Barhoumi's study [27], we can suppose that, in the absence of external NH_2 linker, the chains are adsorbed with a more or less coiled conformation on the metal surface, as illustrated in Figure 5-18A, resulting in fluctuations of the IPRBM intensities. In contrast, for reasons that are not yet clear, we assume that the external NH_2 linker somehow reduces the variety of conformations as illustrated in Figure 5-18B. In other words, the single strand DNA chains with an external NH_2 linker would adopt a more linear and extended conformation, resulting in a 2D monolayer exhibiting an ordered configuration and resulting in a minimization of the SERS intensity fluctuations. One hypothesis is that, during the rinsing procedure, the NH_2 external linker would act like a strong anchoring point. The latter would strengthen the molecule binding on the Ag° surface by maintaining the molecule more extended and less randomly oriented compared to the case of NH_2 free polybases. This overall configuration is illustrated in Figure 5-18B.

In summary, we have shown that the conformation and orientation of single-strand DNA chains can be better controlled by taking advantage of an external NH_2 linker. Thanks to this latter, the polybase chains should be more ordered on the metal surface as attested by the higher reproducibility of SERS spectra. Accordingly, further investigations would be necessary to study the effect of an optimized grafting protocol allowing the relaxation of the oligonucleotide single strands into an extended conformation through an uncoiling thermal treatment as suggested by Barhoumi et al. [26]. In any case, the results clearly show that, for SERS sensor applications, it is preferable to use polybases- NH_2 in order to minimize the SERS intensity fluctuations. More generally, this recommendation is important to monitor the orientation of single strand DNA molecules tethered to metal surface. This ability is crucial for improving the applications related to many fields ranging from DNA nanosensors to nanoelectronics [28].

5. Conclusion

Four single strand polybases (polyA, polyC, polyG, and polyT), modified or not with an external NH_2 linker, have been immobilized with different concentrations on our $\text{Ag}^\circ/\text{TiO}_2$ SERS substrate using a simplified procedure arising from specific assets of this substrate. The label-free SERS detection of these polybases has been performed through Raman spectroscopy measurements and the analysis of SERS spectra has been supported by XPS measurements. Because of the reliability and efficiency of

this platform, we obtained reproducible SERS spectra for the four DNA polybases functionalized or not by a terminal NH₂ group. In particular, the high resolution and signal/noise ratio enabled us to clearly index the main and secondary Raman lines, even for the polybases with a low Raman cross section such as polyC and polyT.

Regardless of the polybase type and whether the polybase was NH₂-modified or not, we have emphasized a polybase concentration dependence of the SERS spectra reproducibility and intensity, which show an optimum for a 5-10 μM range. It suggests that this optimal range of concentrations should be kept for further applicative researches aiming at the SERS detection of DNA multibase oligonucleotides. The optimum concentration range was interpreted in terms of distribution, orientation, and packing density of immobilized molecules. This study also shows that the external NH₂ linker is not necessary for the immobilization of the polybases, which can be bound to the SERS-active Ag⁰ NPs surface through the internal N atoms. In the optimum concentration range, it seems that the polybase molecules undergo a uniform 2D coverage and a flat orientation relative to the Ag⁰ surface. From that point of view, it appears that the NH₂ linker acts like an anchoring point keeping the 2D monolayer in an ordered configuration on the metal surface. In that sense, the NH₂ linker plays, therefore, an essential role in the SERS spectra reproducibility.

To summarize, these fundamental results have demonstrated the feasibility of using our reliable SERS substrate for label-free ssDNA polybases detection. In the next chapter, we will investigate the SERS spectra obtained in the case of polybases mixture and hybridized polybases.

- [1] V. Stambouli, M. Labeau, I. Matko, B. Chenevier, O. Renault, C. Guiducci, *et al.*, "Development and functionalisation of Sb doped SnO₂ thin films for DNA biochip applications," *Sensors and Actuators B: Chemical*, vol. 113, pp. 1025-1033, 2006.
- [2] A. Opdahl, D. Y. Petrovykh, H. Kimura-Suda, M. J. Tarlov, and L. J. Whitman, "Independent control of grafting density and conformation of single-stranded DNA brushes," *Proceedings of the National Academy of Sciences*, vol. 104, pp. 9-14, 2007.
- [3] A. Leitner, "Phosphopeptide enrichment using metal oxide affinity chromatography," *TrAC Trends in Analytical Chemistry*, vol. 29, pp. 177-185, 2010.
- [4] A. I. Eriksson, K. Edwards, A. Hagfeldt, and V. c. A. Hernández, "Physicochemical Characterization of Phosphopeptide/Titanium Dioxide Interactions Employing the Quartz Crystal Microbalance Technique," *The Journal of Physical Chemistry B*, vol. 117, pp. 2019-2025, 2013.
- [5] G. J. Thomas Jr, J. M. Benevides, S. A. Overman, T. Ueda, K. Ushizawa, M. Saitoh, *et al.*, "Polarized Raman spectra of oriented fibers of A DNA and B DNA: anisotropic and isotropic local Raman tensors of base and backbone vibrations," *Biophysical Journal*, vol. 68, pp. 1073-1088, 1995.
- [6] C. Otto, T. J. J. van den Tweel, F. F. M. de Mul, and J. Greve, "Surface-enhanced Raman spectroscopy of DNA bases," *Journal of Raman Spectroscopy*, vol. 17, pp. 289-298, 1986.
- [7] L. Wu, H.-C. Li, H.-F. Zhao, Y. Sun, H.-R. Xu, M. Lu, *et al.*, "Detection of Nucleic Acid Bases by Surface Enhanced Raman Scattering Based on *In Situ* Photo-Reduced Silver Colloids," *Chinese Journal of Analytical Chemistry*, vol. 39, pp. 1159-1164, 2011.
- [8] J.-M. Delabar and M. Majoube, "Infrared and Raman spectroscopic study of 15N and D-substituted guanines," *Spectrochimica Acta Part A: Molecular Spectroscopy*, vol. 34, pp. 129-140, 1978.
- [9] B. Giese and D. McNaughton, "Surface-Enhanced Raman Spectroscopic and Density Functional Theory Study of Adenine Adsorption to Silver Surfaces," *The Journal of Physical Chemistry B*, vol. 106, pp. 101-112, 2001.
- [10] M. Potara, M. Baia, C. Farcau, and S. Astilean, "Chitosan-coated anisotropic silver nanoparticles as a SERS substrate for single-molecule detection," *Nanotechnology*, vol. 23, pp. 055501, 2012.
- [11] F. Feng, G. Zhi, H. S. Jia, L. Cheng, Y. T. Tian, and X. J. Li, "SERS detection of low-concentration adenine by a patterned silver structure immersion plated on a silicon nanoporous pillar array," *Nanotechnology*, vol. 20, p. 295501, 2009.
- [12] M. Mathlouthi, A. M. Seuvre, and J. L. Koenig, "F.T.-I.R. and laser-raman spectra of guanine and guanosine," *Carbohydrate Research*, vol. 146, pp. 15-27, 1986.
- [13] Z.-G. Shang, D. N. Ting, Y. T. Wong, Y. C. Tan, B. Ying, and Y.-J. Mo, "A study of DFT and surface enhanced Raman scattering in silver colloids for thymine," *Journal of Molecular Structure*, vol. 826, pp. 64-67, 2007.
- [14] M. Green, F.-M. Liu, L. Cohen, P. Kollensperger, and T. Cass, "SERS platforms for high density DNA arrays," *Faraday Discussions*, vol. 132, pp. 269-280, 2006.
- [15] J. S. Suh and M. Moskovits, "Surface-enhanced Raman spectroscopy of amino acids and nucleotide bases adsorbed on silver," *Journal of the American Chemical Society*, vol. 108, pp. 4711-4718, 1986.
- [16] S. Liu, G. Zheng, and J. Li, "Raman spectral study of metal-cytosine complexes: A density functional theoretical (DFT) approach," *Spectrochimica Acta Part A: Molecular and Biomolecular Spectroscopy*, vol. 79, pp. 1739-1746, 2011.
- [17] M. Mathlouthi, A. M. Seuvre, and J. L. Koenig, "F.T.-I.R. and laser-raman spectra of cytosine and cytidine," *Carbohydrate Research*, vol. 146, pp. 1-13, 1986.
- [18] J. Florián and V. Hroudá, "Scaled quantum mechanical force fields and vibrational spectra of solid state nucleic acid constituents V: thymine and uracil," *Spectrochimica Acta Part A: Molecular Spectroscopy*, vol. 49, pp. 921-938, 1993.

- [19] E. Papadopoulou and S. E. J. Bell, "Label-Free Detection of Single-Base Mismatches in DNA by Surface-Enhanced Raman Spectroscopy," *Angewandte Chemie International Edition*, vol. 50, pp. 9058-9061, 2011.
- [20] A. Campion and P. Kambhampati, "Surface-enhanced Raman scattering," *Chem. Soc. Rev.*, vol. 27, pp. 241-250, 1998.
- [21] F. Gao, J. Lei, and H. Ju, "Label-Free Surface-Enhanced Raman Spectroscopy for Sensitive DNA Detection by DNA-Mediated Silver Nanoparticle Growth," *Analytical Chemistry*, vol. 85, pp. 11788-11793, 2013.
- [22] G. Rusciano, A. C. De Luca, G. Pesce, A. Sasso, G. Oliviero, J. Amato, *et al.*, "Label-free probing of G-quadruplex formation by surface-enhanced Raman scattering," *Analytical chemistry*, vol. 83, pp. 6849-6855, 2011.
- [23] E. Papadopoulou and S. E. J. Bell, "DNA reorientation on Au nanoparticles: label-free detection of hybridization by surface enhanced Raman spectroscopy," *Chemical Communications*, vol. 47, pp. 10966-10968, 2011.
- [24] T. M. Herne and M. J. Tarlov, "Characterization of DNA Probes Immobilized on Gold Surfaces," *Journal of the American Chemical Society*, vol. 119, pp. 8916-8920, 1997.
- [25] X. Gao, J. P. Davies, and M. J. Weaver, "Test of surface selection rules for surface-enhanced Raman scattering: the orientation of adsorbed benzene and monosubstituted benzenes on gold," *The Journal of Physical Chemistry*, vol. 94, pp. 6858-6864, 1990.
- [26] A. Barhoumi, D. Zhang, F. Tam, and N. J. Halas, "Surface-Enhanced Raman Spectroscopy of DNA," *Journal of the American Chemical Society*, vol. 130, pp. 5523-5529, 2008.
- [27] G. N. Parkinson, M. P. Lee, and S. Neidle, "Crystal structure of parallel quadruplexes from human telomeric DNA," *Nature*, vol. 417, pp. 876-880, 2002.
- [28] S. Ghoshal, D. Mitra, S. Roy, and D. D. Majumder, "Biosensors and Biochips for Nanomedical Applications: a Review," *Sensors & Transducers*, vol. 112, pp. 1726-5479, 2010.

Chapter 6. SERS detection of complementary polybase pairs: mixture versus hybridization effects

1. Introduction

In the previous chapter, thanks to the reliability of our Ag⁰ NPs/TiO₂ substrate, we performed the thorough indexation of SERS spectra of single strand polybases. We also demonstrated the successful control over both the conformation and the surface density of polybases grafted on the Ag⁰ surface following the concentration and the presence of the NH₂ external linker. Based on these promising results, our objective in this chapter is now to investigate the conformation and immobilization density of the corresponding duplex molecules, i.e. single strand polybases hybridized with their complementary polybases. It requires to bring out what are the specific features of SERS spectra of complementary polybase pairs, obtained after *in situ* hybridization directly performed on the Ag⁰ surface. In this view and following a step by step methodology, we have chosen to study the SERS spectra of two hybridized complementary polybase pairs, typically:

- Hybridization of equi-molar polyA-NH₂ with polyT;
- Hybridization of equi-molar polyG-NH₂ with polyC.

To support the results, these SERS spectra will be systematically compared with those obtained after the direct immobilization of mixtures containing the same complementary polybases, typically:

- Mixture of equi-molar polyA-NH₂ with polyT;
- Mixture of equi-molar polyG-NH₂ with polyC.

Since the polybases are not hybridized in these mixtures, the corresponding SERS spectra will serve as negative control, which will allow us to investigate unambiguously the SERS signature of hybridized polybases by comparing the spectroscopic features of mixed and hybridized pairs. To the best of our knowledge, this methodology has not been reported until now in the literature. In this study, we followed the same experimental approach as described in the chapter 5. We performed the spectrum indexation at a fixed polybase concentration (in solution) and then we studied the evolution of the spectrum intensity as a function of the polybase concentration.

2. DNA materials and immobilization process

2.1 *In situ* hybridization

The *in situ* hybridization process with the complementary polybases was carried out directly on the $\text{Ag}^\circ/\text{TiO}_2$ substrate, preliminarily covered by the polybase probes, in four steps illustrated in Figure 6-1. As reported in chapter 5 for the choice of the grafting solution for single polybases, different hybridization buffer solutions have first been tested. Among these, the PBS+NaCl+EDTA buffer solution was finally chosen for two reasons. On the one hand, the integrity of Ag° NPs on the TiO_2 surface was preserved. On the other hand, the SERS spectrum acquisitions were possible and effective, which was not the case when using the other buffer solutions (see Table 6-1).

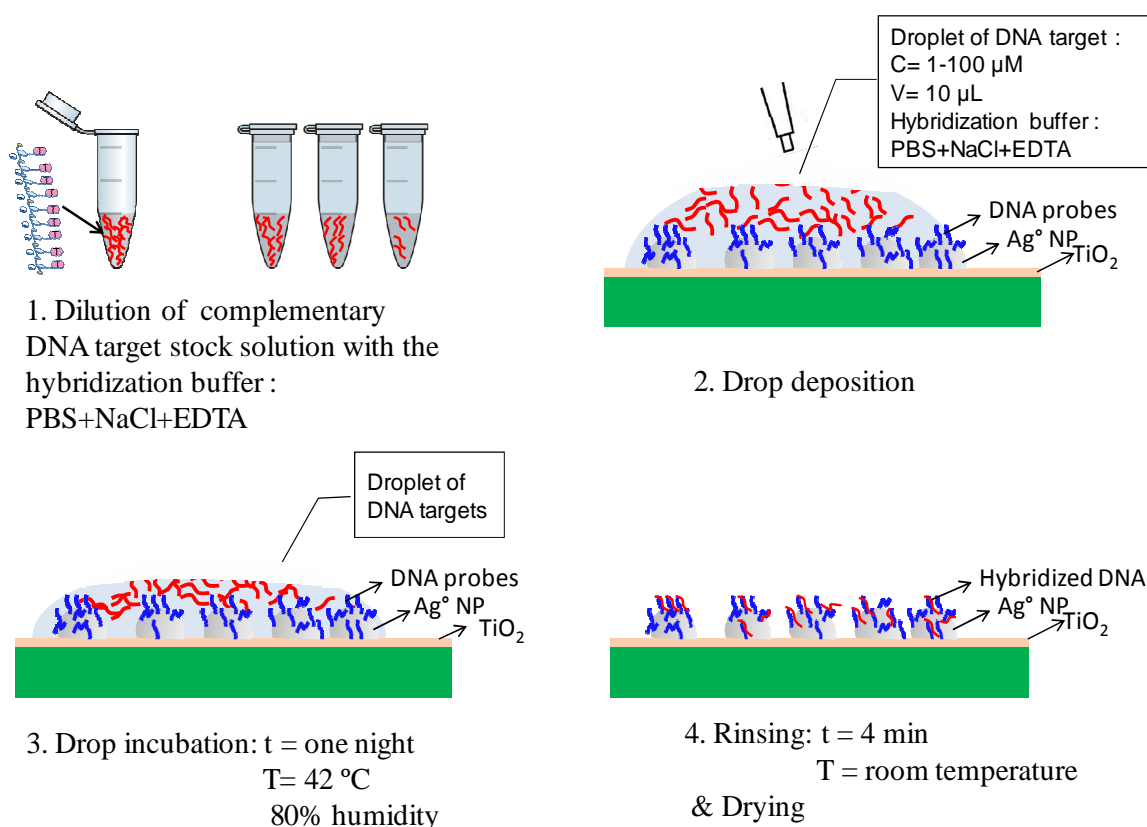


Figure 6-1: Schematic representation of the *in-situ* hybridization process on $\text{Ag}^\circ/\text{TiO}_2$ substrate immediately after DNA probe immobilization.

Tested hybridization solution	Tris-HCl+NaCl	PBS+NaCl+EDTA	Pure deionized water	PBS+NaCl	NaCl	Monobasic sodium phosphate (grafting solution)	2X SSC
Ingredient concentrations	Tris = 10 mM NaCl = 1M	PBS = 10 mM NaCl = 500 mM EDTA = 1 mM	Pure deionized water	PBS = 10 mM NaCl = 500 mM	NaCl = 100 mM	NaH ₂ PO ₄ = 300 mM	Sodium citrate = 300 mM NaCl = 100 mM
pH value	7.6	7.2	Ca. 7	7.2	Ca. 7	4.5	7.7
State of Ag^o/TiO₂ surface	Good: unchanged	Good: unchanged	Good: unchanged	Peel off of Ag ^o NPs	Good: unchanged	Good: unchanged	Peel off of Ag ^o NPs
Acquisition of SERS spectra	No	Yes	Random	No	Random	Random	No

Table 6-1: Preliminarily tested hybridization solutions for DNA hybridization and corresponding results in terms of Ag^o/TiO₂ substrate surface state and SERS spectrum acquisition. The red column corresponds to experimental conditions adopted in next studies.

In a first step of the hybridization process, the complementary target polybases were diluted to desired concentrations in the PBS+NaCl+EDTA buffer solution (pH = 7.2, see composition in Table 6-1). The target polybase concentrations have been varied from 1 to 100 μM. In a second step, a 10 μL volume droplet of the complementary polybase-containing aqueous solution was deposited on the probe-immobilized substrate surface. The third step is a one night incubation at 42 °C, under ~ 80% relative humidity. Different incubation times were preliminarily tested. We found that increasing the incubation time from 45 min to one night improved considerably the SERS signal. It seems that this optimal incubation time yields relatively higher hybridization efficiency. In the fourth step, the droplet was rinsed by immersing the sample in the hybridization solution (PBS+NaCl+EDTA) under soft agitation for 4 minutes. This rinsing step removes the non-hybridized complementary polybases. Then, the sample was dried for one hour at room temperature, ready for SERS experiments. Typical hybridization experiments are summarized in Table 6-2. Practically, we performed the hybridization of paired polybase strands:

- PolyA-NH₂ (probe) hybridized with polyT (targets), named as hybridized polyA-NH₂•polyT;
- PolyG-NH₂ (probe) hybridized with polyC (targets), named as hybridized polyG-NH₂•polyC.

The respective equi-molar concentrations of each polybase have been varied from 1 to 100 μM and are detailed in Table 6-2.

Hybridization	Polybase	Sequences	Concentrations (μM)
PolyA-NH ₂ •polyT	PolyA-NH ₂ (probe)	5' NH ₂ T5-A15 3'	1, 5, 10, 50, 100
	PolyT (target)	5' T20 3'	1, 5, 10, 50, 100
PolyG-NH ₂ •polyC	PolyG-NH ₂ (probe)	5' NH ₂ T5-G15 3'	1, 5, 10, 50, 100
	PolyC (target)	5' T5-C15 3'	1, 5, 10, 50, 100

Table 6-2: Summary table of two pairs of oligonucleotides (polybases) sequences at different concentrations used in the described hybridization experiments.

2.2 Single strand polybase mixture immobilization

In view of the polybase mixture direct immobilization on the $\text{Ag}^{\circ}/\text{TiO}_2$ substrate, the solutions were prepared at room temperature from equi-molar amounts of polybases as follows:

- PolyA-NH₂ (probes) with polyT (targets), named as polyA-NH₂+polyT mixture;
- PolyG-NH₂ (probes) with polyC (targets), named as polyG-NH₂+polyC mixture.

The concentration of each polybase has been varied from 1 to 100 μM . The polybases were diluted in the same optimized grafting solution of monobasic sodium phosphate as described in chapter 5. The immobilization process of the mixture solution drop on the $\text{Ag}^{\circ}/\text{TiO}_2$ surface was carried out just after mixing, using the same direct procedure as described in chapter 5. All the mixture experiments and concentration conditions are summarized in Table 6-3.

Mixture	Polybase	Sequences	Concentrations (μM)
PolyA-NH ₂ +polyT	PolyA-NH ₂	5' NH ₂ T5-A15 3'	1, 5, 10, 50, 100
	PolyT	5' T20 3'	1, 5, 10, 50, 100
PolyG-NH ₂ +polyC	PolyG-NH ₂	5' NH ₂ T5-G15 3'	1, 5, 10, 50, 100
	PolyC	5' T5-C15 3'	1, 5, 10, 50, 100

Table 6-3: Summary table of oligonucleotides sequences with different concentrations used in the described mixture experiments.

2.3 General experimental features

It is important to recall again that, in the following, we always respected equi-molar proportions for the two pairs of polybases (polyA-NH₂ and polyT, polyG-NH₂ and polyC) in both mixture and hybridization experiments.

The SERS spectra were collected using the Raman equipment, described in chapter 5, using the red line (632.8 nm) of a He-Ne laser. For each experiment, as for previous probe polybase characterization, we systematically investigated two different 100 x 100 μm^2 areas of a same 7x7 mm^2 substrate and six spectra were collected in different places of each probed area.

3. Results

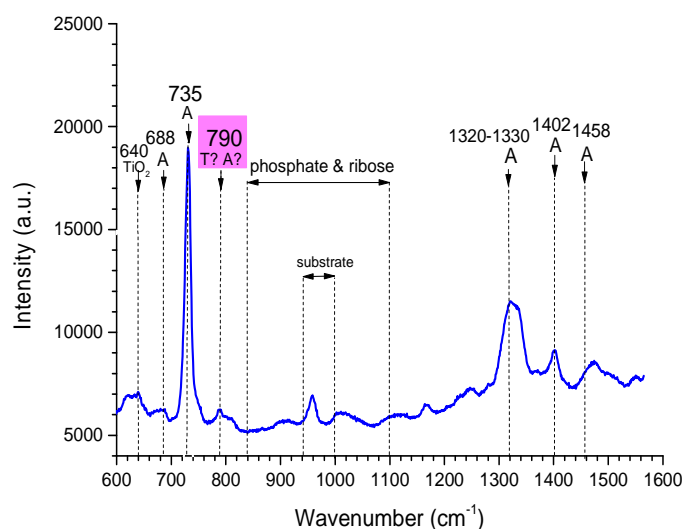
3.1 Equi-molar polyA-NH₂+polyT mixture vs. hybridized polyA-NH₂ • polyT

Similarly to the study of polybases alone (chapter 5), we will first focus on the SERS spectrum indexation of the polybase mixtures and hybridized polybases for a fixed concentration of 5 μM for each polybase. The choice of this concentration value is based on our previous results which systematically showed a maximum of intensities in this range of concentration. Then in a second step, we will focus on the influence of the concentration on the intensity behavior of several important bands.

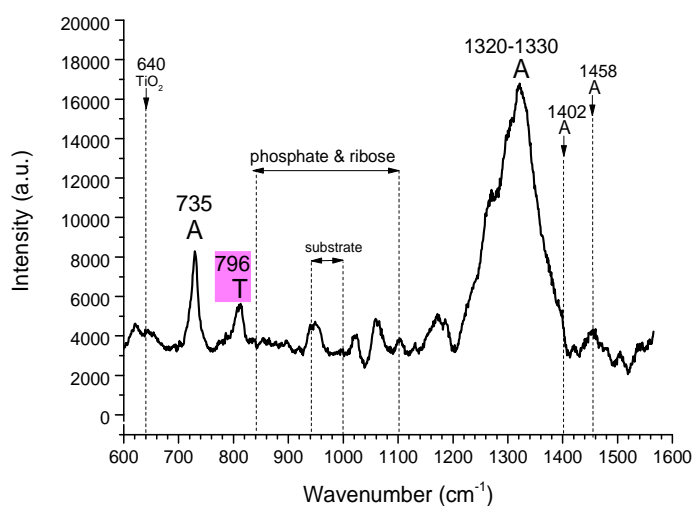
3.1.1 Indexation of SERS spectra at fixed concentration

PolyA-NH₂+polyT mixture:

A typical SERS spectrum of polyA-NH₂+polyT mixture is shown in Figure 6-2 a. The entire characteristic bands of polyA, NH₂-modified or not, have already been detailed in section 3.2.1.1 of chapter 5. Thus, here we only recall the indexation of some of them. The dominant sharp band at 735 cm⁻¹ is attributed to the in plane ring breathing mode (IPRBM) of adenine, while a less intense multi component band centered in a range of 1320 - 1330 cm⁻¹ is attributed to the mixed in-plane stretching mode of the ring skeleton (Table 5-3, chapter 5). We also observe a very weak band located at 790 cm⁻¹. Its indexation can be debated since the thymine ring breathing mode is located at this wavenumber, as well as one of the out of plane vibration modes of adenine (see table 5-3). As a result, this weak peak can be either attributed to polyA-NH₂ or to polyT. Remarkably, this mixture spectrum is very similar to that of polyA-NH₂ alone (Figure 5-10 a, chapter 5). This suggests that, under our experimental mixture conditions, the polyT creates very weak spectral features in SERS spectra. This will be discussed later in the chapter.



(a)



(b)

Figure 6-2: SERS spectra of equi-molar polyA-NH₂+polyT mixture (a) and hybridized polyA-NH₂•polyT (b) obtained for $C_{\text{polyA-NH}_2} = C_{\text{polyT}} = 5 \mu\text{M}$.

Hybridized polyA-NH₂ • polyT:

A typical SERS spectrum of hybridized polyA-NH₂•polyT is shown in Figure 6-2 b. Surprisingly, the spectrum is largely dominated by the adenine 1320-1330 cm⁻¹ multi-component band attributed to the mixed in-plane stretching mode of the ring skeleton, while the 735 cm⁻¹ IPRBM band of adenine is much less intense. This inversed intensity ratio between the 735 and 1330 cm⁻¹ bands will be discussed later in the chapter. Besides, and compared to the mixture spectrum of Figure 6-2 a, the 1320-1330 cm⁻¹ band is dramatically enhanced at two levels, intensity and width, and reveals several satellite bands such as the far 1402 cm⁻¹ one of adenine. Finally, another well resolved band at 796 cm⁻¹ is clearly distinguished, which is attributed to the in plane ring breathing vibration of thymine (see Table 5-3). As a result,

contrary to the spectrum of the polyA-NH₂+polyT mixture, this spectrum exhibits the clear signatures of both polyA-NH₂ and polyT. This feature, added to the strong enhancement of the 1320-1330 cm⁻¹ band of adenine, seems to characterize the hybridized polyA-NH₂•polyT double-strand. This enables us to confirm that the hybridization reaction between the polyA-NH₂ probes immobilized on the Ag⁰ surface and the polyT targets has taken place, which is not the case in the polyA-NH₂+polyT mixture.

3.1.2 Influence of the concentration

In the previous chapter, we have evidenced a concentration dependent intensity of the IRPBM of polybases in the presence or absence of terminal NH₂ group. In the present case, for comparison, we have plotted the evolution of the 735 cm⁻¹ IRPBM intensity of the polyA-NH₂ as a function of the polyA-NH₂ concentration in solution, for both polyA-NH₂+polyT mixture and hybridized polyA-NH₂•polyT (Figures 6-3 a and b, respectively). Striking differences can be observed, which are detailed in the following.

PolyA-NH₂+polyT mixture:

In the case of polyA-NH₂+polyT mixture, the 735 cm⁻¹ band intensity is clearly concentration-dependent (Figure 6-3 a). An optimum concentration yielding a maximal intensity is clearly observed between 5 and 10 μM. Such behavior is remarkably similar to that of polyA-NH₂ alone (Figure 5-9a, chapter 5), and by extension, to all the studied NH₂-modified or not polybases.

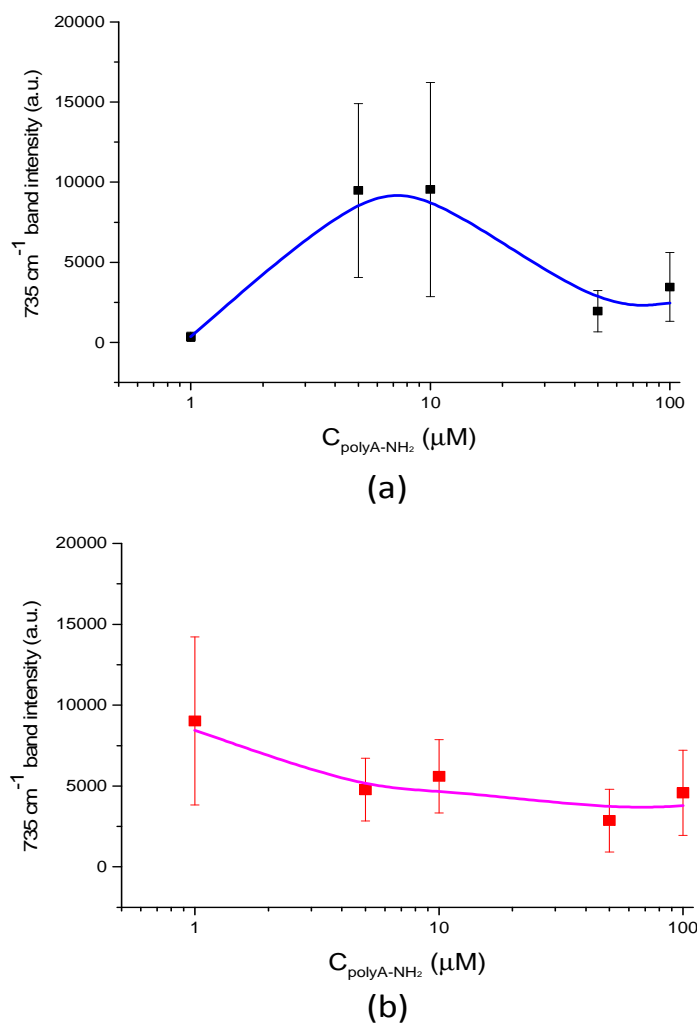


Figure 6-3: Intensity evolutions of the 735 cm⁻¹ in plane ring breathing vibration band of adenine as a function of the polyA-NH₂ concentration in the case of (a) polyA-NH₂+polyT mixture and (b) hybridized polyA-NH₂• polyT.

Hybridized polyA-NH₂ • polyT:

In the same range of concentration, the trend obtained in the case of hybridized polyA-NH₂•polyT is clearly different from the previous one (Figure 6-3 b). This trend depicts a continuous decrease of the intensity when increasing the concentration, with a maximum intensity observed at the lowest concentration, i.e. 1 μM. It is striking that the trend observed in all the cases of polybases alone, and then repeated in the case of polyA-NH₂+polyT mixture (Figure 6-3 a), does not appear in the case of hybridization (Figure 6-3 b). As a result, the SERS signal of hybridized polyA-NH₂•polyT is very pronounced particularly at relative low concentration (i.e. C = 1 μM). This improved detection sensitivity at low concentration upon hybridization may be explained by a particular surface packing density model, which will be discussed later.

Besides, we have studied the evolution of the $1330\text{ cm}^{-1} / 735\text{ cm}^{-1}$ adenine bands intensity ratio as a function of the polyA-NH₂ concentration. The intensity ratio values are reported in Figure 6-4 for the two studied cases: hybridized polyA-NH₂•polyT and polyA-NH₂+polyT mixture. For comparison, we have also reported the values obtained from polyA-NH₂ polybase spectra (after Figure 5-6 of chapter 5). Several observations can be made. On the one hand, in the case of both polyA-NH₂ alone and polyA-NH₂+polyT mixture, the intensity ratio values are similar and remain constant (0.6 ± 0.2) within the whole range of tested concentrations. This similarity confirms the previous result according to which the polyA-NH₂+polyT mixture behaves like polyA-NH₂ alone, meaning that the SERS detection of polyT in the mixture is negligible. On the other hand, for hybridized polyA-NH₂•polyT, the ratio values exhibit a strong concentration dependence. The ratio increases from 1.2 to 2.9 when increasing the concentration from 1 to 50 μM , and then suddenly drops to 1.4 for a concentration of 100 μM . This complex trend has not been explained yet but, in any cases, the values are systematically higher than the 0.6 ratio depicted for polyA-NH₂+polyT mixture and polyA-NH₂ alone. This systematic difference is an additional feature which re-enforces the effectiveness of the hybridization resulting in an enhanced intensity of the 1330 cm^{-1} band regardless of the concentration.

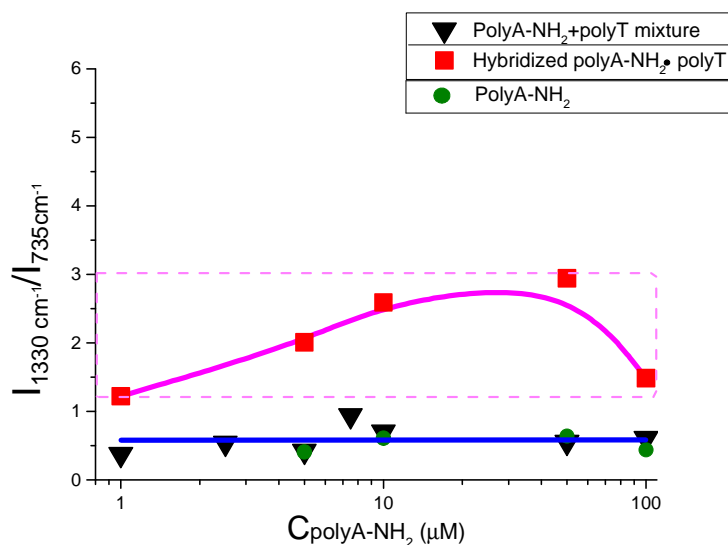


Figure 6-4: $1330\text{ cm}^{-1} / 735\text{ cm}^{-1}$ SERS intensity ratio as a function of polyA-NH₂ concentration for mixture, hybridized, and polyA-NH₂ alone.

3.1.3 Discussion

The clear differences observed between the SERS spectra of hybridized polyA-NH₂•polyT and the corresponding polyA-NH₂+polyT mixture open the way to a discussion. First, we will compare and discuss the hybridized double-strand spectra with the spectra of single strand polybases, i.e. polyA-NH₂ alone, polyT alone, and their mixture, obtained for a same concentration (5 μM). All corresponding

spectra are compiled in Figure 6-5. Then, we will further investigate the different trends observed in concentration-dependent SERS intensities.

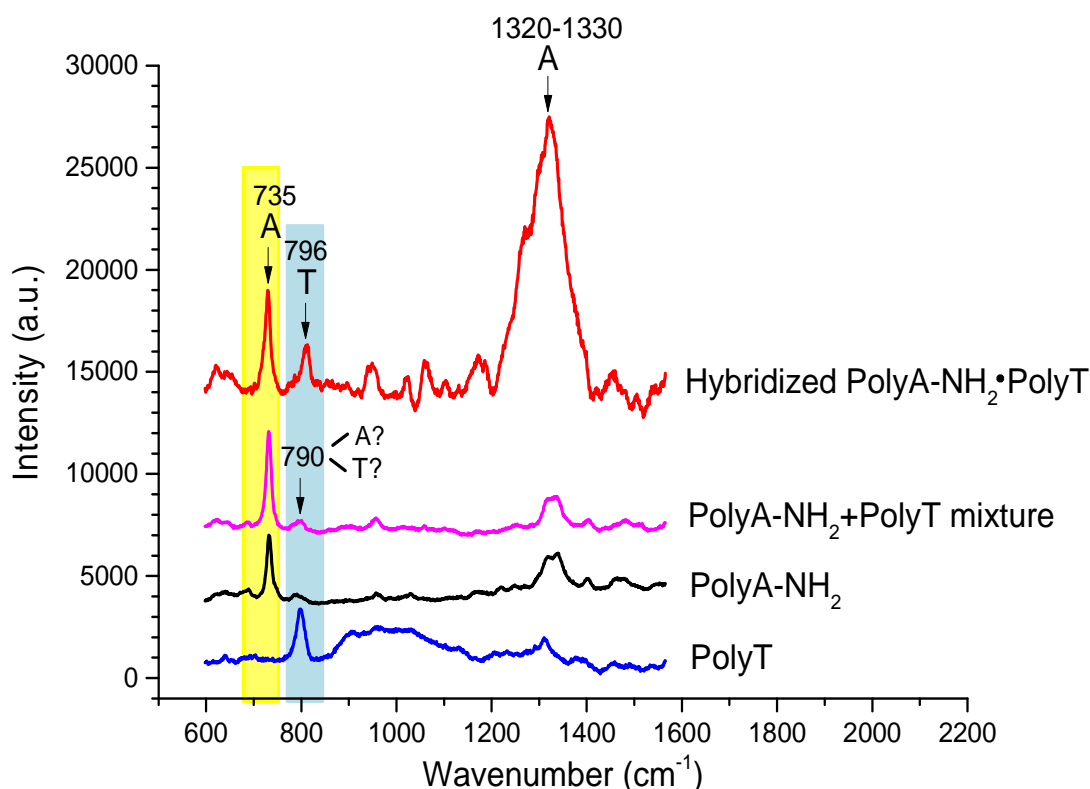


Figure 6-5: SERS spectra of polyA-NH₂ and polyT alone, as well as their equi-molar polyA-NH₂ + polyT mixture and their hybridized polyA-NH₂•polyT pairs, obtained for $C_{\text{polyA-NH}_2} = C_{\text{polyT}} = 5 \mu\text{M}$.

3.1.3.1 PolyA-NH₂+ polyT mixture at fixed concentration: competitive adsorption mechanism

As already mentioned, the spectrum of the polyA-NH₂+polyT mixture is similar to that of polyA-NH₂ alone and, when comparing both spectra with the one of polyT alone, we observe no significant signature of polyT in the mixture spectrum. This feature might result from the weak Raman cross section of thymine [1], but this assumption is denied by the intense SERS spectra of polyT presented in chapter 5. Thus, it is assumed that the absence of thymine band in the mixture spectrum rather suggests that a mechanism of competitive adsorption exists between polyA-NH₂ and polyT upon their immobilization on the Ag⁰ surface. According to this mechanism, the polyT adsorption on the Ag⁰ surface would be hindered, resulting in a predominance of adsorbed polyA-NH₂ at the Ag⁰ surface. This would explain why no signature of polyT is observed in the polyA-NH₂+polyT mixture spectrum. This hypothesis is re-enforced by some studies in the literature, which show that the different bases interact differently with metal (Au in this example) surface. Notably, Demers et al. revealed that there are major differences in the binding affinities of the different bases to gold surface. From reflection-absorption infrared

(RAIR) spectroscopy studies, they deduced different values of desorption heats (ΔH_{des} in KJ/mol) for each base: for thymine, $\Delta H_{\text{des}} = 111 \pm 2$ kJ/mol, and for adenine, $\Delta H_{\text{des}} = 131 \pm 3$ kJ/mol [2]. In other words, the less the energy of desorption, the less the base is adsorbed on the surface, showing that thymine is less adsorbed on Au surface than adenine. This feature is in agreement with our hypothesis. Besides, since adenine (as well as guanine) bases possess the largest number of available N atoms for binding with Ag° surface (Figure 5-16 in chapter 5), it is reasonable to assume that adenine has a highest affinity for Ag° over thymine. To resume, in our case of polyA-NH₂+polyT mixture, the differences between adsorption affinity may lead to a competitive adsorption behavior between polyA-NH₂ and polyT upon their immobilization on the Ag° surface, which would result in a strongly enhanced adsorption of polyA-NH₂ on the Ag° surface, leaving little or no adsorption space for polyT. A consequence of such finding is that the Raman band at 790 cm⁻¹ in the mixture spectrum (Figure 6.2a and 6.5) should be rather attributed to adenine (the out of plane vibrational band) and not to thymine.

3.1.3.2 Hybridization features

a/ Hybridization feasibility

Having established a competitive adsorption model in the case of polyA-NH₂+polyT mixture, we now investigate the behavior of double-strand polybases in the case of in-situ hybridization. Before going further, let us recall that, in standard DNA molecules, the specific recognition between adenine and thymine bases is carried out through the establishment of two hydrogen bonds between some specific N atoms belonging to A and T, respectively, i.e. N6_(adenine)•••H•••O_(thymine) and N1_(adenine)•••H•••N3_(thymine) as shown in Figure 6-6.

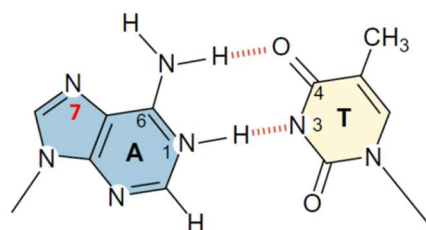


Figure 6-6: Schematic representation of the two hydrogen bonds between specific atoms of adenine and thymine.

To the best of our knowledge, no publication reports on the expected SERS spectra in our *in situ* hybridization case, where a polyA-NH₂ covered Ag° surface is submitted to an aqueous polyT solution. So, in the absence of reference data, our problematic is to prove that hybridization has actually taken

place. That is why, by comparing the SERS spectra of polyA-NH₂+polyT mixture with the one of hybridized polyA-NH₂•polyT, we have attempted to identify the specific SERS features demonstrating hybridization and to deduce from SERS spectra the conformation of the chain and bases relatively to the Ag⁰ surface. As explained before and illustrated in the Figure 6-5, the spectrum of polyA-NH₂+polyT mixture exhibits a very weak band located at 790 cm⁻¹, which is attributed to adenine. In contrast, in the case of hybridized polyA-NH₂•polyT, the typical IPRBM band of thymine is clearly distinguishable at 796 cm⁻¹. So, there is no doubt that this feature evidences the effective presence of polyT in the case of hybridized polyA-NH₂•polyT. Compared to the spectrum of polyA-NH₂+polyT mixture, which was featured by the lack of polyT band, this result shows that polyT is actually present at the Ag⁰ surface and should be strongly bound to the adenine bases through the specific hydrogen pair bonds, as described in Figure 6-6. This important result confirms the feasibility of a hybridization process, which takes place during the incubation step (one night) on the Ag⁰ surface.

The other significant difference between the spectra of polybase mixture and hybridized polybases is the dramatic enhancement and the width of the adenine band at 1320-1330 cm⁻¹ (Figure 6-2 b). This large band combines many peaks corresponding to different in plane vibrations of both adenine and thymine (see table 5-3, chapter 5):

- 1330 cm⁻¹, attributed to the in plane ring skeleton vibration (notably the stretching of C5-N7 and N1-C2, bending of C2-H and C5-N7) of adenine;
- 1380 cm⁻¹, attributed to the in plane bending of C5-Me of thymine;
- 1402 cm⁻¹, attributed to the in plane vibration of adenine (notably the bending of C2-H and the stretching C8-N7, N1-C2).

The enhanced SERS detection of all these vibrations suggests some specific connections with the Ag⁰ surface during hybridization such as N7_(adenine)•••Ag, CH₃_(thymine)••• Ag, as it will be detailed in the following.

b/ Orientation features

As discussed in chapter 5, the preponderant presence of many in plane vibration bands characteristic of adenine (Figure 5-10) and thymine (Figure 5-13), in addition to the weak out of plane vibration bands, demonstrates that the individual adenine and thymine bases are mainly oriented perpendicularly to the Ag⁰ NPs surface [3, 4], which indicates in turn a flat conformation of derived polybases on the Ag⁰ surface before hybridization (Figure 5-18, chapter 5). Since in plane vibration modes are also preponderant after hybridization, it seems reasonable to assume that single strand polyA-NH₂ can hybridize with polyT under flat conformation, as illustrated in Figure 6-7. Similar deductions were reported by Schreiner et al., who have confirmed a flat conformation of polyA (A15) on an Au surface

before and after hybridization with polyT (T15). From XPS and SPR experiments, the authors presented a direct evidence that hybridization can occur even if the DNA probes (A15) are in a directly-adsorbed (flat) conformation [5, 6], which is in complete agreement with our finding.

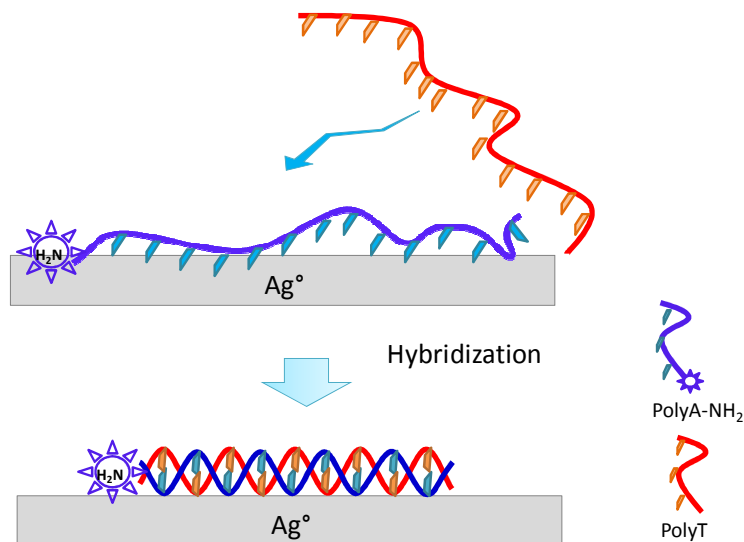


Figure 6-7: Formation of hybridized polyA-NH₂•polyT on the Ag⁰ NPs surface. The polyA-NH₂ is immobilized on the Ag⁰ NPs surface in the known conformations (lying flat), and then hybridization takes place on the Ag⁰ surface and yields to the double-helix lying flat on the Ag⁰ NPs surface.

c/ Immobilization features

Having established the flat hybridized molecule conformation on the Ag⁰ surface, we can now go further by proposing a tentative description of the immobilization process for hybridized polyA-NH₂•polyT. According to our previous studies before hybridization, the polyA-NH₂ single-strand are adsorbed on the Ag⁰ surface possibly through four internal N atoms of the bases, i.e. N1, N3, N7, and NH₂ (Figure 5-16, chapter 5). Upon hybridization with polyT, two of the four internal N atoms, i.e. N6 and N1, which originally interacted with the Ag⁰ surface before hybridization, can now be involved in the hydrogen bonding (Figures 6-6 and 6-8). It means that, during incubation, the bonding between adenine and Ag⁰ surface is disrupted to form the specific hydrogen bonding characteristic of the hybridized bases: N₆(adenine)•••H•••O_(thymine) and N₁(adenine) •••H•••N₃(thymine) (Figure 6-8). Therefore, these N6 and N1 are probably no longer in the proximity of the Ag⁰ surface but, intern N7 atoms, which are clearly not engaged in the hydrogen bonding upon hybridization, are now more available to interact with the Ag⁰ surface (see the green arrow in Figure 6-8). From the presence of a highly enhanced band at 1334 cm⁻¹ in the adenine molecules SERS spectrum, Watanabe et al. deduced that the adsorption of single adenine molecules takes place preferentially through the nitrogen atom N7 of the structural ring [7]. This

conclusion was based on the assumption that the most intense band of the SERS spectrum originates from the corresponding atom directly adsorbed on the surface. Otto and co-workers, however, proposed a slightly different theory. They declared that vibration enhancement originates from the closest proximity of corresponding atom from metal surface [8], which indicates that the direct contact between the corresponding atom and metal surface is not necessary. If we combine the features from both Watanabe and Otto, it is reasonable to assume that, in our case, the hybridization behavior brings the internal N7 atoms of adenine bases into a close proximity of the Ag° surface, and even gives them the possibility to directly interact with the Ag° surface.

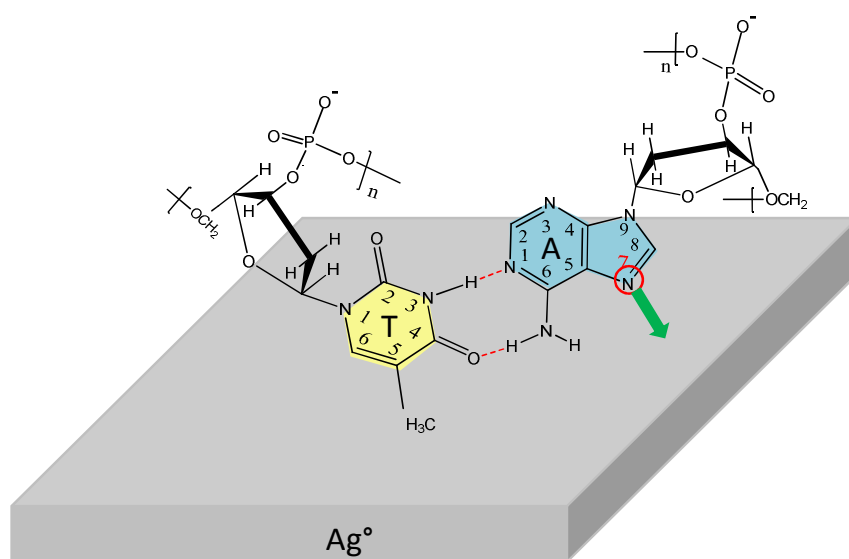


Figure 6-8: Schematic representation showing in details the hydrogen bonding between polyA and polyT single strand pairs and the proximity of adenine N7 atom to the Ag° surface (green arrow).

Thus, through a mechanism which still requires clarification, we assume that the formation of hydrogen bonding through N1 and N6 atoms of adenine with the N and O atoms of thymine upon hybridization makes both kinds of atom moving away from the Ag° surface, but brings the N7 atoms of adenine into a closer proximity of the Ag° surface (as illustrated in Figure 6-8), inducing an enhanced SERS detection of hybridized polybases. These changes accompanying the hybridization are unambiguously reflected in the SERS spectra through the dramatically enhanced adenine band at $1320\text{-}1330\text{ cm}^{-1}$ and the appearance of a thymine band at 796 cm^{-1} .

d/ Summary

Given the significant differences in SERS spectra between single strand polyA-NH₂, polyA-NH₂+polyT mixture, and hybridized polyA-NH₂•polyT, the changes accompanying the hybridization reflected in SERS spectra are important enough to clearly identify the hybridization effect via SERS spectroscopy.

As a result, we can therefore not only confirm the feasibility of hybridization under our experimental conditions, but also tentatively establish the conformation and immobilization features of hybridized polyA-NH₂•polyT on the Ag^o surface.

3.1.3.3 Concentration-dependent SERS intensity

a/ PolyA-NH₂+polyT mixture

As illustrated in Figure 6-3 a, the polyA-NH₂+polyT mixture behaves like the polyA-NH₂ alone, regardless the concentration, because a competitive mechanism leads to the preferential adsorption of polyA-NH₂ on the Ag^o surface. Besides, in the case of polyA-NH₂+polyT mixture, we have formally excluded the adsorption of hybridized pairs and concluded that only polyA-NH₂ is adsorbed. This conclusion is re-enforced by the study of Brabec et al. who showed that the duplex, which might be eventually found in the mixture solution, has a very low probability to adsorb on the Ag^o surface [9].

b/ Hybridized polyA-NH₂•polyT

As detailed in section 4.2 of chapter 5, our study performed on the immobilization of single strand polybases on the Ag^o surface as a function of polybase concentrations enabled us to propose a probe grafting model. This model describes the different distributions, orientations, and packing densities of the polybases on the Ag^o surface, as illustrated in Figure 5-18 of chapter 5. Starting from this model and from the concentration dependent SERS intensity variations in the case of hybridized polyA-NH₂•polyT, we can now propose a new model based on the previous one in order to describe the organization and surface packing density of hybridized molecules on the Ag^o surface. We remind that three domains of concentrations could previously be distinguished for the polyA-NH₂ probes alone.

- The first one corresponds to the medium concentration range of polybases (C= 5-10 μM), in which it is believed that the single strand polybases form a homogeneous 2D monolayer on the Ag^o surface.
- The second one corresponds to the low concentration range (around 1 μM), which yields a weak coverage of the Ag^o surface by polyA-NH₂.
- The third domain corresponds to the high concentration range (around 100 μM), which leads to heterogeneously distributed 3D aggregates of polyA-NH₂.

Let us recall that, in contrast to the medium concentration range, both latter concentration ranges led to SERS spectra of weak intensity and poor reproducibility. In the following, we propose a hybridization model, which describes the packing density and surface coverage in each of these three concentration domains, as illustrated in Figure 6-9.

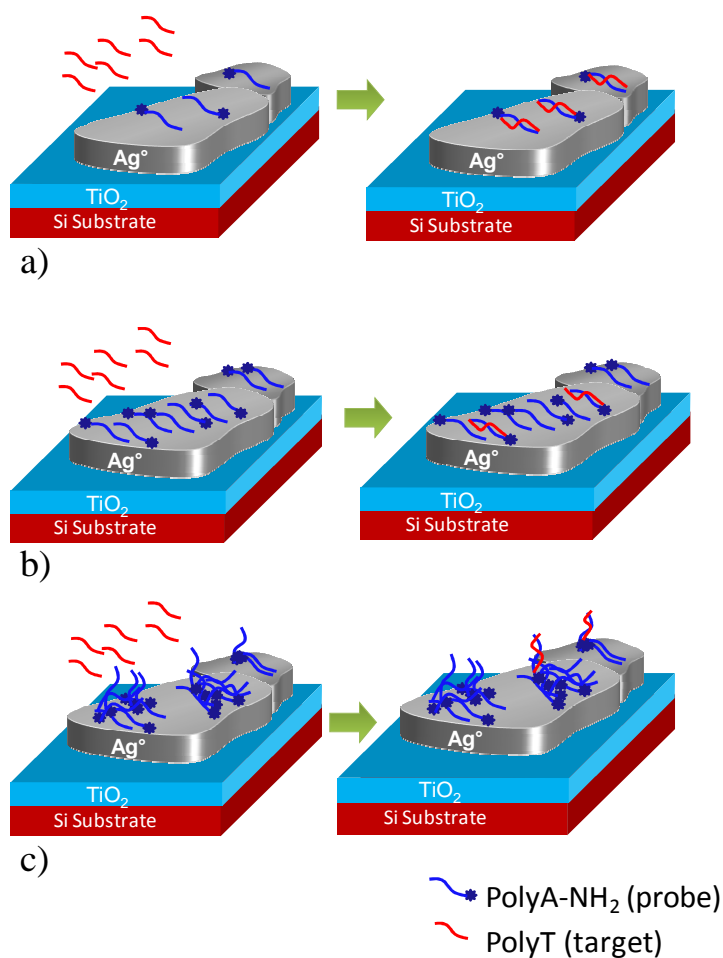


Figure 6-9: Schematic hybridization model depicting the hybridization efficiency according to the surface distribution of polybase probe arising from three concentration ranges of polybases. For the lowest concentrations ($C \sim 1 \mu\text{M}$), loosely distributed probe polybases enable a good hybridization efficiency (a), for the medium concentration range ($5\text{-}10 \mu\text{M}$), a homogeneous 2D monolayer of probe polybases leads to a lower hybridization efficiency (b), for the strongest concentrations ($C \sim 100 \mu\text{M}$), due to some heterogeneous 3D aggregation, the hybridization efficiency is the lowest (c).

Low concentration range

In this concentration range, we have shown that the probe polybases are loosely distributed on the Ag° surface, leaving free spaces between immobilized polyA-NH₂. These spaces can in turn be filled by the polyT target polybases, which should allow an efficient hybridization with the probe polybases (Figure 6-9 a). Such improved hybridization efficiency is accompanied with a highly enhanced intensity of the adenine IPRBM at 735 cm^{-1} , as seen in Figure 6-3 b for a concentration of $1 \mu\text{M}$. It is thus reasonable to assume that the “optimal” grafting density for the polyA-NH₂•polyT hybridization corresponds to the lowest probe concentration in solution ($1 \mu\text{M}$ in this work), which is very different from the case of single strand polyA-NH₂ detection, where an optimal concentration value yielding maximal SERS

intensities was observed between 5 and 10 μM (chapter 5). In other words, at concentrations around 1 μM , the SERS intensities of polyA-NH₂ alone are rather weak, while they appear optimal in the hybridized state. As a result, the detection sensitivity of hybridized polybases seems superior to that of single strand polybases. Such finding is promising since it opens the way for further SERS detection of hybridized molecules at much lower concentrations in solution.

Medium concentration range

In the case of a homogeneous 2D monolayer of polyA-NH₂ arising from the medium concentration range (5-10 μM), the probe polybases are more or less tightly packed, leaving very few space between the immobilized polybases (Figure 6-9 b). Consequently, it may be difficult for polyT to penetrate the 2D layer and to efficiently hybridize [10], which results in a decreased hybridization efficiency compared to the low concentration range and leads to SERS spectra of weaker intensities as illustrated in the Figure 6-3 b.

High concentration range

At strong probe concentrations ($\gg 10 \mu\text{M}$), the probe polybases are expected to constitute 3D aggregates heterogeneously distributed on the Ag^o surface. In these conditions, the excess of molecules forces some polybases to be vertically oriented on the Ag^o surface in an upright conformation. It is assumed that, when these probe aggregates are exposed to the polyT targets, only very few single strand polybases (i.e. probably the standing up ones) have the possibility to interact with their complementary polybases. The rest of probe polybases are densely packed together, leaving no space for the complementary polybases, which finally results in a very poor hybridization efficiency (Figure 6-9 c). It may explain why at high probe concentration, owing to this poor efficiency of hybridization, intensities of derived SERS spectra are weak, as shown in Figure 6-3 b.

In summary, this proposed hybridization model derived from the previously established probe grafting model can fully describe the evolutions of the SERS intensity (735 cm^{-1} band) as a function of the probe polybase concentration.

3.1.4 Summary

For both studied cases, polyA-NH₂+polyT mixture and hybridized polyA-NH₂•polyT, a thorough investigation of the SERS spectra has been performed, first at fixed concentration and then as a function of the concentration. The main important results are the following:

- In the case of polyA-NH₂+polyT mixture, there is no signature of polyT in the spectra and, the spectral behavior of polyA-NH₂+polyT mixture is nearly similar to that of polyA-NH₂ alone. Such behavior is re-enforced by identical trends in the SERS intensities as a function of the polybase concentration in solution. Thus, regardless the concentration, it is inferred that a competitive mechanism between polyA-NH₂ and polyT leads to the preferential adsorption of polyA-NH₂ on the Ag⁰ surface.
- In the case of hybridized polyA-NH₂•polyT, we observe clearly the SERS signature of polyT. This latter is linked to polyA-NH₂ through two specific hydrogen bonds. Remarkably, the adenine band at 1320-1330 cm⁻¹ is dramatically enhanced leading to a 1330 cm⁻¹ / 735 cm⁻¹ intensity ratio which is inversed compared to the case of polyA-NH₂+polyT mixture. This result, in addition with the presence of some very weak out of plane vibration bands, indicates that the hybridized polyA-NH₂•polyT chains are mostly lying flat with their bases orientated perpendicularly to the Ag⁰ surface.
- The clear differences in SERS spectra between polyA-NH₂+polyT mixture and double strands hybridized polyA-NH₂•polyT provide compelling evidence that the hybridization of polyA-NH₂ with polyT has taken place.
- Finally, the behavior of SERS intensity (735 cm⁻¹ band) as a function of concentration in the case of hybridized polyA-NH₂•polyT enables us to propose a hybridization model derived from the previous one concerning the probe polybases immobilized on the Ag⁰ surface. According to this hybridization model, the best hybridization efficiency is encountered at the lowest probe concentration (1 μM). Accordingly, an optimal surface packing density for hybridization is found at 1 μM, at which the hybridized double strands are mainly lying flat and form a homogeneous layer on the Ag⁰ surface.

3.2 Equi-molar polyG-NH₂+polyC mixture vs. hybridized polyG-NH₂ •polyC

In order to support the conclusions drawn from the SERS spectra of polyA-NH₂ with polyT pair, in this section, we study the pair polyG-NH₂ with polyC in both cases of *in situ* hybridization and mixture. The comparison of the different SERS spectral features between the both cases will be emphasized in order to validate the feasibility of an *in situ* hybridization of this new pair.

3.2.1 Indexation of SERS spectra at fixed concentration

Similarly to the case of polyA-NH₂ and polyT pair, we firstly detail here the SERS spectrum indexation of the mixture and hybridized states for a fixed concentration of 5 μM. The corresponding typical spectra

of polyG-NH₂ with polyC in mixture, as well as after hybridization, are presented in the Figures 6-10 a and b, respectively.

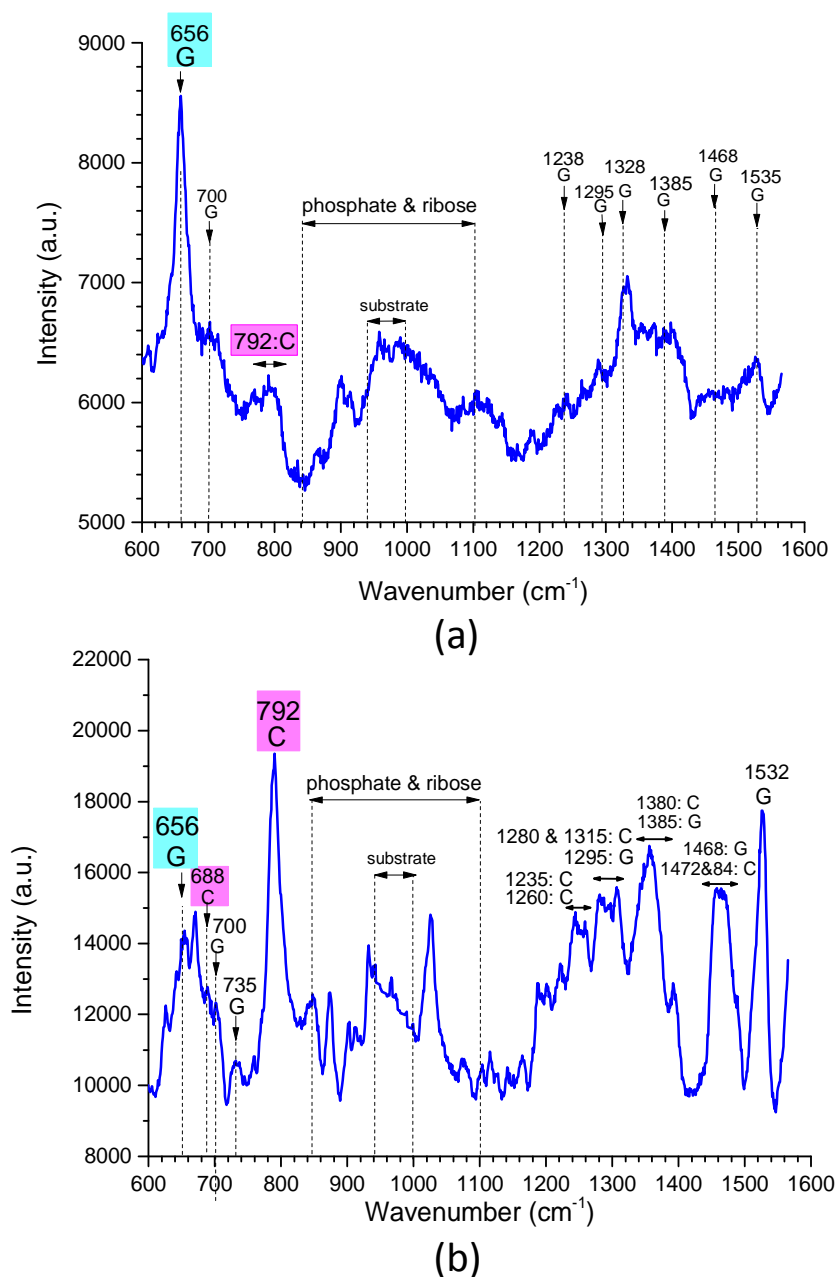


Figure 6-10: SERS spectra of equi-molar polyG-NH₂+polyC mixture (a) and hybridized poly-NH₂+polyC (b) obtained for $C_{polyG-NH_2} = C_{polyC} = 5 \mu M$.

PolyG-NH₂ + polyC mixture:

The mixture spectrum is clearly dominated by several characteristic guanine bands (Figure 6-10 a). The most intense band, located at 656 cm⁻¹, is attributed to the in plane ring breathing mode (IPRBM) of guanine nucleobase (see Table 5-3, chapter 5). In comparison, the in plane ring breathing mode of

cytosine at 792 cm^{-1} is wide and exhibits a weak intensity. At higher frequencies, ranging from 1200 to 1500 cm^{-1} , the spectrum exhibits a group of marked guanine bands, with a dominant band centered at 1328 cm^{-1} being surrounded by two other bands at 1295 cm^{-1} and at 1385 cm^{-1} . All three bands are attributed to in plane stretching modes of guanine. It is worth pointing out that this mixture spectrum is quite similar to that of polyG-NH₂ alone (Figure 5-12 a, chapter 5), in spite of some intensity variations of several bands in the high frequency region. Another observation is that, under our experimental conditions, the intensity of the IPRBM of guanine is clearly superior to that of cytosine.

Hybridized polyG-NH₂•polyC:

Surprisingly, in the spectrum of hybridized polyG-NH₂•polyC, the most intense band of the spectrum at 792 cm^{-1} is assigned to the IPRBM of cytosine (Figure 6-10 b). In comparison, the IPRBM of guanine centered at 656 cm^{-1} is wide and about half less intense. It appears as a combination of several components located at 688 cm^{-1} (attributed to the out of plane bending mode of cytosine, see Table 5-3 of chapter 5) and 700 cm^{-1} (attributed to the in plane bending mode of guanine, see Table 5-3), respectively. A weakly intense and wide band located at 735 cm^{-1} is attributed to the out of plane deformation of guanine. At higher frequencies (1200 - 1500 cm^{-1}), several intense bands can also be observed. Their indexation can be debated, since many characteristic bands of both cytosine and guanine are possibly superimposed in this region. One sharp band of guanine is clearly distinguishable at 1532 cm^{-1} , which is attributed to the in plane stretching of C=C and N3-C4 (Table 5-3). Globally speaking, the clear appearance of cytosine and guanine characteristic bands indicates that both polyG-NH₂ and polyC are present at the Ag^o surface and that the hybridization probably takes place. It is also worth pointing out that, compared to the polyG-NH₂+polyC mixture spectrum, the group of intense bands at high frequencies (1200 - 1500 cm^{-1}) is highly enhanced in the case of hybridized polyG-NH₂•polyC. This trend is rather similar to the case of hybridized polyA-NH₂•polyT (Figure 6-5). Let us recall that in the latter case, the band centered around 1320 - 1330 cm^{-1} (mixed in-plane stretching) was dramatically enhanced at two levels, intensity and width, due to orientation and conformation changes accompanying the hybridization process. In summary, the differences between the polyG-NH₂+polyC mixture and hybridized polyG-NH₂•polyC are clear, here again providing compelling evidence that hybridization has taken place under our experimental conditions.

3.2.2 Influence of concentration

As for the case of polyA-NH₂/ polyT pairs, the intensities of the main guanine band at 656 cm^{-1} (IPRBM) have been plotted as a function of the polyG-NH₂ concentration in solution in the mixture case (Figure 6-11 a). However, unlike the previous study, we do not report the intensity evolutions of this IPRBM in

the case of hybridized polyG-NH₂•polyC, since related intensities were rather weak and difficult to estimate (Figure 6-10 b). Instead, we have plotted the intensity evolutions of the polyC band at 792 cm⁻¹ as a function of the concentrations, since it is the most distinct band in the SERS spectra of hybridized polyG-NH₂•polyC. (Figure 6-11 b).

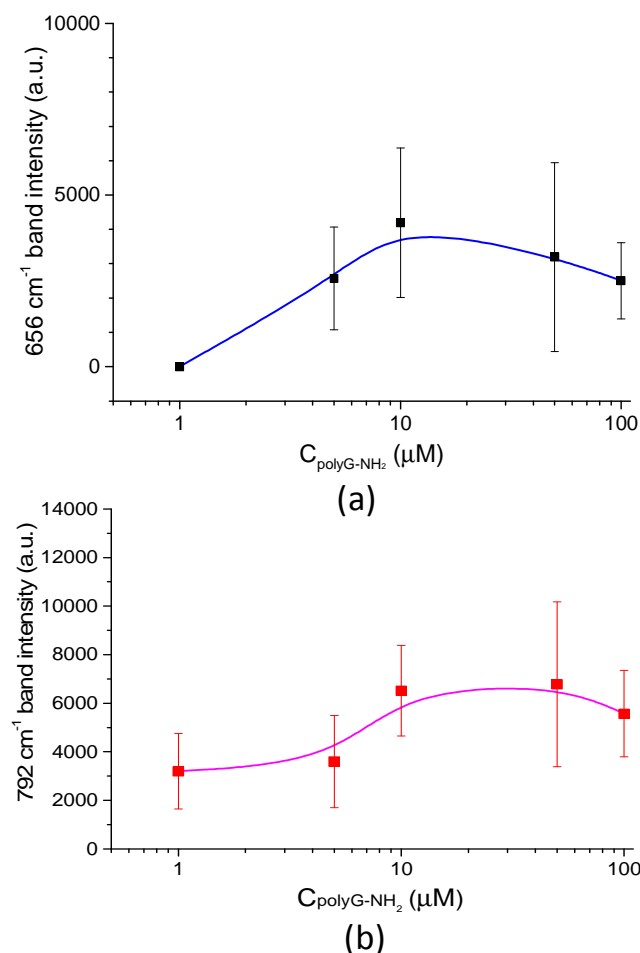


Figure 6-11: Respective intensity evolutions of main Raman band as a function of the concentration in solution: 656 cm⁻¹ band for polyG-NH₂+polyC mixture (a), and 792 cm⁻¹ band for hybridized polyG-NH₂• polyC (b).

PolyG-NH₂ + polyC mixture:

The intensity evolutions of the typical guanine band at 656 cm⁻¹ is clearly concentration-dependent, as seen in Figure 6-11 a, and an optimal concentration yielding a maximal intensity is observed around 10 μM. Such trend is rather similar to that observed for the different studied single strand polybases alone, NH₂-modified or not (chapter 5), as well as in the case of the previously studied polyA-NH₂ + polyT mixture (Figure 6-3 a).

Hybridized polyG-NH₂•polyC:

As previously mentioned, the cytosine band at 792 cm⁻¹ is the most intense band in the spectrum of hybridized polyG-NH₂•polyC. As can be seen in Figure 6-11 b, this band exhibits a moderate concentration-dependent intensity. For this band, a maximal intensity is observed within an optimal concentration range of 10-50 μM. Let us point out that, even at relative low concentration (C = 1 μM), this intensity remains important and is much higher than that obtained in the mixture case for a same concentration (Figure 6-11 a), similarly to the case of hybridized polyA-NH₂•polyT (Figure 6-3 b). This result confirms that the detection sensitivity is significantly improved in the low concentration range in the case of hybridized polybases compared to the case of mixtures and polybases alone.

3.2.3 Discussion

In this section, following the same methodology as that employed for polyA-NH₂ / polyT pairs, we analyze now the results obtained for the hybridized polyG-NH₂•polyC and its corresponding polyG-NH₂+polyC mixture. First, we compare the hybridized double strands spectrum with the spectra of single strand polybases, polyG-NH₂ alone, polyC alone, and their mixture, at a same concentration of 5 μM. All corresponding spectra are compiled in Figure 6-12. Then, we analyze the trends observed in the concentration-dependent SERS intensities for both studied cases, mixture and hybridized.

3.2.3.1 PolyG-NH₂ + polyC mixture

As can be seen in Figure 6-12 in the mixture case, the SERS spectrum is dominated by characteristic guanine bands, notably, the IPRBM at 656 cm⁻¹. Except one wide and weakly intense band at 792 cm⁻¹, there is no significant feature of polyC. As previously discussed for polyT, this feature might be due to the low Raman cross section of this polybase [1], but this assumption is denied by the intense SERS signal of this polybase alone, as presented in chapter 5. Thus, here again, we infer that a competitive mechanism between polyG-NH₂ and polyC leads to the preferential adsorption of guanine. Indeed, as already discussed in the case of polyA-NH₂+polyT mixture, both polybases exhibit different adsorption affinities to the metal surface.

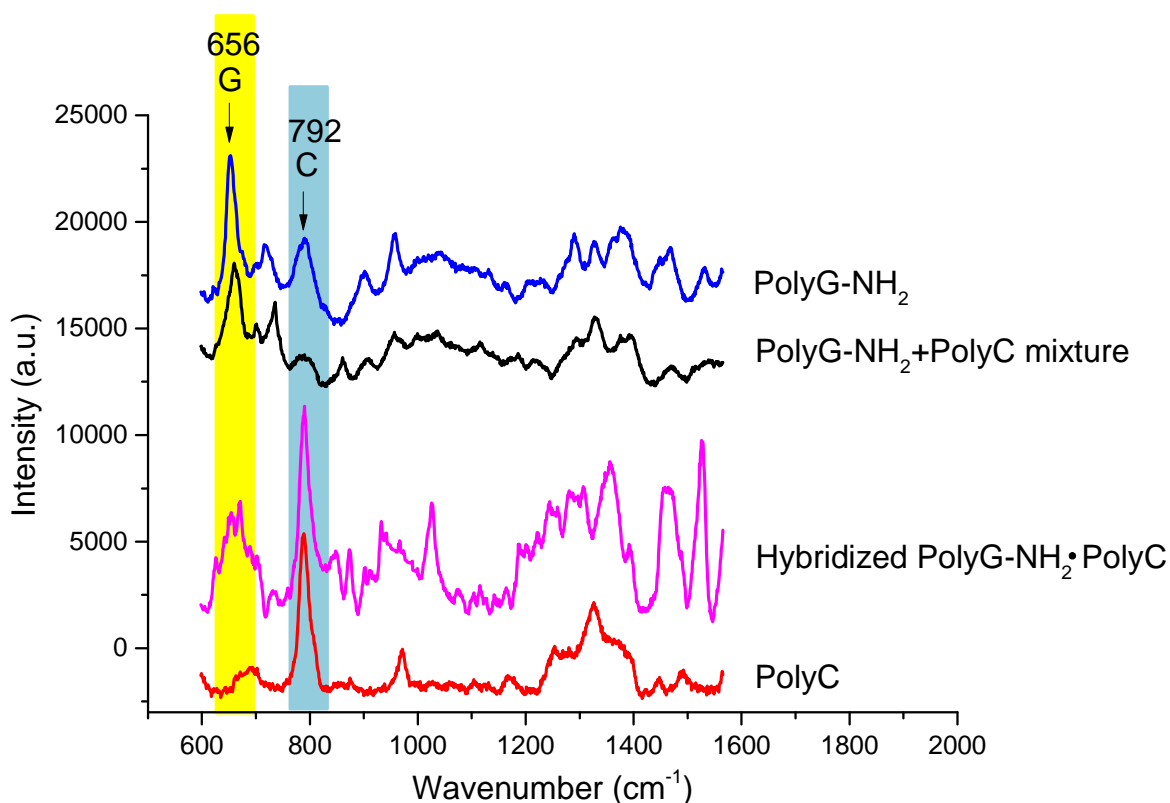


Figure 6-12: SERS spectra of polyG-NH₂ and polyC alone, as well as their equi-molar polyG-NH₂ + polyC mixture and their hybridized polyG-NH₂•polyC pairs, obtained for $C_{\text{polyG-NH}_2} = C_{\text{polyC}} = 5 \mu\text{M}$.

Let us cite again Demers et al., who have reported on the binding affinities of the different bases to gold related to their desorption heats ΔH_{des} . Since the ΔH_{des} value for cytosine ($129 \pm 4 \text{ kJ/mol}$) is weaker than that for guanine ($144 \pm 2 \text{ kJ/mol}$) [2], it can be concluded that cytosine adsorbs less than guanine, in agreement with our observation from SERS spectra. Besides, another important factor may influence the observed variation in affinities, which is the number of available N atoms constituting the individual bases and involved in the binding with the Ag^o surface. Actually, it is not surprising that polyG-NH₂ presents a higher affinity than polyC, since guanine bases possess more available N atoms (four) than cytosine bases (two) (Figure 5-16 in chapter 5). As already mentioned for the polyA-NH₂ + polyT mixture, we cannot either completely rule out the possibility of a duplex polyG-NH₂•polyC formation in the solution. Therefore, the polyG-NH₂ + polyC mixture spectrum may not be simply a combination of both single strand polybase features, but may also include the features of polyG-NH₂•polyC duplex. However, given the fact that we observed a rather similar concentration-dependent trend in SERS intensities of the polyG-NH₂+polyC mixture (Figure 6-11 a) and the polybases alone (chapter 5), it is likely that the polyG-NH₂+polyC mixture follows a behavior similar to that of polyG-NH₂ alone and that no hybridized molecule is present at the Ag^o surface. This last assumption is reinforced by some

published studies showing that the adsorption of duplexes is much lower than that of any individual homo-oligonucleotides [11]. Finally and importantly, a striking similarity in the behavior between polyG-NH₂+polyC and polyA-NH₂+polyT mixtures should be emphasized. In each case, a competitive mechanism takes place, which impinges the adsorption of polybases showing the weakest affinity with the Ag^o surface (polyC and polyT) and leads to the predominant presence of polyG-NH₂ in the former mixture and polyA-NH₂ in the latter one.

3.2.3.2 Hybridization feasibility and immobilization features:

As illustrated in the SERS spectra of Figure 6-12, the differences between polyG-NH₂+polyC mixture and hybridized polyG-NH₂•polyC are clear. For the mixture, the spectra are dominated by characteristic guanine bands while, for the hybridized pair, the most intense band at 792 cm⁻¹ is attributed to cytosine. These differences show that both polyG-NH₂ and their complementary sequences polyC are present in the latter case, which indicates that polyG-NH₂ can hybridize with polyC under our experimental conditions. The specific recognition between G and C originates from the formation of three hydrogen bonds, involving 2 N and 1 O atoms of each base, i.e. O_(guanine)•••H•••NH₂ (cytosine), N1_(guanine)•••H•••N3 (cytosine), and NH₂(guanine)•••H•••O_(cytosine), as can be seen in Figure 6-13.

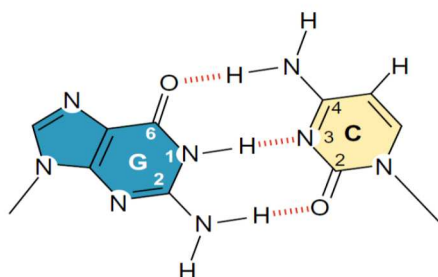


Figure 6-13: Schematic representation of the three hydrogen bonds between specific atoms of guanine and cytosine.

Another interesting feature relies on the fact that, while the in plane vibration modes are mainly detected by SERS, we also observe the appearance of weak out plane bands (i.e. a band at 735 cm⁻¹ for guanine, and the one at 688 cm⁻¹ for cytosine) in all the SERS spectra of the studied hybridized pair (Figure 6-10 b). As mentioned earlier and according to SERS selection rules, the predominant detection of the in plane vibration modes provides compelling evidence that the hybridized pairs are mainly in a flat conformation on the Ag^o surface, similarly to the case of hybridized polyA-NH₂ • polyT illustrated in Figure 6-7, but we cannot either exclude some tilted molecules inducing the presence of weakly intense out of plane bands. It is important to recall that, compared to the mixture spectra, several bands at high frequencies (i.e. in the 1200-1500 cm⁻¹ range) are highly enhanced in the hybridized pair spectra. This trend is remarkably similar to that observed in the case of hybridized polyA-NH₂•polyT. As we already

discussed in the latter case, the enhancement intensity of bands at high frequencies, i.e. the band at 1330 cm^{-1} for polyA-NH₂, can be correlated with conformation changes upon hybridization of polyA-NH₂ with polyC. According to the great similarity between trends observed for both studied hybridized pairs, it is reasonable to assume that the enhancement of high frequency bands in the spectrum of hybridized polyG-NH₂•polyC also originates from conformation changes upon hybridization.

3.2.4 Summary

From this study on polyG-NH₂ / polyC pairs, several important results have been obtained:

- In the mixture case, the lack of cytosine band in the SERS spectra demonstrates that there is a preferential adsorption of polyG-NH₂ on the Ag⁰ surface according to a mechanism of competitive adsorption between polyG-NH₂ and polyC. This result is totally comparable to that of polyA-NH₂+polyT mixture which indicates the preferential adsorption of polyA-NH₂ on the Ag⁰ surface. The main conclusion is that the polyG-NH₂+polyC mixture leads to the presence of polyG-NH₂ alone on the Ag⁰ surface. Besides, the concentration dependency of the SERS intensity for this system is rather similar to the case of the polybases alone showing a maximum of intensity for a concentration around 10 μM .
- In the case of the hybridized polyG-NH₂•polyC, the strong presence of cytosine bands gives a compelling evidence that the hybridization has taken place and that the cytosine is probably bound to the guanine through specific hydrogen bonds. From the enhanced intensity of high frequency (1200-1500 cm^{-1}) bands, and from the main presence of in plane bands, we can also deduce that the hybridized polyG-NH₂•polyC molecules are mainly lying flat on the Ag⁰ surface, even if some molecules can also be orientated perpendicularly.

4. Conclusion

Specific SERS features of complementary polybase pairs have been studied to characterize the *in situ* hybridization of polyA-NH₂ with polyT and polyG-NH₂ with polyC. A comparison of the obtained SERS spectra with those of the corresponding polybase mixtures provides clear spectral differences, which enable to reliably assess the hybridization features. Remarkably, rather similar results are found for both studied pairs, which are summarized in the following.

For both hybridized pairs, the unambiguous presence of polyT and polyC, respectively, is confirmed which is not the case for the corresponding mixtures. In the latter cases, we observed that the mixture behaves like the single strand polybases polyA-NH₂ or polyG-NH₂ alone. We suggest that, compared to

their complementary polyT and polyC moieties, a competitive mechanism leads to the preferential adsorption of polyA-NH₂ and polyG-NH₂ at the Ag^o surface. From this conclusion, we deduce that, in the case of hybridization, the SERS detection of polyT and polyC at the Ag^o surface is justified by their binding with their respective complementary bases through specific hydrogen bonds. We therefore confirm that the *in situ* hybridization has effectively taken place.

For both hybridized systems, and more especially in the case of hybridized polyA-NH₂•polyT, we have also observed a strong enhancement in the intensity of high frequency bands in comparison with the SERS spectra of the mixtures and polybases alone, these latter spectra being essentially featured by a sharp and intense in plane ring breathing modes (IPRBM). The high frequency bands correspond to many different and individual in plane stretching and bending vibration modes. Therefore, in the case of *in situ* hybridization, the enhancement of such bands tends to confirm the changes of orientation and conformation of the individual bases on the Ag^o surface. The bases are more engaged in the pairing hydrogen bonds instead of being connected to the Ag^o surface through their available N intern atoms, as it is the case for polybases alone. Besides, the major presence of in plane vibrations with only some weakly intense out of plane modes tends to prove that the hybridized molecules are mainly lying flat on the surface, similarly to polybases alone.

Finally, a decreasing concentration dependence of the SERS intensity is found in the case of hybridized polyA-NH₂•polyT. This trend has not been confirmed in the case of hybridized polyG-NH₂•polyC. But, for both hybridized pairs, a greater SERS intensity is observed for the lowest concentration studied here (C = 1 μM) compared to the non-hybridized cases. To explain this trend, we have proposed a hybridization model derived from the previous probe grafting model detailed in chapter 5. According to this hybridization model, the hybridization efficiency differs in the three domains of concentrations studied here according to the different surface coverages and packing densities of the polybase probes on the Ag^o surface. Notably, in the lowest concentration domain, the hybridization efficiency is the highest. Further experiments should be performed in much lower concentration domains to investigate the sensitivity and to assess the detection limit of our Ag^o/TiO₂ heterostructure toward the SERS detection of hybridized DNA molecules.

- [1] A. Barhoumi, D. Zhang, F. Tam, and N. J. Halas, "Surface-Enhanced Raman Spectroscopy of DNA," *Journal of the American Chemical Society*, vol. 130, pp. 5523-5529, 2008.
- [2] L. M. Demers, M. Östblom, H. Zhang, N.-H. Jang, B. Liedberg, and C. A. Mirkin, "Thermal Desorption Behavior and Binding Properties of DNA Bases and Nucleosides on Gold," *Journal of the American Chemical Society*, vol. 124, pp. 11248-11249, 2002.
- [3] A. Campion and P. Kambhampati, "Surface-enhanced Raman scattering," *Chemical Society Review*, vol. 27, pp. 241-250, 1998.
- [4] B. Giese and D. McNaughton, "Surface-Enhanced Raman Spectroscopic and Density Functional Theory Study of Adenine Adsorption to Silver Surfaces," *The Journal of Physical Chemistry B*, vol. 106, pp. 101-112, 2001.
- [5] S. M. Schreiner, D. F. Shudy, A. L. Hatch, A. Opdahl, L. J. Whitman, and D. Y. Petrovykh, "Controlled and Efficient Hybridization Achieved with DNA Probes Immobilized Solely through Preferential DNA-Substrate Interactions," *Analytical Chemistry*, vol. 82, pp. 2803-2810, 2010.
- [6] S. M. Schreiner, A. L. Hatch, D. F. Shudy, D. R. Howard, C. Howell, J. Zhao, *et al.*, "Impact of DNA–Surface Interactions on the Stability of DNA Hybrids," *Analytical Chemistry*, vol. 83, pp. 4288-4295, 2011.
- [7] T. Watanabe, O. Kawanami, H. Katoh, K. Honda, Y. Nishimura, and M. Tsuboi, "SERS study of molecular adsorption: Some nucleic acid bases on Ag electrodes," *Surface Science*, vol. 158, pp. 341-351, 1985.
- [8] C. Otto, T. J. J. van den Tweel, F. F. M. de Mul, and J. Greve, "Surface-enhanced Raman spectroscopy of DNA bases," *Journal of Raman Spectroscopy*, vol. 17, pp. 289-298, 1986.
- [9] V. Brabec and K. Niki, "Raman scattering from nucleic acids adsorbed at a silver electrode," *Biophysical Chemistry*, vol. 23, pp. 63-70, 1985.
- [10] M. Green, F.-M. Liu, L. Cohen, P. Kollensperger, and T. Cass, "SERS platforms for high density DNA arrays," *Faraday Discussions*, vol. 132, pp. 269-280, 2006.
- [11] H. Kimura-Suda, D. Y. Petrovykh, M. J. Tarlov, and L. J. Whitman, "Base-Dependent Competitive Adsorption of Single-Stranded DNA on Gold," *Journal of the American Chemical Society*, vol. 125, pp. 9014-9015, 2003.

Conclusion

The goal of this thesis work relies on two important parts.

i/ The first part deals with the investigation on new approaches, aiming at improving the uniformity of an $\text{Ag}^\circ/\text{TiO}_2$ heterostructure elaborated by a low cost and bottom up process. Notably, the photocatalytic reduction parameters leading to the Ag° NPs growth must be clearly defined and controlled in order to optimize the derived SERS substrate performances. The influence of these parameters on the Ag° NPs characteristics, such as morphology, size, surface distribution and density, is crucial for both the SERS activity and the detection performances of the platform in terms of reproducibility, durability, sensitivity, and reliability. This study constitutes the first main objective.

ii/ The second part deals with the extrapolation of this new type of substrate for the label-free SERS detection of DNA molecules. Before considering the problematic of SERS detection of multi-base hybridized DNA molecules, it is essential to improve the reliability of SERS detection on “simpler” single-base DNA molecules. This aspect constitutes the second main objective of this thesis.

As a first issue to address, the formation of Ag° NPs has been studied through a chemically assisted photocatalytic reduction process on the surface of sol-gel deposited TiO_2 thin films exposed to UVA light, in order to propose a low cost liquid solution elaboration procedure of SERS substrates. Different characterization methods have been used to assess how the chemical assistance of the photocatalytic reduction process allows an enhanced uniformity of the Ag° NPs deposition. Tri-sodium citrate (TSC) firstly enables a considerable reduction in the NPs growth kinetic and favors the dispersion of rather small and uniform NPs but, when these NPs are deposited in great amount, they tend to heterogeneously aggregate at the substrate surface. Secondly, an ascorbic acid (AA)-assisted seeded growth procedure, by allowing a self-controlled growth-aggregation process relying on Schottky barrier effects, enables the formation of a great amount of NPs uniformly aggregated. Moreover, various combinations of the seed amount and UVA exposure duration enable to selectively control the amount, aggregation state, and size of deposited NPs. These uniform aggregates obtained in this work are highly susceptible to induce hot spots, thus providing strong local electromagnetic fields and resulting in a large enhancement of Raman signals of the adsorbed molecules.

The SERS performances of the so-obtained $\text{Ag}^\circ/\text{TiO}_2$ heterostructure have firstly been investigated through Raman spectroscopy studies using Rhodamine 6G chosen as a model analyte. The results confirm that the SERS amplification does not seem to intrinsically rely on the shape and size of individual NPs, but is more probably governed by hot spots induced by aggregation features.

Accordingly, the homogeneous aggregation of NPs induced by a TSC-based photocatalytic reduction associated to an AA-based seeded growth leads to good SERS performances, a 10^6 EF and a detection limit of R6G ranging between 10^{-8} and 10^{-10} M, as well as a good reproducibility of the R6G SERS spectra on rather large substrates. As a result, it is considered that our SERS substrates are sufficiently robust and reproducible to be extended to the detection of bio-molecules of applicative interest, such as DNA molecules, whose Raman detection is by far less easy than that of R6G molecule.

Then, we come to the second objective of the thesis dedicated to the SERS detection of DNA molecules. The SERS detection of four single strand DNA polybases (polyA, polyC, polyG, and polyT), modified or not with an external NH_2 linker, has first been considered. These polybases have been immobilized with different concentrations on our $\text{Ag}^\circ/\text{TiO}_2$ SERS substrate using a simplified procedure arising from specific assets of this substrate. Because of the reliability and efficiency of this platform, we obtained reproducible SERS spectra for the four DNA polybases functionalized or not by a terminal NH_2 group. In particular, the high resolution and signal/noise ratio enabled us to clearly index the main and secondary Raman lines, even for the polybases with a low Raman cross section such as polyC and polyT.

Regardless of the polybase type and whether the polybase was NH_2 -modified, we have emphasized a polybase concentration dependence of the SERS spectra reproducibility and intensity, which shows an optimum for a 5-10 μM range. This optimal range of concentrations should, therefore, be kept for further applicative researches aiming at the SERS detection of DNA multibase oligonucleotides. The optimum concentration range was interpreted in terms of distribution, orientation, and packing density of immobilized molecules. This study also shows that the external NH_2 linker is not necessary for the immobilization of the polybases, which can be bound to the SERS-active Ag° NPs surface through the internal N atoms. In the optimum concentration range, it seems that the polybase molecules undergo a uniform 2D coverage and a flat orientation relative to the Ag° surface. From that point of view, it appears that the NH_2 linker acts like an anchoring point keeping the 2D monolayer in an ordered configuration on the metal surface. In that sense, the NH_2 linker plays, therefore, an essential role in the SERS spectra reproducibility.

We have then extended our studies to complementary hybridized polybase pairs, polyA- NH_2 with polyT and polyG- NH_2 with polyC, obtained after *in situ* hybridization. Their specific SERS features have been emphasized by comparing the obtained SERS spectra with those of the corresponding polybase mixtures (not hybridized). Evidences for the determination of hybridization spectrum features were obtained with remarkably similar results found for both pairs. In the case of the two hybridized pairs, the unambiguous presence of polyT and polyC is confirmed, which is not the case for the corresponding mixtures. In the latter cases, we observed that the mixtures behave like the single strand polybases alone, i.e. polyA- NH_2

and polyG-NH₂. Consequently, we suggest that a competitive mechanism leads to a preferential adsorption of polyA-NH₂ and polyG-NH₂ at the Ag⁰ surface. In contrary, the observed presence of polyT and polyC in SERS spectra for the case of hybridization was justified by their binding to their respective complementary bases through specific hydrogen bonds. A consequence of these specific bindings is the change of the base orientation relatively to the Ag⁰ surface, which resulted in a strong enhancement of the high frequency bands in comparison with the SERS spectra of the mixtures and polybases alone. Therefore, we confirmed that the *in situ* hybridization has effectively taken place.

Besides, the major presence of in plane vibration bands, along with only some very weak out of plane vibration bands, tends to prove that the hybridized molecules are mainly lying flat on the Ag⁰ surface, similarly to single strand polybases. Finally, by varying the hybridized polybase concentration, we could emphasize a decreasing concentration dependence of the SERS intensity, the result being clearer in the case of polyA-NH₂ with polyT than in the case of polyG-NH₂ with polyC. Notably, compared to polybases alone or in mixture, a much higher SERS intensity is observed after hybridization for the lowest studied concentration (C=1 μM). To explain this observation, we proposed a hybridization model where the hybridization efficiency differs according to the surface coverage and packing densities of the polybase probes on the Ag⁰ surface. Accordingly, in the lowest concentration domain, the hybridization efficiency is the highest. Further experiments should be performed at much lower concentrations to investigate the sensitivity and assess the detection limit of our SERS substrate toward the detection of hybridized DNA.

In summary, this thesis provides an insight on a cycle of understanding (how to control surface architecture), innovation (proposition of a highly reliable SERS substrate), and potential application (DNA molecules detection). A major strength in our proposed Ag⁰/TiO₂ SERS substrate, which differs from others in the literature, is the controlled fabrication of ordered aggregates with enhanced properties. Since it still remains a challenging task to rationalize the chemical approach to predict/control the morphology of nanostructures, such organized structure should find its scope in the area of biosensor devices. Moreover, the robust nature of our substrate has been demonstrated by its applications to rather complex DNA molecules detection. Methodologies presented in this thesis not only provided excellent tool to study but also to improve our understanding of DNA-Ag⁰ NPs surface interactions.

In the future, such understanding, innovation, and application cycle should continue to progress, promising more advance toward objectives in the medical diagnostic field. Thus, further works related to this thesis should address the following items.

- As the elaboration conditions of our heterostructure lead to a large variety of NPs Ag⁰ aggregates morphologies, it should be interesting to study how these morphologies influence and enable to optimize the SERS detection.
- New experimental studies should be conducted in order to better understand how the data arising from SERS spectra enable to better understand the binding, orientation, and ordering of DNA molecules on the Ag⁰/TiO₂ heterostructure.
- The first studies on the hybridization of polybases on our SERS substrate should be continued in order to provide entries for further more complex studies dealing with the SERS detection of multibase DNA molecules and their hybridization.
- These studies on the SERS detection of multibase DNA molecules and their hybridization should in particular enable to assess essential questions dealing with the potential of our Ag⁰/TiO₂ heterostructure in the view of medical diagnostic applications, for instance the unique use or reusability of the proposed SERS substrates.

List of publications

Publications in peer-reviewed journals

- "Controlled growth of silver nanoparticles through a chemically assisted photocatalytic reduction process for SERS substrate applications", L. He, D. Riassetto, P. Bouvier, L. Rapenne, O. Chaix-Pluchery, V. Stambouli, M. Langlet, *J Photochem Photobiol A : Chem*, 277 (2014) 1.
- "New insights in SERS label free detection of DNA on Ag⁰/TiO₂ substrate", L. He, M. Langlet, P. Bouvier, C. Calers, C. M. Pradier, V. Stambouli, *J Phys Chem C*, 118 (2014) 25658.
- "On the role of the NH₂ external linker on the SERS intensities of DNA homo-oligonucleotide single strand SERS spectra", L. He, M. Langlet, V. Stambouli, submitted to *Sensors & Actuators: B. Chemical* (2014).
- "SERS detection of complementary polybase pairs on a Ag⁰ / TiO₂ heterostructure: mixture versus hybridization effects", L. He, M. Langlet, V. Stambouli, redaction in progress (2014).

Communications and posters in conferences and workshops

- "Nouveaux aperçus dans la synthèse de substrats SERS Ag⁰/TiO₂ pour la détection sans marquage de biomolécules", L. He, M. Langlet, O. Chaix, V. Stambouli, 9^{ème} Journée Sol-Gel Rhône-Alpes-Auvergne, St Etienne, 5 Avril 2012 (communication).
- "New insights in Ag⁰/TiO₂ SERS substrates for the label-free DNA detection", L. He, I. Sow, M. Langlet, O. Chaix-Pluchery, V. Stambouli, E-MRS Spring Meeting, Strasbourg (France), 14-18 Mai 2012 (poster).
- "Chemically assisted photocatalytic routes for the low cost fabrication of Ag⁰/TiO₂ SERS substrates", L. He, M. Langlet, O. Chaix-Pluchery, V. Stambouli, 2^{èmes} journées plénières du GDR PMSE, Porquerolles (France), 1-3 octobre 2012 (poster).
- "Chemically assisted photocatalytic routes for the low cost fabrication of Ag⁰/TiO₂ SERS substrates", L. He, M. Langlet, O. Chaix-Pluchery, V. Stambouli, 1st International Conference on Enhanced Spectroscopy, Porquerolles (France), 3-5 octobre 2012 (poster).
- "Substrats SERS Ag⁰/TiO₂ pour la détection de molécules organiques", L. He, V. Stambouli, M. Langlet, 10^{ème} Journée Sol-Gel Rhône-Alpes-Auvergne, St Etienne, 11 Avril 2014 (communication).
- "Ag⁰/TiO₂ sensor for the SERS detection of organic molecules", L. He, V. Stambouli, M. Langlet, EUROPT(R)ODE XII, 12th conference on Optical Chemical Sensor & Biosensor, Athens, 13-16 Avril 2014 (poster).
- "TiO₂-Ag⁰ plasmonic sensor for the SERS detection of organic molecules", L. He, M. Langlet, O. Chaix-Pluchery, V. Stambouli, Journées plénières du GdR Plasmonique Moléculaire et Spectroscopies Exaltées, 2-3 juin 2014, Université P. Diderot, Paris (communication).

Titre / Title

ELABORATION ET EVALUATION D'UNE NOUVELLE HETEROSTRUCTURE $\text{Ag}^\circ/\text{TiO}_2$ DESTINEE A LA DETECTION PAR EFFET SERS SANS MARQUAGE D'ADN.

ELABORATION AND ASSESSMENT OF A NEW $\text{Ag}^\circ/\text{TiO}_2$ HETEROSTRUCTURE INTENDED TO THE LABEL-FREE SERS DETECTION OF DNA.

Résumé: Des substrats SERS, élaborés selon une approche simple et à moindre coût, ont été étudiés pour la détection sans marqueurs d'ADN en vue d'applications dans le domaine du diagnostic médical. Un protocole de réduction photocatalytique assistée chimiquement conduisant à des hétérostructures $\text{Ag}^\circ/\text{TiO}_2$ a été optimisé. Nous avons montré en quoi l'utilisation d'un agent encapsulant et d'une procédure de nucléation-croissance permettent de contrôler la formation et l'agrégation de NPs Ag° à la surface de couches minces TiO_2 . L'agrégation contrôlée des NPs conduit à des points chauds induisant une très forte amplification de l'effet SERS. Les performances des substrats SERS ont tout d'abord été validées par détection Raman de la molécule modèle R6G. Des études de fond, portant sur la détection de polybases dérivées des quatre nucléobases constituant la structure de l'ADN, adénine, cytosine, guanine et thymine, ont ensuite été réalisées. Le potentiel de détection des hétérostructures $\text{Ag}^\circ/\text{TiO}_2$ a permis l'indexation quasi-intégrale des bandes Raman des quatre polybases étudiées, modifiées ou non avec des groupements NH_2 , et nous a permis de discuter des effets d'accrochage, d'orientation et d'agencement des molécules d'ADN sur les substrats SERS. Des études complémentaires ont finalement confirmé le potentiel de nos hétérostructures en fournissant différents aperçus sur l'hybridation des polybases et l'association de différentes polybases sur un même substrat SERS.

Summary: SERS substrates, elaborated through a simple and low-cost procedure, have been studied for the label-free detection of DNA in the view of applications in the medical diagnostic field. A chemically assisted photocatalytic reduction protocol leading to an $\text{Ag}^\circ/\text{TiO}_2$ heterostructure has been optimized. We have shown how the use of an encapsulating agent and a nucleation-growth procedure enable to control the formation and aggregation of Ag° NPs at the surface of TiO_2 thin films. The controlled aggregation of NPs leads to hot points inducing a very strong amplification of the SERS effect. Performances of the SERS substrate have first been evaluated through the Raman detection of the R6G model molecule. Thorough studies dealing with the detection of polybases derived from the four nucleobases constituting the DNA structure, adenine, cytosine, guanine, and thymine, have then been conducted. The detection potential of the $\text{Ag}^\circ/\text{TiO}_2$ heterostructure enabled a nearly exhaustive indexation of the Raman bands for the four studied polybases, modified or not with NH_2 groups, and to discuss on binding, orientation, and ordering effects of the DNA molecules on the SERS substrate. Complementary studies finally enabled us to confirm the potential of our heterostructure by providing different insights on the polybase hybridization and the association of different polybases on a same SERS substrate.

Mots clefs / Keywords

ADN, détection sans marqueurs, effet SERS, NPs Ag° , dioxyde de titane, activité photocatalytique.
DNA, label-free detection, SERS effect, Ag° NPs, titanium dioxide, photocatalytic activity.

Résumé

1. Introduction

La détection rapide et fiable de biomolécules, telles que des protéines, des métabolites, des peptides ou encore des séquences d'ADN, est d'une importance cruciale pour progresser efficacement dans le domaine du diagnostic médical. Dans ce domaine, la recherche vise à développer des approches toujours plus efficaces et sensibles et ne nécessitant pas l'usage de marqueurs fluorescents dont l'usage est contraignant et onéreux. Parmi les différentes approches étudiées, les méthodes par spectroscopie laser jouent un rôle central car elles sont capables d'identifier et de caractériser les molécules d'intérêt, ceci en fournissant des données sur leur empreinte digitale et leur évolution structurale. En particulier, les techniques spectroscopiques basées sur la vibration moléculaire, telles que la spectroscopie Raman, ont attiré une attention croissante en raison de leur richesse en informations structurales via la détection spécifique de bandes de vibration. Plus récemment, le développement des nanotechnologies a ouvert un nouvel horizon pour la détection biomoléculaire. Ainsi, la spectroscopie Raman exacerbée de surface (en anglais, Surface Enhanced Raman Spectroscopy : SERS) tire profit des propriétés optiques de nanostructures métalliques (par exemple Ag° ou Au°), résultant en un signal Raman fortement amplifié. Cette spécificité permet de surmonter les problématiques découlant de la faible sensibilité de la spectroscopie Raman classique, et le SERS fournit ainsi un outil puissant pour la détection biomoléculaire, notamment des molécules d'ADN, ceci sans nécessiter l'utilisation de marqueurs fluorescents.

Par ailleurs, les spectres SERS de molécules adsorbées sur une nanostructure métallique solide sont beaucoup plus stables et reproductibles que ceux obtenus à partir de suspensions colloïdales de nanoparticules (NPs) métalliques. Des études fondamentales ont en particulier montré que, sur des substrats solides, des « points chauds » situés à la jonction entre des NPs métalliques voisines provoquent une augmentation spectaculaire du champ électromagnétique et conduisent ainsi à une très forte intensification de l'effet SERS. La sensibilité élevée des substrats SERS étudiés à l'heure actuelle repose donc sur la possibilité de créer uniformément un grand nombre de points chauds sur un substrat solide via la dispersion homogène d'agrégats de NPs métalliques à la surface du substrat ou la structuration appropriée d'un substrat métallique. Toutefois, les méthodes actuellement proposées pour la fabrication de tels substrats solides (par exemple la lithographie par faisceau d'électrons ou encore la lithographie nanosphère) sont généralement trop coûteuses et / ou reposent sur des procédures de fabrication trop complexes pour envisager des applications pratiques. La fabrication simplifiée et à moindre coût de substrats SERS solides, présentant une bonne reproductibilité spectrale sur de grandes

dimensions et un important facteur d'amplification par rapport à des spectres Raman classiques (en anglais, enhancement factor : EF), demeure donc un défi très actuel. L'objectif de la thèse est de répondre à ce défi en proposant de nouvelles approches de fabrication de substrats SERS solides.

La synthèse de NPs métalliques par voie chimique ou photochimique sur des supports solides est une approche à moindre coût qui peut répondre aux critères de fonctionnement d'un substrat SERS performant. Par exemple, certaines études publiées dans la littérature ont montré la possibilité de faire croître chimiquement ou photochimiquement des NPs Ag⁰ sur des supports solides, mais ces études ne sont pas suffisamment détaillées pour envisager la croissance contrôlée de NPs métalliques compatibles avec des substrats SERS exploitables pour des applications. Il existe en particulier un véritable intérêt à mener des recherches approfondies sur les mécanismes conduisant à la croissance contrôlée de NPs Ag⁰ via un processus de réduction photocatalytique. L'objectif de la thèse est donc double. Elle vise tout d'abord à étudier les conditions d'élaboration d'une hétérostructure Ag⁰ / TiO₂ formée par réduction photocatalytique à la surface d'une couche mince TiO₂ en vue d'optimiser les performances du substrat SERS en découlant. Elle vise par ailleurs à extrapoler ce nouveau type de substrat à la détection SERS sans marqueur de biomolécules d'intérêt applicatif, i.e. des molécules d'ADN, et à évaluer les performances de notre plateforme SERS (reproductibilité, sensibilité, sélectivité, fiabilité).

2. Etude d'une hétérostructure Ag⁰ / TiO₂

2.1 Optimisation des conditions d'élaboration

L'approche développée au cours de cette thèse repose sur l'activité photocatalytique du dioxyde de titane (TiO₂) une fois cristallisé dans sa forme polymorphe anatase. Sous exposition UVA d'énergie supérieure au gap de l'anatase ($E > E_g = 3,20 \text{ eV}$; $\lambda < 380 \text{ nm}$), le TiO₂ va créer des porteurs de charge trous et électrons qui, après migration vers la surface, sont capables d'induire toutes sortes de réactions d'oxydo-réduction (figure 1). Dans ce travail, nous nous sommes tout particulièrement intéressés au pouvoir réducteur des électrons photo-générés afin de réduire du nitrate d'argent (AgNO₃) adsorbé à la surface de couches minces TiO₂ et ainsi former des NPs Ag⁰. Les couches minces TiO₂ ont été déposées par voie sol-gel, sur des substrats de silicium de 3 x 3 cm², en utilisant un protocole optimisé au LMGP pour élaborer des films photocatalytiques. Après dépôt à température ambiante par spin-coating d'un sol à base d'alkoxyde de titane, le film xérogel résultant est traité à 500°C en vue de le cristalliser dans la phase anatase du TiO₂. Les couches minces obtenues présentent une épaisseur de 40 nm, homogène sur toute la surface de l'échantillon, et se traduisent par une très bonne activité photocatalytique.

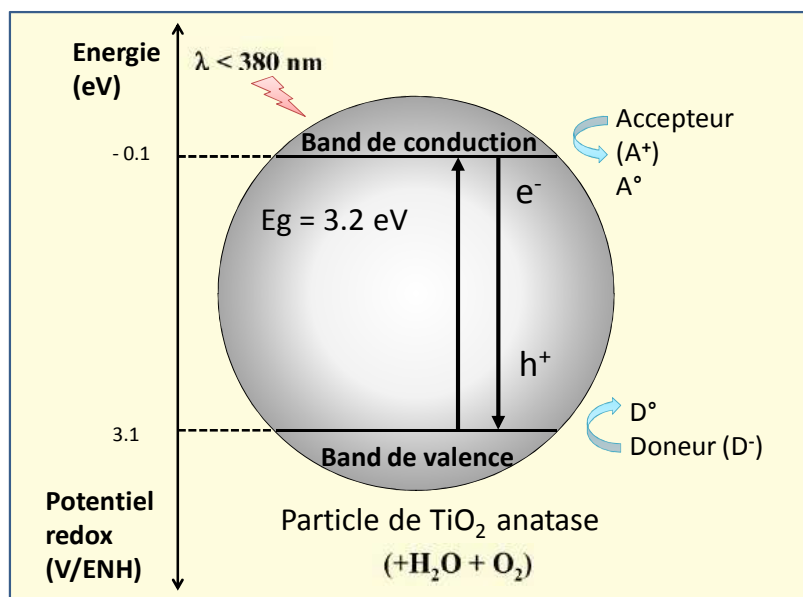


Figure 1. Principe de la photocatalyse : création de porteurs de charge trous et électrons sous exposition du TiO₂ aux UVA.

Les substrats de 3 x 3 cm² recouverts d'une couche TiO₂ ont ensuite été immergés dans une solution aqueuse de nitrate d'argent et exposés pendant des durées variables à la lumière UVA émise par des lampes PLS-11W (Philips). Cette procédure permet de mettre en œuvre un processus de réduction photocatalytique qui conduit à une hétérostructure Ag^o / TiO₂ consistant en des NPs métalliques Ag^o sphériques déposées sur la surface du film TiO₂. Ces NPs sont toutefois réparties de façon très hétérogène sur la surface TiO₂ et elles présentent une distribution de taille extrêmement large allant de quelques nanomètres à plusieurs centaines de nanomètres (figure 2). Cette hétérogénéité a pu être expliquée par des effets de barrières Schottky aux interfaces Ag^o-TiO₂, lesquels favorisent la croissance rapide des plus grosses NPs au détriment des plus petites.

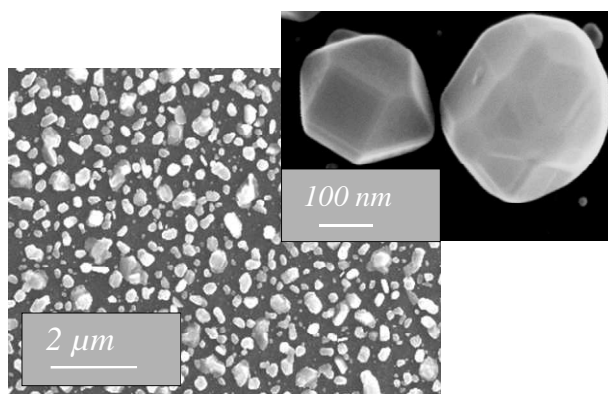


Figure 2. Images MEB de NPs Ag[°] formées par réduction photocatalytique.

Le protocole a donc fait l'objet de différentes optimisations en assistant par voie chimique le processus de réduction photocatalytique. Nous avons tout d'abord mis à profit le pouvoir encapsulant du tri-sodium citrate (TSC) dilué dans la solution aqueuse de nitrate d'argent. Ce pouvoir encapsulant permet de ralentir et mieux contrôler la croissance des NPs Ag[°] au cours de l'exposition aux UVA. Ces études nous ont permis d'optimiser des premières conditions expérimentales en fixant la concentration de nitrate d'argent en solution à 2 mM et le rapport molaire TSC / AgNO₃ à 5. Il est à noter que, contrairement au protocole sans TSC qui conduisait à des NPs séparées, l'utilisation du TSC conduit à des agrégats de NPs sphériques. Les NPs constituant ces agrégats présentent une petite taille uniforme avec un diamètre compris entre 50 et 100 nm. Rappelons que les agrégats de NPs présentent un intérêt particulier car ils sont susceptibles de provoquer des points chauds conduisant à une amplification importante de l'effet SERS. Toutefois, et malgré les effets bénéfiques du TSC, l'agrégation des NPs devient inhomogène et les agrégats coexistent avec des particules isolées de toute petite taille lorsque les NPs Ag[°] sont formées en quantité importante (par exemple après des durées d'exposition UVA longues) (figure 3). Comme nous le verrons par la suite, ces observations ne sont pas compatibles avec la reproductibilité des spectres SERS mesurés en différents endroits d'un même échantillon.

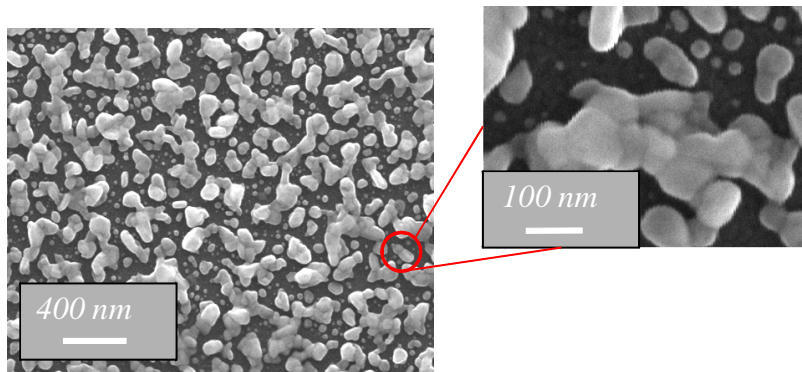


Figure 3. Images MEB de NPs Ag[°] formées par réduction photocatalytique assistée TSC après 60 min d'exposition aux UVA.

Nous avons donc poursuivi notre optimisation de la plateforme SERS en complétant le protocole de réduction photocatalytique assisté TSC par un processus de nucléation-croissance. Pour ce faire, nous avons tiré profit du faible pouvoir (chimiquement) réducteur de l'acide ascorbique (AA). Un protocole de dépôt multicouche en solution liquide (éthanol) par spin-coating, basé sur le dépôt de nitrate d'argent suivi du dépôt d'AA, a ainsi été mis au point. Ce protocole conduit à des nuclei Ag[°], de petite taille homogène avec un diamètre moyen compris entre 15 et 25 nm, distribués uniformément sur la surface du film TiO₂, et dont la quantité peut être ajustée en faisant varier le nombre d'opérations de dépôt de l'AA sans pour autant modifier significativement leur taille (figure 4).

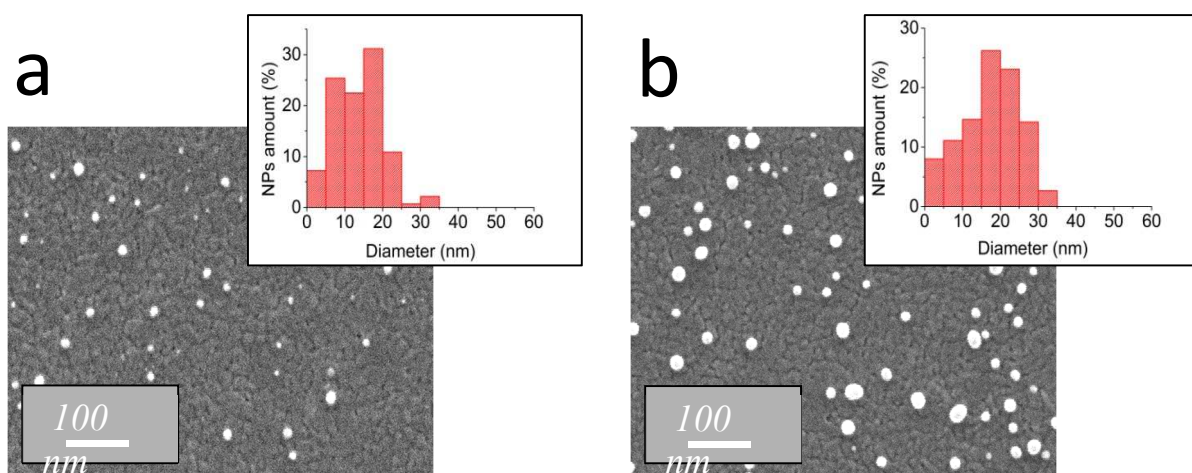


Figure 4. Images MEB et distribution de taille de nuclei Ag° formés après une opération de dépôt (gauche) et cinq opérations de dépôt d'AA (droite).

La croissance de NPs Ag° par réduction photocatalytique assistée TSC a ensuite été mise en œuvre sur les substrats recouverts de nuclei Ag° , ceci dans les mêmes conditions que précédemment. Dans ce nouveau mode opératoire, les effets de barrières Schottky sont toujours présents mais, du fait de la taille uniforme des nuclei formés initialement, ils conduisent à une croissance et une agrégation uniformes des NPs tout au long de l'exposition aux UVA. Il a ainsi été possible de former des agrégats homogènes et d'éliminer la majorité des toutes petites particules isolées (figures 5). La quantité et la dimension des agrégats, i.e. leur taux de recouvrement sur la surface TiO_2 , augmente continuellement en augmentant la quantité de nuclei ou encore la durée d'exposition aux UVA mais, dans toutes les conditions testées, les NPs constituant ces agrégats présente une taille constante et uniforme comprise entre 50 et 100 nm. Cette observation a été attribuée à une auto-régulation de la croissance des NPs régie par le phénomène d'agrégation, i.e. la croissance cesse une fois que les NPs entre en contact au sein des agrégats.

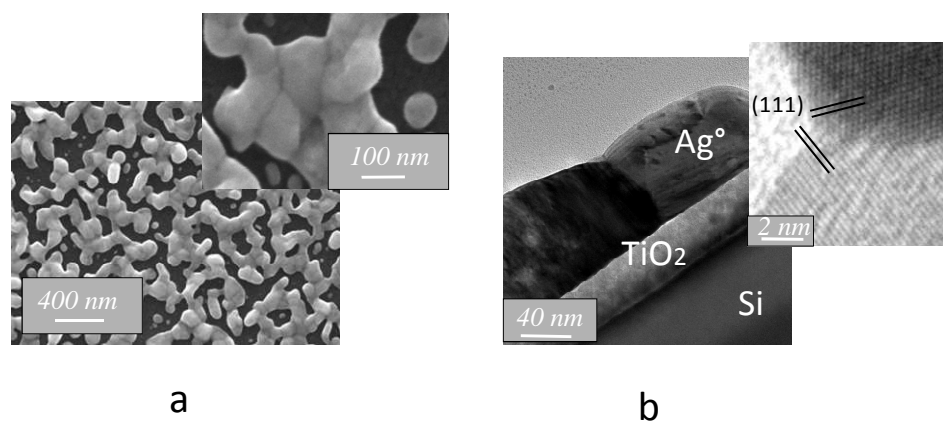


Figure 5. Images MEB (gauche) et MET (droite) à faible grossissement sur la tranche (image principale) et à haute résolution (insert) de NPs Ag° formées par réduction photocatalytique assistée TSC après 60 min d'exposition aux UVA en présence de nuclei Ag° obtenus après trois opérations de dépôt d'AA. L'image MET à haute résolution illustre les plans réticulaires (111) de la structure cristallographique de l'argent métallique

2.2 Premières évaluations SERS

Les optimisations décrites précédemment nous ont permis d'optimiser des hétérostructures Ag^0/TiO_2 se traduisant par une grande quantité d'agrégats homogènes et distribués uniformément à la surface du substrat. Comme nous l'avons déjà mentionné, ce résultat permet d'envisager une intensité SERS importante, via la création d'un très grand nombre de points chauds, et une bonne reproductibilité des spectres SERS mesurés en différents endroits du substrat. Afin de valider les performances SERS de ces hétérostructures, des mesures par spectroscopie Raman ont été réalisées pour détecter la rhodamine 6G (R6G), retenue comme analyte modèle en raison de sa très forte section efficace Raman, et en utilisant l'émission à 514 nm d'un laser argon. Pour ces mesures, les échantillons de dimension $3 \times 3 \text{ cm}^2$ ont été clivés en petits morceaux rectangulaires de dimension $3 \times 4 \text{ mm}^2$, puis un volume de 10 μL de R6G, diluée en concentrations variables (entre 10^{-3} et 10^{-10} M) dans de l'eau ou de l'éthanol, a été étalé sur ces petits morceaux et finalement séché à 60°C . Afin d'évaluer la reproductibilité des spectres, les mesures Raman ont été réalisées en différents endroits de plusieurs zones de $100 \times 100 \mu\text{m}^2$ d'un même substrat ainsi que sur des substrats différents élaborés dans des conditions similaires. Une solution de R6G diluée à 10^{-3} M a tout d'abord été étalée sur des substrats de silicium nu (en l'absence de NPs Ag^0) pour collecter des spectres Raman pur (non SERS) de référence. Les spectres obtenus montrent des bandes Raman de faible intensité avec un très faible rapport signal sur bruit, ce qui illustre la faible sensibilité de la spectroscopie Raman classique (figure 6). Par ailleurs, ces bandes poussent sur une ligne de base fortement pentue qui a été attribuée à la fluorescence de la R6G.

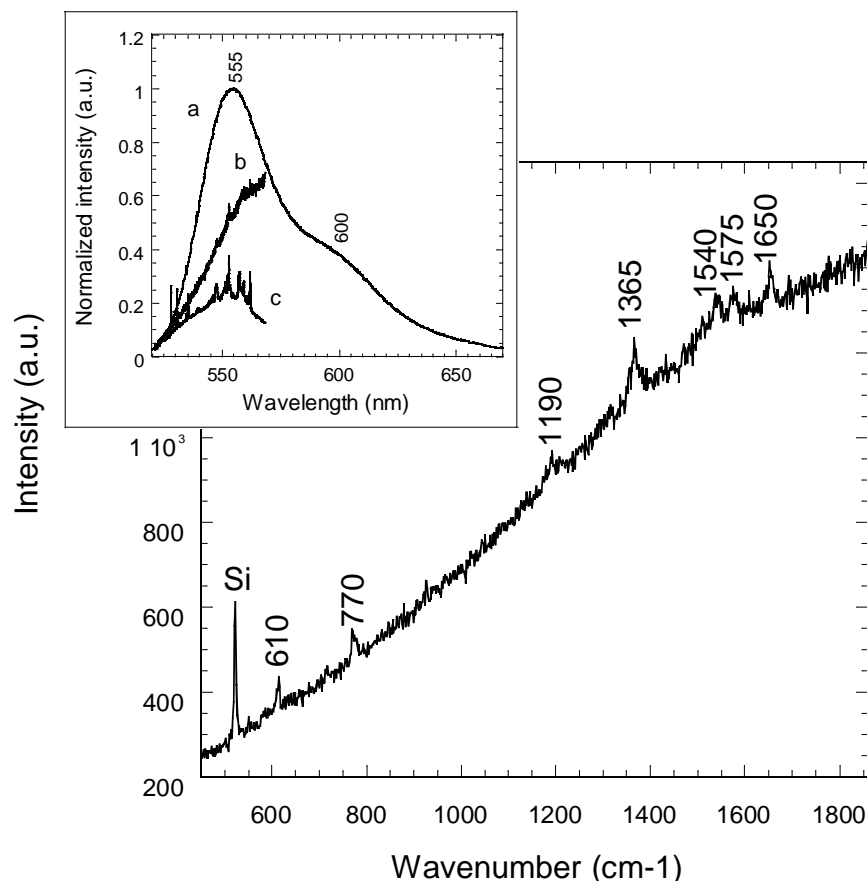


Figure 6. Spectre Raman pur de la R6G (10^{-3} M en solution) étalée sur silicium.

Afin d'évaluer les performances SERS de nos plateformes, nous nous sommes ensuite plus particulièrement intéressés à une hétérostructure $\text{Ag}^\circ / \text{TiO}_2$ modèle. Cette hétérostructure a été élaborée par réduction photocatalytique assistée TSC pendant 60 min d'exposition UVA et en présence de nuclei Ag° . Ces derniers étaient obtenus en déposant l'AA en trois opérations de dépôt. Par rapport aux spectres Raman pur, les spectres collectés sur cette hétérostructures $\text{Ag}^\circ / \text{TiO}_2$ présentent une très forte intensité ainsi qu'un bien meilleurs rapport signal sur bruit et la ligne de base induite par la fluorescence de la R6G apparaît fortement atténuée. La forte intensité des spectres SERS a ainsi permis d'indexer sans ambiguïté toutes les bandes Raman de la R6G. L'intensité de ces bandes décroît logiquement en réduisant la quantité de R6G adsorbée, i.e. la concentration de R6G en solution, mais la détection demeure possible même pour de très faibles concentrations. Il a ainsi été possible de définir un seuil de détection correspondant à des concentrations de l'ordre de 10^{-8} - 10^{-10} M (figure 7).

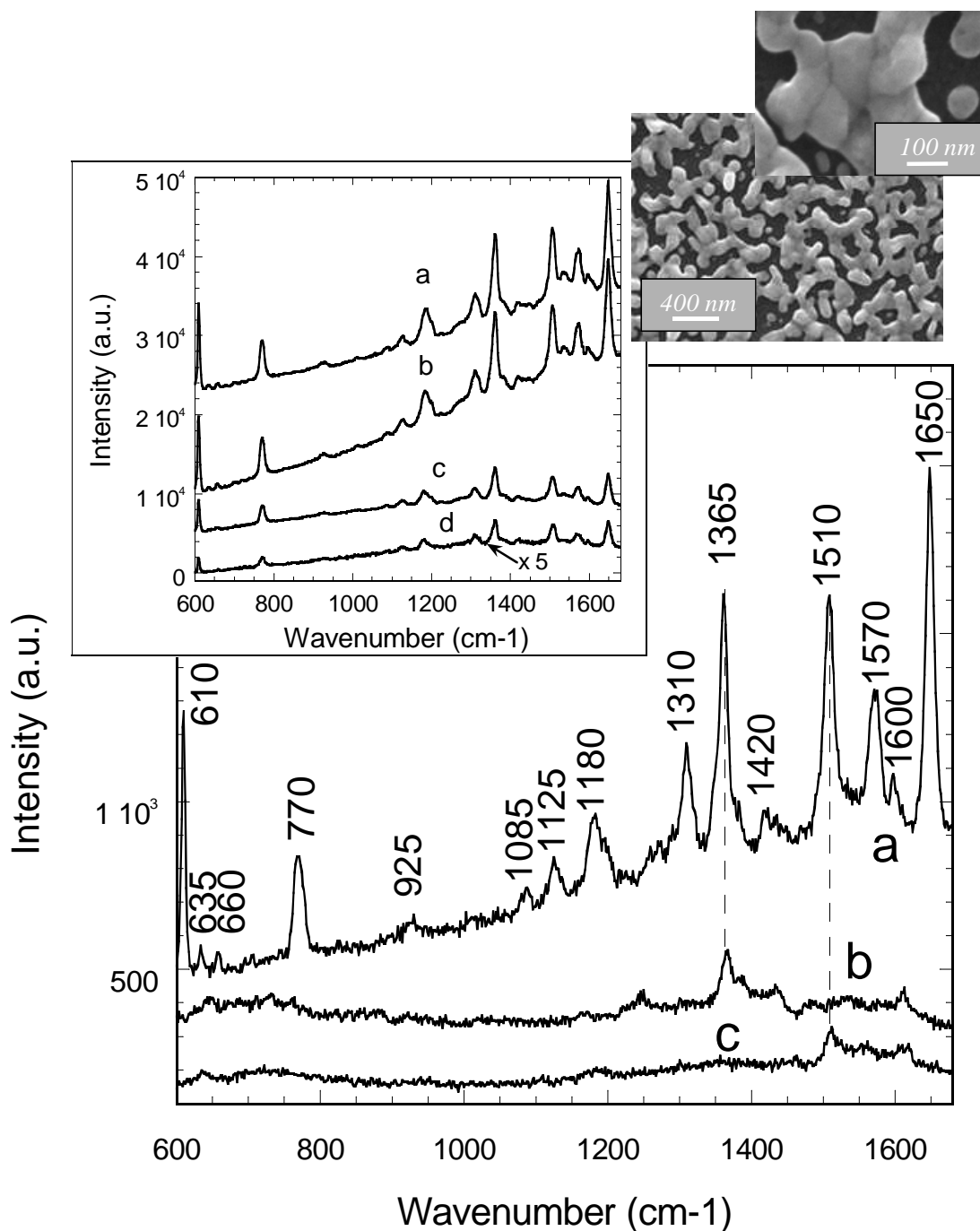


Figure 7. Spectres SERS de la R6G étalée sur l'hétérostructure modèle (60 min UVA en présence de nuclei Ag°) pour des concentrations variables de R6G en solution : (insert) 10^{-4} M (a), 10^{-5} M (b), 10^{-6} M (c), 10^{-7} M (d), et (figure principale) 10^{-8} M (a), 10^{-9} M (b), 10^{-10} M (c).

Une normalisation des spectres SERS, obtenus pour une concentration de 10^{-8} M, avec les spectres Raman pur obtenus pour une concentration de 10^{-3} M, nous a aussi permis de déduire un EF de 10^6 . Des performances bien meilleures ont déjà été mentionnées dans la littérature portant sur des substrats SERS

solides, mais les méthodes d'élaboration proposées sont trop onéreuses et / ou complexes pour adresser des applications pratique. A l'inverse, les performances de notre plateforme SERS apparaissent à l'état de l'art si on considère les résultats publiés dans la littérature concernant des méthodes simples et à moindre coût.

Le grand intérêt de notre approche repose également sur la reproductibilité des spectres SERS. Il est à noter que les aspects reproductibilité sont assez peu évoqués dans la littérature traitant de substrats SERS solides, et lorsqu'ils sont abordés, la reproductibilité des spectres n'est évaluée que sur des zones de petites dimensions (de 10×10 à $100 \times 100 \mu\text{m}^2$). A titre de comparaison, nous nous sommes tout d'abord intéressés à une hétérostructure élaborée dans les mêmes conditions que notre hétérostructure modèle mais en l'absence de nuclei Ag° . Dans ce premier cas, l'intensité des bandes Raman fluctue sur environ un ordre de grandeur lorsque les spectres sont collectés en différents endroit d'une même zone de $100 \times 100 \mu\text{m}^2$ (figure 8). Comme indiqué précédemment, les agrégats de NPs obtenus en l'absence de nuclei Ag° ne sont pas uniformes et les points chauds en résultant sont donc répartis de façon hétérogène sur la surface du substrat, ce qui explique la mauvaise reproductibilité des spectres SERS.

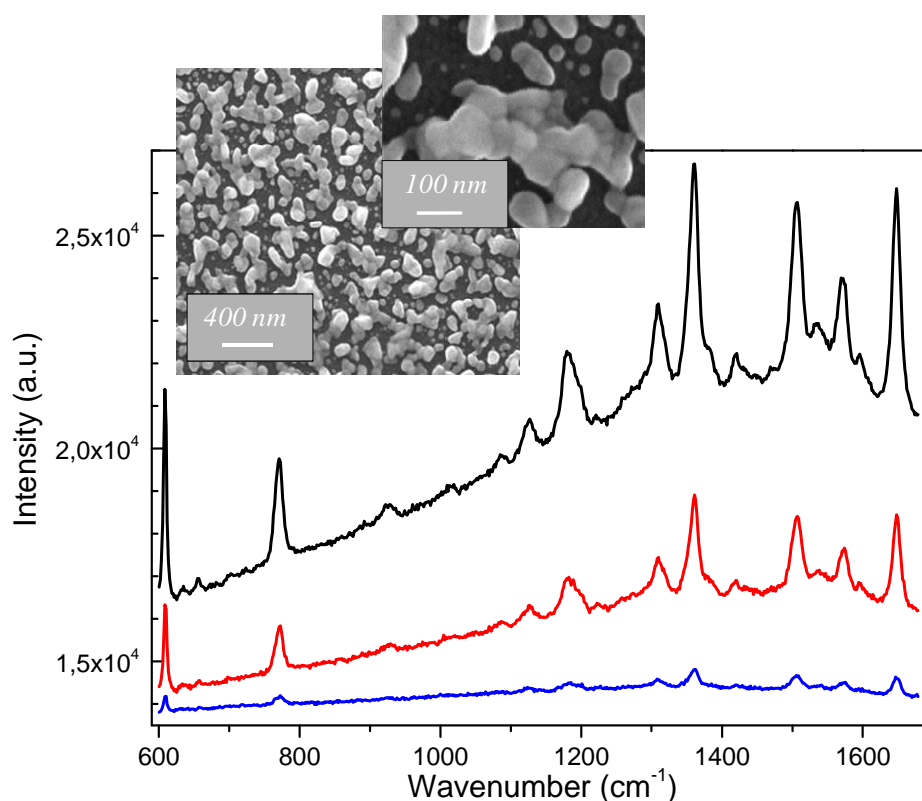


Figure 8. Spectres SERS mesurés sur une hétérostructure élaborée sans nuclei Ag° (60 min UVA) en différents endroits d'une zone de $100 \times 100 \mu\text{m}^2$.

A l'inverse, la reproductibilité des spectres mesurés sur notre hétérostructure modèle est particulièrement probante. Les spectres mesurés en différents endroits d'une même zone de $100 \times 100 \mu\text{m}^2$ se traduisent par une déviation standard relative (DSR) en intensité de l'ordre de 10% (figure 9). Ce résultat est à la hauteur des meilleures performances reportées dans la littérature pour la détection SERS de la R6G sur des zones de petites tailles. Qui plus est, la DSR en intensité demeure similairement faible (environ 12%) lorsque les spectres sont mesurés en différents endroits d'un même substrat de $3 \times 4 \text{ mm}^2$ (figure 10). A notre connaissance, aucune publication ne reporte de telles performances sur des substrats SERS d'aussi grande taille.

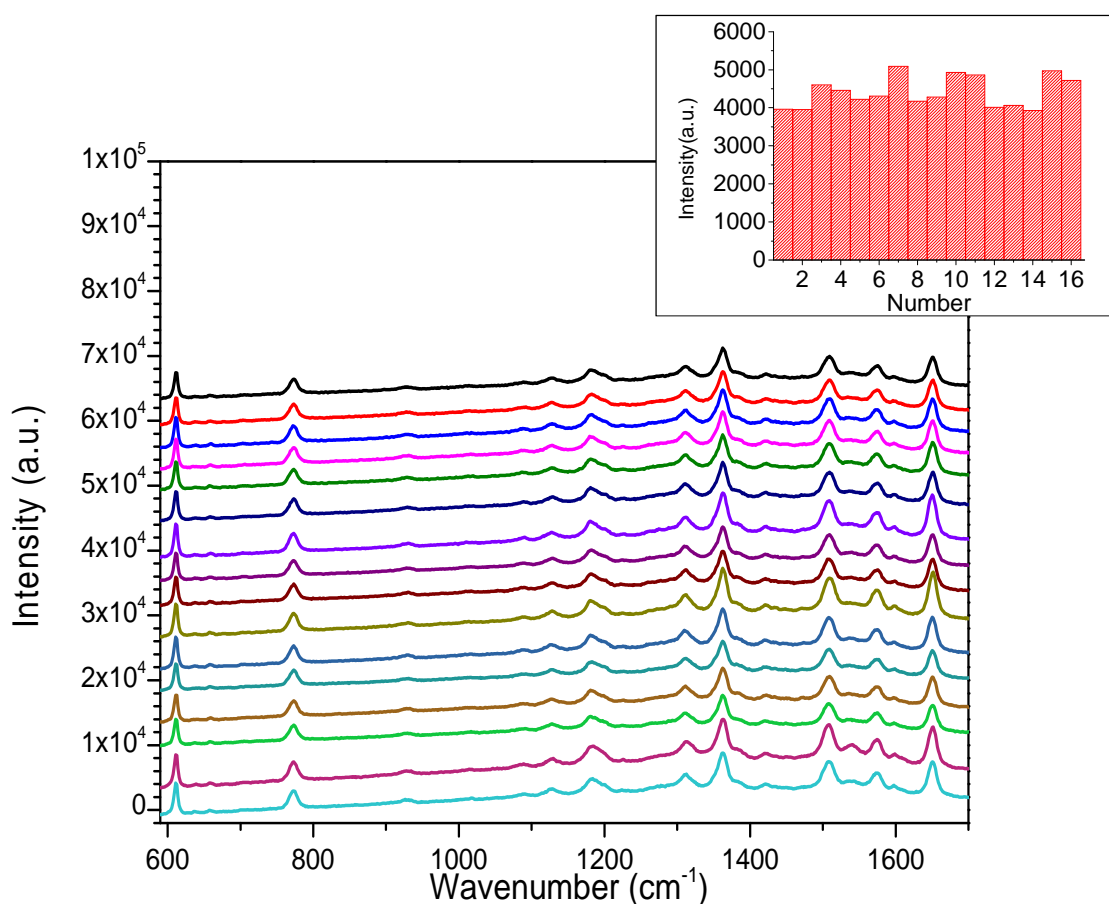


Figure 9. Spectres SERS mesurés sur l'hétérostructure modèle (60 min UVA en présence de nuclei Ag°) en différents endroits d'une zone de $100 \times 100 \mu\text{m}^2$ et histogramme associé de l'intensité de la bande à 610 cm^{-1} .

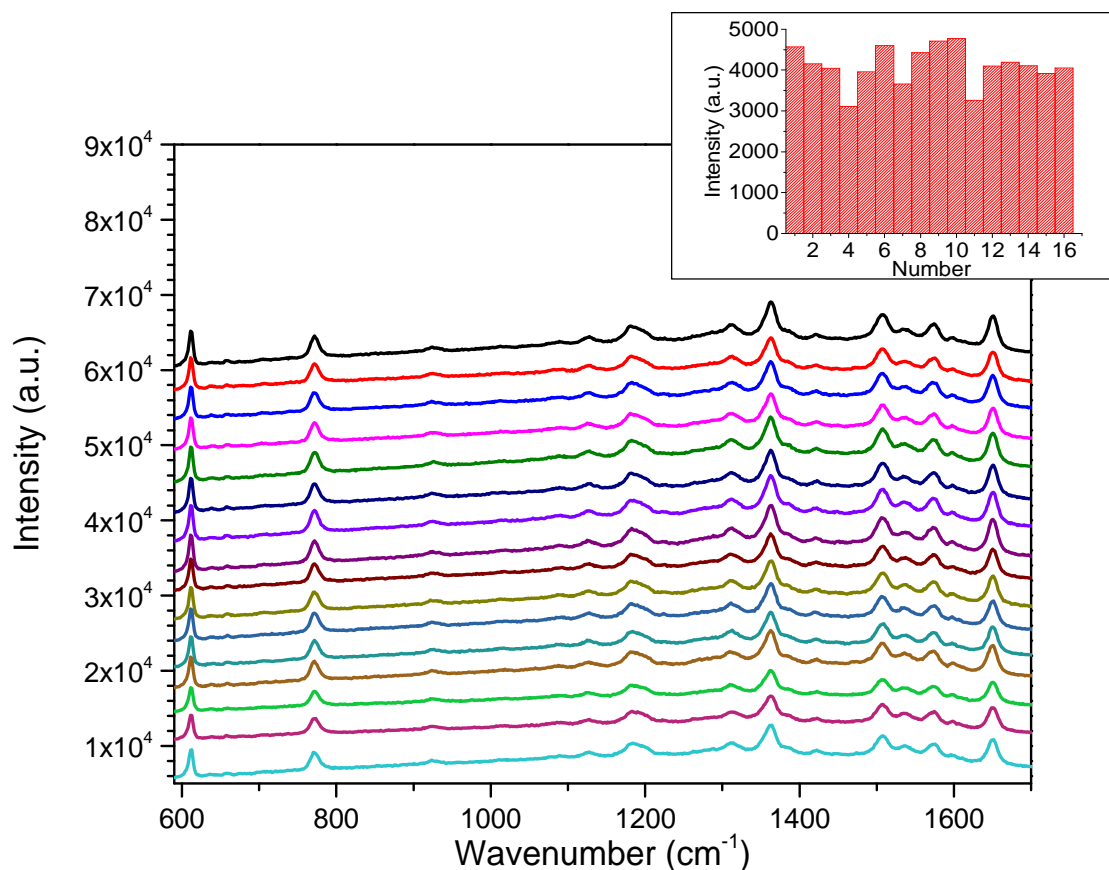


Figure 10. Spectres SERS mesurés sur l'hétérostructure modèle (60 min UVA en présence de nuclei Ag⁰) en différents endroits d'un échantillon de 3 x 4 mm² et histogramme associé de l'intensité de la bande à 610 cm⁻¹.

Nous avons également évalué la reproductibilité des spectres sur différents échantillons élaborés dans des conditions similaires. Les mesures Raman montrent que 80% des spectres présentent une DSR en intensité d'environ 20% tandis que les autres spectres divergent de cette tendance mais en présentant systématiquement une intensité environ deux fois plus forte. Ces données indiquent évidemment une plus grande dispersion en intensité par rapport à des mesures réalisées sur un même substrat. Mais il faut noter que cette plus grande dispersion tient compte non seulement de la reproductibilité entre échantillons mais aussi de la reproductibilité sur la surface totale des échantillons élaborés (3 x 3 cm²). En ce sens, les évaluations demeurent donc extrêmement probantes en termes de reproductibilité. Finalement, nous avons aussi testé des échantillons après un mois de vieillissement dans le noir. Les variations d'intensité causées par ce vieillissement se cantonnent à la gamme des fluctuations mentionnées précédemment lorsqu'on compare différents échantillons élaborés dans des conditions identiques, ce qui indique un effet négligeable du vieillissement. Toutes ces observations démontrent la fiabilité et la robustesse de notre plateforme SERS et l'intérêt de mettre en œuvre un protocole de nucléation-croissance pour optimiser la procédure de réduction photocatalytique assistée TSC en vue de

produire des points chauds uniformément distribués à la surface de l'hétérostructure $\text{Ag}^0 / \text{TiO}_2$ et conduisant à des spectres SERS intenses et reproductibles.

3. Détection SERS d'homonucléotides simple brin

3.1 Choix des molécules et protocole d'immobilisation

Les études se sont ensuite poursuivies en utilisant exclusivement l'hétérostructure modèle définie dans ce qui précède. Les performances de la plateforme SERS en découlant nous ont encouragés à nous pencher sur des biomolécules d'intérêt applicatif, i.e. des molécules d'ADN. L'intérêt d'étudier de telles molécules dans le domaine du diagnostic médical porte à terme sur la possibilité de détecter des molécules d'ADN multibases et leur hybridation. Toutefois, avant de s'engager dans de tels objectifs complexes, il est impératif de maîtriser parfaitement des approches plus simples. C'est la raison pour laquelle une grosse partie du travail de thèse a porté sur la détection SERS d'homo-oligonucléotides simple brin (sans hybridation), encore appelés polybases pour des raisons de simplicité. Ces polybases découlent de la polymérisation de nucléotides identiques dérivés des quatre nucléobases qui constituent la structure de l'ADN multibases : adénine (A), cytosine (C), guanine (G) et thymine (T). Les homonucléotides ainsi obtenus seront labélisés polyA, polyC, polyG et polyT. Nos études ont porté sur la détection SERS des quatre types de polybases, fonctionnalisées ou non avec un groupement externe aminé NH_2 (respectivement labélisées polyX- NH_2 ou polyX, où X = A, C, G ou T). Après l'étape de réduction photocatalytique, les molécules d'ADN ont été immobilisées sur des substrats clivés en morceaux de $7 \times 7 \text{ mm}^2$, et leur détection SERS a été effectuée sur différentes zones de $100 \times 100 \mu\text{m}^2$ en utilisant l'émission à 632,8 nm d'un laser hélium-néon.

Avant d'entamer des travaux de fond sur les polybases, il a été nécessaire de mener des études préliminaires concernant leur mode d'immobilisation sur la plateforme SERS. Ces études ont permis d'optimiser le pH de la solution (4,5) et la nature du milieu de dilution (solution aqueuse de NaH_2PO_4 ; C = 0.3 M). Par ailleurs, outre les performances SERS de notre plateforme, celle-ci présente également d'autres atouts qui nous ont permis de mettre au point un protocole d'immobilisation simplifié ne nécessitant pas une procédure multi-étapes complexe traditionnellement utilisée pour greffer des molécules d'ADN sur un substrat de silicium.

Cette procédure simplifiée repose sur :

- La superhydrophilie photo-induite du dioxyde de titane qui conduit à un étalement parfait (un angle de mouillage proche de 0°) d'une solution aqueuse sur une surface TiO_2 après exposition aux UVA. Dans nos conditions, cette propriété était générée lors de la procédure de réduction photocatalytique,

dans les zones TiO₂ non-recouvertes d'agrégats Ag⁰. Elle a permis l'étalement uniforme des solutions aqueuses et l'immobilisation uniforme des polybases sur les hétérostructures Ag⁰ / TiO₂.

- Le greffage direct des molécules d'ADN sur les NPs Ag⁰ via la création de liaisons Ag-N qui seront discutées plus loin. Après étalement de la goutte liquide, ce greffage a été réalisé en incubant la goutte pendant douze heures à température ambiante, puis en rinçant les échantillons et en les séchant ensuite pendant une heure à température ambiante.

3.2 Etudes expérimentales

Des mesures par XPS ont tout d'abord montré que les molécules d'ADN se greffent préférentiellement sur les agrégats Ag⁰ de notre hétérostructure et non pas dans les zones TiO₂ nues, ce qui renforce l'hypothèse d'un greffage par liaisons Ag-N. Des premières mesures par spectroscopie Raman réalisées sur cette hétérostructure ont par ailleurs montré que, quelle que soit la nature des polybases, fonctionnalisées ou non avec des groupements NH₂, l'intensité des bandes Raman présente systématiquement un très net optimum pour des concentrations de polybase en solution comprises entre 5 et 10 μM. Par la suite, l'essentiel des études a donc été réalisé en utilisant cette gamme de concentration. Pour toutes les polybases, modifiées ou non avec des groupements NH₂, les spectres ainsi obtenus sont composés de bandes Raman intenses et bien résolues avec un très bon rapport signal sur bruit, y compris dans le cas des polyC et polyT qui présentent pourtant une très faible section efficace Raman (figure 11). La qualité des spectres nous a ainsi permis d'indexer la quasi-intégralité des bandes Raman caractéristiques des polybases étudiées (tableau 1).

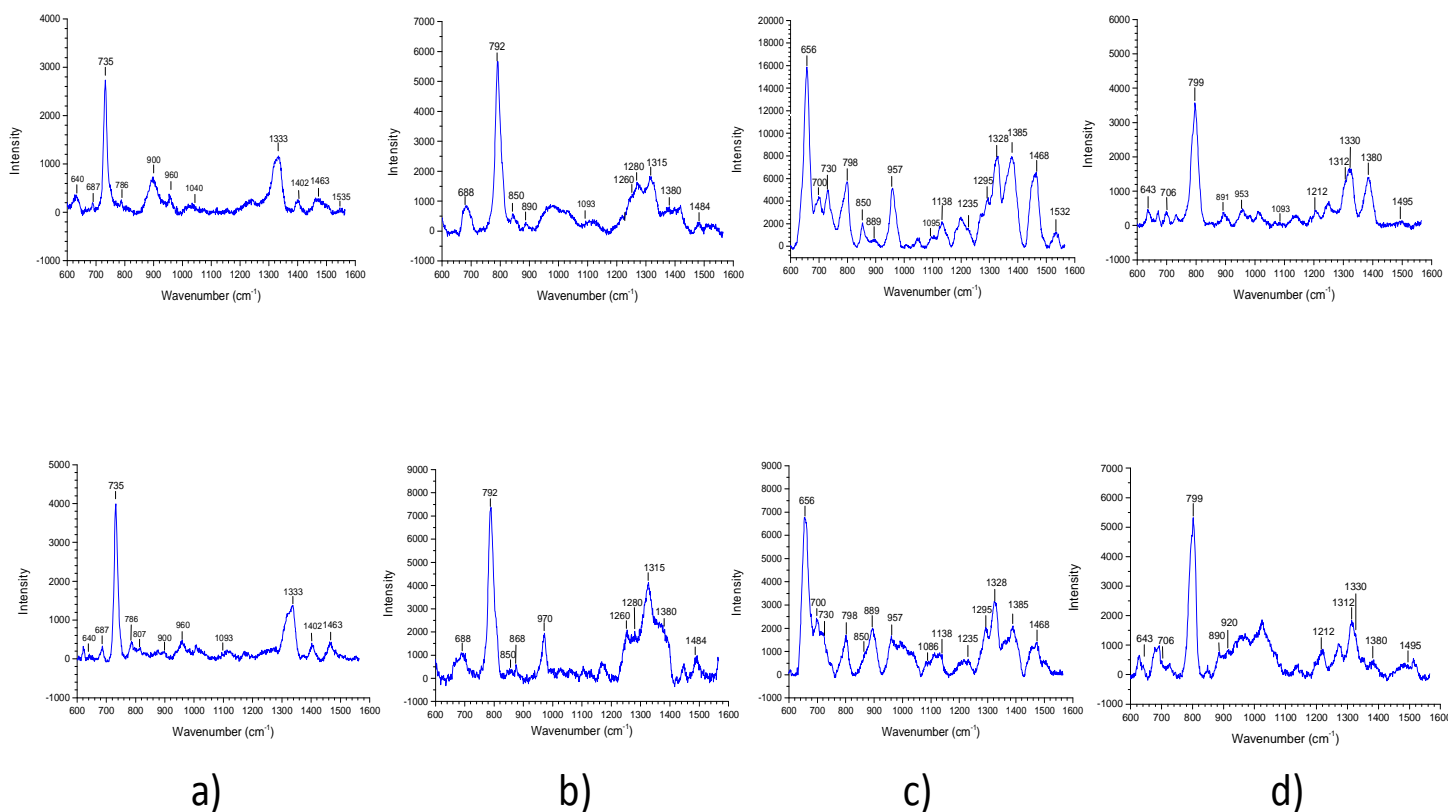


Figure 11. Spectres SERS mesurés sur l'hétérostructure modèle pour polyA (a), polyC (b), polyG (c) et polyT (d) modifiées (haut) ou non (bas) avec des groupements NH₂.

Band position (cm ⁻¹)	Tentative assignments				Ref.
	PolyA	PolyC	PolyG	PolyT	
656			In, breath R6		[6-8]
687	Out, def R5, R6 (tors C4-C5-C6, w N3-C4-N9)				[9-11]
688		Out, bend C5-C4, N3-C4			[6]
700			In, bend (ring)		[9, 12]
706				In, ring breath	[13]
730			Out, def R6 (w N1-C2-N3), tors NH ₂		[7]
735	In, ring breath				[9-11, 14]
786	Out, def R6 (w C4-C5-C6, w C8-H)				[9-11, 14]
792		In, ring breath			[6, 15-17]
798			Mentioned but not indexed in ref.		[6]
799				In, ring breath	[6, 13, 18]
850			In, def R6-R5		[8, 9, 12]
889			In, NH bend		[8]
957			In, def R5 (sqz N7-C8-N9)		[6, 7]
1138			In, bend C8-H, str C4-N9, rock NH ₂		
1212				In, str C5-C6, bend CH ₃ , str N3-C4, C6-N1	[7, 13, 18]
1235			In, pyrimidic character		[8, 9, 12]
1260		In, str C4-N3			[17]
1280		In, str C2-N3			[16, 17]
1295			In, str N7-C8, C2-N3, bend N1-H		[7]
1312				In, bend N3-H, C6-H	[7, 13]
1315		In, str N1-C6+ C5-C6			[6, 15]
1328			In, bend C8-H, str C5-N7-C8		[6]
1333	In, ring skeleton vibration: str C5-N7, N1-C2, bend C2-H, C8-H				[6, 9-11, 14]
1380		In, bend C=C-H			[6, 15, 17]
1380				In, bend C5-Me	[6, 13, 18]
1385			In, str C2-N3, C6-N1, C5-C6, C4-N9, C5-N7		[6, 8]
1402	In, bend C2-H, str C8-N7, N1-C2				[9, 10]
1463	In, str C2-N3, N1-C6, bend C2-H, sciss NH ₂				[9-11]
1463				In, sciss CH ₃ , bend C6-H	[13, 18]
1468			In, str N7=C8 & C8-N9		[8, 9, 12]
1472		In, str C4-N3 + C2-N3			[15, 17]
1484		In, str N1-C6 + str N3-C4			[6]
1495				bend C6-H, N-H	[7, 13, 18]
1532			In, str C=C, str N3-C4		[8, 9]
1535	In, str N3-C4, N1-C6, C5-N7, N7-C8, sciss NH ₂				[9, 12]

Tableau 1. Indexation des bandes Raman mesurées sur l'hétérostructure modèle pour les quatre polybases étudiées.

Cette indexation est particulièrement à souligner car l'essentiel des travaux publiés portant sur la détection SERS de molécules d'ADN concernent l'adénine ou ses molécules dérivées et, à notre connaissance, aucune étude antérieure n'avait encore porté sur la détection SERS et l'indexation des bandes Raman des quatre polybases sur un même type de substrat. Ce constat ne fait que renforcer nos conclusions sur la robustesse de notre plateforme SERS. Cette indexation a en particulier permis de montrer que, pour les quatre bases étudiées, les spectres Raman sont dominés par des bandes de vibration « in plane ». Une exception notable à cette tendance est toutefois à souligner. En effet, lorsque la concentration des polybases en solution excède largement la gamme optimale de concentration, i.e. dans nos conditions, pour des concentrations supérieures à 50 μM , l'intensité relative des bandes de vibration « out of plane » augmente sensiblement. Il est important de noter que ce phénomène a systématiquement été reproduit, que les polybases soient modifiées ou non avec des groupements NH_2 . Par ailleurs, à concentration égale et même nature de polybase, les principales bandes Raman présentent des intensités moyennes dont l'ordre de grandeur est comparable que les polybases soient modifiées ou non avec les groupements NH_2 . Toutes ces observations amènent à la conclusion que ces groupements ne jouent pas un rôle essentiel sur le greffage des molécules d'ADN.

Nos études ont également montré que la concentration de polybase en solution joue un rôle essentiel dans la reproductibilité des spectres. En effet, de part et d'autre de la gamme de concentration optimale définie précédemment (5-10 μM), l'intensité des bandes Raman fluctue sur environ un ordre de grandeur lorsque les spectres sont collectés en différents endroits d'une même zone de 100 x 100 μm^2 . A l'inverse, pour une concentration comprise entre 5 et 10 μM , la reproductibilité des spectres apparaît très probante (figure 12).

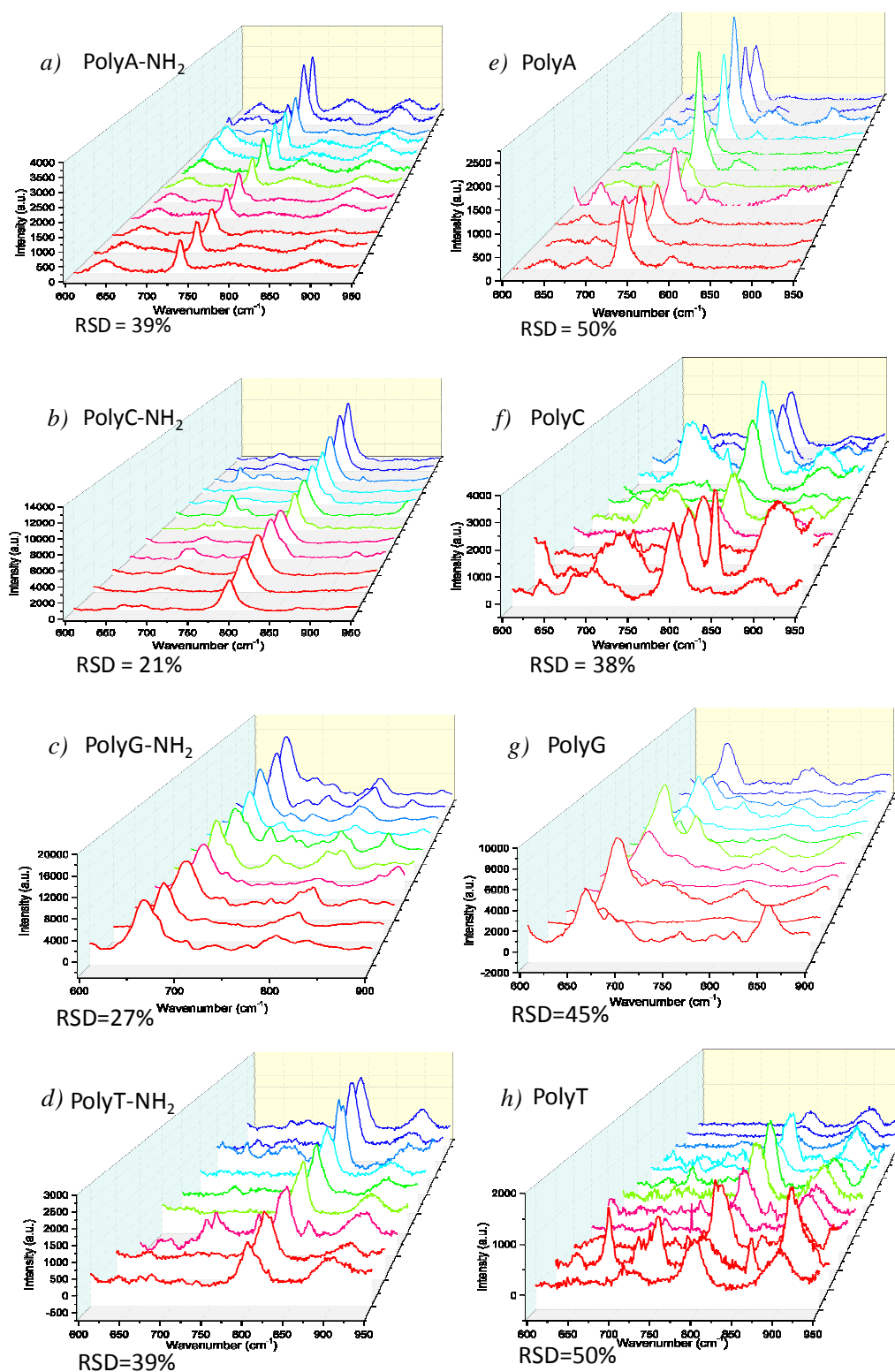


Figure 12. Spectres SERS mesurés sur l'hétérostructure modèle en six endroits différents de deux zones de $100 \times 100 \mu\text{m}^2$ d'un même échantillon de $7 \times 7 \text{mm}^2$ pour polyA-NH₂ (a), polyC-NH₂ (b), polyG-NH₂ (c), polyT-NH₂ (d) et polyA (e), polyC (f), polyG (g), polyT (h). La concentration de polybase en solution a été fixée à $5 \mu\text{M}$.

Afin de quantifier cette reproductibilité, nous avons mesuré pour chaque polybase la DSR en intensité de la principale bande de vibration « in plane » détectée en six endroits de deux zones distinctes de $100 \times 100 \mu\text{m}^2$ d'un même échantillon de $7 \times 7 \text{mm}^2$. En présence de groupements NH_2 externes, la DSR en intensité déduite des douze spectres de chaque base est respectivement de 39%, 21%, 27% et 39% pour polyA- NH_2 , polyC- NH_2 , polyG- NH_2 et polyT- NH_2 . Ces valeurs de DSR sont évidemment plus élevées que celles mesurées dans le cas de la R6G, mais elles révèlent tout de même une bonne reproductibilité des spectres, quelles que soient les polybases étudiées. A notre connaissance, une telle reproductibilité n'a jamais été reportée dans la littérature SERS pour les quatre bases détectées sur un même type de substrat. Toutefois, cette reproductibilité apparaît moins bonne lorsque les polybases ne sont pas modifiées avec des groupements NH_2 . La DSR en intensité déduite des douze spectres collectés pour chaque base est ainsi respectivement de 50%, 38%, 45% et 50% pour polyA, polyC, polyG et polyT. Ces mesures indiquent donc que, à nature de base identique, la DSR est systématiquement plus faibles en présence de groupements externes NH_2 (figure 13). Ce constat implique à son tour que, si ces groupements ne jouent pas un rôle essentiel sur le greffage des molécules d'ADN, ils semblent très favorablement influencer la reproductibilité des spectres.

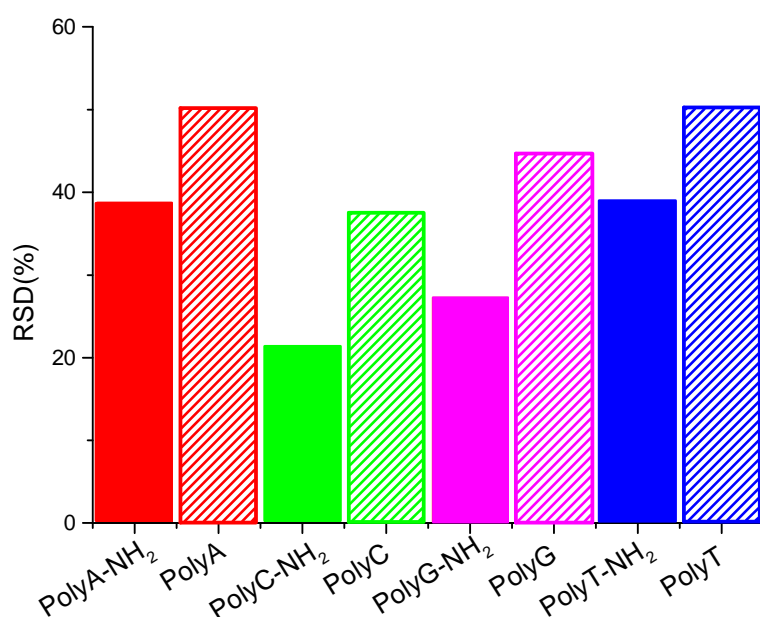


Figure 13. DSR en intensité de la principale bande de vibration « in plane » des quatre polybases étudiées, modifiées ou non avec des groupements NH_2 , déduite de spectres SERS mesurés sur l'hétérostructure modèle en six endroits différents de deux zones de $100 \times 100 \mu\text{m}^2$ d'un même échantillon de $7 \times 7 \text{mm}^2$.

3.3 Discussion : effets d'accrochage, d'orientation et d'agencement

Les résultats obtenus au cours de cette étude peuvent être discutés en termes d'accrochage, d'orientation et d'agencement des molécules d'ADN à la surface de l'hétérostructure $\text{Ag}^\circ / \text{TiO}_2$. Ces différents aspects sont en effet susceptibles d'influencer fortement les spectres SERS. Les analyses par XPS ont confirmé que le greffage des polybases sur l'hétérostructure implique un accrochage préférentiel sur les NPs Ag° via la formation de liaisons Ag-N. Toutefois, les spectres SERS nous amènent à la conclusion que les groupements externes NH_2 ne jouent pas un rôle essentiel dans ce processus. On peut donc en conclure que cet accrochage implique les groupements NH_2 structuraux des molécules d'ADN, ou encore des atomes d'azote internes constituant les liaisons NH et CN. L'implication au moins partielle de ces atomes internes est renforcée par le cas particulier de polyT. En effet, cette polybase ne présente pas de groupements NH_2 structuraux, or la forte intensité des bandes Raman observées dans le cas de cette polybase sans groupements NH_2 externes démontre que son greffage est tout aussi efficace que celui des autres polybases. Par ailleurs, pour des concentrations de polybase en solution suffisamment faibles (dans les conditions étudiées, $C \ll 50 \mu\text{M}$), les spectres SERS sont dominés par les modes de vibration « in plane ». Dans ces conditions, les lois de sélection SERS découlant de la théorie du champ électromagnétique permettent de conclure que le plan des nucléobases constituant les polybases est globalement orienté perpendiculairement à la surface des NPs Ag° . Ces plans étant eux-mêmes perpendiculaires à l'axe de la chaîne homo-oligonucléotide, la prédominance des modes de vibration « in plane » indique donc que les polybases sont probablement orientées horizontalement sur la surface de l'hétérostructure $\text{Ag}^\circ / \text{TiO}_2$.

Les spectres SERS indiquent également que la concentration de polybase en solution joue un rôle prédominant sur l'intensité des bandes Raman et leur reproductibilité, ainsi que sur l'apparition de modes de vibration « out of plane ». Cette influence de la concentration peut être discutée en termes de densité et d'orientation des polybases à la surface de l'hétérostructure $\text{Ag}^\circ / \text{TiO}_2$ (figure 14). Pour de faibles concentrations, l'intensité des bandes est faible et très irréproducible, ce qui peut être attribué à une trop faible densité de surface des polybases greffées sur l'hétérostructure. Dans une gamme de concentration intermédiaire (5-10 μM), les spectres présentent au contraire une bonne reproductibilité et des bandes Raman intenses, ce qui est attribuable à une couverture optimale de l'hétérostructure par les polybases. Celles-ci peuvent alors être décrites comme formant une monocouche 2D à la surface de l'hétérostructure. Rappelons que, pour toutes ces concentrations, les polybases sont supposées être orientées parallèlement à la surface du substrat. Enfin, pour de fortes concentrations, l'intensité des bandes redevient faible et très irréproducible et on observe également une augmentation de l'intensité relative des modes de vibration « out of plane ». Dans cette gamme de concentration, alors que la

quantité de matière déposée est supposée plus importante qu'à plus faible concentration, des mesures par XPS ont montré une plus faible couverture de l'hétérostructure par les polybases. Cette observation peut expliquer que, la quantité de polybases en contact avec les NPs Ag° et donc susceptibles d'être détectées par effet SERS étant plus faible, l'intensité des bandes Raman diminue. Ces analyses XPS suggèrent également que, lorsque la quantité de polybases déposées en solution liquide devient excessive, ces dernières tendent à s'agréger en agglomérats 3D distribués de façon hétérogène à la surface du substrat, ceci possiblement au cours de l'étape de rinçage/séchage terminant la procédure de greffage. La distribution hétérogène de ces agrégats expliquerait alors la mauvaise reproductibilité des spectres SERS. Il est enfin possible que, pour des raisons d'encombrement stérique, les polybases constituant les agrégats ne soient pas orientées parallèlement à la surface du substrat mais présentent au contraire des orientations aléatoires, ce qui expliquerait alors l'apparition des modes de vibration « out of plane ».

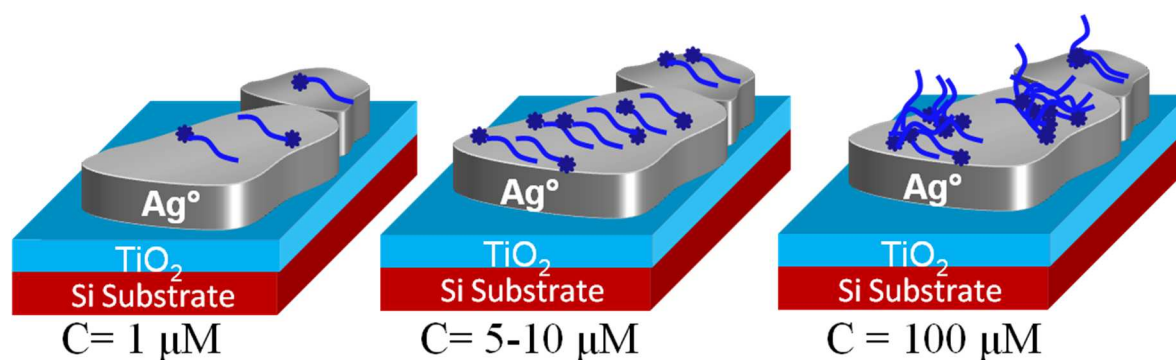


Figure 14. Représentation schématisée du modèle proposé pour la distribution et l'orientation des polybases à la surface de l'hétérostructure $\text{Ag}^\circ / \text{TiO}_2$ pour une faible ($1\mu\text{M}$), moyenne ($5 - 10\mu\text{M}$) et forte ($100\mu\text{M}$) concentration de polybase en solution.

Enfin, nous avons montré que, dans la gamme de concentration optimale, tandis que les groupements NH_2 externes n'influencent pas significativement l'intensité moyenne des bandes Raman, ils jouent un rôle favorable dans la reproductibilité des spectres. Pour des concentrations suffisamment faibles de polybase en solution, nous avons vu que les polybases sont orientées parallèlement à la surface du substrat, qu'elles soient modifiées ou non avec des groupements NH_2 . Toutefois, en raison de la flexibilité de la chaîne polybase liée à sa structure torsadée, les nucléobases la constituant ne sont pas nécessairement ancrées uniformément sur la surface des NPs Ag° . Ceci peut expliquer que, même si les nucléobases conservent une orientation perpendiculaire au substrat favorisant la prépondérance des modes de vibration « in plane », elles ne sont pas détectées de façon reproductible. Toutefois, les groupements NH_2 externes sont peut-être capables d'offrir des points d'ancrage sur la surface du substrat, lesquels permettraient le greffage de chaînes polybases plus rigides et linéaire dont la détection

serait ainsi plus reproductible. Ce phénomène de linéarisation a déjà été reporté dans la littérature en mettant à profit un traitement thermique post-greffage adéquat.

L'ensemble de cette discussion ne vise évidemment pas à expliquer tous les phénomènes observés au cours de notre étude, mais elle ouvre des pistes de compréhension qui devront par la suite être validées par de nouvelles expérimentations.

4. Détection SERS de paires de polybases : effets de l'hybridation versus mélange

Suite aux résultats probants concernant la détection SERS d'homonucléotides sur notre hétérostructure $\text{Ag}^\circ / \text{TiO}_2$, la toute fin de thèse a été consacrée à quelques études complémentaires visant à renforcer le potentiel de notre plateforme SERS dans le domaine de la détection de molécules d'ADN. Pour ces études, le protocole d'immobilisation était le même que celui décrit précédemment et la détection SERS a de nouveau été effectuée en utilisant l'émission à 632,8 nm d'un laser hélium-néon. Ces études se sont orientées sur l'hybridation des polybases et l'association de différentes polybases sur un même substrat SERS.

4.1 Choix des molécules et protocole d'immobilisation

La mise en évidence des caractéristiques organisationnelles des doubles brins sur la surface d'argent nécessite de mettre en évidence quelles sont leurs caractéristiques spécifiques dans les spectres SERS. Dans cette perspective et selon une méthodologie étape par étape, nous avons choisi d'étudier les spectres de SERS de deux paires de polybases complémentaires, typiquement:

- hybridation polyA-NH₂ avec polyT (quantité équimolaire)
- hybridation polyG-NH₂ avec polyC (quantité équimolaire)

Pour confirmer ces résultats, les spectres SERS obtenus sont systématiquement comparés avec les spectres SERS obtenus après immobilisation directe de mélanges contenant des polybases complémentaires, typiquement:

- Mélange polyA-NH₂ avec polyT (quantité équimolaire);
- Mélange polyG-NH₂ avec polyC (quantité équimolaire).

Les polybases n'étant pas hybridées dans les mélanges, les spectres SERS correspondant servent de témoins négatifs ici, ce qui permettra d'étudier sans ambiguïté la signature SERS des polybases hybridées en confrontant les différentes caractéristiques spectroscopiques entre les deux types de spectres SERS : hybridation versus mélange.

Au meilleur de notre connaissance, une telle étude n'a pas été rapportée jusqu'à présent dans la littérature.

Le protocole d'immobilisation des polybases hybridées a été mis au point. Il fait intervenir un temps d'incubation dans un tampon d'hybridation (PBS, NaCl, EDTA) à 42° durant une nuit dans un milieu à 80% d'humidité. Dans de telles conditions, les nanoparticules d'argent sont préservées et l'acquisition des spectres SERS avec un bon signal/bruit est optimisée.

4.2 Résultats

4.2.1 Cas de polyA-NH₂ et polyT : mélange (polyA-NH₂ + polyT) versus hybridation (polyA-NH₂ • polyT)

L'étude approfondie des spectres SERS dans les deux cas a été effectuée, d'abord à concentration fixe, puis, en fonction de la concentration. Les principaux et importants résultats sont les suivants.

Dans le cas du mélange poly-NH₂ + polyT, il n'y a pas de signature de polyT dans les spectres (Figure 15). On observe ainsi que le comportement de ce mélange est pratiquement similaire à celui de polyA-NH₂ seul. Par ailleurs, cette observation sur ce comportement est confirmée par la tendance de l'intensité du signal SERS qui est identique à celle observée dans le cas du polyA-NH₂ seul en fonction de la concentration, montrant un maximum d'intensité dans une plage de concentration 5 -10 uM. Ainsi, quelle que soit la concentration, nous en avons déduit qu'un mécanisme d'adsorption compétitive se produit entre polyA-NH₂ et polyT. Il en résulte une adsorption préférentielle de polyA-Ag⁰ NH₂ sur la surface.

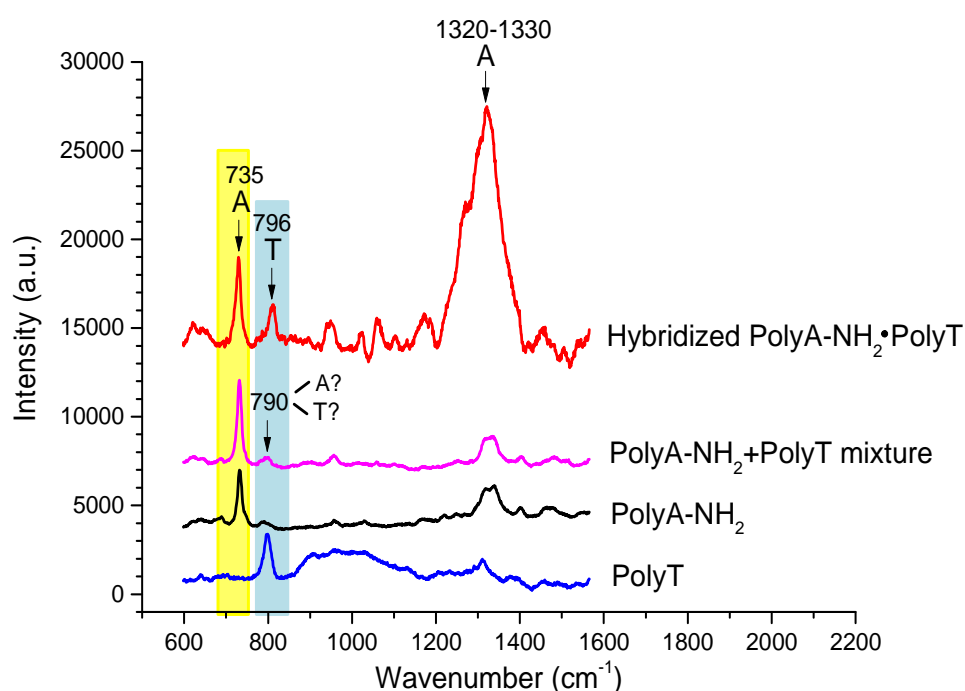


Figure 15: spectres de SERS de polyA-NH₂, polyT, du mélange équimolaire polyA-NH₂ + polyT et de l'hybridé poly-NH₂ • polyT. C_{polyA-NH₂} = C_{polyT} = 5 μ m.

- Dans le cas des molécules hybridées poly-NH₂ • polyT, à l'inverse du mélange, nous avons observé clairement la signature de la bande de polyT. Cela indique que polyT est bien lié à polyA-NH₂ grâce aux deux liaisons hydrogène spécifiques et qu'il s'agit là d'une preuve de la signature des molécules hybridées. En outre, de manière remarquable, l'intensité de la bande de l'adénine à 1330 cm⁻¹ (stretching mode) est considérablement renforcée, révélant un rapport d'intensité 1330 cm⁻¹ / 735 cm⁻¹, qui est inversé par rapport au cas de mélange poly-NH₂ + polyT. Ce résultat, complété par la présence de bandes out of plane de très faible intensité, indique que les bases sont toujours orientées perpendiculairement à la surface Ag, comme dans le cas des polybases seules, mais que les atomes d'azote liés à l'argent ne sont plus les mêmes, notamment le N7 est davantage lié à l'argent, alors que les autres atomes d'N sont engagés dans les liaisons hydrogène. Enfin, il en résulte aussi que les molécules hybridées poly-A-NH₂ • polyT sont pour la plupart couchées à plat sur la surface d'argent, comme nous l'avons schématisé en Figure 16.

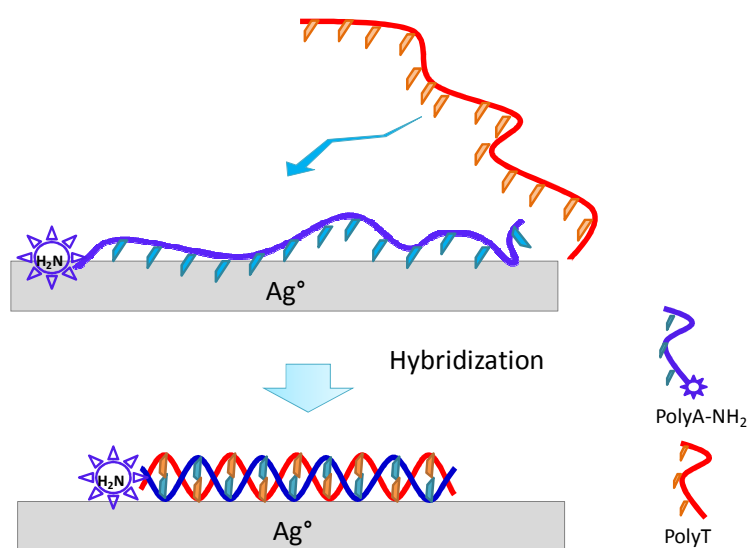


Figure 16: Formation de la molécule hybridée poly-NH₂ • polyT sur la surface Ag °. De même que polyA-NH₂ est immobilisé à plat sur la surface Ag °, la double hélice obtenue après hybridation in situ est également couchée à plat sur la surface Ag °.

Ainsi, les différences entre les spectres de SERS du mélange poly-NH₂ + polyT et de la molécule double brin hybridée polyA-NH₂ • polyT ont été clairement établies. Elles fournissent des preuves convaincantes que l'hybridation in situ de polyA-NH₂ avec polyT a bien eu lieu. Par ailleurs, dans le cas

de l'hybridation poly-NH₂ • polyT, l'étude de l'évolution de l'intensité du signal SERS en fonction de la concentration, nous a permis de proposer un nouveau modèle, nommé "modèle d'hybridation". Ce dernier est dérivé du précédent qui concernait l'organisation, la couverture de surface et la conformation des polybases sondes immobilisées sur la surface de l'Ag ("greffage modèle sonde»). Ce nouveau modèle décrit 3 zones de concentration selon lesquelles l'efficacité de l'hybridation varie : elle est maximum à la plus faible concentration de sonde (1 uM) (Figure 17). Dans ce cas, l'hybridation peut s'effectuer optimalement, et la couche hybridée forme une couche homogène.

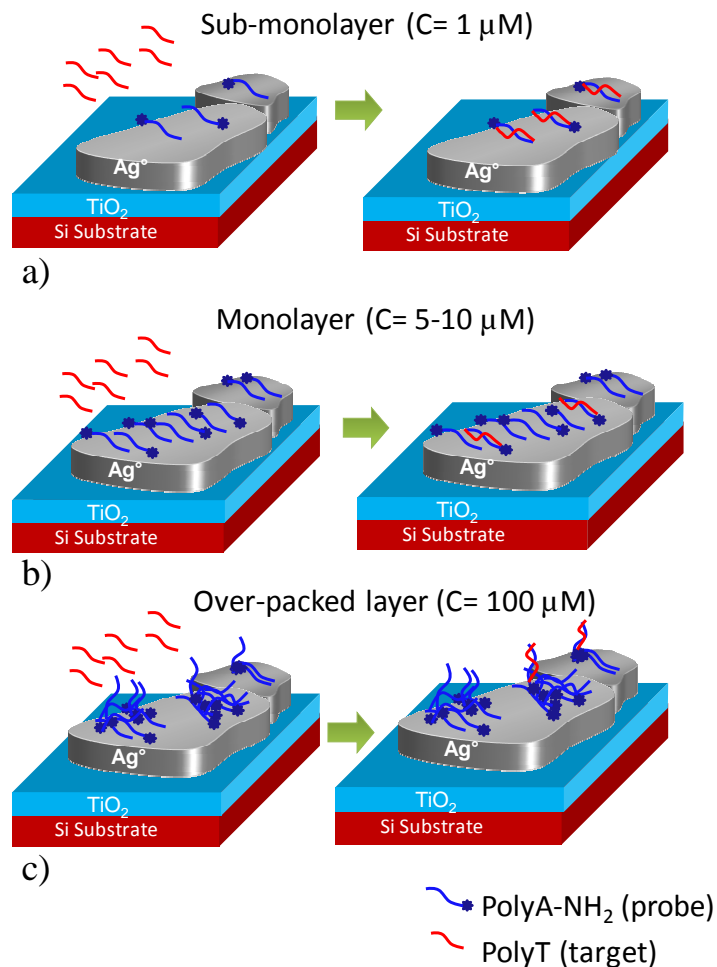


Figure 17: Schéma du modèle, nommé "modèle d'hybridation", présentant l'efficacité d'hybridation selon la distribution des polybases. La mono-couche est obtenue pour la concentration la plus faible ($C = 1 \mu\text{M}$), elle permet une bonne efficacité d'hybridation (a), cas de la monocouche (correspondant à la concentration de la sonde 5-10 μM), où les molécules sont serrées, et ce qui conduit à une faible efficacité d'hybridation (b), pour la plus forte concentration ($C = 100 \mu\text{M}$), en raison d'une agrégation 3D, le rendement d'hybridation est le plus bas (c).

4.2.2 Cas de polyG-NH₂ et polyC : mélange (polyG-NH₂ + polyT) et hybridation (polyG-NH₂ • polyT)

L'étude de la paire polyG-NH₂ avec polyC (hybridation versus mélange) a permis de dégager plusieurs résultats importants.

- Dans le cas du mélange, l'indexation des spectres SERS met en évidence l'absence de bande de polyC (Figure 18). Cela démontre qu'il existe une adsorption préférentielle de polyG-NH₂ sur la surface Ag⁰, selon un mécanisme d'adsorption compétitive entre polyG et poly C-NH₂. Ce résultat est tout à fait comparable à celui du mélange polyA + polyT-NH₂ qui produisait l'adsorption préférentielle de polyA-NH₂ sur la surface Ag⁰. Egalement, l'intensité du signal SERS du mélange polyG-NH₂ + poly C suivant la concentration est tout à fait semblable au cas des polybases seules, montrant un maximum d'intensité dans une plage de concentration 5 -10 uM.

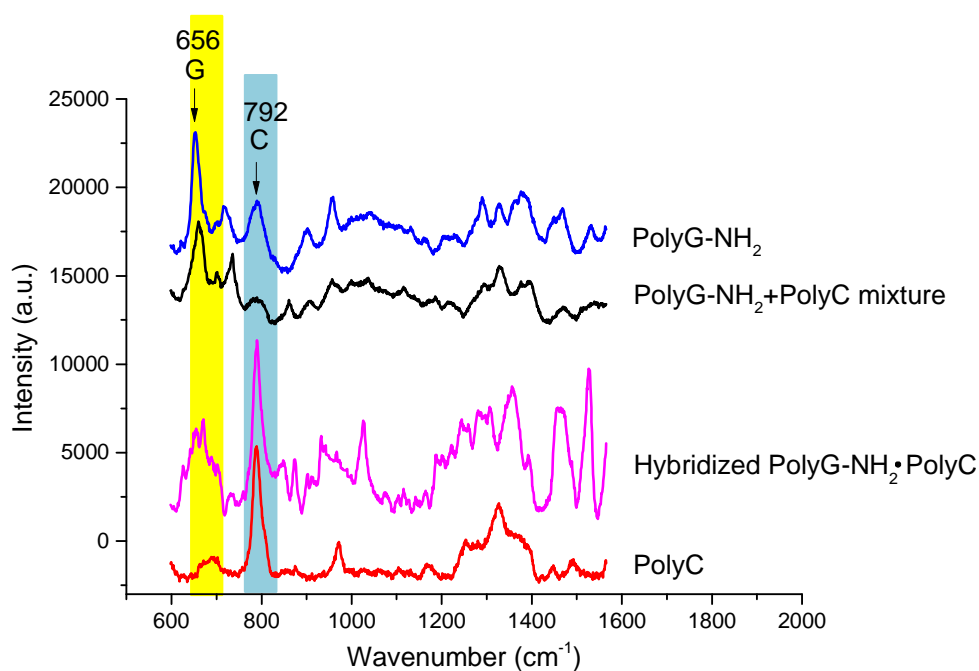


Figure 18: spectres SERS de polyG-NH₂, polyC, mélange équimolaire polyG-NH₂ + polyC et hybridation polyG-NH₂ • polyC. $C_{\text{polyG-NH}_2} = C_{\text{polyC}} = 5 \mu\text{M}$.

- Dans le cas de l'hybridation polyG-NH₂•polyC, la présence de la bande de polyT prouve que l'hybridation a bien eu lieu et que la cytosine est probablement liée à la guanine à travers les liaisons spécifiques hydrogène. A partir de l'intensité accrue des bandes situées aux hautes fréquences (1200-1500 cm⁻¹), nous pouvons déduire que les molécules hybridées polyG-NH₂ • polyC sont principalement couchées à plat sur la surface Ag⁰, même si certaines molécules peuvent être orientées

perpendiculairement. Cette dernière hypothèse est déduite de la présence de bandes out of plane de faible intensité.

5. Conclusion

Ce travail de thèse a porté sur un nouveau type de substrat SERS, élaboré selon des approches simples et à moindre coût, et sur l'évaluation de ses performances pour la détection sans marqueurs de molécules d'ADN en vue d'applications dans le domaine du diagnostic médical. Nous avons ainsi mis au point un protocole de réduction photocatalytique assistée chimiquement conduisant à des hétérostructures $\text{Ag}^\circ / \text{TiO}_2$, et montré en quoi l'utilisation d'un agent encapsulant (TSC) et d'une procédure de nucléation-croissance permettent de contrôler la formation et l'agrégation de NPs Ag° à la surface de couches minces TiO_2 . L'agrégation contrôlée des NPs conduit à son tour à des points chauds induisant une très forte amplification de l'effet SERS. Les performances de nos substrats SERS ont tout d'abord été validées par des mesures par spectroscopie Raman portant sur la détection de la molécule R6G choisie comme analyte modèle. Ces mesures démontrent de bonnes performances de détection (un seuil de détection de 10^{-8} - 10^{-10} M et un EF de 10^6) et une très bonne reproductibilité des spectres SERS collectés sur des substrats de large dimension (plusieurs dizaines de mm^2). Forts de ces performances, nous nous sommes ensuite penchés sur la détection SERS de molécules biologiques d'intérêt applicatif. Des études de fond, portant sur la détection d'homo-nucléotides (polybases) dérivés des quatre nucléobases constituant la structure de l'ADN, adénine (A), cytosine (C), guanine (G) et thymine (T), ont ainsi été réalisées. Le potentiel de détection de nos hétérostructures $\text{Ag}^\circ / \text{TiO}_2$ a conduit à l'indexation quasi-intégrale des bandes Raman des quatre bases étudiées, modifiées ou non avec des groupements NH_2 , et nous a ensuite permis de discuter des effets d'accrochage, d'orientation et d'agencement des molécules d'ADN sur les hétérostructures $\text{Ag}^\circ / \text{TiO}_2$. Des études complémentaires ont finalement permis de confirmer le potentiel de détection de nos hétérostructures en fournissant différents aperçus sur l'hybridation des polybases et l'association de différentes polybases sur un même substrat SERS.

Puis, pour la première fois à notre connaissance, nous avons réalisé l'étude approfondie des spectres SERS obtenus après hybridation in situ de paires de polybases complémentaires appariées : polyA- NH_2 avec polyT et polyG- NH_2 avec polyC. Cette étude a permis de mettre en évidence les caractéristiques spectrales spécifiques de chaque paire appariée, et ce de manière non ambiguë, grâce à la confrontation avec les spectres des mélanges des bases paires correspondantes, non appariées.

Dans le cas de l'hybridation (polyA- NH_2 avec polyT, et polyG- NH_2 avec polyC), nous avons mis en évidence la présence formelle de polyT et de polyC, prouvant leur engagement dans les liaisons hydrogène spécifiques avec polyA- NH_2 et polyG- NH_2 , respectivement. Par ailleurs, cela nous a permis de montrer que les mélanges se comportent exactement comme les solutions de bases simple brin seuls

en raison d'une adsorption préférentielle d'une part, de polyA dans le cas du mélange polyA-NH₂ avec polyT, et d'autre part, de polyG-NH₂ dans le cas du mélange polyG-NH₂ avec polyC, au profit de polyT et de polyC. Nous avons donc émis l'hypothèse d'un mécanisme d'adsorption compétitif qui est en accord avec d'autres données de la littérature telles que les chaleurs de désorption de chacune des bases et de leurs nombres d'atomes d'azote disponibles pour réaliser la liaison base et surface d'argent.

Enfin, concernant les paires de bases appariées et hybridées, comme dans l'étude des cas des polybases simple brins, nous avons pu mettre en évidence que les molécules hybridées sont orientées en position couchée sur les nanoparticules d'argent. Les études en concentration ont montré que l'efficacité de l'hybridation est d'autant meilleure que la concentration des brins sur la surface est faible.

Ce travail de thèse ouvre de très nombreuses perspectives de poursuite.

- Les conditions d'élaboration de nos hétérostructures conduisant à des morphologies très variées des agrégats de NPs Ag⁰, il sera intéressant d'étudier en quoi ces morphologies influencent et permettent d'optimiser les performances de détection SERS.

- De nouvelles études expérimentales devront être menées en vue de mieux comprendre comment les données issues des spectres SERS permettent d'analyser les effets d'accrochage, d'orientation et d'agencement des molécules d'ADN sur les hétérostructures Ag⁰ / TiO₂.

- Les premières études portant sur l'hybridation des polybases et l'association de différentes polybases sur un même substrat SERS devront être poursuivies en vue de fournir des entrées pour des études ultérieures plus complexes sur la détection de molécules d'ADN multibases et leur hybridation.

- Les études sur la détection de molécules d'ADN multibases et leur hybridation permettront de répondre à différentes questions portant sur le potentiel des hétérostructures Ag⁰ / TiO₂ en vue d'applications dans le domaine du diagnostic médical, par exemple l'usage unique ou multiple des substrats SERS proposés.